FINAL REPORT ~ FHWA-OK-20-01 Revision 1

DEVELOPMENT OF RATING TOOL FOR PRESTRESSED CONCRETE BRIDGES VULNERABLE TO SHEAR

Royce W. Floyd, Ph.D., P.E.
Jin-Song Pei, Ph.D.
Cameron D. Murray, Ph.D., EIT
John Toshima, M.Sc.
Afnan Ali, M.Sc.
Stephen Roswurm, Graduate Research Assistant

School of Civil Engineering and Environmental Science (CEES)
Gallogly College of Engineering
The University of Oklahoma
Norman, Oklahoma

January 2020

OKLAHOMA Transportation

The Oklahoma Department of Transportation (ODOT) ensures that no person or groups of persons shall, on the grounds of race, color, sex, religion, national origin, age, disability, retaliation or genetic information, be excluded from participation in, be denied the benefits of, or be otherwise subjected to discrimination under any and all programs, services, or activities administered by ODOT, its recipients, sub-recipients, and contractors. To request an accommodation please contact the ADA Coordinator at 405-521-4140 or the Oklahoma Relay Service at 1-800-722-0353. If you have any ADA or Title VI questions email ODOT-ada-titlevi@odot.org.

DEVELOPMENT OF RATING TOOL FOR PRESTRESSED CONCRETE BRIDGES VULNERABLE TO SHEAR

FINAL REPORT ~ FHWA-OK-20-01 Revision 1

ODOT SP&R ITEM NUMBER 2280

Submitted to:
Office of Research and Implementation
Oklahoma Department of Transportation

Submitted by:
Royce W. Floyd, Ph.D., P.E.
Jin-Song Pei, Ph.D.
Cameron D. Murray, Ph.D., EIT
John Toshima, M.Sc.
Afnan Ali, M.Sc.
Stephen Roswurm, Graduate Research Assistant
School of Civil Engineering and Environmental Science (CEES)
The University of Oklahoma

OKLAHOMA
Transportation

January 2020

TECHNICAL REPORT DOCUMENTATION PAGE

1. REPORT NO.	2. GOVERNMENT ACCESSION NO.	3. RECIPIENT'S CATALOG NO.
FHWA-OK-20-01 Revision 1		

4. TITLE AND SUBTITLE	5. REPORT DATE
Development of Rating Tool for Prestressed Concrete Bridges Vulnerable to Shear	Jan 2020
	6. PERFORMING ORGANIZATION CODE

7. AUTHOR(S)	8. PERFORMING ORGANIZATION REPORT
Royce W. Floyd, Ph.D., P.E., Jin-Song Pei, Ph.D., Cameron D. Murray, Ph.D., EIT, John Toshima, Afnan Ali, Stephen Roswurm	

9. PERFORMING ORGANIZATION NAME AND ADDRESS	10. WORK UNIT NO.
Donald G. Fears Structural Engineering Laboratory School of Civil Engineering and Environmental Science The University of Oklahoma, 303 E. Chesapeake St., Norman, OK 73019	11. CONTRACT OR GRANT NO. ODOT SPR Item Number 2280

12. SPONSORING AGENCY NAME AND ADDRESS	13. TYPE OF REPORT AND PERIOD COVERED
Oklahoma Department of Transportation Office of Research and Implementation 200 N.E. 21st Street, Room G18 Oklahoma City, OK 73105	Final Report Oct 2017 - Sep 2019
	14. SPONSORING AGENCY CODE

15. SUPPLEMENTARY NOTES

Revision 1: no technical changes

16. ABSTRACT

A study was conducted examining the factors affecting shear capacity and load rating, two potential methods for assessing condition of in-service prestressed concrete bridge girders, and a simple procedure for assessing whether and how a bridge should be rated for shear was developed. First, a detailed literature review was conducted to collect results of experimental shear testing on older prestressed concrete girders and the comparison of those results to capacity calculation methods. This was followed by a parametric study to examine the effect of different design items on load distribution and the difference between AASHTO load distribution equations and grillage models for more than two hundred different bridge configurations. Two methods for assessing condition of in-service girders were examined and further refined. The results of previous shear testing and the grillage model parametric study indicate that there may be conservativism built in when AASHTO load distribution factors are used that leaves open the possibility of increased load ratings for some older bridges. Using a grillage model can increase load ratings, reducing the potential need to load post or take some bridges out of service without sacrificing accuracy and safety. The proposed procedure uses a set of simple criteria to identify bridges potentially vulnerable to shear and modifications to the typical rating procedure to produce an accurate shear rating.

17. KEY WORDS	18. DISTRIBUTION STATEMENT
Structural Design, Bridge Design, Load Rating, Prestressed Concrete, Grillage Model, Bayesian	No restrictions. This publication is available from the Office of Research and Implementation, Oklahoma DOT.

19. SECURITY CLASSIF. (OF THIS REPORT)	20. SECURITY CLASSIF. (OF THIS PAGE)	21. NO. OF PAGES	22. PRICE
Unclassified	Unclassified	274	N/A

Form DOT F 1700.7 (08/72)

SI* (MODERN METRIC) CONVERSION FACTORS

APPROXIMATE CONVERSIONS TO SI UNITS

SYMBOL	WHEN YOU KNOW	MULTIPLY BY	TO FIND	SYMBOL
		LENGTH		
in	inches	25.4	millimeters	mm
ft	feet	0.305	meters	m
yd	yards	0.914	meters	m
mi	miles	1.61	kilometers	km
		AREA		
in^2	square inches	645.2	square millimeters	mm^2
ft^2	square feet	0.093	square meters	m^2
yd^2	square yard	0.836	square meters	m^2
ac	acres	0.405	hectares	ha
mi^2	square miles	2.59	square kilometers	km^2
		VOLUME		
fl oz	fluid ounces	29.57	milliliters	mL
gal	gallons	3.785	liters	L
ft^3	cubic feet	0.028	cubic meters	m^3
yd^3	cubic yards	0.765	cubic meters	m^3
	NOTE: volumes greater than 1000 L shall be shown in m^3			
		MASS		
oz	ounces	28.35	grams	g
lb	pounds	0.454	kilograms	kg
T	short tons (2000 lb)	0.907	megagrams (or "metric ton")	Mg (or "t")
		TEMPERATURE (exact degrees)		
°F	Fahrenheit	5 (F-32)/9 or (F-32)/1.8	Celsius	°C
		ILLUMINATION		
fc	foot-candles	10.76	lux	lx
fl	foot-Lamberts	3.426	$candela/m^2$	cd/m^2
		FORCE and PRESSURE or STRESS		
lbf	poundforce	4.45	newtons	N
lbf/in^2	poundforce per square inch	6.89	kilopascals	kPa

APPROXIMATE CONVERSIONS FROM SI UNITS

SYMBOL	WHEN YOU KNOW	MULTIPLY BY	TO FIND	SYMBOL
		LENGTH		
mm	millimeters	0.039	inches	in
m	meters	3.28	feet	ft
m	meters	1.09	yards	yd
km	kilometers	0.621	miles	mi
		AREA		
mm^2	square millimeters	0.0016	square inches	in^2
m^2	square meters	10.764	square feet	ft^2
m^2	square meters	1.195	square yards	yd^2
ha	hectares	2.47	acres	ac
km^2	square kilometers	0.386	square miles	mi^2
		VOLUME		
mL	milliliters	0.034	fluid ounces	fl oz
L	liters	0.264	gallons	gal
m^3	cubic meters	35.314	cubic feet	ft^3
m^3	cubic meters	1.307	cubic yards	yd^3
		MASS		
g	grams	0.035	ounces	oz
kg	kilograms	2.202	pounds	lb
Mg (or "t")	megagrams (or "metric ton")	1.103	short tons (2000 lb)	T
		TEMPERATURE (exact degrees)		
°C	Celsius	1.8C+32	Fahrenheit	°F
		ILLUMINATION		
lx	lux	0.0929	foot-candles	fc
cd/m^2	$candela/m^2$	0.2919	foot-Lamberts	fl
		FORCE and PRESSURE or STRESS		
N	newtons	0.225	poundforce	lbf
kPa	kilopascals	0.145	poundforce per square inch	lbf/in^2

*SI is the symbol for the International System of Units. Appropriate rounding should be made to comply with Section 4 of ASTM E380.(Revised March 2003).

ACKNOWLEDGEMENTS

The authors appreciate Mr. Walt Peters for his support and technical guidance offered to this project. The authors also appreciate the technical input provided by Mr. Wes Kellogg from the ODOT Bridge Division. The authors further acknowledge significant technical contributions from Professors James L. Beck and Joseph P. Wright on methods for assessing the condition of aged girders.

The following students who participated in the project and contributed are acknowledged: Mr. Connor Casey and Mr. Stephen Tanksley, former master's students from OU CEES.

REVISIONS

Revision 1: August 11, 2020 - no technical changes

EXECUTIVE SUMMARY

A large number of bridges in Oklahoma were designed between 1960 and 1990 using a potentially less conservative design shear demand and a different shear capacity calculation than used currently. In light of these changes to the AASHTO Bridge Design Specifications since many older prestressed concrete bridge girders were designed, accurate load rating of bridges for shear is important to prevent adequate bridges from being rated deficient. This report documents a study examining the factors affecting shear capacity and load rating, two potential methods for assessing condition of in-service prestressed concrete bridge girders, and a simple procedure for assessing whether and how a bridge should be rated for shear. First, a detailed literature review was conducted to collect results of experimental shear testing on older prestressed concrete girders and the comparison of those results to capacity calculation methods. This was followed by a parametric study to examine the effect of different design items on shear load distribution and the difference between AASHTO load distribution equations and grillage models for more than two hundred different bridge configurations. Two methods for assessing condition of in-service girders, based on end region bond behavior and flexural stiffness, were examined and further refined.

Most of the girders in the tests examined in this study reached or exceeded expected capacities even when minor end region corrosion was present. The AASHTO modified compression field theory methods were found to be the best for use in rating older girders due to their balance of accuracy and conservativism. The results of previous shear testing and the grillage model parametric study indicate that there may be conservativism built in when AASHTO load distribution factors are used that leaves open the possibility of increased load ratings for some older bridges. Replacing the code shear distribution factors with grillage model derived load distribution for load rating these types of bridges may be beneficial in some cases. Using a grillage model can increase load ratings, reducing the potential need to load post or take some bridges out of service without sacrificing accuracy and safety. The proposed procedure uses a set of simple criteria to identify bridges potentially vulnerable to shear and modifications to the typical rating procedure to produce an accurate shear rating.

Table of Contents

ACKNOWLEDGEMENTS vi

EXECUTIVE SUMMARY vii

List of Figures xii

List of Tables xxiv

1.0 Introduction and Literature Review 1

1.1 Overview 1

1.2 Problem Statement 2

1.3 Project Objectives 2

1.4 Shear in Prestressed Concrete Members 3

1.4.1 ACI Code Equations for Shear 4

1.4.2 AASHTO Standard Specifications Shear Equations 7

1.4.3 AASHTO Load and Resistance Factor Design Shear Procedures 8

1.4.4 Changes in AASHTO Demands 12

1.4.5 Strut and Tie Models 13

1.4.6 Bond-Shear Models 13

1.5 Previous Testing of Older Bridge Girders 14

1.6 Previous Studies on Ultimate Bridge Capacity 17

1.7 Live Load Distribution 20

1.7.1 Overview 20

1.7.2 AASHTO LRFD Distribution Factor Procedures 20

1.7.3 Previous Studies on Load Distribution 24

1.8 Grillage Modeling 27

1.9 Impact of Diaphragm on Load Distribution 30

1.10 Load Rating of Bridges 31

1.11 Literature Review Summary 34
2.0 Design Items Affecting Shear Capacity and Load Distribution 35
2.1 Overview 35
2.2 Modeling Procedures 36
2.2.1 Grillage Modeling Methods 36
2.2.2 Validation of Grillage Models 40
2.2.3 Plate Modeling Methods 49
2.2.4 Validation of Plate Models 51
2.3 Parametric Study 53
2.3.1 Selection of Variables for Parametric Modeling 53
2.3.2 Load Cases 57
2.4 Type-II Girder Model Results 62
2.4.1 Overview of Results 62
2.4.2 Effects of Girder Spacing 63
2.4.3 Effects of Diaphragms 69
2.4.4 Effects of Deck Thickness 71
2.4.5 Effects of Span Length 71
2.5 Type III Girder Model Results 78
2.5.1 Overview 78
2.5.2 Effects of Girder Spacing 78
2.5.3 Effects of Diaphragms 91
2.5.4 Effects of Deck Thickness 92
2.5.5 Effects of Span Length 93
2.5.6 Quantitative Comparison of Load Distribution Factors 93

2.6 Summary of Grillage Parametric Study 96
2.7 Comparison of Plate and Grillage Models 99
2.8 Collection of Previous Experimental Results 108
2.9 End Region Corrosion 115
2.10 Inspection Data Interpretation 116
3.0 Methods for Assessing Condition of Aged Girders 121
3.1 Overview 121
3.2 Technique #1: Bond Transfer Inverse Modeling Using Draw-In Data 122
3.2.1 Introduction 122
3.2.2 Strand Draw-in Data Collection 126
3.2.3 Improving Model in Floyd et al. (2018) 129
3.2.4 Other Literature Review 132
3.3 Technique #2: Piecewise EI Identification 132
3.3.1 Introduction 132
3.3.2 Methodology and Coding 136
3.3.3 Analysis, Results and Discussion 148
3.3.4 Summary 162
4.0 Examination of Sample Oklahoma Bridges 162
4.1 Selected Oklahoma Bridges 162
4.2 Results of Oklahoma Bridge Models 163
4.3 Discussion of Oklahoma Bridge Models 165
5.0 Recommendations for Identifying and Rating Bridges Susceptible to Shear 168
5.1 Overview 168
5.2 Procedure 170

5.2.1 Step 1: Identifying Bridges Vulnerable to Shear 170
5.2.2 Step 2: Collect Additional Information 170
5.2.3 Step 3: Determine if a Grillage Model May be Beneficial 171
5.2.4 Step 4: Rate Bridge for Shear 172
5.2.5 Step 5: Examine Available Experimental Data 172
5.3 Example: U.S. 412 over Verdigris River O'Flow (NBI 19101) 173
6.0 Summary and Conclusions 177
6.1 Summary 177
6.2 Conclusions 178
6.2.1 Factors Affecting Shear Capacity and Load Rating 178
6.2.2 Conclusions on Methods for Assessing Condition of Aged Girders 180
6.2.3 Overall Conclusions 181
6.3 Limitations 181
6.4 Suggestions for Future Research 182
References 182
Appendix A: Additional Parametric Study Results 193
A.1 Type-IV Girders 193
A.1.1 Effects of Girder Spacing 193
A.1.2 Effects of Diaphragms 194
A.1.3 Effects of Deck Thickness 194
A.1.4 Effects of Span Length 194
A.1.5 Quantitative Comparison of Load Distribution Factors 205
A.2 BT-63 Girders 207
A.2.1 Effects of Girder Spacing 207

A.2.2 Effects of Diaphragms 208
A.2.3 Effects of Deck Thickness 208
A.2.4 Effects of Span Length 208
A.2.5 Quantitative Comparison of Load Distribution Factors 219
A.3 BT-72 Girders 221
A.3.1 Effects of Girder Spacing 221
A.3.2 Effects of Diaphragms 221
A.3.3 Effects of Deck Thickness 222
A.3.4 Effects of Span Length 222
A.3.5 Quantitative Comparison of Load Distribution Factors 232
Appendix B: Distribution factor data 235
Appendix C: Strand Draw-in Data 244

List of Figures

Figure 1.1. General free body diagram (taken from Ross and Naji, 2014) 14
Figure 1.2. Grillage example 28
Figure 1.3. Equivalent shape to find torsion constant (from O'Brien and Keogh 1997) (dimensions in mm) 29
Figure 2.1. Typical grillage model configuration 38
Figure 2.2. Type-III girder section and the equivalent section used to determine properties 39
Figure 2.3. Section and plan of test bridge 41
Figure 2.4. Longitudinal members used in grillage: interior girder (left), exterior girder (right) 41
Figure 2.5. Transverse grillage members at diaphragm locations 42
Figure 2.6. Grillage support conditions 43
Figure 2.7. Comparison of load versus deflection relationships for grillage model and scale bridge loaded at girder A5 44

Figure 2.8. Comparison of load versus deflection relationships for grillage model and scale bridge loaded at girder A4 45
Figure 2.9. Comparison of load versus girder strain relationships for grillage model and scale bridge loaded at girder A5 46
Figure 2.10. Comparison of load versus girder strain relationships for grillage model and scale bridge loaded at girder A4 46
Figure 2.11. Distribution factor comparison for grillage model and scale bridge load test (load at A5) 48
Figure 2.12. Distribution factor comparison for grillage model and scale bridge load test (load at A4) 48
Figure 2.13. Representation of an element used for plate models (Sotelino and Chung, 2006) 50
Figure 2.14. Wireframe and extruded view of a typical plate model 51
Figure 2.15. Oklahoma prestressed concrete bridges between 30 and 108 ft (1960-1979) 54
Figure 2.16. Roadway widths for bridges of interest 55
Figure 2.17. HS-20 truck loads 58
Figure 2.18. Locations of HS-20 truck for grillage model 59
Figure 2.19. Critical lateral location of design truck for exterior girder, one lane loaded case 60
Figure 2.20. Critical location of design truck for interior girder, one lane loaded case .. 60
Figure 2.21. Lane load width and clearance for HS-20 truck (MoDOT, 2007) 61
Figure 2.22. Critical location of design truck for exterior girder, two lanes loaded case 61
Figure 2.23. Critical location of truck for interior girder, two lanes loaded case 62
Figure 2.24. Distribution factors for exterior girders, one lane loaded versus girder spacing 64
Figure 2.25. Distribution factors for exterior girders, 2+ lanes loaded versus girder spacing 65
Figure 2.26. Distribution factors for interior girders, one lane loaded versus girder spacing 66
Figure 2.27. Distribution factors for interior girders, 2+ lanes loaded versus girder spacing 67
Figure 2.28. Potential conservativism of distribution factors for each girder spacing examined with diaphragms 68
Figure 2.29. Potential conservativism of distribution factors for each girder spacing examined without diaphragms 69

Figure 2.30. Difference in distribution factors for diaphragm versus no diaphragm for interior girders 70
Figure 2.31. Difference in Distribution factors for diaphragm versus no diaphragm for exterior girders 70
Figure 2.32. Distribution factors for interior girders with one lane loaded, 6 ft girder spacing 72
Figure 2.33. Distribution factors for interior girders with one lane loaded, 9 ft girder spacing 72
Figure 2.34. Distribution factors for interior girders with one lane loaded, 12 ft girder spacing 73
Figure 2.35. Distribution factors for interior girders with 2+ lanes loaded, 6 ft girder spacing 73
Figure 2.36. Distribution factors for interior girders with 2+ lanes loaded, 9 ft girder spacing 74
Figure 2.37. Distribution factors for interior girders with 2+ lanes loaded, 12 ft girder spacing 74
Figure 2.38. Distribution factors for exterior girders with one lane loaded, 6 ft spacing 75
Figure 2.39. Distribution factors for exterior girders with one lane loaded, 9 ft spacing 75
Figure 2.40. Distribution factors for exterior girders with one lane loaded, 12 ft spacing 76
Figure 2.41. Distribution factors for exterior girders with 2+ lane loaded, 6 ft spacing .. 76
Figure 2.42. Distribution factors for exterior girders with 2+ lane loaded, 9 ft spacing .. 77
Figure 2.43. Distribution factors for exterior girders with 2+ lane loaded, 12 ft spacing 77
Figure 2.44. Grillage model and AASHTO load distribution factors for 45 ft span interior Type-III girders, one lane loaded case versus girder spacing 79
Figure 2.45. Grillage model and AASHTO load distribution factors for 60 ft span interior Type-III girders, one lane loaded case versus girder spacing 80
Figure 2.46. Grillage model and AASHTO load distribution factors for 75 ft span interior Type-III girders, one lane loaded case versus girder spacing 80
Figure 2.47. Grillage model and AASHTO load distribution factors for 45 ft span exterior Type-III girders, one lane loaded case versus girder spacing 81
Figure 2.48. Grillage model and AASHTO load distribution factors for 60 ft span exterior Type-III girders, one lane loaded case versus girder spacing 81
Figure 2.49. Grillage model and AASHTO load distribution factors for 75 ft span exterior Type-III girders, one lane loaded case versus girder spacing 82
Figure 2.50. Grillage model and AASHTO load distribution factors for 45 ft span interior Type-III girders, two lanes loaded case versus girder spacing 82

Figure 2.51. Grillage model and AASHTO load distribution factors for 60 ft span interior Type-III girders, two lanes loaded case versus girder spacing 83

Figure 2.52. Grillage model and AASHTO load distribution factors for 75 ft span interior Type-III girders, two lanes loaded case versus girder spacing 83

Figure 2.53. Grillage model and AASHTO load distribution factors for 45 ft span exterior Type-III girders, two lanes loaded case versus girder spacing 84

Figure 2.54. Grillage model and AASHTO load distribution factors for 60 ft span exterior Type-III girders, two lanes loaded case versus girder spacing 84

Figure 2.55. Grillage model and AASHTO load distribution factors for 75 ft span exterior Type-III girders, two lanes loaded case versus girder spacing 85

Figure 2.56. Percentage difference between AASHTO equations and grillage model derived load distribution factors for 45 ft span Type-III interior girders, one lane loaded case 86

Figure 2.57. Percentage difference between AASHTO equations and grillage model derived load distribution factors for 60 ft span Type-III interior girders, one lane loaded case 86

Figure 2.58. Percentage difference between AASHTO equations and grillage model derived load distribution factors for 75 ft span Type-III interior girders, one lane loaded case 87

Figure 2.59. Percentage difference between AASHTO equations and grillage model derived load distribution factors for 45 ft span Type-III interior girders, two lanes loaded case 87

Figure 2.60. Percentage difference between AASHTO equations and grillage model derived load distribution factors for 60 ft span Type-III interior girders, two lanes loaded case 88

Figure 2.61. Percentage difference between AASHTO equations and grillage model derived load distribution factors for 75 ft span Type-III interior girders, two lanes loaded case 88

Figure 2.62. Percentage difference between AASHTO equations and grillage model derived load distribution factors for 45 ft span Type-III interior girders, two lanes loaded case 89

Figure 2.63. Percentage difference between AASHTO equations and grillage model derived load distribution factors for 60 ft span Type-III interior girders, two lanes loaded case 89

Figure 2.64. Percentage difference between AASHTO equations and grillage model derived load distribution factors for 75 ft span Type-III interior girders, two lanes loaded case 90

Figure 2.65. Percentage difference between AASHTO equations and grillage model derived load distribution factors for 45 ft span Type-III exterior girders, two lanes loaded case 90

Figure 2.66. Percentage difference between AASHTO equations and grillage model derived load distribution factors for 60 ft span Type-III exterior girders, two lanes loaded case 91

Figure 2.67. Percentage difference between AASHTO equations and grillage model derived load distribution factors for 75 ft span Type-III exterior girders, two lanes loaded case 91

Figure 2.68. Grillage model showing the critical load case for exterior girder one lane loaded condition 92

Figure 2.69. Linear trendlines for effect of girder spacing on distribution factors for interior Type-III girders, one lane loaded case 94

Figure 2.70. Linear trendlines for effect of girder spacing on distribution factors for exterior Type-III girders, one lane loaded case 94

Figure 2.71. Linear trendlines for effect of girder spacing on distribution factors for interior Type-III girders, two lanes loaded case 95

Figure 2.72. Linear trendlines for effect of girder spacing on distribution factors for exterior Type-III girders, two lanes loaded case 95

Figure 2.73. Comparison of plate and grillage models for 12 ft spacing and 2 lanes loaded case for BT-72 girders with 150 ft span 101

Figure 2.74. Comparison of plate and grillage models for 12 ft spacing and 2 lanes loaded case for Type III girders with 75 ft span 101

Figure 2.75. Comparison of plate and grillage models for 12 ft spacing and 2 lanes loaded case for BT-72 girders with 120 ft span 102

Figure 2.76. Comparison of plate and grillage models for 12 ft spacing and 2 lanes loaded case for Type-III girders with 45 ft span 102

Figure 2.77. Comparison of plate and grillage models for 12 ft spacing and 1 lane loaded case for BT-72 girders with 150 ft span 103

Figure 2.78. Comparison of plate and grillage models for 12 ft spacing and 1 lane loaded case for Type-III girders with 75 ft span 103

Figure 2.79. Comparison of plate and grillage model for 12 ft spacing and 1 lane loaded case for BT-72 girders with 120 ft span 104

Figure 2.80. Comparison of plate and grillage model for 12 ft spacing and 1 lane loaded case for Type-III girders with 45 ft span 104

Figure 2.81. Comparison of plate and grillage model for 6 ft spacing and 2 lanes loaded case for BT-72 girders with 150 ft span 105

Figure 2.82. Comparison of plate and grillage model for 6 ft spacing and 2 lanes loaded case for Type-III girders with 75 ft span 105

Figure 2.83. Comparison of plate and grillage models for 6 ft spacing and 2 lanes loaded case for BT-72 girders with 120 ft span 106

Figure 2.84. Comparison of plate and grillage models for 6 ft spacing and 2 lanes loaded case for Type III girders with 45 ft span 106
Figure 2.85. Comparison of plate and grillage models for 6 ft spacing and 1 lane loaded case for BT-72 girders with 150 ft span 107
Figure 2.86. Comparison of plate and grillage models for 6 ft spacing and 1 lane loaded case for Type-III girders with 75 ft span 107
Figure 2.87. Comparison of plate and grillage models for 6 ft spacing and 1 lane loaded case for BT-72 girders with 120 ft span 108
Figure 2.88. Comparison of plate and grillage models for 6 ft spacing and 1 lane loaded case for Type-III girders with 45 ft span 108
Figure 2.89. Comparison of experimental shear to calculated capacity for girders tested by Floyd et al. (2016) relative to a/d ratio 109
Figure 2.90. Comparison of experimental shear to calculated capacity for girders tested by Floyd et al. (2016) relative to failure type 110
Figure 2.91. Comparison of experimental shear to calculated capacity for girders tested by Osborn et al. (2012) relative to a/d ratio 111
Figure 2.92. Comparison of experimental shear to calculated capacity for girders tested by Osborn et al. (2012) relative to failure type 111
Figure 2.93. Comparison of experimental shear to calculated capacity for girders tested by Shahawy et al. (1993) relative to a/d ratio 112
Figure 2.94. Comparison of experimental shear to calculated capacity for girders tested by Shahawy et al. (1993) relative to failure type 112
Figure 2.95. Comparison of experimental shear to calculated capacity for girders tested by Ross et al. (2011) relative to a/d ratio 113
Figure 2.96. Comparison of experimental shear to calculated capacity for girders tested by Ross et al. (2016) relative to failure type 114
Figure 2.97. Comparison of experimental shear to calculated capacity for girders tested by Floyd et al. (2016), Osborn et al (2012). and Ross et al. (2011) relative to a/d ratio 114
Figure 2.98. Comparison of experimental shear to calculated capacity for girders tested by Floyd et al. (2016), Osborn et al (2012). and Ross et al. (2011) relative to failure type 115
Figure 2.99. Section of sample inspection report showing Main Span Material and Design Type (item 43) and Year Built (item 27) 117
Figure 2.100. Section of sample inspection report showing Girder Spacing/Number (item 243) and Span Lengths (item 244) 118
Figure 2.101. Section of sample inspection report showing Width Curb to Curb (item 51) and Width Out to Out (item 52) 118

Figure 2.102. Section of sample inspection report showing Element Notes for Beam Ends (Element 719) and Steel Bearing Assembly (Element 916) 120

Figure 2.103. Section of sample inspection report showing Element Condition States for Beam Ends (Element 719) and Steel Bearing Assembly (Element 916) 120

Figure 2.104. Bearing plate corrosion and spalling at the prestressed beam end 121

Figure 3.1. Displacements of the strand and concrete at the end of a prestressed concrete beam, following Figures 11 and 13 in Chapter VII of Guyon (1953) but with a minor correction on both the concrete and strand ends. 123

Figure 3.2. One-year prestress loss for selected normal- and lightweight self-consolidating concrete beam specimens by assuming the ultimate creep coefficient to be 2.35 124

Figure 3.3. Measured vs. predicted strand draw-in, and predicted end movement of strand and concrete for two LWSCC and one NWSCC specimen. 125

Figure 3.4. Time evolution of strain distribution for both strand and concrete and estimated transfer length in comparison with 3λ for a lightweight self-consolidating concrete beam specimen LWSCC-12 with $w_c = 120.45$ pcf, $f'_c = 6700$ psi, $k = 1/2.35$, and $\eta = 7.114\ \mathrm{day}$. Only the left half is presented due to symmetry. 126

Figure 3.5. Prestressed beam specimen cross-section and elevation 127

Figure 3.6. Sample strand draw-in time history measured for prestressed beam specimen PC11 127

Figure 3.7. Internal instrumentation plan for SPTC prestressed beam 128

Figure 3.8. Plot of strain measured along the length of the beam using DEMEC surface gages, internal VSWGs, and fiber optic sensors at 1 and 28 days of age 129

Figure 3.9. An example of significantly improved results of predicted draw-in for specimen LWSCC-12 131

Figure 3.10. An illustrative example using $N = 3$, $J = 4$ and $K = 1$: (a) test setup and (b) real and (c) – (f) virtual bending moment diagrams utilized in the MATLAB code Leastsquares.m 137

Figure 3.11. A flowchart of the developed code for piecewise EI identification 143

Figure 3.12. A flowchart of the involved additional preprocessing 143

Figure 3.13. Raw load and displacement time histories of a typical test including irrelevant data 144

Figure 3.14. Filtered (with a low-pass filter) and reduced (as shown in circles) multi-channel data measurements for further analysis 145

Figure 3.15. Visual representation of validation of the least-squares and Bayesian methodologies using a simple beam - with uniform EIs, for the test 1 setup 146

Figure 3.16. Validation of the least-squares and Bayesian methodologies using a simple beam - with varying piecewise constant EIs, for the test 10 setup 147

Figure 3.17. Validation of the least-squares and Bayesian methodologies using a simple beam - with varying piecewise constant EIs, for the test 15 setup 147

Figure 3.18. Panel (a) shows a typical test result involving a potentially malfunctioning LVDT L1 (located approximately 50 in. left of the beam centerline). Panel (b) shows the strategy adopted to remove all readings from the possibly unreliable LVDT L1 148

Figure 3.19. 1, 3, 6, 9, 10, and example arbitrary substructure divisions applied to a simulated Girder A 154

Figure 3.20. Test 1 “Uncorrected” identification for 1 (top), 3, 6, and 9 (bottom) substructure divisions 156

Figure 3.21. Test 1 “L1 Corrected” identification for 1 (top), 3, 6, and 9 (bottom) substructure divisions 157

Figure 3.22. Test 1 “L1-KL Corrected” identification for 1 (top), 3, 6, and 9 (bottom) substructure divisions 158

Figure 3.23. One EI value for Girder A when Bayesian analysis was applied to the one substructure case: distribution of EI identification for each test is based on data category 159

Figure 3.24. Three EI values for Girder A when Bayesian analysis was applied to the three substructure case: distribution of EI identification for each test is based on data category 160

Figure 3.25. Ten EI values for Girder A when Bayesian analysis was applied to the ten substructure case: distribution of EI identification for each test is based on data category 161

Figure 4.1. Comparison of distribution factors for selected Oklahoma bridges 164

Figure 4.2. Distribution factor ratios for specific Oklahoma bridges 165

Figure 4.3. AASHTO DF/Grillage model DF for Oklahoma bridges 166

Figure 4.4. Grillage derived rating factors/AASHTO LRFD rating factors for Oklahoma bridges of interest 168

Figure 5.1. Flow chart of suggested procedures for examining bridges potentially susceptible to shear. 169

Figure 5.2. Portion of inspection report for the U.S. 412 Bridge over Verdigris River O’Flow (NBI 19101) showing span type and year built 174

Figure 5.3. Portion of inspection report for the U.S. 412 Bridge over Verdigris River O’Flow (NBI 19101) showing span lengths and girder spacing 174

Figure 5.4. Portion of inspection report for the U.S. 412 Bridge over Verdigris River O’Flow (NBI 19101) showing Element Notes 175

Figure A.1. Distribution factors for the interior girders, one lane loaded versus girder spacing, Type-IV with 75 ft span 195

Figure A.2. Distribution factors for the interior girders, one lane loaded versus girder spacing, Type-IV with 90 ft span 195

Figure A.3. Distribution factors for the interior girders, one lane loaded versus girder spacing, Type-IV with 105 ft span 196

Figure A.4. Distribution factors for the exterior girders, one lane loaded versus girder spacing, Type-IV with 75 ft span 196

Figure A.5. Distribution factors for the exterior girders, one lane loaded versus girder spacing, Type-IV with 90 ft span 197

Figure A.6. Distribution factors for the exterior girders, one lane loaded versus girder spacing, Type-IV with 105 ft span 197

Figure A.7. Distribution factors for the interior girders, two lanes loaded versus girder spacing, Type-IV with 75 ft span 198

Figure A.8. Distribution factors for the interior girders, two lanes loaded versus girder spacing, Type-IV with 90 ft span 198

Figure A.9. Distribution factors for the interior girders, two lanes loaded versus girder spacing, Type-IV with 105 ft span 199

Figure A.10. Distribution factors for the exterior girders, two lanes loaded versus girder spacing, Type-IV with 75 ft span 199

Figure A.11. Distribution factors for the exterior girders, two lanes loaded versus girder spacing, Type-IV with 90 ft span 200

Figure A.12. Distribution factors for the exterior girders, two lanes loaded versus girder spacing, Type-IV with 105 ft span 200

Figure A.13. Percentage difference between AASHTO equations and grillage models, for one lane loaded and interior girder, Type-IV with 75 ft span 201

Figure A.14. Percentage difference between AASHTO equations and grillage models, for one lane loaded and interior girder, Type-IV with 90 ft span 201

Figure A.15. Percentage difference between AASHTO equations and grillage models, for one lane loaded and interior girder, Type-IV with 105 ft span 201

Figure A.16. Percentage difference between AASHTO equations and grillage models, for one lane loaded and exterior girder, Type-IV with 75 ft span 202

Figure A.17. Percentage difference between AASHTO equations and grillage models, for one lane loaded and exterior girder, Type-IV with 90 ft span 202

Figure A.18. Percentage difference between AASHTO equations and grillage models, for one lane loaded and exterior girder, Type-IV with 105 ft span 202

Figure A.19. Percentage difference between AASHTO equations and grillage models, for two lanes loaded and interior girder, Type-IV with 75 ft span 203

Figure A.20. Percentage difference between AASHTO equations and grillage models, for two lanes loaded and interior girder, Type-IV with 90 ft span 203

Figure A.21. Percentage difference between AASHTO equations and grillage models, for two lanes loaded and interior girder, Type-IV with 105 ft span 203

Figure A.22. Percentage difference between AASHTO equations and grillage models, for two lanes loaded and exterior girder, Type IV with 75 ft span 204

Figure A.23. Percentage difference between AASHTO equations and grillage models, for two lanes loaded and exterior girder, Type IV with 90 ft span 204

Figure A.24. Percentage difference between AASHTO equations and grillage models, for two lanes loaded and exterior girder, Type IV with 105 ft span 204

Figure A.25. Linear trendlines for effect of girder spacing on distribution factors for Type-IV girders, interior girder one lane loaded case 205

Figure A.26. Linear trendlines for effect of girder spacing on distribution factors for Type-IV girders, exterior girder one lane loaded case 206

Figure A.27. Linear trendlines for effect of girder spacing on distribution factors for Type-IV girders, interior girder two lanes loaded case 206

Figure A.28. Linear trendlines for effect of girder spacing on distribution factors for Type-IV girders, exterior girder two lanes loaded case 207

Figure A.29. Distribution factors for the interior girders, one lane loaded versus girder spacing, BT-63 with 105 ft span 209

Figure A.30. Distribution factors for the interior girders, one lane loaded versus girder spacing, BT-63 with 120 ft span 209

Figure A.31. Distribution factors for the interior girders, one lane loaded versus girder spacing, BT-63 with 135 ft span 210

Figure A.32. Distribution factors for the exterior girders, one lane loaded versus girder spacing, BT-63 with 105 ft span 210

Figure A.33. Distribution factors for the exterior girders, one lane loaded versus girder spacing, BT-63 with 120 ft span 211

Figure A.34. Distribution factors for the exterior girders, one lane loaded versus girder spacing, BT-63 with 135 ft span 211

Figure A.35. Distribution factors for the interior girders, two lanes loaded versus girder spacing, BT-63 with 105 ft span 212

Figure A.36. Distribution factors for the interior girders, two lanes loaded versus girder spacing, BT-63 with 120 ft span 212

Figure A.37. Distribution factors for the interior girders, two lanes loaded versus girder spacing, BT-63 with 135 ft span 213

Figure A.38. Distribution factors for the exterior girders, two lanes loaded versus girder spacing, BT-63 with 105 ft span 213

Figure A.39. Distribution factors for the exterior girders, two lanes loaded versus girder spacing, BT-63 with 120 ft span 214

Figure A.40. Distribution factors for the exterior girders, two lanes loaded versus girder spacing, BT-63 with 135 ft span 214

Figure A.41. Percentage difference between AASHTO equations and grillage models, for one lane loaded and interior girder, BT-63 with 105 ft span 215

Figure A.42. Percentage difference between AASHTO equations and grillage models, for one lane loaded and interior girder, BT-63 with 120 ft span 215

Figure A.43. Percentage difference between AASHTO equations and grillage models, for one lane loaded and interior girder, BT-63 with 135 ft span 215

Figure A.44. Percentage difference between AASHTO equations and grillage models, for one lane loaded and exterior girder, BT-63 with 105 ft span 216

Figure A.45. Percentage difference between AASHTO equations and grillage models, for one lane loaded and exterior girder, BT-63 with 120 ft span 216

Figure A.46. Percentage difference between AASHTO equations and grillage models, for one lane loaded and exterior girder, BT-63 with 135 ft span 216

Figure A.47. Percentage difference between AASHTO equations and grillage models, for two lanes loaded and interior girder, BT-63 with 105 ft span 217

Figure A.48. Percentage difference between AASHTO equations and grillage models, for two lanes loaded and interior girder, BT-63 with 120 ft span 217

Figure A.49. Percentage difference between AASHTO equations and grillage models, for two lanes loaded and interior girder, BT-63 with 135 ft span 217

Figure A.50. Percentage difference between AASHTO equations and grillage models, for two lanes loaded and exterior girder, BT-63 with 105 ft span 218

Figure A.51. Percentage difference between AASHTO equations and grillage models, for two lanes loaded and exterior girder, BT-63 with 120 ft span 218

Figure A.52. Percentage difference between AASHTO equations and grillage models, for two lanes loaded and exterior girder, BT-63 with 135 ft span 218

Figure A.53. Linear trendlines for effect of girder spacing on distribution factors for BT-63 girders, interior girders one lane loaded case 219

Figure A.54. Linear trendlines for effect of girder spacing on distribution factors for BT-63 girders, exterior girders one lane loaded case 220

Figure A.55. Linear trendlines for effect of girder spacing on distribution factors for BT-63 girders, interior girders two lanes loaded case 220

Figure A.56. Linear trendlines for effect of girder spacing on distribution factors for BT-63 girders, exterior girders two lanes loaded case 221

Figure A.57. Distribution factors for the interior girders, one lane loaded versus girder spacing, BT-72 with 120 ft span 222

Figure A.58. Distribution factors for the interior girders, one lane loaded versus girder spacing, BT-72 with 135 ft span 223

Figure A.59. Distribution factors for the interior girders, one lane loaded versus girder spacing, BT-72 with 150 ft span 223

Figure A.60. Distribution factors for the exterior girders, one lane loaded versus girder spacing, BT-72 with 120 ft span 224
Figure A.61. Distribution factors for the exterior girders, one lane loaded versus girder spacing, BT-72 with 135 ft span 224
Figure A.62. Distribution factors for the exterior girders, one lane loaded versus girder spacing, BT-72 with 150 ft span 225
Figure A.63. Distribution factors for the interior girders, two lanes loaded versus girder spacing, BT-72 with 120 ft span 225
Figure A.64. Distribution factors for the interior girders, two lanes loaded versus girder spacing, BT-72 with 135 ft span 226
Figure A.65. Distribution factors for the interior girders, two lanes loaded versus girder spacing, BT-72 with 150 ft span 226
Figure A.66. Distribution factors for the exterior girders, two lanes loaded versus girder spacing, BT-72 with 120 ft span 227
Figure A.67. Distribution factors for the exterior girders, two lanes loaded versus girder spacing, BT-72 with 135 ft span 227
Figure A.68. Distribution factors for the exterior girders, two lanes loaded versus girder spacing, BT-72 with 150 ft span 228
Figure A.69. Percentage difference between AASHTO equations and grillage models, for one lane loaded and interior girder, BT-72 with 120 ft span 228
Figure A.70. Percentage difference between AASHTO equations and grillage models, for one lane loaded and interior girder, BT-72 with 135 ft span 229
Figure A.71. Percentage difference between AASHTO equations and grillage models, for one lane loaded and interior girder, BT-72 with 150 ft span 229
Figure A.72. Percentage difference between AASHTO equations and grillage models, for one lane loaded and exterior girder, BT-72 with 120 ft span 229
Figure A.73. Percentage difference between AASHTO equations and grillage models, for one lane loaded and exterior girder, BT-72 with 135 ft span 230
Figure A.74. Percentage difference between AASHTO equations and grillage models, for one lane loaded and exterior girder, BT-72 with 150 ft span 230
Figure A.75. Percentage difference between AASHTO equations and grillage models, for two lane loaded and interior girder, BT-72 with 120 ft span 230
Figure A.76. Percentage difference between AASHTO equations and grillage models, for two lane loaded and interior girder, BT-72 with 135 ft span 231
Figure A.77. Percentage difference between AASHTO equations and grillage models, for two lane loaded and interior girder, BT-72 with 150 ft span 231
Figure A.78. Percentage difference between AASHTO equations and grillage models, for two lane loaded and exterior girder, BT-72 with 120 ft span 231

Figure A.79. Percentage difference between AASHTO equations and grillage models, for two lane loaded and exterior girder, BT-72 with 135 ft span 232

Figure A.80. Percentage difference between AASHTO equations and grillage models, for two lane loaded and exterior girder, BT-72 with 150 ft span 232

Figure A.81. Linear trendlines for effect of girder spacing on distribution factors for BT-72 girders, interior girders one lane loaded case 233

Figure A.82. Linear trendlines for effect of girder spacing on distribution factors for BT-72 girders, exterior girders one lane loaded case 233

Figure A.83. Linear trendlines for effect of girder spacing on distribution factors for BT-72 girders, interior girders two lanes loaded case 234

Figure A.84. Linear trendlines for effect of girder spacing on distribution factors for BT-72 girders, exterior girders two lanes loaded case 234

List of Tables

Table 1.1. Table to find beta (β) adapted from Appendix B5 of AASHTO 2015 11

Table 1.2. Distribution factor equations for 1 design lane loaded 21

Table 1.3. Distribution factor equations for 2+ design lanes loaded 22

Table 1.4. Multiple presence factors from AASHTO LRFD 24

Table 1.5. Bridge condition ratings 31

Table 1.6. Bridge condition factor 33

Table 2.1. Summary of properties used in scale bridge grillage 42

Table 2.2. Method to find distribution factors from deflections for the interior girder (load on girder A5) load case 47

Table 2.3. Method to find distribution factors from deflections for the exterior girder (load on girder A4) load case 47

Table 2.4. Types of 3D FE models described by Sotelino and Chung (2006) 49

Table 2.5. Comparison of bridge test with grillage and plate models for interior girders (load on girder A5) 52

Table 2.6. Comparison of bridge test with grillage and plate models for exterior girders (load on girder A4) 52

Table 2.7. Type- II girder bridge grillage models (deck thickness (in.) on interior of table) 56

Table 2.8. Type-III girder bridge grillage models (deck thickness (in.) on interior of table) 56

Table 2.9. Type-IV girder bridge grillage models (deck thickness (in.) on interior of table) 56
Table 2.10. BT-63 girder bridge grillage models (deck thickness (in.) on interior of table) 57
Table 2.11. BT-72 girder bridge grillage models (deck thickness (in.) on interior of table) 57
Table 2.12. Conservativism of AASHTO LRFD code for varying slab thickness 71
Table 2.13. Range of difference between AASHTO and grillage distribution factors (%) 96
Table 2.14. Summary of distribution factor vs spacing trendline slopes 97
Table 2.15. Type III girder bridge plate models (deck thickness in in. on interior of table) 100
Table 2.16. BT-72 girder bridge plate models (deck thickness in in. on interior of table) 100
Table 2.17. List of Sample Inspection Reports Examined 116
Table 3.1. Study of rate of convergence for predicted end movement using LWSCC-12 131
Table 3.2. Results from validation of the least-squares and Bayesian methodologies using a simple beam – with uniform EIs, for the test 1 setup 146
Table 3.3. Results from validation of the least-squares and Bayesian methodologies using a simple beam – with varying piecewise constant EIs, for the test 10 setup 147
Table 3.4. Results from validation of the least-squares and Bayesian methodologies using a simple beam - with varying piecewise constant EIs, for the test 15 setup 148
Table 4.1. Shear distribution factors for selected Oklahoma bridges 164
Table 4.2. Shear load ratings for the three Oklahoma bridges of interest (using AASHTO distribution factors) 167
Table 4.3. Shear load ratings for the three Oklahoma bridges of interest (using grillage derived distribution factors) 167
Table 5.1. Range of difference between AASHTO and grillage distribution factors (%) 171
Table 5.2. Difference between AASHTO and grillage distribution factors (%) for Type II girders 176
Table 5.3. Shear load rating using AASHTO distribution factors 176
Table B.1. Distribution factors from STAAD and model parameters for Type II girders 235
Table B.2. AASHTO distribution factors for parametric models for Type II girders 237
Table B.3. Girder properties for Type II girder parametric bridge models 239

Table B.4. Continued properties for Type II girder parametric bridge models 241
Table B.5. Properties for grillage models of selected Oklahoma bridges (part 1)..... 243
Table B.6. Properties for grillage models of selected Oklahoma bridges (part 2)..... 243
Table C.1. Draw-in data for specimen PC3 244
Table C.2. Draw-in data for specimen PC4 244
Table C.3. Draw-in data for specimen PC5 245
Table C.4. Draw-in data for specimen PC6 245
Table C.5. Draw-in data for specimen PC7 245
Table C.6. Draw-in data for specimen PC8 246
Table C.7. Draw-in data for specimen PC9 246
Table C.8. Draw-in data for specimen PC10 246
Table C.9. Draw-in data for specimen PC11 247
Table C.10. Draw-in data for specimen PC12 247
Table C.11. Draw-in data for specimen PC13 247

1.0 Introduction and Literature Review

1.1 Overview

A large number of bridges in Oklahoma were designed and put into service between 1960 and 1990 using the quarter point rule for shear design from the AASHTO Standard Specifications (e.g. AASHTO 1973). This method considered the applied shear at the quarter-span point to be the critical value for the design demand, which often resulted in larger shear reinforcement spacings near the beam ends than what is typical for new construction. The current AASHTO LRFD Specifications (2015) consider the critical location for shear to be much closer to the support, which can result in a larger design demand and smaller shear reinforcement spacings. The methods for calculating shear capacity included in the AASHTO LRFD Specifications have also evolved considerably over time and a number of additional methods have been proposed by researchers. According to ODOT engineers, as many as 1000 bridges in Oklahoma may have been designed using the quarter point rule for shear, potentially leaving these bridges vulnerable to a lower load rating compared to newer bridges when evaluated using the current LRFD Specifications. This problem can potentially be exacerbated when larger axle loads are required, such as for implements of husbandry or emergency situations. In addition to the differences in design criteria, long-term exposure to the often harsh climate of Oklahoma can cause deterioration of the mechanical properties and structural behavior of the girders. An accurate understanding of the effects of deterioration should be considered when calculating capacity for the girders. As the state of Oklahoma pushes to get the number of structurally deficient bridges down to less than 1% of all highway bridges in Oklahoma by the end of the decade, it is important that additional bridges are not labeled structurally deficient or load posted unnecessarily. In rating a bridge, all available information should be collected and examined to ensure that safety and economy are effectively balanced.

Shear capacity of prestressed concrete girder bridges and load rating of these bridges has been studied over the years to better understand their ultimate behavior related to shear. In light of changes to the code since many older girders were designed and constructed, accurate load rating of bridges for shear is important to prevent

adequate bridges from being rated deficient. This is especially true for the case of overloaded trucks or when there is some end region damage due to corrosion. It is important to have accurate information to use for rating these bridges which can be obtained from typical bridge inspections and innovative methods for determining material properties of older girders.

1.2 Problem Statement

A substantial quantity of research sponsored by ODOT has been conducted by the PIs over the last decade related to shear behavior and evaluating condition of prestressed concrete bridge girders. The availability of this information combined with information found in the literature and results of analytical studies performed by the research team presents an opportunity to create a procedure for more accurately rating bridges for shear; specifically bridges designed using older versions of the AASHTO Specifications.

1.3 Project Objectives

The objectives of the research described in this report were intended to extend the results of previous research sponsored by ODOT related to shear in prestressed concrete bridge girders and evaluation of deterioration in in-service bridges in order to create useful guidance for accurate ratings of older bridges. These objectives were:

1) Identify trends in girder design, construction, and deterioration affecting girder shear capacity,
2) Develop procedures for assessing condition of aged girders specifically related to material properties, effective prestress, and section deterioration,
3) Develop procedures to identify characteristics important to shear capacity from typical inspection data,
4) Create a set of specifications/recommendations that provide guidance on how to analyze and rate bridges potentially susceptible to shear considering all available information.

1.4 Shear in Prestressed Concrete Members

Shear in prestressed concrete members differs from shear in reinforced concrete. The presence of an internal axial force (fully effective beyond the transfer length) alters the stress trajectories in the member. The horizontal compression from the prestress has the effect of flattening the angle of the diagonal tension forces (and resulting cracks), which can mobilize a greater number of shear stirrups and thus increase ductility. The structural designer's goal is typically to create a member that has sufficient ductility so that there are noticeable deflections and visible cracking before a sudden, catastrophic failure. This is typically done by designing the member such that flexural capacity is the controlling factor. Shear in concrete members can be a sudden and an unpredictable failure mode. As such there has been extensive research in shear over the years. Shear cracking is usually split into two categories: web-shear and flexure-shear cracking. Web-shear cracks initiate in the web of a member and flexure shear cracks begin as flexural cracks (vertical) before re-orienting themselves to the load point and becoming diagonal.

Aside from the typical web-shear and flexure-shear type failures, often a shear failure is associated with loss of bond in the prestressing strands. Recent work has sought to present a uniform system of characterizing failures where strand slip occurs (Naji et al. 2017). This work uses the shear span to depth ratio (*a/d*) to describe the testing location. This nomenclature is common in shear tests. Bond-shear failures are associated with cracking near the supports and strand slip or bond loss. A bond-shear failure is defined as a failure with cracking near the supports, strand slip, and no flange crushing. When flange crushing occurs, and the *a/d* is less than 2.5, the failure can be characterized as bond-shear/flexure. If the *a/d* is greater than 2.5 and less than 4.5, and when the nominal moment is exceeded, the failure can be characterized as flexure-bond. When the nominal moment is not reached, the terminology is bond-flexure. This effort was useful in providing guidance for evaluating a failure where slip occurs.

Some important early work regarding shear in prestressed concrete girders was performed at the University of Illinois in the mid-1960s (MacGregor et al. 1965). These researchers tested 104 prestressed concrete beams in shear, varying the locations and

amounts of transverse reinforcement and concrete strength, among other variables. The researchers found that transverse reinforcement helped to restrain cracking and improved ductility after web cracks occurred and used this finding to create an empirical equation for shear capacity of girders with transverse steel. Following this work, MacGregor published another paper with code recommendations which were eventually adopted by the ACI 318 Building Code Requirements for Structural Concrete (ACI 2014) and are still used today (MacGregor & Hanson 1969). The ACI equations are largely empirical and the methodology has not changed much since the 1970s. However, the code that bridge designers currently use is the AASHTO LRFD Bridge Design Specifications (AASHTO 2015). Compared to the ACI shear methodology, the AASHTO code methodology has changed considerably over time. The following discussions of shear capacity calculation methods may overlap with the codes and previous reports (Floyd et al. 2016, Pei et al. 2008), but are included for the sake of completeness.

1.4.1 ACI Code Equations for Shear

The ACI treatment of shear in prestressed concrete is given in Chapters 9 and 22 of the 2014 code (ACI 2014) and involves a separate calculation of the contribution of the steel (V_s) and the concrete (V_c) to the shear resistance. The nominal shear capacity (V_n) of a section is given by Equation 1.1:

$$V_n = V_c + V_s \tag{1.1}$$

The method of separating the shear capacity of the concrete and steel is common in the design codes. For prestressed concrete members, the ACI code offers two methods to calculate shear capacity of the concrete: a simplified method and a more complex method that takes into account different cracking behavior and failure mechanisms. Both methods account for the tensile strength of the concrete based on the square root of the compressive strength. The complex method provides an equation for web-shear cracking and flexure-shear cracking to find the controlling type of cracking at a given section (and the capacity related to these two types). The simplified method is given in Equation 1.2.

$$V_c = \left(0.6\lambda\sqrt{f'_c} + 700\frac{V_u d_p}{M_u}\right) b_w d \tag{1.2}$$

where:

λ = Modification factor for lightweight aggregate; 1.0 for normalweight concrete

f'_c = Specified compressive strength of concrete (psi)

V_u = Factored applied shear at section (lb)

d_p = Depth to centroid of prestress force from extreme compression fiber (in.)

M_u = Factored moment at section (in.-lb)

b_w = Width of web (in.)

d = Distance from extreme compression fiber to centroid of tensile reinforcement (in.)

For this equation, the concrete strength contribution is also limited by the relationship given in Equation 1.3:

$$2\lambda\sqrt{f'_c}b_w d \le V_c \le 5\,\lambda\sqrt{f'_c}b_w d \tag{1.3}$$

Generally speaking, the square root of concrete compressive strength provides an empirical relationship to the tensile strength in the shear equations. For the more complex method in ACI, the concrete contribution related to flexure-shear capacity is given by Equations 1.4, 1.5, 1.6, and 1.7.

$$V_{ci} = 0.6\lambda\sqrt{f'_c}b_w d_p + V_d + \frac{V_i M_{cre}}{M_{max}} \tag{1.4}$$

where:

$$d_p \ge 0.8h \tag{1.5}$$

$$M_{cre} = \left(\frac{I}{y_t}\right)\left(6\lambda\sqrt{f'_c} + f_{pe} - f_d\right) \tag{1.6}$$

$$V_{ci} \ge 1.7\lambda\sqrt{f'_c}b_w d \tag{1.7}$$

and:

V_{ci} = Nominal shear strength provided by concrete when diagonal cracking results from combined shear and moment (lb)

V_d = Shear force at section due to un-factored dead load (lb)

V_i = Factored shear force at section due to externally applied loads associated with M_{max} (lb)

M_{cre} = Maximum factored moment due to external loads (in.-lb)

M_{max} = Maximum factored moment due to external loads (in.-lb)

y_t = Distance from centroid of gross section to tension face (in.)

I = Moment of inertia of cross-section (in^4)

f_{pe} = Stress in concrete due to effective prestress force at tension face (psi)

f_d = Stress due to unfactored dead load at tension face (psi)

h = Height of section (in.)

Note: other variables are as previously defined

The nominal shear force required to cause web-shear cracking is given by Equations 1.8 and 1.9.

$$V_{cw} = \left(3.5\lambda\sqrt{f'_c} + 0.3f_{pc}\right)b_w d_p + V_p \quad (1.8$$

where:

$$d_p \geq 0.8h \quad (1.9)$$

and:

V_{cw} = Nominal shear strength provided by concrete when diagonal cracking results from high principal tensile stress in web (lb)

f_{pc} = Compressive stress in concrete after losses at centroid of the section resisting external loads or at the junction of the web and the flange when the centroid is within the flange (psi)

V_p = Vertical component of effective prestress force at section (lb)

The shear strength supplied by the transverse reinforcement is given by Equation 1.10. For vertical shear stirrups, the ACI code assumes a crack angle of 45 degrees. This approach likely overestimates the angle of shear cracking for prestressed beams but will give a conservative value for the steel contribution to shear strength. A minimum amount of shear steel is required if the nominal resistance of the concrete is less than 50% of the ultimate shear demand.

$$V_s = \frac{A_v f_{yt} d}{s} \tag{1.10}$$

where:

A_v = Area of shear reinforcement within spacing, s (in^2)

f_{yt} = Yield strength of transverse reinforcement (psi)

s = Spacing of shear reinforcement at section (in.)

The ACI methodology has changed little since the 1970s. ACI also allows the use of a strut-and-tie model (STM) for analysis and design in discontinuity regions of concrete beams. Discontinuity regions, or D-regions, are locations in beams near points of sudden change in load or geometry. For bridge girders, locations near the supports are D-regions, and in these locations the assumptions of Bernoulli beam theory become less accurate. This explains the need for different mathematical models for shear capacity near the ends, as well as why accurate equations for shear capacity have proven difficult to derive over the years.

1.4.2 AASHTO Standard Specifications Shear Equations

In the older AASHTO Standard Bridge Specifications (hereafter referred to as AASHTO-STD) (AASHTO 1973), the shear capacity of a member is handled in a similar fashion to the ACI 318 code. This code was selected here because it was in use at the time the full-scale girders tested in Floyd et al. (2016) were cast. As for the equations in ACI 318, these equations were largely empirical. The AASHTO-STD used a load factor design (LFD) philosophy for concrete, whereas the current code uses the LRFD philosophy. The sum the contributions of the steel and the concrete to shear resistance in AASHTO-STD is given in Equation 1.11.

$$V_n = V_c + V_s = 0.06 f'_c b' jd + \frac{2 A_v f_{sy} jd}{s} \tag{1.11}$$

where:

b' = Width of web (in.)

j = Ratio of distance between centroid of compression force and centroid of tension force and total depth

f_{sy} = Tensile capacity of shear reinforcement (psi)

This procedure is quite similar to the ACI method, although it is less complicated with regards to the contribution of concrete to shear strength. As for the steel contribution to shear strength, the “2” in the numerator of the second term in Equation 11 corresponds to a crack angle of 26.6 degrees, as opposed to 45 degrees in the ACI code. A smaller crack angle makes sense because prestress forces are known to flatten stress trajectories in girders, but if the actual crack angle is greater than 26.6 degrees, which is often the case, the steel capacity will be overestimated. A minimum shear steel requirement is given by AASHTO-STD provided in Equation 1.12.

$$A_v \geq \frac{100b's}{f_{sy}} \tag{1.12}$$

There is no upper limit on shear reinforcement in AASHTO-STD. However, the concrete contribution to shear strength is constrained by an upper limit on compressive strength of 3000 psi. A conservative result of this requirement is that most girders designed using this code required a larger amount of shear steel. This conservativism with regards to concrete strength could improve the ductility of girders from this time period loaded in shear.

1.4.3 AASHTO Load and Resistance Factor Design Shear Procedures

The AASHTO Bridge Design Specification has also changed considerably overall since the 1970s. The current code now uses a probabilistic LRFD design philosophy. For the rest of this dissertation, the 2015 version will be referred to as the AASHTO LRFD code. In 2004, the code switched to a “sectional design model” using Modified Compression Field Theory (MCFT). The so-called sectional model refers to the division of a member into design spans (typically at tenth points along the span), each of which would have a different demand and capacity.

MCFT was developed in the late 1980s to provide a general method for determining stresses in reinforced concrete members without the use of a computer (Vecchio & Collins 1986). MCFT assumes that, when shear cracks form, an array of diagonal compression struts are formed in the girder web. These struts also carry some tension, the sum of which is the concrete contribution to shear strength. When using MCFT in the context of AASHTO LRFD, the designer may determine the factors theta

(*θ*) and beta (*β*) using tables provided in the code. The factor *θ* is the crack angle (or angle of diagonal compressive stress) and *β* describes the ability of the concrete to transmit tension and shear. This meant MCFT was an iterative process that designers disliked because of its complexity and the challenge of performing the calculations by hand (Hawkins et al. 2005). Due to the complications associated with MCFT, revisions were published in 2008 allowing the use of MCFT without iteration, simplifying the design process by providing beta/theta equations. The revision also allowed designers to use a method similar to the ACI code (simplified method), and this revision is reflected in the current standard (AASHTO 2015). However, the current code allows the designer to use the simplified method, or MCFT by beta/theta equations or tables.

For all of the current AASHTO methods, the nominal shear resistance (V_n) is represented by the sum of the concrete and steel contributions to shear strength (V_c, V_s) and an additional component, V_p, representing additional resistance to shear from the prestressing force. The overall shear strength formulation is given in AASHTO LRFD Section 5.8.3.3.

1.4.3.1 AASHTO Simplified Method

The AASHTO LRFD code simplified method is similar to the ACI method in that the concrete contribution to shear strength is determined based on flexure-shear and web-shear cracking (Hawkins et al. 2005). The simplified procedures are given in AASHTO LRFD Section 5.8.3.4.3. Shear resistance is taken as the sum of the concrete shear strength, steel contribution to shear strength, and a term to account for the influence of prestress force on shear strength. Concrete contribution to shear strength is taken as the lesser of the resistance when cracking is caused by combined shear and moment or the resistance when cracking occurs in the web due to shear only (Equations 1.13, 1.14, and 1.15).

$$V_c = lesser\ of\ V_{ci}, V_{cw} \tag{1.13}$$

$$V_{ci} = 0.02\sqrt{f'_c}\,b_v d_v + V_d + \frac{V_i M_{cre}}{M_{max}} \geq 0.06\sqrt{f'_c}\,b_v d_v \tag{1.14}$$

$$V_{cw} = \left(0.06\sqrt{f'_c} + 0.30 f_{pc}\right) b_v d_v + V_p \tag{1.15}$$

where:

b_v = Effective web width taken as the minimum web width within d_v (in.)

d_v = Effective shear depth taken as the distance between the resultant tensile and compressive forces due to flexure (in.)

Note: All force units in kips; some variables same as in previous equations

The steel contribution in the AASHTO LRFD code is generally a function of the crack angle, rebar spacing, effective section depth, stirrup angle, reinforcement area, and yield strength of the reinforcement. When vertical shear reinforcement is used, the steel contribution to shear strength is given by Equation 1.16. As in MCFT, the crack angle is represented by the Greek letter theta (θ).

$$V_s = \frac{A_v f_y d_v}{s} cot\theta \tag{1.16}$$

For the simplified method, the term *cot* θ simplifies to 1.0 if $V_{ci} < V_{cw}$, otherwise it can be found using Equation 1.17.

$$cot\theta = 1.0 + 3\left(\frac{f_{pc}}{\sqrt{f'_c}}\right) \leq 1.8 \tag{1.17}$$

The simplified method provides an alternative to MCFT that is more familiar and comfortable for designers used to the ACI and AASHTO-STD methods.

1.4.3.2 AASHTO MCFT Method

Some drawbacks of MCFT were listed previously, but the benefits of MCFT are important. While the typical moment capacity methods are rationally derived, and work across various section types (columns, beams, slabs), shear methods have typically been empirically derived for many types of structures. The benefit of MCFT is that it is a rational method for reinforced and prestressed shear design for all types of members. In order to find shear resistance by MCFT, the factors β and θ must be determined. In LRFD, the MCFT can be used two ways: the first is with beta/theta equations and the second is through the use of beta/theta tables given in Appendix B5 of AASHTO. An example of one of the AASHTO tables is reproduced in Table 1.1. The values of β and θ

depend on the amount of transverse reinforcement provided. ε_x refers to the longitudinal strain in the web of the member. An expression for ε_x is also given in Appendix B5.

Table 1.1. Table to find beta (β) adapted from Appendix B5 of AASHTO 2015

v_u/f'_c	ε_x *1000 ≤ -0.2	ε_x *1000 ≤ -0.1	ε_x *1000 ≤ -0.05	ε_x *1000 ≤ 0	ε_x *1000 ≤ 0.125	ε_x *1000 ≤ 0.25	ε_x *1000 ≤ 0.5	ε_x *1000 ≤ 0.75	ε_x *1000 ≤ 1
≤ 0.075	6.32	4.75	4.1	3.75	3.24	2.94	2.59	2.38	2.23
≤ 0.1	3.79	3.38	3.24	3.14	2.91	2.75	2.5	2.32	2.18
≤ 0.125	3.18	2.99	2.94	2.87	2.74	2.62	2.42	2.26	2.13
≤ 0.15	2.88	2.79	2.78	2.72	2.6	2.52	2.36	2.21	2.08
≤ 0.175	2.73	2.66	2.65	2.6	2.52	2.44	2.28	2.14	1.96
≤ 0.2	2.63	2.59	2.52	2.51	2.43	2.37	2.14	1.94	1.79
≤ 0.225	2.53	2.45	2.42	2.4	2.34	2.14	1.86	1.73	1.64
≤ 0.25	2.39	2.39	2.33	2.33	2.12	1.93	1.7	1.58	1.5

Note: v_u is the average factored shear stress on the concrete in ksi

Because of the perceived complexity of MCFT (specifically regarding use of tables), a new procedure based on equations instead of tables was developed by Bentz, Vecchio, & Collins (2006) to simplify the MCFT procedure. If the minimum amount of shear steel is not provided, the equation for β assumes no transverse reinforcement. These simplified calculations should be more conservative for almost all combinations of β and θ as compared to the original tabular method. The equation for β is shown in Equations 18 and 19 (found in AASHTO LRFD Section 5.8.3.4.2). A minimum transverse steel requirement is given in AASHTO LRFD Section 5.8.2.5.

If $A_v \geq$ Minimum A_v,

$$\beta = \frac{4.8}{(1+750\varepsilon_s)} \tag{1.18}$$

else,

$$\beta = \frac{4.8}{(1+750\varepsilon_s)} \frac{51}{(39+s_{xe})} \tag{1.19}$$

where:

ε_s = Net longitudinal tensile strain at the centroid of the tension reinforcement

s_{xe} = A spacing factor given in the AASHTO LRFD code

The crack angle, θ, can be found by the relationship in Equation 1.20.

$$\theta = 29 + 3500\varepsilon_s \tag{1.20}$$

Once the values of β and θ are found, the concrete and steel contributions to shear strength can be calculated, as in the tabular method. The concrete contribution is a function of β and is given in Equation 1.21.

$$V_c = 0.0316\beta\sqrt{f'_c}b_v d_v \tag{1.21}$$

Finally, the steel contribution in AASHTO LRFD is generally a function of the crack angle, rebar spacing, depth, stirrup angle, area, and yield strength of the reinforcement. This relationship is given in Equation 1.22. Note, the simplified method uses a simpler version of this equation (see Equation 1.16).

$$V_s = \frac{A_v f_y d_v (cot\theta + cot\alpha) sin\alpha}{s} \tag{1.22}$$

where:

α = Angle of inclination of transverse reinforcement

1.4.4 Changes in AASHTO Demands

Of particular interest in relation to girders which have been in service for many years is whether the codes in use at the time those bridges were constructed are adequate for today's loads and compatible with the current code requirements. Generally, codes tend to become less conservative over time as more information is available to the designer and the probability of failure can be reduced; however, there are cases where older equations are less conservative. For this project, one concern is on the demand side of the equation. In the 1970s, the critical section for shear was permitted to be taken at the "quarter-point" of the girder (known as the quarter-point rule). In other words, the maximum shear force used in design could be taken at a quarter of the length into the girder (AASHTO 1973). Today, maximum shears are calculated at a location much closer to the support, possibly resulting in increased shear stresses (AASHTO 2015). It is difficult to say what general effect this has on older designs because the geometry, detailing, and demand on individual bridges varies greatly. It is possible that this provision would result in a larger shear reinforcement spacing near the ends of the girder than would result from currently used methods.

1.4.5 Strut and Tie Models

Another option allowed by both ACI and AASHTO LRFD is the strut-and-tie model (STM). At regions near discontinuities (e.g. loads, supports, cross section changes); St. Venant's Principle is no longer an accurate assumption. These D-regions can be defined as sections of the beam within a distance equal to the member depth from the discontinuity. At these locations, Bernoulli beam theory does not provide accurate results for the shear capacity because the strain distribution is not linear. The STM was developed in the late 1980's to solve these types of problems (Schlaich et al. 1987). STM creates a truss analogy where diagonally cracked concrete forms compressive "struts," and the longitudinal and transverse reinforcement form tension "ties." The strength of the individual struts and ties are then compared to the force demands calculated using the truss model. The STM does not provide a unique solution like the sectional methods, but will give a lower bound shear strength. STM has been used to verify details in concrete members but can be difficult to apply (Hawkins et al. 2005).

1.4.6 Bond-Shear Models

Ross and Naji (2014) describe a method for calculating the bond-shear capacity of a prestressed concrete member. These procedures are similar to the AASHTO 5.8.3.5 provisions for longitudinal reinforcement in end regions with modifications to account for bond failure. Bond-shear failures are initiated by the formation of cracks in the end region that reduce the available development length. When the available development is reduced, the precompression in the ends is also reduced, lowering the shear capacity. This model allows the calculation of the shear force required to initiate this type of failure. The method was verified experimentally for a/d ratios of 1.0 to 4.4. The method is based on moment equilibrium about the top of a shear crack including the forces in the bottom strands, harped strands, shear steel, and reaction force at the support. The full procedure is well laid out in Ross and Naji (2014). Figure 1.1 is taken from Ross and Naji (2014) and shows the free body diagram used for this method.

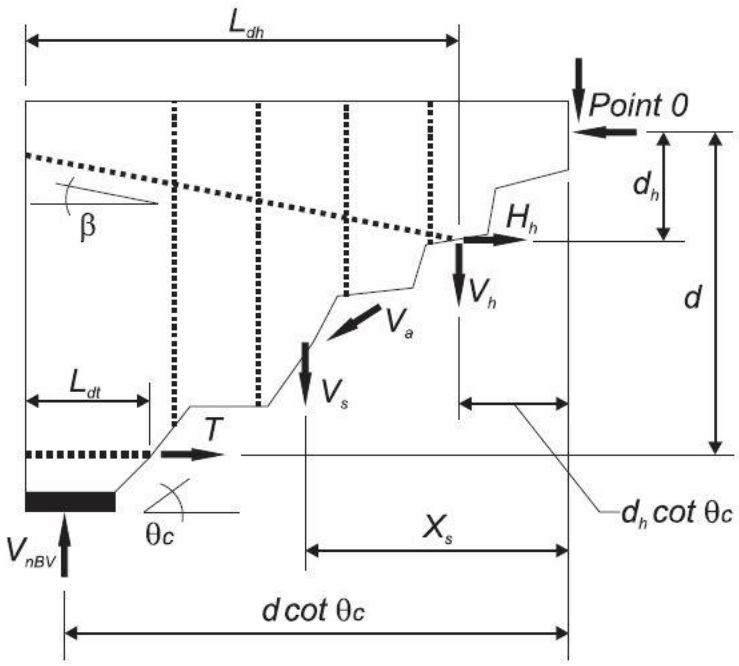

Figure 1.1. General free body diagram (taken from Ross and Naji, 2014)

1.5 Previous Testing of Older Bridge Girders

There are several types of experimental studies of shear in prestressed concrete beams that encompass most published research. Traditionally, researchers will build scale sections, typically no more than 24 in. tall and 20 ft long (e.g. Hanson and Hulsbos 1964; Peterman et al. 2000; Zwoyer and Siess 1954; Elzanaty et al. 1986). Occasionally full-scale replicas will be constructed for lab testing, although relatively few labs around the country have the capability to test sections this large (>24 in. depth) (Shahawy et al. 1993, Shahawy and Batchelor 1996; Morcous et al. 2011). The most uncommon research in this area is testing of full-scale, aged girders, taken from bridges that have been in service for many years. However, many of these full-scale tests look at flexural capacity, and not shear capacity. Tests of these older girders are important because they can provide insight into the residual performance of older bridges, they allow researchers to evaluate the effects of time (e.g., corrosion and prestress losses), and they can provide a benchmark to judge other similar bridges still in service. Many bridges in the U.S. were designed and built more than 30 years ago with a design life of only 50 years, so understanding the behavior of these bridges is useful for rating and

prioritizing bridges for repair and replacement. This section will review some of the past testing of girders taken out of service throughout the U.S.

In Connecticut in 1987, the Walnut Street Bridge was taken out of service and researchers at the University of Connecticut were able to retrieve two girders from the bridge for testing. The girders were 27 in. deep box girders, one of which was in good condition and the other showed minor signs of cracking and spalling. The girders were tested at 1/3 points causing a constant maximum moment in the middle 1/3 of the girder. The researchers found that beam behavior was still ductile, the ultimate strength was higher than predicted, and strain compatibility accurately estimated behavior. The researchers observed little shear cracking (Shenoy & Frantz 1991). Design details of the girders were not available.

In the 1950s, the Ohio Department of Transportation constructed some bridges with prestressed inverted T beams. At the time they were constructed, some were tested in the laboratory. Over 40 years later some of these bridges were taken out of service and two specimens were tested at the University of Cincinnati to compare to the original results. The samples were tested using a single point load at mid-span. The researchers found that the beams remained strong and ductile even after 40 years in service. Prestress losses were around 20-26% based on the observed cracking moment and the beam performance was very similar to the new beams tested in the 1950s. There was no shear cracking observed during the tests (Halsey & Miller, 1996). As these bridges were designed in the 1950s, it is likely they were designed using the American Association of State Highway Officials (AASHO) code which used the Allowable Stress Design (ASD) philosophy as opposed to the Load Factor Design (LFD) adopted in the 1970s.

In Pennsylvania in 1996, two girders were tested to determine the residual prestress by finding the decompression load after 28 years in service. The girders tested were found to be in excellent condition with no cracking occurring during service. Prestress losses of 18% were found, roughly 60% of the predicted losses. These girders were not tested to failure and no shear testing was performed (Pessiki et al. 1996).

A study performed in Minnesota looked at the shear capacity at both ends of a girder taken from a bridge in the state. The goal of these tests was to consider whether previous codes (pre-1980) led to girders under designed for shear. Despite a smaller amount of shear steel than would be required today, the girder carried a greater applied shear than the factored demands in the newer LRFD code (Runzell et al. 2007).

The Florida Department of Transportation recovered four Type-III AASHTO girders while reconstructing some bridges on I-75. The girders were 30 years old at the time and were tested with a single point load and an *a/d* ratio of 1.2 to 5.4. The girders were cut from the bridge such that a 28 in. wide section of deck was left atop the girders. The researchers found that the girders did not exhibit reduced capacity compared to code estimates for shear and moment strength despite their age. For *a/d* ratios of 3 or less, bond-shear failures were observed. When *a/d* was 4, shear compression failure was observed. For *a/d* of 5, a flexural failure was observed. Analysis found that MCFT and the ACI provisions provided conservative failure values for situations with *a/d* less than 3 despite the bond-shear failure, which is not explicitly accounted for by these methods (Ross et al. 2011; Hamilton et al. 2009).

Seven girders from a 42-year-old bridge in Utah were obtained to determine effective prestress force and two were tested to evaluate ultimate shear capacity. The shear tests were performed at *a/d* = 1.5 using a single point load. The authors found that the code equations were conservative for the failure loads observed in testing. The research showed that the STM method was more accurate for loads near a discontinuity and a finite element model showed that concrete compressive strength had a larger effect on shear capacity than stirrup spacing (Osborn 2010; Osborn et al. 2012).

Prior work at the University of Oklahoma has also focused on shear capacity of aged prestressed concrete girders. In 2008, a 40-year-old bridge girder was tested in order to compare experimental values with code values from the 1973 AASHTO-STD and 2004 AASHTO LRFD Specifications. The research also compared the AASHTO-STD, AASHTO LRFD and ACI specifications for shear. The results showed that all codes were conservative with regards to shear failure at *a/d* = 1 (Martin et al. 2011). A second project conducted between 2013 and 2016 (Floyd et al. 2016) consisted of four

shear testing two AASHTO Type II girders taken from an Oklahoma bridge after 46 years in service. This project examined behavior at additional *a/d* ratios of 2.0, 2.5, 3.0 and 3.83, included a girder with a concrete deck, and the girders exhibited some minor corrosion of the prestressing strands at one end. The project also examined full bridge behavior through testing of a scaled four girder bridge section. The girders exhibited capacity significantly exceeding the calculated demands on the bridge and the AASHTO LRFD MCFT method using the beta/theta tables was found to be the best predictor of experimental shear capacity. Corrosion damage was observed to result in bond-shear failures that did not reduce the accuracy of the MCFT prediction, but did reduce the accuracy of the AASHTO simplified procedure. In all tests a 2 in. bonded concrete deck overlay contributed to potential premature failure of the girder, which was not expected.

1.6 Previous Studies on Ultimate Bridge Capacity

There is a dearth of information on the ultimate behavior of bridges as a unit, particularly prestressed concrete bridges. Obviously, opportunities to bring full-scale bridge sections to their ultimate capacity are limited, and constructing a bridge in a laboratory setting can be cost and space prohibitive. However, there have been several studies that examined the ultimate behavior of bridges. Studies of the behavior of full bridge sections are important because their behavior is fundamentally different from that of individual bridge girders. Bridge decks represent a complex system that shares force effects by distribution through the deck and the girders. Elastic analysis of these sections is complex; ultimate behavior is even more vexing. Ultimate bridge tests can provide insight into how bridges behave after the elastic limit of their components is reached.

Jorgenson and Lawson (1972) tested a three-span reinforced concrete slab bridge to failure. The bridge was 10 years old when tested and was being taken out of service when the highway was realigned. A four-wheel patch loading and line loading pattern was placed on the bridge. The section was analyzed as a channel loaded about its weak axis, as the cross-section of the bridge was a flat slab with curbs on each side. Based on the maximum moment applied via line load at failure, the bridge could theoretically support eight HS-20 trucks before permanent deformation occurred and 20

HS-20 trucks before collapse, indicating a very high strength given that the span was only about 25 ft (Jorgenson & Lawson 1972).

Burdette and Goodpasture (1973) performed what they described as “the first failure tests of full-size bridges performed in this country (USA).” Four bridges were tested, including superstructures consisting of AASHTO Type-III girders, reinforced concrete T-beams, and rolled steel sections. The Type-III girder bridge had a 70-degree skew, making it a particularly unusual case and difficult to use for making generalizations. All bridges were described as structurally sound at the time of testing (they were soon to be inundated by the construction of a reservoir). Rolling load and vibration tests were performed before the ultimate load test. Load was arranged in such a way as to simulate the HS-20 truck and apply maximum moment to the bridges. The load was applied through small holes in the bridge deck anchored to the bedrock below the bridge. The researchers noted diaphragm cracking in the concrete bridges at early stages of loading, but this cracking seemed to have little effect on load-deflection behavior. In the Type-III girder bridge, failure initiated with cracking along the web-deck interface and diagonal shear cracks appeared near the supports. The slab was observed to “dish,” or deflect more noticeably at the interior girders compared to the exterior girders. The girder separated from the deck near the load, and at this point the behavior changed and more load was carried by the adjacent girders. The final failure occurred when diagonal cracks propagated in the interior girders (Burdette and Goodpasture 1973).

In 1994, researchers at the University of Cincinnati performed a destructive test on a 38-year-old two lane “concrete slab bridge”. The bridge had a 30-degree skew and exhibited significant deterioration due to freeze/thaw and alkali-silica reaction. One lane of the bridge was loaded in a way as to simulate the HS-20 truck. Despite the bridge being decommissioned for structural reasons, the deck held a large ultimate load (22 HS-20 trucks). The researchers observed that previous damage to the deck affected the final failure mechanism (punching shear). Although punching shear occurred at a lower than estimated load, the overall performance of the bridge exceeded design capacities (Miller et al. 1994).

A 2011 study at the University of Delaware involved the destructive testing of a scale steel bridge (Bechtel et al. 2011). The authors here noted that in the few examples of destructive bridge tests since the 1970s (some listed above), a common finding was a large reserve of strength relative to the design code predictions and rating techniques. The bridge tests listed in this study were all for steel or reinforced concrete superstructures, not prestressed concrete. The increase in bridge strength relative to design strength is attributed to redistribution of force not accounted for in the code. The scale test performed in the study showed that the ability of the bridge to carry load efficiently hinged on the condition of the deck; i.e., the deck was unable to distribute load effectively when significant damage occurred. The researchers concluded that efforts to test bridge sections to failure must be made due to the uniqueness of individual bridge designs (Bechtel et al. 2011). The authors emphasized that analytical models must always be verified against the results of destructive tests to ensure their accuracy.

A recent Minnesota Department of Transportation study involved testing of older girders in shear and the full-scale testing of a bridge constructed in the laboratory to investigate load distribution, ultimate bridge behavior, and the effects of secondary elements (diaphragms and parapet walls) (Dymond et al. 2016). The bridge test showed a reserve of strength in the bridge system relative to the component level capacities, which was attributed to the use of elastic load distribution factors. The study also examined distribution factors using a variety of computer models. 2D grillage models were found to be accurate as a means of finding elastic distribution factors. A major result of the study was a screening tool to help determine which bridges are in need of load rating and which methods to use to determine the demands for these bridges (Dymond et al. 2016). Grillages were recommended to find distribution factors in some cases, and ignoring diaphragms and parapet walls were seen as reasonable simplifications.

1.7 Live Load Distribution

1.7.1 Overview

The concept of live load distribution was developed in the 1930s and 40s and has been in use by AASHTO ever since (Westergaard 1930; Newmark et al. 1946). The method is a simplification of bridge behavior to avoid more complex analyses, especially for typical bridge types. Live load distribution factors are an approximate method of analyzing shears, moments, and deflections in the beams that support a highway bridge deck. According to Taly (2014), there are three main steps to analyzing a bridge structure using distribution factors.

1. Bending moments and shears are calculated based on the notional truck and lane loads in the code. These loads are placed on a beam (whether continuous or simple) in a manner such as to cause maximum force effects. The beam is analyzed based on principles of structural mechanics. At this step, the actual details of the bridge (spacing, superstructure type, etc.) are unimportant.
2. The live load effects on a single girder are determined by multiplying the moments and shears from step 1 by distribution factors. These factors are calculated for both shear and moment, and for interior and exterior girders (four total factors). These factors are based on the spacing, superstructure type, and other geometric details.
3. If the bridge is built with a skew, i.e. not perpendicular to supports, a skew factor must also be applied.

These distribution factors are applied to the load effects (moments and shears) after accounting for other factors that affect the load. These other factors include the impact factor (IM), load factors, and skew correction factors.

1.7.2 AASHTO LRFD Distribution Factor Procedures

The work described in this report focused on 4-girder or more beam-slab type bridges consisting of a series of parallel girders with a slab connecting them. The distribution factors for these types of bridges are given in AASHTO LRFD Section 4.6.2.2 (AASHTO, 2015). Table 1.2 contains the code equations for distribution factors

Table 1.2. Distribution factor equations for 1 design lane loaded

Force effect	Distribution Factor	Range of Applicability
Moment in Interior Beams	$0.06 + \left(\frac{S}{14}\right)^{0.4}\left(\frac{S}{L}\right)^{0.3}\left(\frac{K_g}{12.0Lt_s^3}\right)^{0.1}$	$3.5 \le S \le 16.0$ $4.5 \le t_s \le 12.0$ $20 \le L \le 240$ $N_b \ge 4$ $10{,}000 \le K_g \le 7{,}000{,}000$
Moment in Exterior Beams	Lever Rule	$-1.0 \le d_e \le 5.5$
Shear in Interior Beams	$0.36 + \frac{S}{25}$	$3.5 \le S \le 16.0$ $35 \le L \le 240$ $4.5 \le t_s \le 12.0$ $N_b \ge 4$
Shear in Exterior Beams	Lever Rule	$-1.0 \le d_e \le 5.5$

Note: S = Girder spacing, L = Span length, t_s = slab thickness, N_b = Number of beams, K_g = see Equation 1.23, d_e = distance from center of exterior girder to curb

for beam-slab bridges with one design lane loaded. The “lever rule” referenced in this table is an analogy used in the code to determine distribution factors in some specific cases. For an exterior girder, it involves placing a wheel load 2 ft from the curb on a bridge and treating the slab as simply supported across the first two girders. Using statics, the reaction at the exterior girder can be found as a ratio of the dimensions of the section, this ratio is used as the distribution factor for the exterior girder. In effect, it is a simple and relatively accurate tool for assessing load distribution in exterior girders or for bridges with only three girders. In order to use the following equations, the deck must have a constant width and the beams must be parallel.

Equations 1.23 and 1.24 show some of the parameters for distribution factor calculations.

$$K_g = n\left(I + Ae_g^2\right) \tag{1.23}$$

$$n = \frac{E_b}{E_D} \tag{1.24}$$

where:

n = Modular ratio

E_b = Modulus of beams (ksi)

E_D = Modulus of deck (ksi)

A = Gross area of beam (in^2)

e_g = distance between center of gravity of deck and beam (in.)

AASHTO LRFD also contains equations for load distribution with two design lanes loaded. At the design stage, it is assumed that the number of design lanes (N_L) is equal to the integer part of the ratio of clear roadway width to 12.0 ft (one design lane). In cases where a bridge must support multiple design lanes, there are separate DF cases to check for two or more design lanes loaded in addition to a single lane loaded (as in Table). The DF equations for two or more design lanes are given in Table 1.3.

Table 1.3. Distribution factor equations for 2+ design lanes loaded

Force effect	Distribution Factor	Range of Applicability
Moment in Interior Beams	$0.075 + \left(\frac{S}{9.5}\right)^{0.6}\left(\frac{S}{L}\right)^{0.2}\left(\frac{K_g}{12.0Lt_s^3}\right)^{0.1}$	$3.5 \le S \le 16.0$ $4.5 \le t_s \le 12.0$ $20 \le L \le 240$ $N_b \ge 4$ $10{,}000 \le K_g \le 7{,}000{,}000$
Moment in Exterior Beams	$e \times DF_{interior}$ $e = \frac{d_e}{9.1}$	$-1.0 \le d_e \le 5.5$
Shear in Interior Beams	$0.2 + \frac{S}{12} - \left(\frac{S}{35}\right)^{2.0}$	$3.5 \le S \le 16.0$ $35 \le L \le 240$ $4.5 \le t_s \le 12.0$ $N_b \ge 4$
Shear in Exterior Beams	$e \times DF_{interior}$ $e = 0.6 + \frac{d_e}{10}$	$-1.0 \le d_e \le 5.5$

One important takeaway from these equations is that girder spacing is the most important parameter for load distribution. This makes sense; all other things equal a longer span will result in a more flexible beam, and load transfer occurs through the slab acting as a beam. Some other factors that can affect load distribution but are less influential in these equations include span length, slab thickness, stiffness of beams, stiffness of slabs, and presence/dimensions of diaphragms. The superstructure of a bridge acts as a stiffened plate (Taly, 2014) with many complex variables from these various components of the structure. Distribution factors serve as a simplification of this complex system, but more detailed analyses could result in a more accurate picture of load distribution in a given bridge.

In addition to the procedures listed previously, the AASHTO LRFD code provides an additional procedure for finding distribution factors for exterior girders when end diaphragms are present. This is often referred to as “special analysis” and it is given in

AASHTO LRFD Section 4.6.2.2.2d (AASHTO, 2015). Using this special analysis, the distribution factor is taken as the greater of the distribution factors based on the equations above, or the distribution factor obtained assuming that the bridge deflects and rotates as a rigid cross-section. This process is given by Equation 1.25.

$$R = \frac{N_L}{N_b} + \frac{X_{ext}\sum^{N_L} e}{\sum^{N_b} x^2} \tag{1.25}$$

where:

R = Reaction on exterior girder in terms of lanes

e = Eccentricity of a design truck or design lane load from the center of gravity of all girders (ft)

x = Horizontal distance from the center of gravity of the pattern of girders to each girder (ft)

X_{ext} = Horizontal distance from the center of gravity of all girders to the exterior girder (ft)

This so-called special analysis requires placement of design trucks in adjacent lanes in such a way as to create the maximum resultant on the exterior girder. There are additional factors to account for skew of bridges, but this study focused on straight bridges only.

Finally, there is another factor included in the distribution factor equation in the tables above known as the “multiple presence factor.” This factor must be applied to the lever rule and the “special analysis” since it is not already accounted for in these methods. The multiple presence factor is based on an evaluation of multiple load cases and is meant to represent the worst-case loading scenario. For this study, the multiple presence factor was removed for comparison to computer model results. These factors are merely an increase in loading to account for the possibility of truck loads larger than the HL-93 for the case of one design lane loaded (Cross, et al., 2009). The multiple presence factors from LRFD are given in Table 1.4.

Table 1.4. Multiple presence factors from AASHTO LRFD

Number of loaded lanes, N_L	Multiple presence factor, m
1	1.20
2	1.00
3	0.85
3+	0.65

1.7.3 Previous Studies on Load Distribution

There has been a large amount of research on load distribution in bridges and the subject is a source of considerable debate in the research community. Many load distribution paradigms have been proposed, and the current methods have been derided both as too simple and not simple enough. This section highlights several of the more comprehensive studies on live load distribution in bridges.

Distribution factors have been used for bridge design in the U.S. since the 1930s as a simplification of the complex behavior of bridge decks. Likely the first load distribution relationships for bridges were proposed by Westergaard (Westergaard 1930). Further development of the concept continued in 1946 (Newmark et al., 1946). At this time load distribution was based on the theory that the bridge deck deforms as an elastic plate. In truth, the deck is a plate stiffened by supporting beams (Taly, 2014). The initial work by Newmark et al. (1946) was included in the AASHTO Standard Specifications up to 2002 (AASHTO, 2002). The Standard Specifications used so-called *S/D* (spacing divided by a constant in the denominator), or “S-over” equations which were found to be less accurate for some bridge types (Zokaie, 2000). The AASHTO LRFD distribution factors were developed based on a series of studies performed in the late 80s and early 90s (Nutt et al. 1988; Zokaie et al. 1991a; Zokaie et al. 1991b). These studies were intended to increase the applicability of the distribution factor equations to more bridge types.

More recently, efforts have been made to further improve distribution factors. The most comprehensive push to change the equations was explained in the National Cooperative Highway Research Program (NCHRP) Report 592 (Mertz, 2006). The goal of this NCHRP project was to simplify the distribution factor equations. The study looked at the effects of skew, diaphragms, vehicle position, and a variety of bridge types and

dimensions. As a simplification, the report recommended the use of simple equilibrium formulae (i.e., lever rule), or a kinematic assumption (uniform distribution of load). After these methods are used, the results are scaled up or down by calibration factors based on the specific bridge parameters. Despite a greater degree of accuracy, the new methods proposed by Mertz did not gain much traction. According to Dymond et al. (2016), the methods were criticized as not enough of a simplification to warrant a change. Additionally, the use of grillage analyses was seen as the future of load distribution analysis (Dymond et al. 2016).

Since 2000, there have been several studies to investigate load distribution using either computer models or field testing. Barr, Eberhardt, and Stanton (2001) evaluated code equations for load distribution in prestressed concrete girder bridges using finite-element models and load tests on a real bridge. Twenty-four different variations of 3D finite element (FE) models were developed for bridge superstructures to compare load distribution factors from models and three codes. The finite element models were developed to investigate the effects of lifts (haunches), intermediate diaphragms, end diaphragms, continuity, skew angle, and load type. This study paid particular attention to the diaphragms, continuity, skew, and load type. AASHTO LRFD distribution equations were found to be conservative to a degree that varied among the different configurations tested... End diaphragms were found to reduce distribution factors and intermediate diaphragms were observed to have little effect on load distribution. Distribution factors found using the lane loading were lower than those for the truck loading, indicating that a truck is the conservative case for distribution factor estimation. The researchers also found that the specific bridge examined in their work could have been designed for a girder release strength reduced from 7.4 ksi to 6.4 ksi or the bridge could alternatively, have been designed for 39% higher load based on their finite-element modeling (Barr et al. 2001).

Altay et al. (2003) instrumented three prestressed concrete bridges to investigate the effects of larger truck loads on bridges in Minnesota. The researchers found that shear cracking tended to occur for wide bridges with a high ratio of live load stress to dead load stress. Additionally, it was noted that increases in permit truck weights could lead to shear cracking, which could “significantly effect service life”. Distribution factors

were found to be conservative and interior diaphragms were found to influence load distribution and stresses in the girders (Altay et al., 2003).

Sotelino et al. (2004) suggested a simplified load distribution factor procedure and also compared load distribution factors based on a number of finite-element models of both steel and concrete bridges. The study also considered the effects of diaphragms on load distribution. For prestressed concrete bridges the AASHTO LRFD Distribution factors were found to be conservative by 30%. Secondary elements (end and interior diaphragms) were found to increase transverse distribution of moment; load distribution factors were 39% less when these elements were considered (Sotelino et al., 2004).

Patrick et al. (2006) observed the effects of live load placement on load distribution using grillage models. The study investigated truck placement in design lanes for the purpose of speeding up computation time in computer analysis of bridges. The analysis was performed for both steel and prestressed concrete girder bridges. The researchers concluded that vehicle spacing has little effect on distribution factors (Patrick et al. 2006).

A study by Yousif and Hindi (2007) compared load distribution factors calculated using the AASHTO LRFD 2004, 2D grillage models (frame elements), and 3D finite element (FE), shell and frame elements, models. AASHTO LRFD load distribution factors have range of applicability which is defined in terms of span length, slab thickness, girder spacing, and longitudinal stiffness. All AASHTO LRFD prestressed concrete girder sections (Type I-VI) were covered in this study by Yousif and Hindi (2007). The live load used in the analysis was the vehicular live load and lane load as specified by AASHTO LRFD 2004. Studies in the past had shown that load distribution factors from AASHTO LRFD may give either conservative results or unconservative results for specific bridge parameters (Yousif and Hindi, 2007). Therefore, the study covered FE models of different bridge configurations within the limits specified by AASHTO to examine a wide range of variables and improve the applicability of the load distribution factor (Yousif and Hindi, 2007). The torsional constant proposed by Eby et al. (1993) was used for the girders as it correlated with experimental data with a minor error of ±3%. The torsional constant plays a significant role in the determination of load

distribution factor. The 2004 AASHTO LRFD gave load distribution factor in a range with a maximum of approximately 55% more than FE analysis and a minimum 20% less than from the FE model. Yousif and Hindi (2007) observed that the AASHTO LRFD equations seemed to give reasonable results using parameters within the intermediate zone of the applicable range and tended to deviate at the extreme ends of the range. The authors concluded that range of applicability of the load distribution factors should be reconsidered because in some cases the deviation was too conservative and in some cases the deviation was unsafe (Yousif and Hindi, 2007).

Despite efforts to improve distribution factors, the current equations are still being used in AASHTO LRFD. The research community has also observed the benefits of simple computer models to come up with Distribution factors. Absent in the literature are specific studies of individual types of bridges to discern trends. For example: in Oklahoma, AASHTO Type-II girders are commonly used in spans between 30 and 70 ft and at spacings between 6 and 12 ft. It is valuable to have references in the literature that look at common arrangements like these to highlight the combinations of variables that warrant further attention at the design or load rating stage. In particular, bridges that were designed under older codes and are now being load rated can be earmarked for special attention when they are used in a certain configuration that is deemed to be of particular concern.

1.8 Grillage Modeling

A simple and safe method of computer analysis of a bridge system is the use of a “grillage model.” Grillage models are so called because they consist of a grillage of beam elements used to represent the girders and slab of a simple bridge. The benefits of this style of analysis include: ease of comprehension and use, inexpensive cost, accuracy, and applicability to a wide range of bridge types (Hambly 1991). According to Hambly (1991), it is not simple to make a set of general rules for creating a grillage model, but this text is often cited as a guide for building grillage models. Some modeling suggestions given in this text include: placing grillage beams at locations of designed strength (main girders, diaphragms), transverse spacing of beams should be less than 1/4 of the effective span, longitudinal spacing and transverse spacing should be

relatively similar, and point loads should be used to represent distributed loads. Figure 1.2 shows a simple example of a grillage analogy for a bridge.

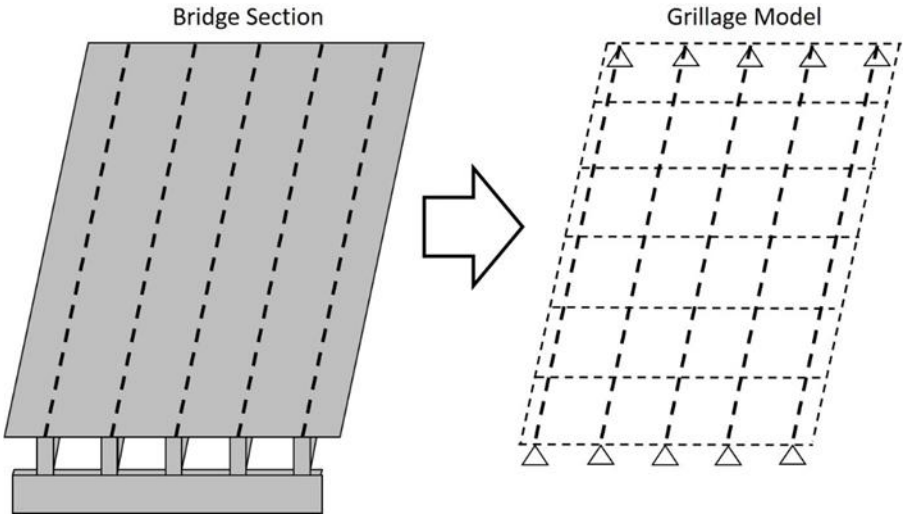

Figure 1.2. Grillage example

For bridges like those consisting of simply supported prestressed girders, Hambly suggests using longitudinal grillage members coincident with the girders and using transverse beams at 1/4 to 1/8 of the effective span. Diaphragms at the supports are to be modeled with grillage beams, and there are special rules for diaphragms at the center of the span. Hambly states that for many concrete and steel I-girders, the torsional constant, *C*, can be ignored since these sections often have a torsion stiffness much smaller than their bending stiffness.

More guidance for grillage modeling of beam and slab bridges is given by O'Brien and Keogh (1999). In this text, beam and slab bridges are described as bridge systems where a large portion of the stiffness is concentrated at discrete locations (beams), and the slab provides load distribution between these beams. The authors note the importance of modeling the slab properly, as the stiffness of the slab directly determines the ability of the slab to transfer load between beams. Diaphragms are described as providing additional load transfer, and if they are wide enough they are likely to contribute to shear strength at the support. Spacing of transverse members is recommended at one to three times the spacing of longitudinal members (O'Brien and Keogh, 1999).

O’Brien and Keogh (1999) recommend using an approximation for torsional stiffness that sums the stiffness of rectangles that approximate the section. This approximation is reasonably accurate for beam-slab type bridges. The approximation for torsional stiffness given in this text was reported by Ghali and Neville (1997), and it consists of representing a complex shape, such as an I-shaped prestressed concrete beam, as a series of rectangles. More complex methods of estimating the torsional constant exist, but the accuracy of simplified methods is adequate according to Ghali and Neville (1997). An example of this rectangular approximation of more complex shapes is given in Figure 1.3. The equation for the torsion constant of a rectangular section is given by Equation 1.26 (Ghali & Neville 1997). This can be summed to approximate a non-rectangular shape with rectangles.

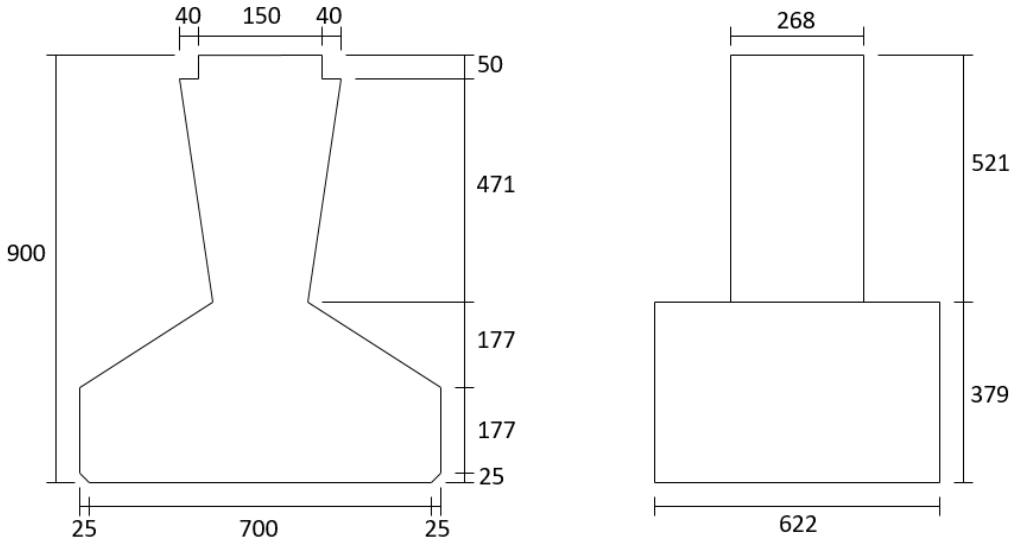

Figure 1.3. Equivalent shape to find torsion constant (from O'Brien and Keogh 1997) (dimensions in mm)

$$J = ba^3\left[\frac{1}{3} - 0.21\frac{a}{b}\left(1 - \frac{a^4}{12b^4}\right)\right] \tag{1.26}$$

Grillage modeling techniques were pioneered for computer use by Lightfoot and Sawko in the late 1950s (Lightfoot & Sawko 1959). Because these models have proven useful in accurately representing bending stresses (Hambly 1991), they have been used in bridge research somewhat regularly. A National Cooperative Highway Research Program (NCHRP) study used grillage modeling to examine shear distribution factors in

2006 (Mertz 2006). The researchers found that grillage models compare well with more rigorous FE models, especially for load distribution. As such, grillage models were used as the basis for the findings of the report. The effectiveness of grillages was also corroborated by Dymond et al. (2016) and Peterson-Gauthier (2013).

Turer and Shahrooz (2011) conducted a study to compare 1D beam element model, 2D grillage, and 3D FE models for concrete deck on steel beams. 2D grillage and 3D FE models were developed for the same bridge configuration. Typically, a 1D model is used for analysis and gives quick and conservative results in most cases. Drawbacks that come with 1D beam analysis are oversimplified geometry, weakness in modelling in the transverse direction (i.e. diaphragm, cross bracing), and irregularities such as skew. A 2D model can mitigate the limitations of 1D models because it provides the capability to have elements in the transverse direction such as diaphragms or cross bracing. 3D models are superior to both 2D and 1D models in defining the geometric dimensions, continuity, material properties and support conditions. The 3D models have a high number of elements, usually in the thousands, depending on the size of mesh and take more time for analysis than 2D and 1D models. Through their study the authors found that 2D models were merely a step behind 3D models in accuracy (Turer and Shahrooz, 2011)**.**

1.9 Impact of Diaphragm on Load Distribution

The contribution of diaphragms on the load distribution is controversial especially when the radius of the curvature of the alignment of the bridge is infinity (i.e. a straight bridge). There is inconsistency among different state DOTs regarding the usage of diaphragms. The Texas Department of Transportation (TxDOT) bridge design manual says that intermediate diaphragms are not required for structure performance unless required for erection stability of girder sizes extended beyond their normal span limits (TxDOT 2015). On the other hand, in Oklahoma Department of Transportation's (ODOT) standard drawings, end and intermediate diaphragms are present, and the Louisiana Department of Transportation and Development (LADOTD), as per their design manual, does not require diaphragms when the span length is less than 50 ft (LADOTD 2002). Construction of intermediate diaphragms is an extra burden on the

schedule and cost of the project. There are benefits described by the Garcia (1999) in his study about intermediate diaphragms, such as that diaphragms help with lateral load transfer, reduce deflection, provide support to girders during construction, and redistribute impact load if an over height truck hits the bottom of girder. However, it is difficult to predict the real stiffness contribution of diaphragms to load distribution due to typically weak connections between the diaphragm and girder (Cai et al., 2007).

1.10 Load Rating of Bridges

Evaluating old bridges is an important step in maintaining infrastructure, especially as heavier vehicles travel over bridges that may not have been designed for that level of load. These evaluations are important from two standpoints; first, they ensure that older bridges are still safe to traverse, and second, they save money by extending the usable life of older bridges.

The AASHTO specification for evaluating in-service bridges is known as the AASHTO Manual for Bridge Evaluation (AASHTO 2011). This document will be referred to in this report as the AASHTO Manual. This document provides standard guidance to bridge owners to help maintain safe bridges. The guidance provided applies to every bridge on public roads with a span of 20 ft or longer. The FHWA collects all bridge condition information in a database called the National Bridge Inventory (NBI) for the purpose of being consistent across all bridge owners. The NBI provides a rating for the substructure, superstructure, and deck of a bridge. These ratings are assigned based on visual inspection on a scale of 0-9, as given in Table 1.5.

Table 1.5. Bridge condition ratings

Code	NBI Rating Definition
N	Not applicable
9	Excellent
8	Very good
7	Good
6	Satisfactory
5	Fair
4	Poor
3	Serious
2	Critical
1	Imminent failure
0	Failed

The AASHTO Manual suggests quality control standards including education standards and training for bridge inspection personnel, but needless to say there is some subjectivity involved in rating bridges visually on a numerical scale. In previous research by the authors, it was noted that rating variability between bridges and owners was not uncommon (Pough et al. 2017). These structure evaluations are used for load rating and load posting of bridges, so their accuracy is important.

The AASHTO Manual uses a process known as load and resistance factor rating (LRFR) similar to the LRFD probabilistic concept used in the bridge design code. The general load rating equation for any live load effect from this document is given in Equation 1.27.

$$RF = \frac{\phi_c \phi_s \phi R_n - \gamma_{DC} DC - \gamma_{DW} DW \pm \gamma_P P}{\gamma_L LL(1+IM)} \quad (1.27)$$

where:

RF = Rating factor
R_n = Nominal member resistance
DW = Dead-load effect due to wearing surface and utilities
DC = Dead load effect due to structural components and attachments
P = Permanent loads other than dead loads
LL = Live load effect
IM = Dynamic load factor
γ = LRFD load factor
ϕ = LRFD resistance factor
ϕ_c = Condition factor
ϕ_s = System factor

This fraction represents the additional capacity available for live load after the dead loads are applied (RF). The condition factor (ϕ_c) is based on the result of the bridge inspection as referenced in the previous section. There are only three possible values of the condition factor (1.00, 0.95, and 0.85) even though the condition of the bridge is rated on a scale of 1-9. A summary of how the condition factor is selected is given in Table 1.6. Note that bridges below a “poor” rating of 4 cannot be load rated.

Table 1.6. Bridge condition factor

Structural Condition of Member	ϕ_c	NBI Rating Code
Good or satisfactory	1.00	6 to 9
Fair	0.95	5
Poor	0.85	4

The system factor (ϕ_s) is based on the spacing of girders, e.g. for a typical 4 girder prestressed concrete bridge the factor is 1.00. The LRFD load factors for all possible limit states used in this equation are given in the AASHTO Manual Table 6A.4.2.2-1.

When a rating factor is determined, the rating factor can be directly multiplied by the load case being considered. For example, if the HL-93 load case is being considered, the allowable load of a bridge is the rating factor times the HL-93 load. A RF greater than 1.0 indicates a greater capacity than the loads considered, and a number less than one indicates that the allowable load must be proportionally reduced and posted. The rating is done on a component basis, so the weakest component of a bridge system controls for rating the entire structure (Fu, 2013).

The process for rating an existing bridge includes determining the live load demands on the bridge the same way as for a new bridge, using distribution factors. Additionally, shear resistance is calculated using the LRFD equations. There are two levels of load rating: an inventory rating and an operating rating. The inventory rating refers to the bridge's ability to carry current design loads for an indefinite period of time. The operating rating has to do with the maximum permissible live load; this level is not intended to be reached with regularity, or the life of the bridge will be diminished (Sanayei et al. 2015). The difference between the two is a question of structural reliability; the load factor applied for the inventory rating is higher than the operating rating, indicating a greater uncertainty and duration of the load. If a bridge passes the inventory rating (RF>1) for the HL-93 loading, the structure will have adequate capacity for all AASHTO legal loads. Bridges that pass at the operating level but not the inventory rating must be checked for loads greater than the AASHTO trucks.

For the case of shear, the AASHTO manual states, “In-service concrete bridges that show no visible signs of shear distress need not be checked for shear when rating for the design load or legal loads.” In other words, where shear cracking is not apparent bridge owners must only check the RF for permit loads. However, demands may be higher than they were taken when the girders were designed (quarter-point rule), and shear capacity calculations have changed over the years. Permitting owners to ignore shear load ratings unless cracking is visible is problematic if the actual capacity of a bridge is low compared to current methods, or if the current demands exceed the demands at the time the bridge was designed.

1.11 Literature Review Summary

The literature review revealed a dearth of experimental research on shear behavior of older AASHTO Type-II prestressed concrete girders and of the ultimate behavior of bridge systems loaded in shear. The work detailed in this report addresses how to account for these two items in rating older bridges related to shear. Most of the past research in the area of lateral load distribution factors has been focused on the distribution of moment. It is observed that the past researchers have confidence in the plate and grillage models which were used in the study described in this report. Even in the study by Eamon at el. (2016) which used AASHTO LRFD 6th Ed. (AASHTO 2012) showed that AASHTO equations are conservative for some cases and in some cases AASHTO LRFD gives smaller load distribution factors than results from field tests indicate. The load distribution factor equations are the same in AASHTO LRFD 6th Ed. (2012) and AASHTO LRFD 7th Ed. (2015). Therefore, an examination of AASHTO I-Girders (which are commonly used by ODOT), shear load distribution, 2D grillage models and comparison with 3D plate models is warranted to provide recommendations for use of grillage models for load rating of shear critical bridges in the state of Oklahoma in the future. Grillage modeling represents a modernization of the distribution factor formulation that can be applied to a wide variety of bridges. The parametric study described in this report is combined with experimental data and field observation to provide information about common types of bridges in Oklahoma, which can be used by ODOT to help make decisions about older bridges. For bridges that do not show signs

of shear cracking, grillage models combined with the shear capacity analyses recommended herein can provide an accurate rating of prestressed concrete bridges.

2.0 Design Items Affecting Shear Capacity and Load Distribution

2.1 Overview

Data from shear tests in Oklahoma and from the literature and results of grillage modeling of various bridge configurations were examined to identify trends in girder design and capacity affecting shear behavior, including effects of end region deterioration. This examination included two primary items. The first aspect was a parametric study of various bridge configurations analyzed using grillage models to identify important variables to consider when calculating load demands necessary when rating bridges for shear. This parametric study was intended to distill the process into relatively simple rules to guide modeling and advice to inform engineering judgement in the load rating process. The results of both aspects were combined to provide guidance to ODOT engineers toward specific items that should be given extra consideration in the load rating process.

The second was to compile a summary of test data from previous research focused on shear capacity of aged girders that included the various girder types, configurations used in testing, and comparison of the measured shear capacities to the shear strengths calculated using the methods included in the completed SPR 2256 (Floyd et al. 2016). These results were organized to associate experimental shear capacity data with as many details as possible of the bridge from which the girders were taken. Expected capacities calculated by the various researchers or by the research team were compiled for comparison to the experimental results. This summary was examined to identify trends in actual capacity versus calculated capacity to provide additional qualitative and quantitative assessment information for engineers working on rating a specific bridge.

This chapter contains information about the modeling techniques used, their derivation, and the decision making related to the parametric study and the real-world bridges modeled as part of the study. All grillage models were built in the finite element

analysis program STAAD.Pro made by Bentley Systems. It should be noted at the beginning that any discussion of “conservativism” of the code methods here is only in relation to the grillage models, not a description of their overall level of conservativism compared to bridge behavior. This chapter also contains information on experimental behavior of older girders beyond that described in Section 1.5 and includes information on how inspection reports can be used to identify parameters important for bridge rating.

2.2 Modeling Procedures

Several options were considered for modeling the bridge sections examined in this study. Originally, a detailed finite element model containing solid elements to represent the concrete and rod elements to model the steel at discrete locations was planned. After performing preliminary analyses using ANSYS workbench it was decided that a simpler modeling paradigm would be more appropriate to understand bridge behavior. After consulting the work of other authors who have studied bridge behavior (Hambly 1991; Lightfoot & Sawko 1959; Mertz 2006) it was decided that grillage models provide an efficient and accurate way to predict the response of a bridge system to external loads. Three-dimensional models considering the bridge deck as a plate separated from the beam centroids were also considered.

2.2.1 Grillage Modeling Methods

The grillage modeling method simulates the superstructure of the bridge by having discrete members coinciding with the centroid of the bridge beams, resulting in a two-dimensional (2D) model. The grillage modeling technique used to examine the behavior of the bridge superstructure in the current research was validated using experimental results from a previous project conducted at OU (Floyd et al. 2016). 2D grillage model results have also been compared with 3D model results and were found to be satisfactory by other researchers (Turer and Shahrooz 2011).

The grillage model was assembled by discretizing the bridge into longitudinal grillage members (prestressed girders), and transverse members (slabs and diaphragms). The width of slab used to determine properties for the interior girders was selected based on the tributary width, specified by AASHTO LRFD Section 4.6.2.6.

Exterior girder tributary slab widths were chosen in a similar way, but terminating at the edge of the slab. In the transverse direction, the slab (including diaphragms if present) was divided into a series of discrete sections. For superstructures with diaphragms, the diaphragm was defined by its section properties including the slab section based on tributary width. For superstructures without diaphragms the members in the transverse direction were defined using the respective section properties of each slab element's tributary width. The major steps in developing a grillage model for each bridge configuration examined were defining the geometry, assigning member properties, assigning supports, and applying loads, which are all explained in the following sections. All grillage models were built and analyzed using the finite element based analysis program STAAD.Pro made by Bentley Systems.

2.2.1.1 Defining the Geometry

All elements of the superstructure were defined using line elements. The longitudinal elements (beams) were defined by having a line element at the centroid of the beam cross-section. The diaphragm elements, if required, were also defined like the longitudinal elements by having a line element along the centroid of the cross-section. The deck was broken into the flanges of the diaphragms or slab elements in the transverse direction and as part of the beams in longitudinal direction. Line elements were broken at every intersection of beam, slab and diaphragm to connect the elements. A dummy beam was assigned at the edges of the deck with negligible stiffness to connect the ends of the transverse elements. A typical grillage model layout with the different elements identified is shown in Figure 2.1. A sensitivity study of mesh spacing was done by Peterson-Gauthier (2013) where transverse grillage spacings of half and twice what was typically used were considered. In general, a finer mesh gave results which were about 1% closer to a 3D finite element model and the grillage model with double spacing gave the results which were 1% farther away (Peterson-Gauthier, 2013). In the current study eight or nine transverse beam elements were used to define deck, end diaphragm and mid-span diaphragm. The width and spacing of these transverse elements varied with span length.

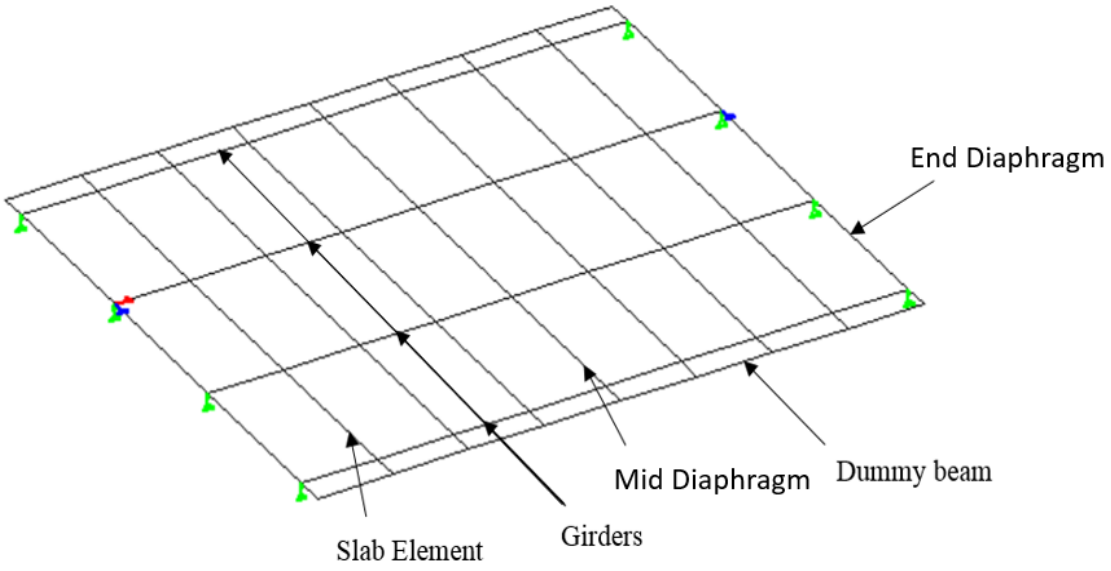

Figure 2.1. Typical grillage model configuration

2.2.1.2 Member Properties

Sectional properties determined for each element, such as area, moment of inertia, and torsional constant, were used to define the element properties in STAAD.Pro. Girder flange widths were determined using the tributary width from AASHTO LRFD Section 4.6.2.6 and the beam line elements were given section properties based on this composite section. Concrete material properties such as compressive strength and elastic modulus were also defined as part of this step. The girder cross-sections were simplified into smaller rectangular elements to enable the user to easily calculate the girder section properties. An example for a Type III girder is shown in Figure 2.2. The torsional stiffnesses of the individual rectangles were summed to obtain the torsional stiffness of the section. The equations described by Ghali and Neville (1997) were used to determine the torsional stiffness of the rectangular sections in this study.

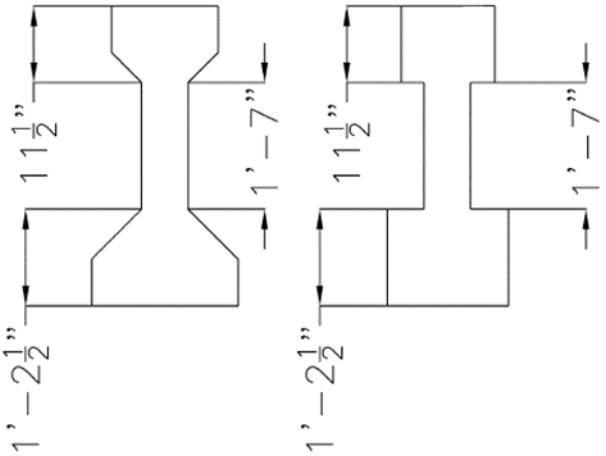

Figure 2.2. Type-III girder section and the equivalent section used to determine properties

2.2.1.3 Support Conditions

All the supports in the model were restrained in the vertical direction. Because the bearing conditions of in-service bridges are typically elastomeric pads and the scale bridge test used to verify the model included elasticity of the support (elastomeric bearing pads), an elastic modulus of 300 kips/in. based on validation testing described in Section 2.2.2 was assigned to the supports.

2.2.1.4 Load Application

Deck systems with four longitudinal I-girders were used to provide enough deck width to capture the effects of load distribution. The HS-20 truck load was applied at critical locations described in Section 2.3.2 for the three girder spacings used in this study: 6 ft (deck width = 22 ft), 9 ft (deck width = 31 ft) and 12 ft (deck width = 40 ft). The 40 ft deck width sections had a maximum of 3 lane widths (based on a 12 ft wide design lane from AASHTO LRFD 3.6.1.1.1) which could be placed on the deck simultaneously. The other two deck widths used had a maximum of two loaded design lanes. The HS-20 truck load predefined in STAAD.Pro was used for all loadings.

After running the analysis for the critical load case, the reactions at the support were extracted from the post-processing mode in STAAD.Pro. The reactions obtained from the model were then filtered and sorted to obtain the critical numbers. Reactions

obtained for a particular case were also added up and compared with the applied loads to check the quality of the model. The reaction at a particular beam support was then divided with the sum of reactions at that end of the bridge to get the load distribution factor for that particular support.

2.2.2 Validation of Grillage Models

The first step in modeling was to compare the response of the computer model to the scale bridge section tested by Floyd et al. (2016). This was necessary to ensure the applicability of the modeling technique. The scale bridge consisted of four approximately half-scale girders combined with a half-scale composite concrete deck. A diagram of the bridge configuration and loading conditions is shown in Figure 2.3. LVDTs used to measure deflection are shown as rectangles, wire pots as circles, strain gages as black rectangles and the load cell as a cross. Elastic level loadings were placed on both exterior (A4) and interior (A5) girders at the quarter-span point, and the bridge was loaded to ultimate failure on interior girder A5 as described in Floyd et al. (2016). Load, deflection, and concrete strain at strategic points were recorded during each test. Several iterations of model comparison were performed, first checking the deflections of the scale bridge against the deflections predicted by the grillage model. The grillage was assembled by discretizing the bridge into longitudinal grillage members (prestressed girders), and transverse members (slabs and diaphragms). The cross-sections of the members used for the longitudinal grillage of the scale bridge are shown in Figure 2.4. The 46 in. width of slab used to determine properties for the interior girders was selected based on the tributary width, specified by AASHTO LRFD Section 4.6.2.6 to determine the effective slab (AASHTO 2015). Exterior girder tributary widths were chosen in a similar way, terminating at the edge of the slab and12 in. away from the girder centerline.

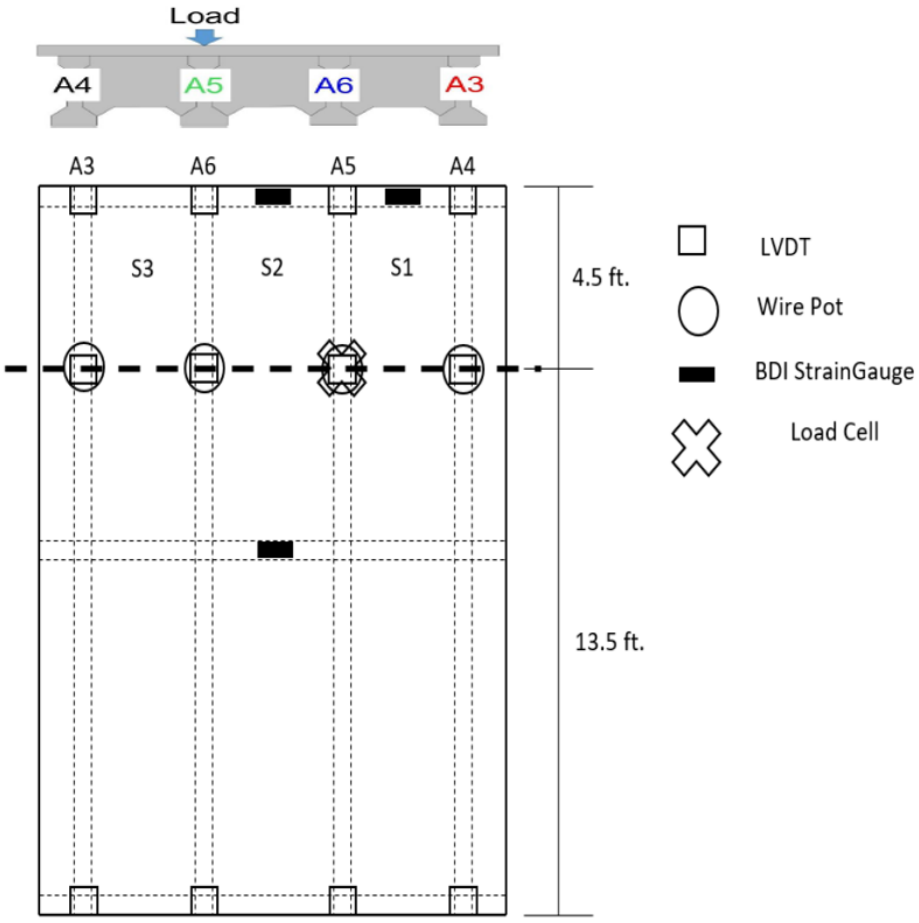

Figure 2.3. Section and plan of test bridge

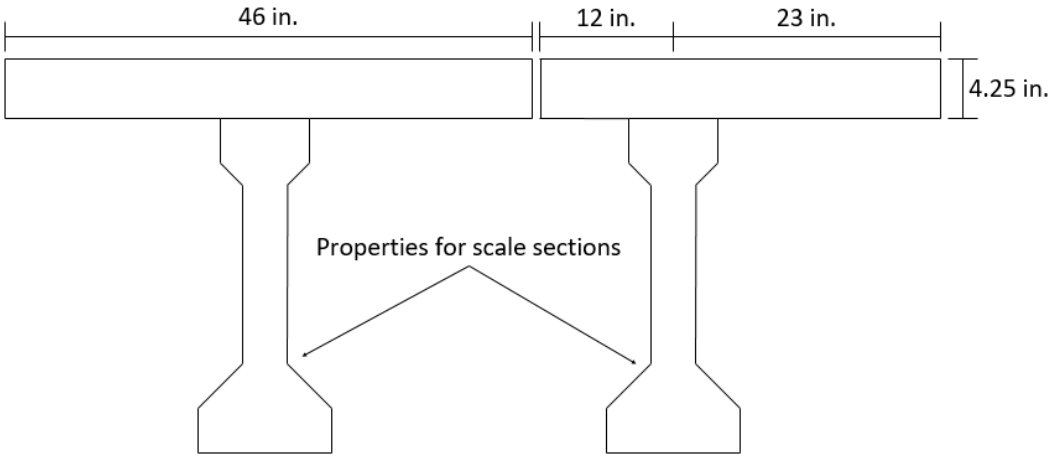

Figure 2.4. Longitudinal members used in grillage: interior girder (left), exterior girder (right)

The slab was divided into eighths along the girder span, so that each slab section was 2.25 ft wide (8 x 2.25 ft = 18 ft). Eighths were chosen based on general guidance from Hambly (1991). For most slab sections, the cross-section was simply a 4.25 in. by 27 in. (2.25 ft) rectangle. At the ends and mid-span, the slab member properties included the added stiffness from the diaphragms (Figure 2.5). Dummy beams were provided along the outside edge of the deck for geometric reasons. These beams were given negligible stiffness. Once the dimensions of the members were chosen, the bending and torsional stiffnesses and areas were calculated, and these could then be input into the model. The moment of inertia was calculated for bending in the direction of the member's span, and the torsional stiffness was calculated based on recommendations listed the literature review (Section 1.8). The properties used for the grillage members are given in Table 2.1.

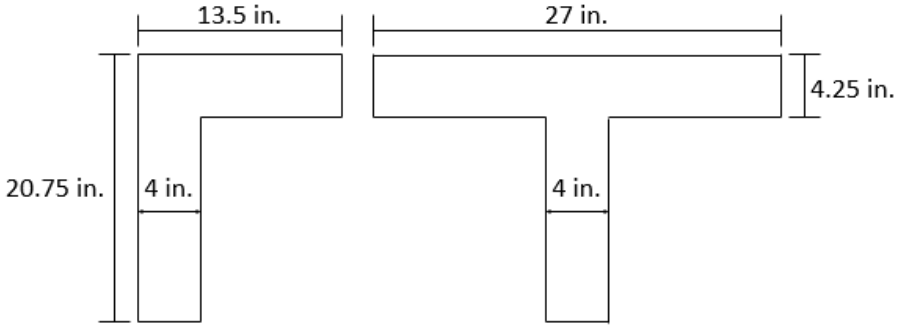

Figure 2.5. Transverse grillage members at diaphragm locations

Table 2.1. Summary of properties used in scale bridge grillage

Property	Interior girder	Exterior girder	Slab	Slab + middle diaphragm	Slab + end diaphragm
Area (in^2)	280.8	238.9	102.7	161.8	110.4
Torsion Stiffness (in^4)	511.9	511.9	309.2	683.2	510.5
Bending Stiffness (in^4)	20,302.2	18,739.4	102.7	2,273.2	1,987.7

The compressive strengths for the girders and deck differed for all bridge configurations examined. For all grillage models, the difference in modulus of the deck and the girders was accounted for using a modular ratio (E_{girder}/E_{deck}). This information was based on modulus tests performed on cores from the old girder and deck concrete and companion cylinders made when the scale sections were constructed, described in

Floyd et al. (2016). The modular ratio was used to adjust the areas and moments of inertias contributed by the decks.

Support conditions were selected to be consistent with the test setup for the scale bridge (Figure 2.6), which consisted of neoprene bearing pads. One support was restrained in every direction (x, y, z) in order to ensure model stability. The support across the bridge from the fully constrained support only allowed displacement in one direction. All other supports only restrained vertical deflections. Because the bearing conditions of the actual test included elasticity of the support (elastomeric bearing pads), an elastic modulus was assigned to the supports. The vertical stiffness given to the supports was 500 MN/m (2,855 k/in.), representing “a rubber bearing on a stiff concrete structure” (Hambly 1991). After comparing deflections at the supports from the physical testing to the model, the stiffness of the bearing was reduced to 300 k/in., which was more consistent with the response of the tested section. This large discrepancy was unusual, but given that the experimentally verified value agreed well, it was determined to be best for use in future models.

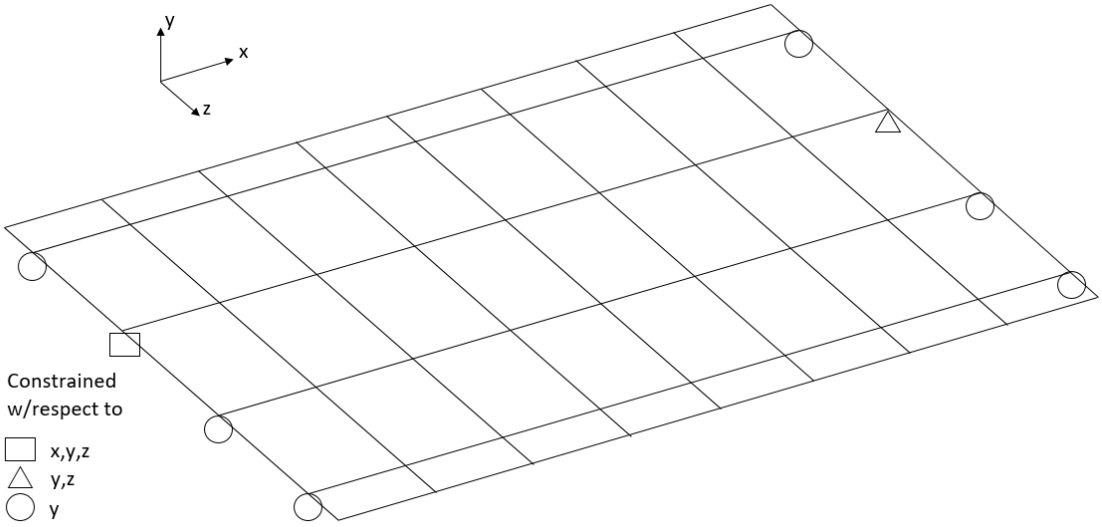

Figure 2.6. Grillage support conditions

Initially, load versus deflection relationships from the scale bridge tests were compared to load versus deflection relationships from the model. The two load cases used were: 1) a single point load directly atop girder A4 (exterior) at the quarter span point (from elastic testing) and 2) a single point load directly atop girder A5 (interior) at

the quarter span point. Additional elastic tests over the slab (S1 and S2) described in Floyd et al. (2016) could not be used for model validation because the loads and resulting deflections and strains were so small. For the interior girder load case (load on A5), the deflections for all girders from the destructive test up to the cracking load (40 kips) were used for comparison. For the exterior case (load on A4), the load was 20 kips and the deflections used for comparison were from the elastic testing. Figure 2.7 shows the agreement between the model and the scale bridge response when load was applied at girder A5 (interior case). Figure 2.8 shows the agreement between the model and the scale bridge response when load was applied at girder A4 (exterior case). The numbers after the girder (e.g. A41, A51) refer to the number of the specific elastic test, i.e. some of the examples shown were the result of multiple elastic tests.

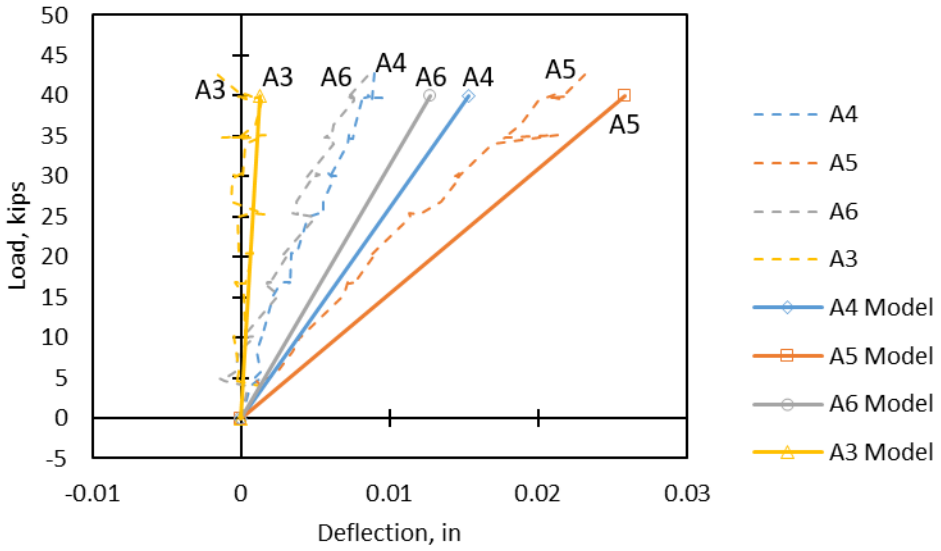

Figure 2.7. Comparison of load versus deflection relationships for grillage model and scale bridge loaded at girder A5

Referring to Figure 2.7, the deflection of girder A5 differs from the model by 18% at the maximum load. For load point A4 (Figure 2.8), the difference in deflections between the model and experimental results is 4% at the maximum load. Deflections for some of the other girders do show larger differences. However, matching the behavior of the loaded girder was determined to be the most important parameter. Based on the two load locations, there seemed to be good agreement between the models and the experimental results. An important factor to consider in interpreting these deflections is

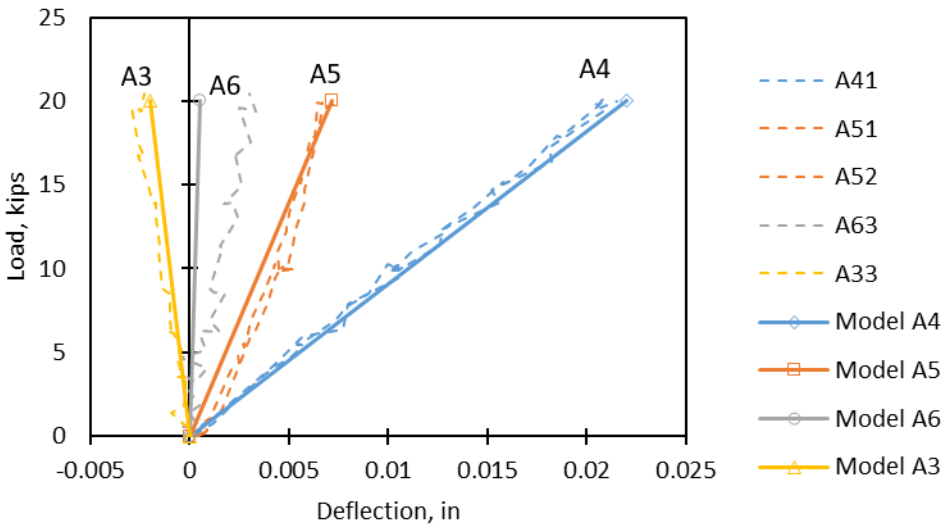

Figure 2.8. Comparison of load versus deflection relationships for grillage model and scale bridge loaded at girder A4

their magnitude. The extremely small deflections measured for both load cases means some variation is expected. The magnitude of deflections for the loads examined is on the same order as the noise in the signal from the sensors used in the experimental tests, accounting for some of this error. Based on these results, it was decided that the behavior of the model was an acceptable representation of the recorded response, despite some percentage difference. The differences were on the same magnitude of those observed in similar research (Petersen-Gauthier, 2013).

Another factor considered for acceptance of the modeling paradigm was strain in the bottom flange of the girders at the load point. Figure 2.9 and Figure 2.10 show strains measured at the load point on all girders compared to strains given by the model at the same locations. These figures show reasonable agreement with the behavior of the actual bridge. It is worth noting that grillage models are not excellent at representing local phenomena in the members as compared to more detailed finite element methods, but the objectives of this research were focused more on the overall structural behavior. The reasonable agreement of deflections and strains was seen as further validation of the modeling methods.

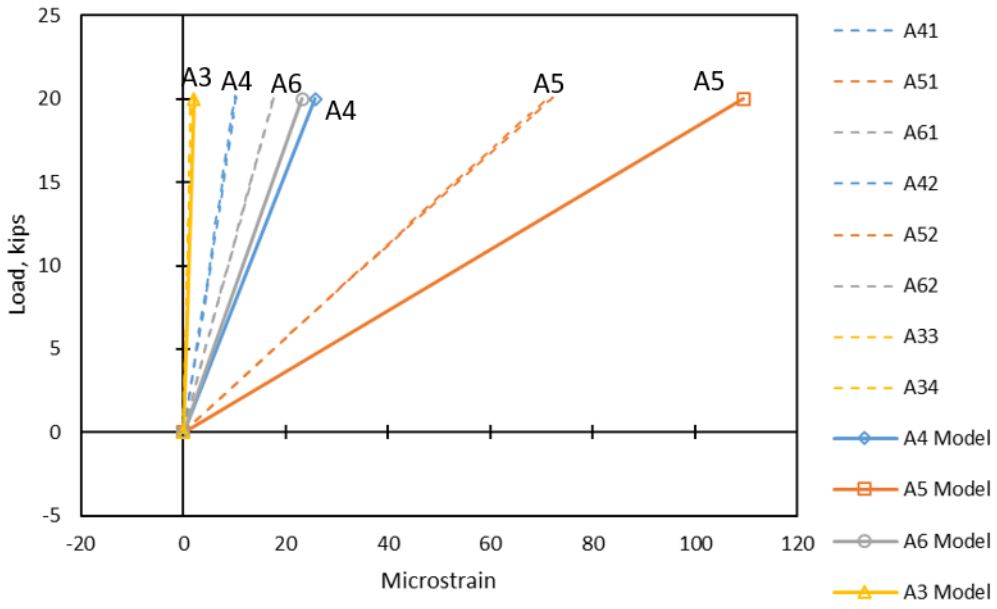

Figure 2.9. Comparison of load versus girder strain relationships for grillage model and scale bridge loaded at girder A5

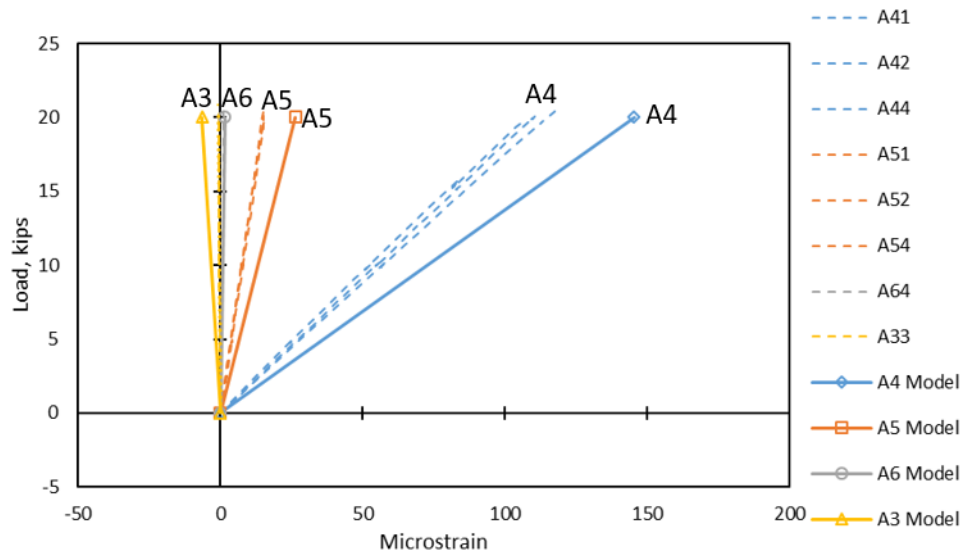

Figure 2.10. Comparison of load versus girder strain relationships for grillage model and scale bridge loaded at girder A4

Another method used to verify the modeling procedure was comparing the amount of shear force observed at each support. Since the models were intended to be used to evaluate shear distribution factors, this is likely the most important parameter. The way this comparison was achieved was by summing the support deflections for

each girder (at the loaded end of the bridge) and using the proportion of individual support deflections to total support deflection to represent the same proportion of the total load on the bridge. This method was used for the support deflections of the scale bridge in the elastic range (at 40 kips of load) with the load on an interior girder (A5) and the same response of the model at 40 kips. This procedure is similar to that used in other research to determine distribution factors for tests and models (Cross et al., 2006). The results obtained from this method are summarized in Table 2.2. Table 2.3 also shows the distribution factors for the case where a 20 kip load was applied over an exterior girder (A4). For both load cases, 75% of the total load is assumed to go to the support with the largest shear (based on statics and the loading configuration). This assumption is accurate based on the magnitude and proportion of deflections at every support.

Table 2.2. Method to find distribution factors from deflections for the interior girder (load on girder A5) load case

Girder	Support Deflection from Test (in.)	As Reaction Force from Test (kips)	Distribution Factor from Test	Support Deflection from Model (in.)	As Reaction Force from Model (kips)	Distribution Factor from Model
A4	0.019	5.15	**0.172**	0.022	6.67	**0.222**
A5	0.058	15.44	**0.515**	0.053	16.06	**0.535**
A6	0.033	8.91	**0.297**	0.026	7.88	**0.263**
A3	0.002	0.51	**0.017**	-0.002	-0.61	**-0.020**
Total	0.113	30.00	**1.000**	0.099	30.00	**1.000**

Table 2.3. Method to find distribution factors from deflections for the exterior girder (load on girder A4) load case

Girder	Support Deflection from Test (in.)	As Reaction Force from Test (kips)	Distribution Factor from Test	Support Deflection from Model (in.)	As Reaction Force from Model (kips)	Distribution Factor from Model
A4	0.027	9.45	**0.630**	0.043	12.90	**0.860**
A5	0.018	6.31	**0.421**	0.011	3.30	**0.220**
A6	0.002	0.76	**0.051**	-0.001	-0.30	**-0.020**
A3	-0.004	-1.52	**-0.101**	-0.003	-0.90	**-0.060**
Total	0.044	15.00	**1.000**	0.05	15.00	**1.000**

The comparison of distribution factors for the end with the highest shear (end nearest the load point) when load was placed directly above girder A5 is given in Figure 2.11, and shows very good agreement between the model and the actual response. When load was placed on an exterior girder (Figure 2.12) the distribution factor differences were larger, but still show reasonable agreement.

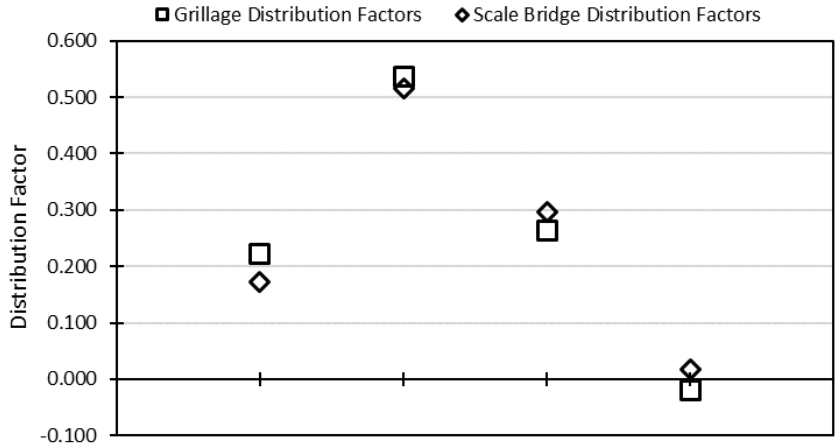

Figure 2.11. Distribution factor comparison for grillage model and scale bridge load test (load at A5)

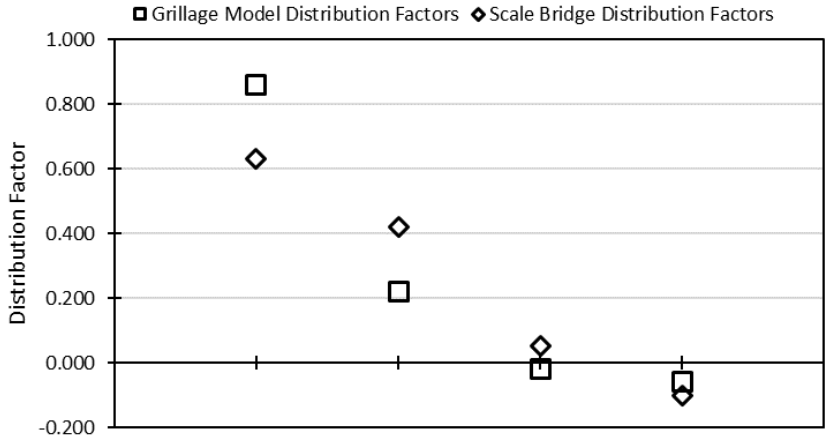

Figure 2.12. Distribution factor comparison for grillage model and scale bridge load test (load at A4)

In addition to the full bridge, individual models were created for girders A and C as tested in the lab by Floyd et al. (2016). These models showed good agreement with the deflections from the elastic portion of the destructive test, further validating the modeling procedures.

2.2.3 Plate Modeling Methods

Investigation of methods for creating three-dimensional (3D) grillage models considering separation between the girder and slab centroids using STAAD.Pro was conducted to further examine torsional effects, which may not be captured effectively using 2D grillage models. It was determined that a more effective mechanism was to model the beams in the same fashion as for the 2D grillage models, but to model the transverse deck as a plate. 3D finite element based plate models were compared to experimental data and 2D analyses to identify effects not captured by the 2D grillage models. The 3D grillage model was used to examine the scale bridge tested and described by Floyd et al. (2016) and model and experimental results were compared in order to verify performance of the model. Type III and BT-72 girder bridge configurations were then examined using this modeling method to bracket the size of girders investigated and to compare with results from the 2D grillage models.

In grillage models the slab is taken as a frame element and the centroids of the slab and girders coincide resulting in a 2D model. Such discrepancies between the model and an actual bridge can be overcome by developing 3D models. There are different ways to develop 3D models of a bridge superstructure. Several of these were summarized in a study by Sotelino and Chung (2006). They characterized the geometry using the different combinations of elements shown in Table 2.4. Plate elements were used for the deck and beam elements combined with shell elements were used for the girder as shown in Figure 2.13. The model type 4 in Table 2.4 was found to be the most economical model, and was found to be capable of accurately predicting the flexural behavior of the bridge girders including deflection, strain, and lateral distribution (Sotelino and Chung, 2006).

Table 2.4. Types of 3D FE models described by Sotelino and Chung (2006)

Model Type	**Girder Web**	**Girder Flanges**
1	Shell Element	Shell Element
2	Shell Element	Beam Element
3	Beam Element	Shell Element
4	Beam Element	

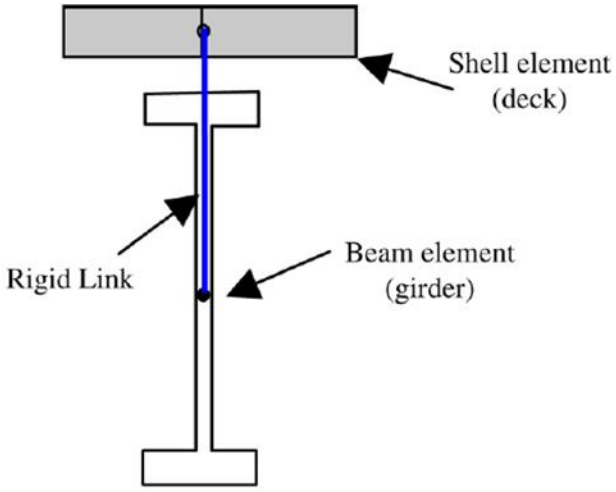

Figure 2.13. Representation of an element used for plate models (Sotelino and Chung, 2006)

For the models considered in this study, all the applied forces on the deck were out-of-plane forces. Therefore, the plate element was selected for the deck and the line element was selected for the girders. An example plate model is shown in Figure 2.14. In the program (STAAD.Pro) this plate element has both membrane (in-plane effect) and bending (out-of-plane effect) attributes which provides the capabilities required for modeling the expected behavior of the bridge deck. Bending effects can be shut off by defining the element as plane stress. A four noded quadrilateral plate element with the thickness defined was considered for the plate model. Initially, models were developed with and without offsets between the centroid of the deck and centroid of the girder. There was a difference in the results between models when girder spacing was 12 ft, but the difference was negligible in case of 6 ft spacing. It was decided to proceed with an offset between the centroid of deck and centroid of the girder in an attempt to more accurately represent the actual bridge. Offsets were also provided for the diaphragms.

The beam sections used in the study were not predefined in the program. Therefore, prismatic sections with the proper dimensions were defined, which are shown as lines in the extruded view in Figure 2.14. The mesh sizes used for the deck and girders were defined such that the nodes for each coincided with one other. The mesh size of plate was 2 in. x 3 in. for the plate model. Application of loads and analysis of the data to determine load distribution factors were conducted in the same manner as

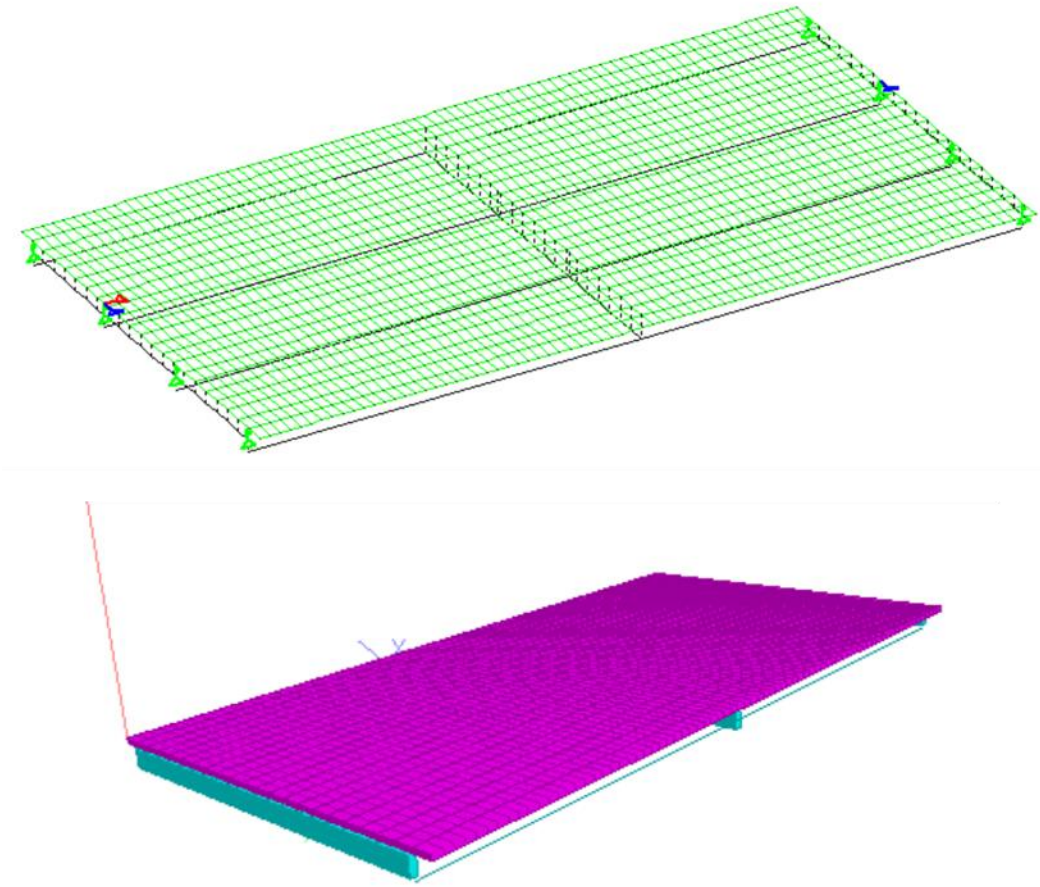

Figure 2.14. Wireframe and extruded view of a typical plate model

for grillage models. To make the comparison between plate and grillage models only Type-III and BT-72 girder were considered, and only certain parameters were included. For instance, only the 6 ft and 12 ft girder spacings were considered to reduce the number of models and subsequently time required for data analysis.

2.2.4 Validation of Plate Models

A plate model was developed for the scale bridge and model results compared to experimental results as described for the grillage model in Section 2.2.2. The geometry of the bridge, loading configurations, and applied loads in the plate model were same as used in the grillage model and tested bridge. The reactions and deflections for the bridge test and grillage models in Tables 2.5 and 2.6 are repeated from Section 2.2.2. The configuration of the tested half-scale bridge used for comparison is shown in Figure 2.3.

Table 2.5. Comparison of bridge test with grillage and plate models for interior girders (load on girder A5)

Girder	Support Deflection from Test (in.)	As Reaction Force from Test (kips)	Support Deflection from Grillage (in.)	As Reaction Force from Grillage (kips)	Support Deflection from Plate Model (in.)	As Reaction force from Plate Model (kips)
A4	0.019	5.150	0.022	6.670	0.022	6.650
A5	0.058	15.440	0.053	16.060	0.053	15.927
A6	0.033	8.910	0.026	7.880	0.027	8.157
A3	0.002	0.510	-0.002	-0.610	0.004	-0.737
Total	0.113	30.000	0.099	30.000	0.106	30.000

Table 2.6. Comparison of bridge test with grillage and plate models for exterior girders (load on girder A4)

Girder	Support Deflection from Test (in.)	As Reaction Force from Test (kips)	Support Deflection from Grillage (in.)	As Reaction Force from Grillage (kips)	Support Deflection from Plate Model (in.)	As Reaction force from Plate Model (kips)
A4	0.027	9.450	0.043	12.900	0.043	12.913
A5	0.018	6.310	0.011	3.300	0.011	3.193
A6	0.002	0.760	-0.001	-0.300	0.002	-0.344
A3	-0.004	-1.520	-0.003	-0.900	0.003	-0.762
Total	0.044	15.000	0.050	15.000	0.059	15.000

The results from the plate model shown in Tables 2.5 and 2.6 are quite close to those from grillage models. The principles of statics are proven by all the models. When the 40 kips load is applied 4.5 ft from one end of the bridge then the total reaction on the end of the bridge nearest the load will be 30 kips and on the other end 10 kips. The summation of support reactions on the end of the bridge nearest the load is 30 kips for both types of models. The summation of all the support reactions was 40 kips for the 40 kips load on beam A5 case and 20 kips when the load of 20 kips was applied on beam A4. The deflections and the support reactions from the plate models were comparable with the grillage model and tested bridge results which validates the applicability of the plate models used.

2.3 Parametric Study

2.3.1 Selection of Variables for Parametric Modeling

Full-scale bridge models were created using the same procedures as were applied successfully to the scale bridge. These full-scale bridge models were constructed to compare distribution factors given in the AASHTO LRFD with the distribution of load in the bridge models. The objective was to compare distribution factors for these model bridges with varying span length, girder type, girder spacing, and deck thickness, as well as with or without diaphragms to identify bridge design items with significant impact on shear load distribution. Distribution factors were determined to use for comparison between variable combinations. Comparisons were also made between the model derived distribution factors and those determined using the AASHTO LRFD equations to determine which method produced more conservative results for given situations.

The types of bridges selected for modeling in this study were selected by considering actual bridge dimensions found in Oklahoma. A spreadsheet containing the NBI data for all Oklahoma bridges was used to identify the types of bridges of interest to the current study. First, bridges were limited to those built between 1960 and 1979. This year range was chosen to only study bridges composed of girders similar to those tested in the lab by Floyd et al. (2016). The results were also limited to bridges open to traffic, with zero-degree skew (since there is a skew correction for distribution factors in the code), and beam-slab type bridges with prestressed concrete superstructures. Of all of these bridges, the lengths were between 30 ft and 108 ft, as shown in Figure 2.15. AASHTO Type-II girders were the primary focus of this study and are used today for typical span lengths between 30 ft and 55 ft according to the standard ODOT drawings for highway bridges (ODOT, 2016).

The filtered bridge data identified 257 bridges meeting the criteria listed in the previous paragraph. The lengths of these bridges are shown in the histogram in Figure 2.15. Based on this histogram, a range of potential Type-II girder lengths was selected (30 ft to 67.5 ft). The value of 67.5 ft was selected to maintain even increments for bridge lengths. The bridge inventory does not list what type of cross-section each bridge

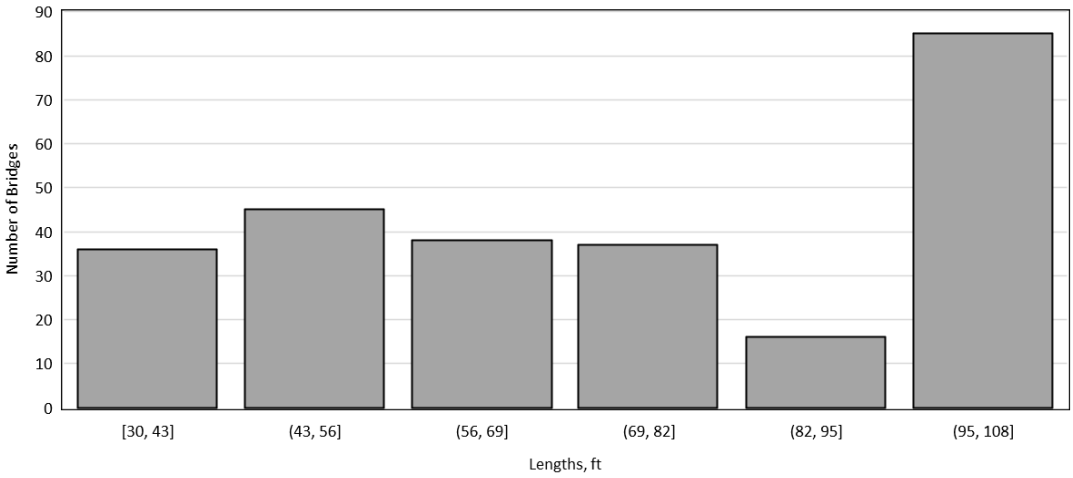

Figure 2.15. Oklahoma prestressed concrete bridges between 30 and 108 ft (1960-1979)

consists of, however AASHTO Type-II girders tend to fit into this span length range. The Florida Department of Transportation has design aids that allow span lengths for Type-II girders up to 81 ft (FDOT, 2013); in Oklahoma shorter lengths are more common. In addition to Type-II girders, other girder types typical to Oklahoma and Texas were considered. The girders selected for the study were Type-III, Type-IV, BT-63 and BT-72. All these girders are used by ODOT except BT-63. ODOT uses Type-IV and BT-72 for longer spans skipping BT-63 in the progression of sizes, but this girder section is used by surrounding states and may be used by ODOT in the future. The selection of the different span lengths was dependent on the type of girder. Typical span lengths were chosen from standard bridge drawings available on the Oklahoma Department of Transportation (ODOT) website (ODOT 2016). At least one span length was chosen near the low end, high end and middle of the typical span range for each girder type.

Next, common bridge widths were sorted (Figure 2.16). The most common bridges of this type appear to be able to support 2, 3, or 4 lanes of traffic. Unfortunately, the inventory data does not contain any indication of the girder spacing. Based on conversations with ODOT engineers, typical girder spacings at this time were between 7 ft and 9 ft (or less). The Little River Overflow bridge (NBI # 19269) considered in this project had a girder spacing of 11.75 ft, which was considered to be a relatively extreme case. The girder spacings selected for this study were 6 ft, 9 ft, and 12 ft, to provide a

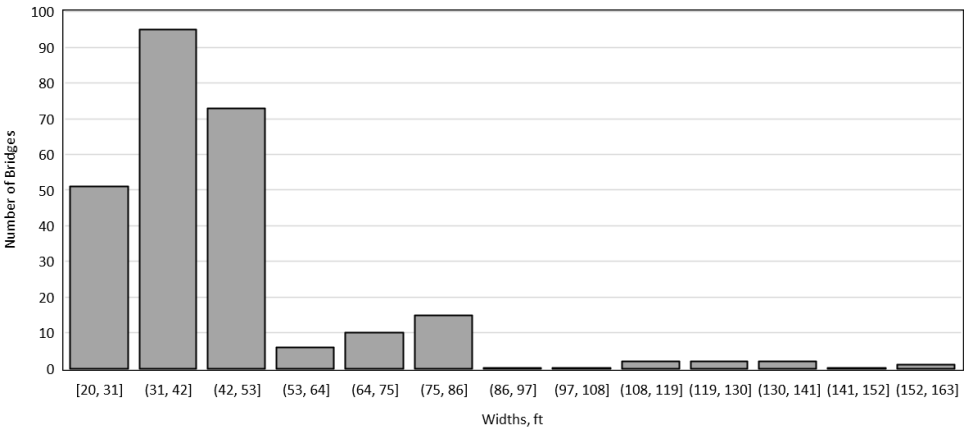

Figure 2.16. Roadway widths for bridges of interest

range including extremes of small and large spacings. For all cases a four girder bridge was considered with a width varying based on the girder spacing for simplicity (lever rule only is used for load distribution in three girder bridges). Another important question for modeling purposes is the width of deck overhang on each side of the outside girder. The inventory data does not contain this information. Since the I-244 bridge considered extensively in previous research (Floyd et al. 2016) had a 2 ft clearance from the center of the outside girder to the edge of the bridge, this distance was selected for the parametric models. Obviously, a larger slab overhang will increase distribution to the outside girder. However, since the I-244 bridge used as basis for much of the previous research (Floyd et al. 2016) was taken to be a typical highway bridge, it was assumed that similar bridges will tend to have a shorter overhang due to the large live loads they support. For simplicity, no curb width was assumed and the roadway width was considered to be the distance between exterior girders. The distance a load is placed from the extreme edge of the deck will mostly affect the distribution to the exterior girder, which is generally designed using the lever rule.

At the time these bridges were designed, deck thickness was determined based on girder spacing. Unfortunately, deck thicknesses are also not given in the bridge inventory data. Based on drawings obtained from the time period in question, it is inferred that most bridges tended to have slab thicknesses between 7 in. and 9 in. Because of this, these two thicknesses were used for the current study. All the ODOT standard bridges include end and midspan diaphragms, but to study the impact of the

diaphragm on shear load transfer, the bridge superstructure without diaphragms was also considered in this study. Tables 2.7-2.11 contain all the parameters examined in this parametric study. These parameters resulted in examination of 192 bridge configurations with varying girder type, deck thickness, girder spacing, span length, and presence or lack thereof of diaphragms using grillage models and 32 configurations using plate models. All the models fall within the range of applicability defined in AASHTO LRFD for the equations of load distribution factors (AASHTO 2014).

Table 2.7. Type- II girder bridge grillage models (deck thickness (in.) on interior of table)

Spacing (ft)	30 ft Span	30 ft Span	42.5 ft Span	42.5 ft Span	55 ft Span	55 ft Span	67.5 ft Span	67.5 ft Span	Presence of Diaphragms
6	7	9	7	9	7	9	7	9	Diaphragm
6	7	9	7	9	7	9	7	9	No Diaphragm
9	7	9	7	9	7	9	7	9	Diaphragm
9	7	9	7	9	7	9	7	9	No Diaphragm
12	7	9	7	9	7	9	7	9	Diaphragm
12	7	9	7	9	7	9	7	9	No Diaphragm

Table 2.8. Type-III girder bridge grillage models (deck thickness (in.) on interior of table)

Spacing (ft)	45 ft Span	45 ft Span	60 ft Span	60 ft Span	75 ft Span	75 ft Span	Presence of Diaphragms
6	7	9	7	9	7	9	Diaphragm
6	7	9	7	9	7	9	No Diaphragm
9	7	9	7	9	7	9	Diaphragm
9	7	9	7	9	7	9	No Diaphragm
12	7	9	7	9	7	9	Diaphragm
12	7	9	7	9	7	9	No Diaphragm

Table 2.9. Type-IV girder bridge grillage models (deck thickness (in.) on interior of table)

Spacing (ft)	75 ft Span	75 ft Span	90 ft Span	90 ft Span	105 ft Span	105 ft Span	Presence of Diaphragms
6	7	9	7	9	7	9	Diaphragm
6	7	9	7	9	7	9	No Diaphragm
9	7	9	7	9	7	9	Diaphragm
9	7	9	7	9	7	9	No Diaphragm
12	7	9	7	9	7	9	Diaphragm
12	7	9	7	9	7	9	No Diaphragm

Table 2.10. BT-63 girder bridge grillage models (deck thickness (in.) on interior of table)

Spacing (ft)	105 ft Span	105 ft Span	120 ft Span	120 ft Span	135 ft Span	135 ft Span	Presence of Diaphragms
6	7	9	7	9	7	9	Diaphragm
6	7	9	7	9	7	9	No Diaphragm
9	7	9	7	9	7	9	Diaphragm
9	7	9	7	9	7	9	No Diaphragm
12	7	9	7	9	7	9	Diaphragm
12	7	9	7	9	7	9	No Diaphragm

Table 2.11. BT-72 girder bridge grillage models (deck thickness (in.) on interior of table)

Spacing (ft)	120 ft Span	120 ft Span	135 ft Span	135 ft Span	150 ft Span	150 ft Span	Presence of Diaphragms
6	7	9	7	9	7	9	Diaphragm
6	7	9	7	9	7	9	No Diaphragm
9	7	9	7	9	7	9	Diaphragm
9	7	9	7	9	7	9	No Diaphragm
12	7	9	7	9	7	9	Diaphragm
12	7	9	7	9	7	9	No Diaphragm

2.3.2 Load Cases

Loading of the bridges was an important modeling question that required careful consideration. In all cases only the application of the AASHTO LRFD design truck load (AASHTO 2015) was considered for determination of the distribution factors. A lane load of 0.64 klf is assigned to every 12 ft design lane defined. For this study the lane load does not affect the distribution of load on girders and therefore was not considered. Guidance for applying loads to the grillage models was taken from a similar study (Cross, et al. 2009). For the work described in this report, the HS-20 truck loading (Figure 2.17) was placed with the rear axle at the end of the span, to maximize the shear force. The spacing between the 32 kips axles can be between 14 ft and 30 ft, but the 14 ft spacing yields maximum shear at support, and a 14 ft spacing was used for all models.

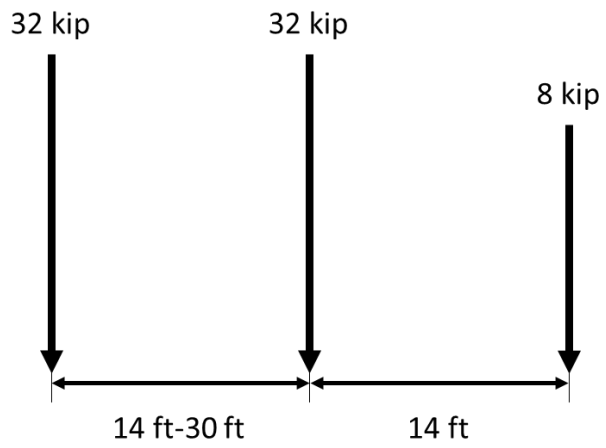

Figure 2.17. HS-20 truck loads

The loading locations along the width of the bridge are given in Figure 2.18. Transverse spacing of wheels for HS-20 truck is 6.0 ft. Load cases were created to determine the most critical location of load across the width of the bridge. For instance, for a single lane loaded, load cases were defined by placing the HS-20 design truck defined in the AASHTO LRFD close to the deck railing and then moving the truck load in the transverse direction in 1.0 ft increments until the truck load was in the middle of bridge (AASHTO 2014). The first tire load was placed 2 ft from the curb for maximum load on the exterior girder (as recommended by AASHTO). Since all bridge models were symmetric more load cases were not required. Next trucks were placed in each possible lane (12 ft away), then a design truck was placed with each tire load positioned over an interior girder. These represented the cases for each design lane loaded individually, and the interior girders loaded for maximum effect. Finally, each design lane was loaded with a design truck (multiple lanes loaded). Since there are three girder spacings considered, the bridges have one, two, and three design lanes. Not shown in this figure is the case of a design truck centered over the interior girder. This load case governed in some cases. For bridges with 6 ft girders spacing, there was only one 12 ft design lane. In this case, a truck was placed 2 ft from the curb on both sides of the bridge for the two lanes loaded case.

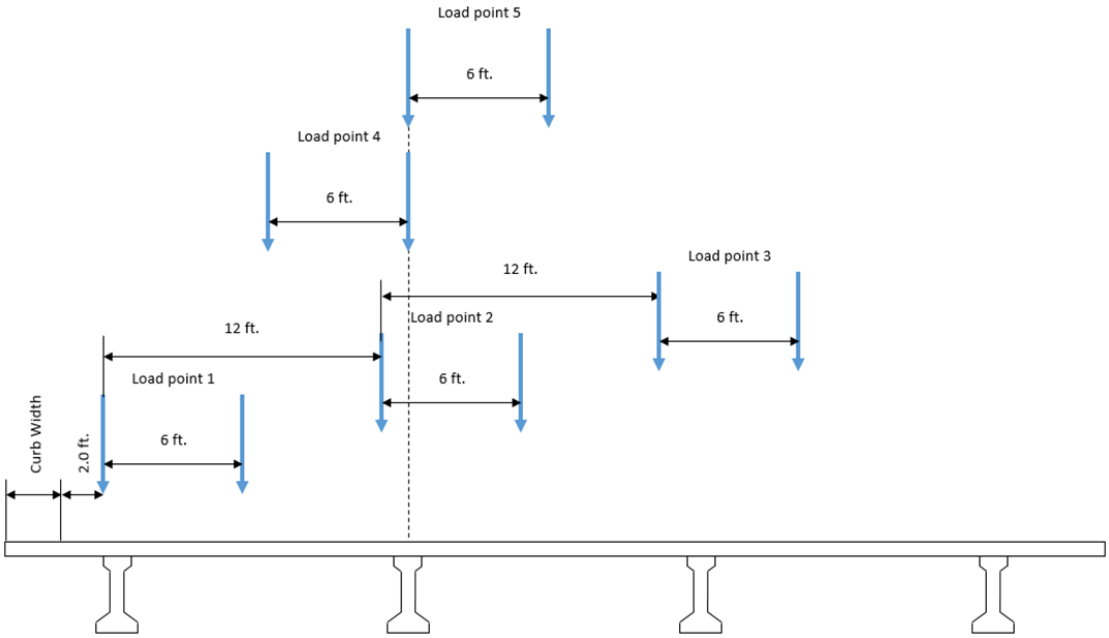

Figure 2.18. Locations of HS-20 truck for grillage model

Determining the critical location of the design truck in the transverse direction required a number of iterations, but since all the bridge geometries considered in this research were symmetric, iterations for only one-half of the bridge width were considered. Determination of the critical transverse load location was broken into four categories: one lane loaded for exterior girders, one lane loaded for interior girders, two lanes loaded for exterior girders, and two lanes loaded for interior girders.

2.3.2.1 One Lane Loaded Case for Exterior Girder

For this case the critical load location for each girder spacing was when the truck is placed right over the exterior girder as shown in Figure 2.19.

2.3.2.2 One Lane Loaded Case for Interior Girders

For this case the truck was placed on the bridge cross-section as shown in Figure 2.19, then it was moved in the transverse direction in 1 ft increments to determine the location that would cause the maximum shear on the interior girder. It was found that the truck placed centered on the interior girder (Figure 2.20) resulted in maximum shear on the interior girder for all girder spacing values used in this study.

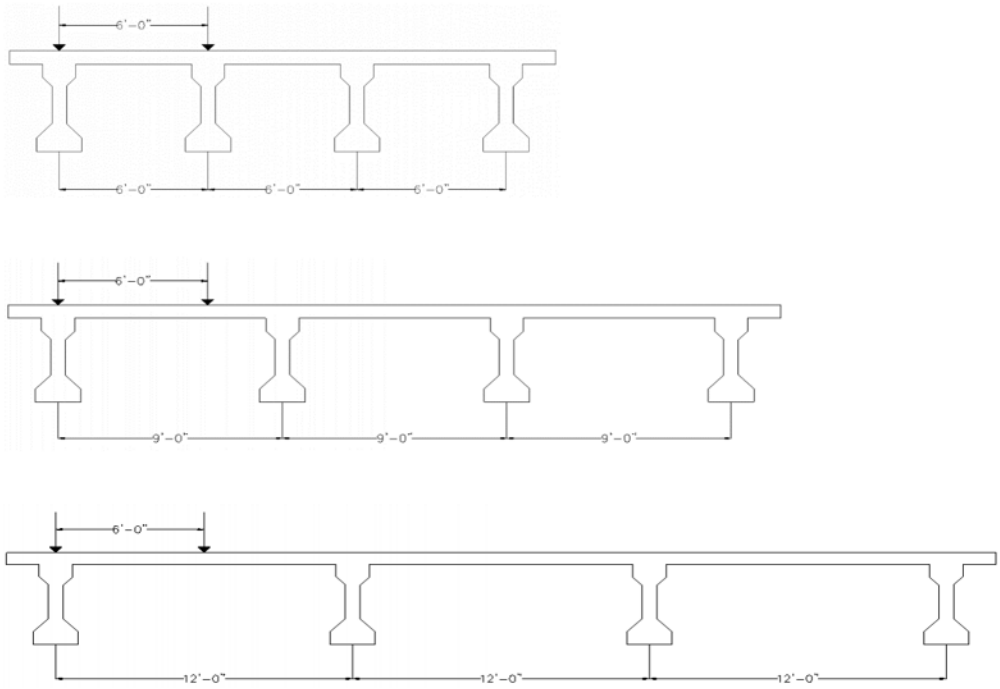

Figure 2.19. Critical lateral location of design truck for exterior girder, one lane loaded case

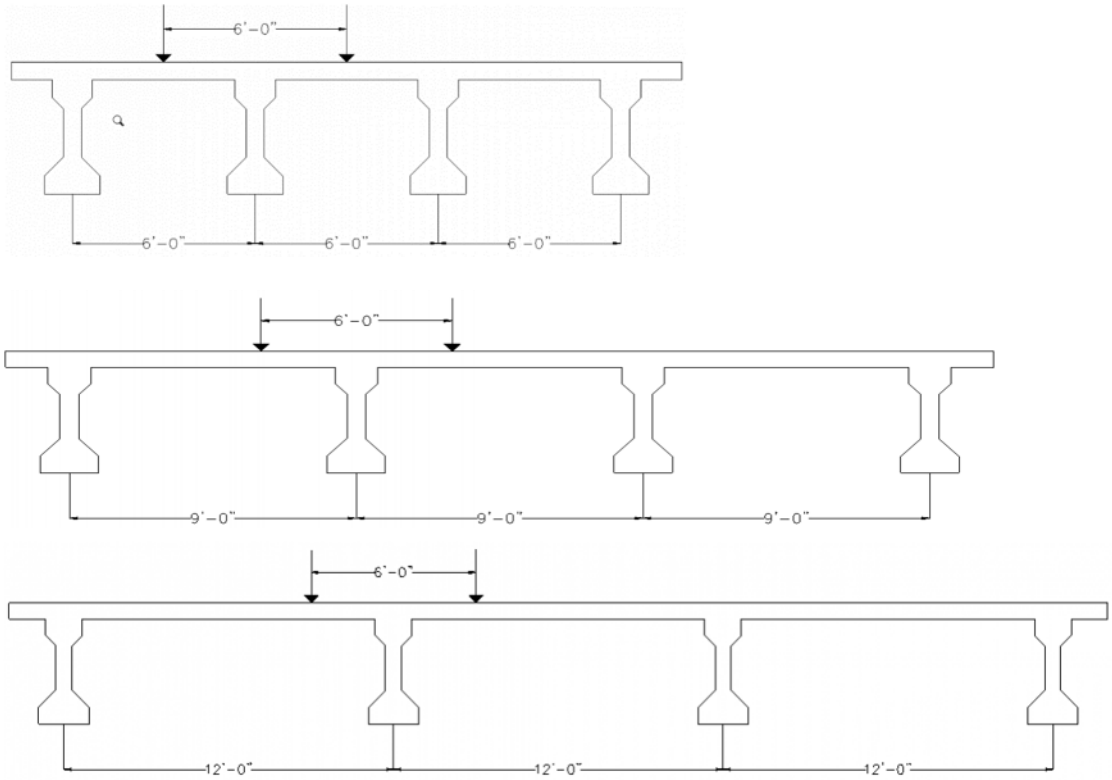

Figure 2.20. Critical location of design truck for interior girder, one lane loaded case

2.3.2.3 Two Lanes Loaded Case for Exterior Girder

When two or more trucks are placed side by side on the bridge deck the lateral spacing between them should be 4 ft based on the distribution of the design truck within the design lane shown in Figure 2.21. Two trucks placed side by side with one on the exterior girder, as shown in Figure 2.22, resulted in the highest shear on the exterior girder.

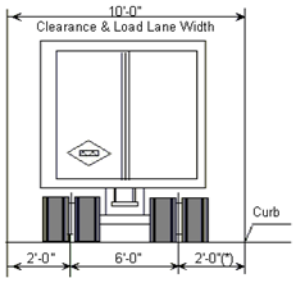

Figure 2.21. Lane load width and clearance for HS-20 truck (MoDOT, 2007)

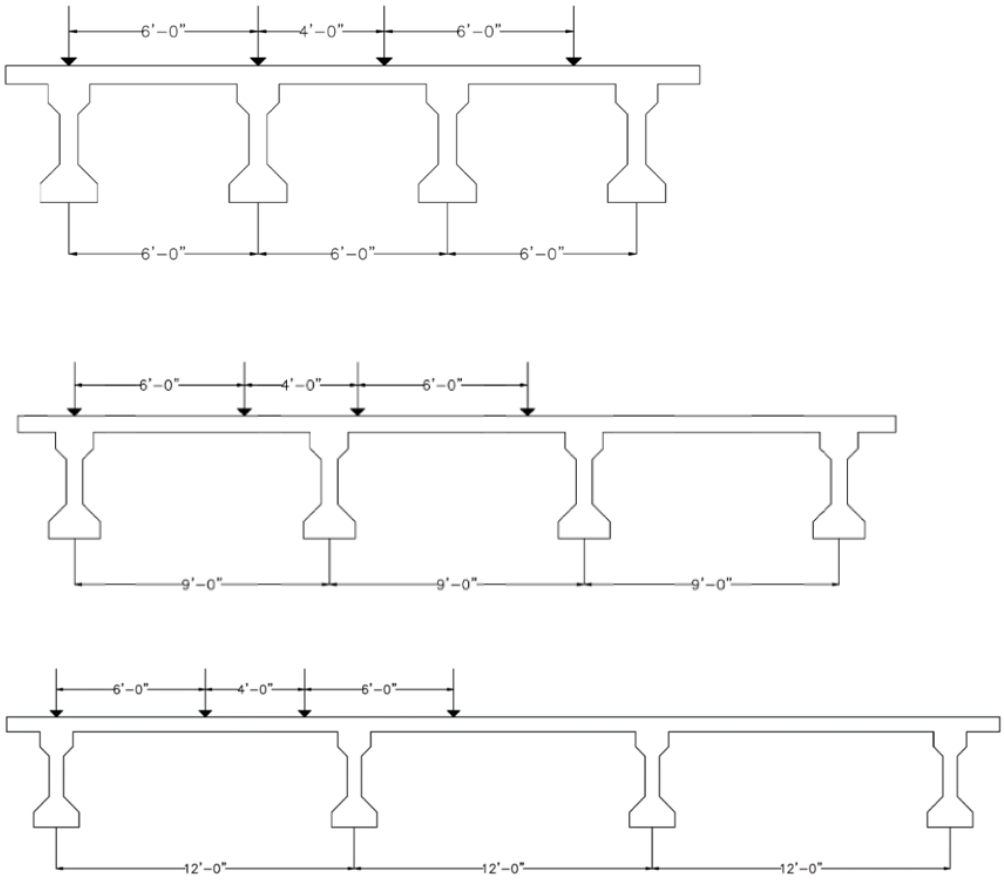

Figure 2.22. Critical location of design truck for exterior girder, two lanes loaded case

2.3.2.4 Two Lanes Loaded Case for Interior Girder

For girder spacings of 6 ft and 9 ft the critical load placement for the two design lanes loaded case for an interior girder was the same as shown in Figure 2.22. When the girder spacing was 12 ft the critical load case was as shown in Figure 2.23.

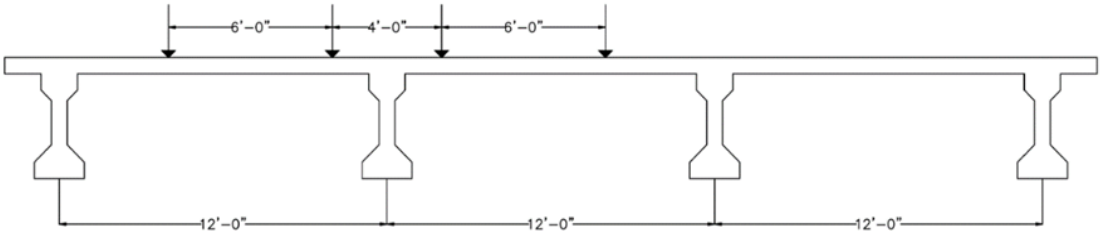

Figure 2.23. Critical location of truck for interior girder, two lanes loaded case

The reactions from each load case were summed, and the fraction of the total reaction at each girder was compared to the AASHTO Distribution factors. For the two or more lanes loaded case, the reaction at each support was divided by the static reaction of the design truck placed on a simple beam of the same length. Because exact materials properties were not known, the deck concrete was assumed to have a 4,500 psi compressive strength at 28 days, and the girder concrete was assumed to be 6,000 psi. These values were based on the properties of the girders tested in the lab by Floyd et al. (2016) and on the ODOT standard specifications. Using these values of compressive strength and ACI equation 19.2.2.1.b (ACI Committee 318, 2014), this resulted in a modulus for the deck of 3,824 ksi and a modulus for the girder of 4,415 ksi. It is recognized that these values are unlikely to be correct for larger depth girder types, but they were used for all bridge models for the sake of consistency.

2.4 Type-II Girder Model Results

2.4.1 Overview of Results

The results obtained from the grillage modeling, were compared with the load distribution factors calculated using equations available in AASHTO LRFD. All of these distribution factor equations already include the multiple presence factor. Therefore, all the results obtained from AASHTO LRFD equations were divided by the respective multiple presence factor to ensure the correct comparison with the grillage model

derived results. In general, the AASHTO LRFD equations produced larger load distribution factors compared to the grillage models examined in this study. Though the AASHTO LRFD equations were generally found to produce larger distribution factors compared to the grillage models, in few of the cases the load distribution factor from the model was found to be greater than the value given by the AASHTO LRFD equations.

Since AASHTO Type-II girders were the primary focus of this research, the results from those models are discussed in the greatest detail. Substantial discussion of the results for the Type-III girder bridges is also included, but only discussion of the results from the rest of the models is presented in the main body of the report. Detailed results for the Type-IV, BT-63, and BT-72 girder models are included in Appendix A.

This section will discuss the effects of various parameters (girder spacing, deck thickness, span length, diaphragm vs. no diaphragm) on AASHTO LRFD Distribution factors and distribution factors derived from grillage models. The section properties used to build these models and the distribution factors collected from grillage models and from the AASHTO LRFD equations are given in Appendix B. The results presented in this section are separated by interior and exterior girders in the span and by loading (one lane loaded or two or more lanes loaded). These cases are considered separately in the code so they were separated for the discussion of grillage modeling results. This section merely presents the results and explains the trends that were seen. The results are discussed in more detail and in context of the other girder types in Section 2.6.

In this section, differences in distribution factors between the code and the grillage models are discussed. A discussion of how these differences are expressed is warranted as a prelude to this section. Since a DF represents a fraction of the total shear at one end of a bridge, differences in the factors will be expressed as the absolute difference between the two. For example, where the AASHTO DF is 0.4 and the grillage model derived factor is 0.35, the difference is 0.05, or 5% of the total shear at that end of the bridge.

2.4.2 Effects of Girder Spacing

First, the effects of girder spacing were examined. Distribution factor equations in the code have always appreciated the effect of spacing on load distribution. Clearly a

longer deck span will reduce the distribution of load to adjacent girders, and thus will increase the DF for the girder in question. Figure 2.24 shows the distribution factors for 6, 9, and 12 ft girder spacings for each span length, deck thickness and diaphragm condition modeled for exterior girders with one lane loaded (note: the lines on figures in this section do not indicate a trend necessarily, but are in place to indicate the AASHTO distribution factors). As expected, the distribution factors increased with increasing spacing. The AASHTO distribution factors appear to show good agreement with the results of the parametric models examined, generally being conservative by a value of about 0.05 (or 5% greater shear at that end). For the case of 6 ft girder spacing, the AASHTO equations appear to be unconservative (by about 0.025 or 2.5% less shear) for the case of no diaphragms (smaller distribution factor means less conservative). For exterior girders, the code allows the end of the span to be modeled as a rigid body

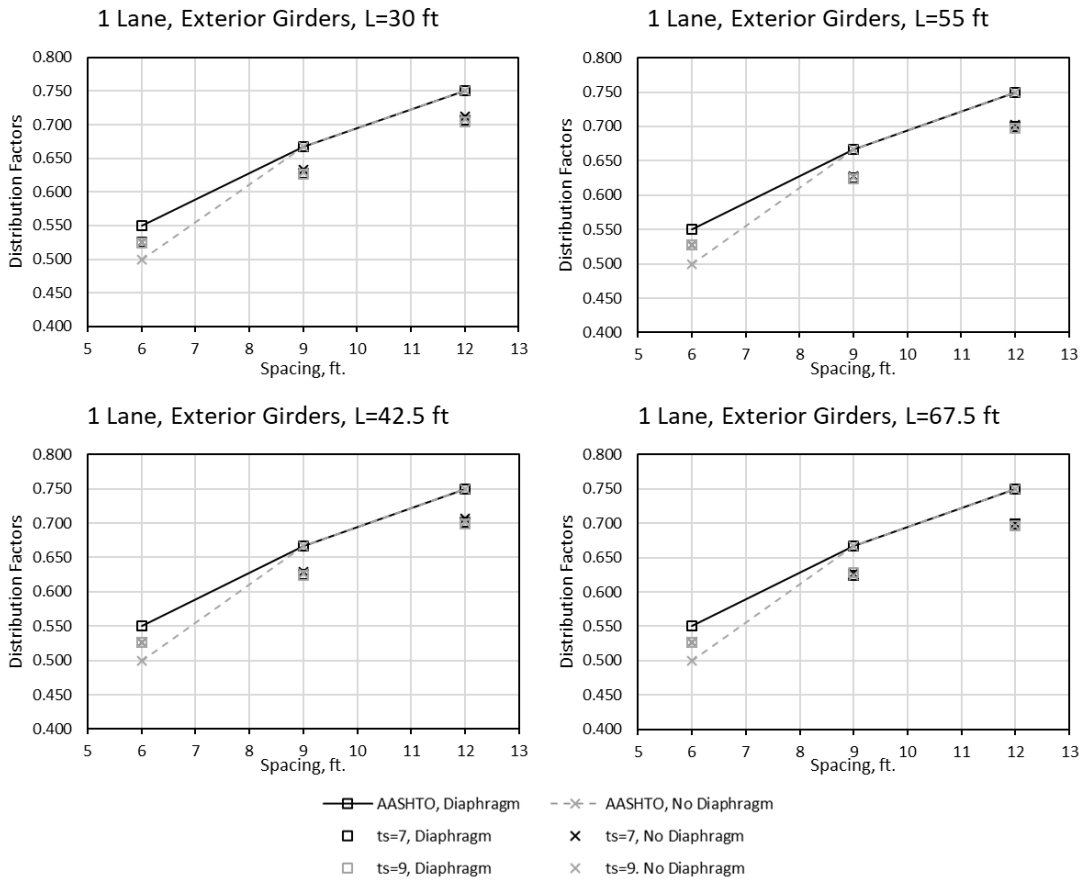

Figure 2.24. Distribution factors for exterior girders, one lane loaded versus girder spacing

when diaphragms are present. This assumption is known as “special analysis.” In this study, the special analysis was used when diaphragms were present (solid line in figures), and it was occasionally the controlling distribution factor case in the AASHTO LRFD code. Based on the modeling presented here, diaphragms do not appear to have a significant effect on load distribution for exterior girders compared to the effect of spacing.

Next, the same parameters were compared for exterior girders with two or more lanes loaded. For the 6 ft girder spacing case, two lanes loaded was achieved by placing a truck 2 ft from the deck’s edge on each side of the bridge. This arrangement produces a situation that is smaller than the design lane width of 12 ft, but arranging loads more closely spaced than a typical design lane may be necessary for load rating of narrower bridges. Again, there is a trend of increasing distribution factors with increasing girder spacing (Figure 2.25). This finding is unsurprising. The distribution

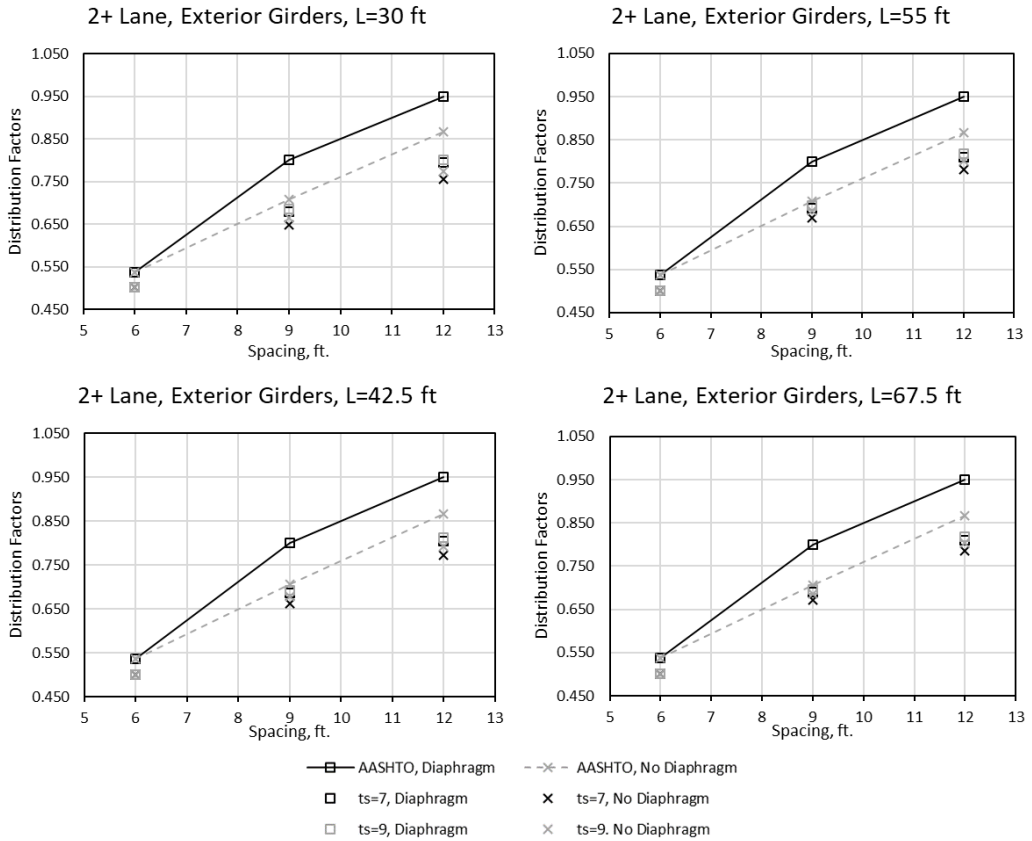

Figure 2.25. Distribution factors for exterior girders, 2+ lanes loaded versus girder spacing

factors appear to vary more for exterior girders with two or more lanes loaded with respect to deck thickness and presence of diaphragms based on the grillage models. In other words, for two or more lanes loaded, these variables have a more pronounced effect than for one lane loaded. The AASHTO LRFD distribution factors are conservative, especially when diaphragms are present and the “special analysis” is used. However, for the 6 ft girder spacing there appears to be very little influence from diaphragms or deck thickness. Based on the grillage models examined, it is a more conservative assumption to use the rigid section special analysis method. The controlling AASHTO LRFD code equations appear to become more conservative with larger girder spacings.

Next, interior girder distribution factors were examined for the same variable combinations. Again, these were separated by number of lanes loaded. Results for the case of one lane loaded are given in Figure 2.26. For this case, AASHTO distribution

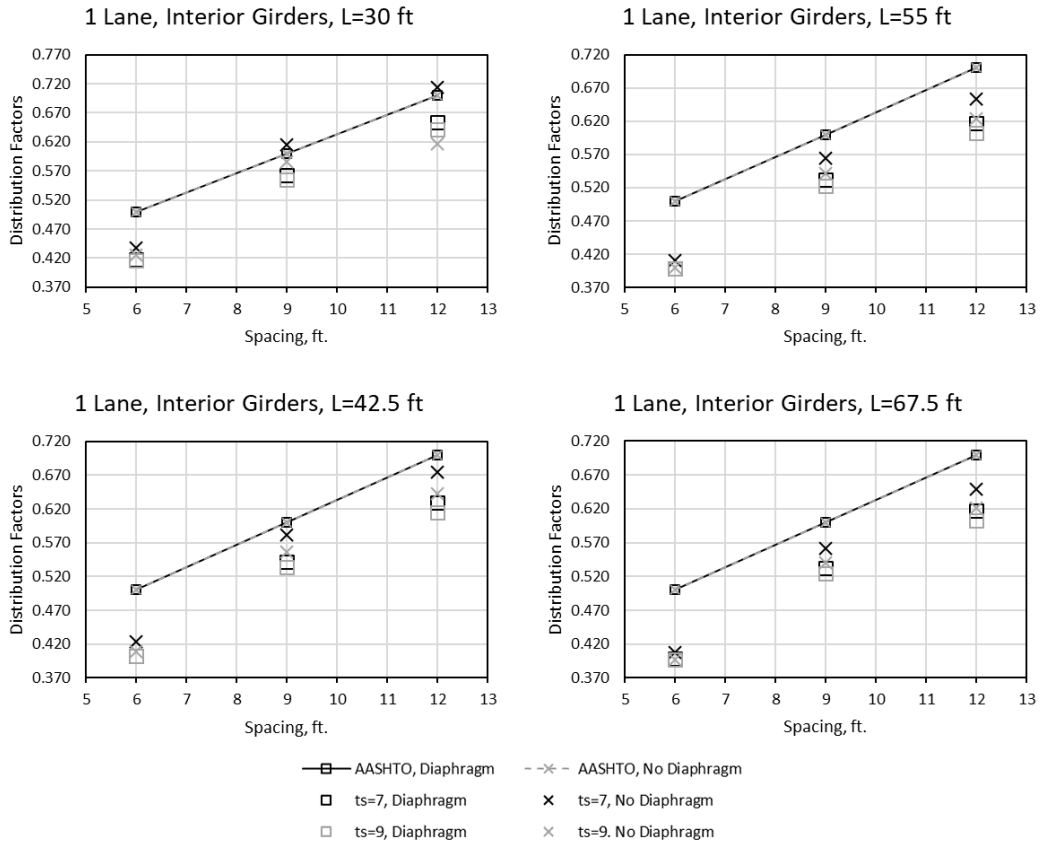

Figure 2.26. Distribution factors for interior girders, one lane loaded versus girder spacing

factors were generally conservative. However, the code distribution factors were slightly unconservative for thinner decks with shorter spans and wider girder spacings (top left in Figure 2.26). Distribution factors from the grillage models tended to vary more as span length increased, i.e. the effects of deck thickness and the presence of diaphragms are more pronounced as span length is increased.

Figure 2.27 shows the distribution factors for interior girders with two or more lanes loaded. AASHTO distribution factors were conservative for all variable combinations considered for this case. It appears that the code distribution factors are less conservative for larger girder spacings and very conservative for smaller girder spacings.

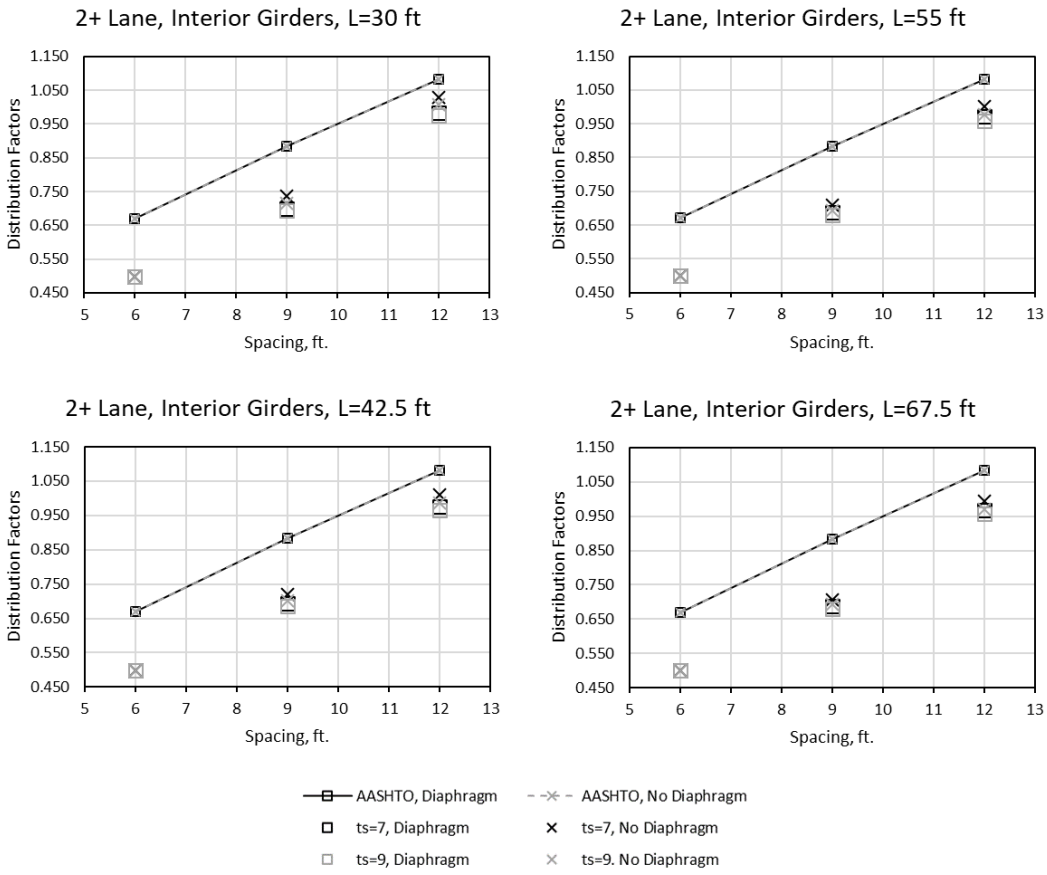

Figure 2.27. Distribution factors for interior girders, 2+ lanes loaded versus girder spacing

As stated previously, spacing is the factor which influences load distribution the most. For bridges with middle and end diaphragms, the influence of girder spacing on

ratio of AASHTO DF to grillage model DF is shown in Figure 2.28. This ratio is intended as a measure of the conservativism of the AASHTO factors as compared to those determined using grillage models. The grillage factors should be compared to real bridges in the future, to verify their accuracy. For interior girders, the code tends to become less conservative at larger girder spacings. At a spacing of 6 ft the interior girder AASHTO distribution factors are 1.35 times the grillage model values for any span length. Conversely, at a 12 ft spacing this factor is between 1.1 and 1.15. On the other hand, exterior girders show the opposite trend of increasing conservativism with larger girder spacing. At a 6 ft spacing the code is only conservative by a factor of about 1.05 for exterior girders. This increases to between 1.13 and 1.16 for a 12 ft girder spacing. In general, it appears that the effects of deck thickness and span length have more of an effect on load distribution at larger girder spacings.

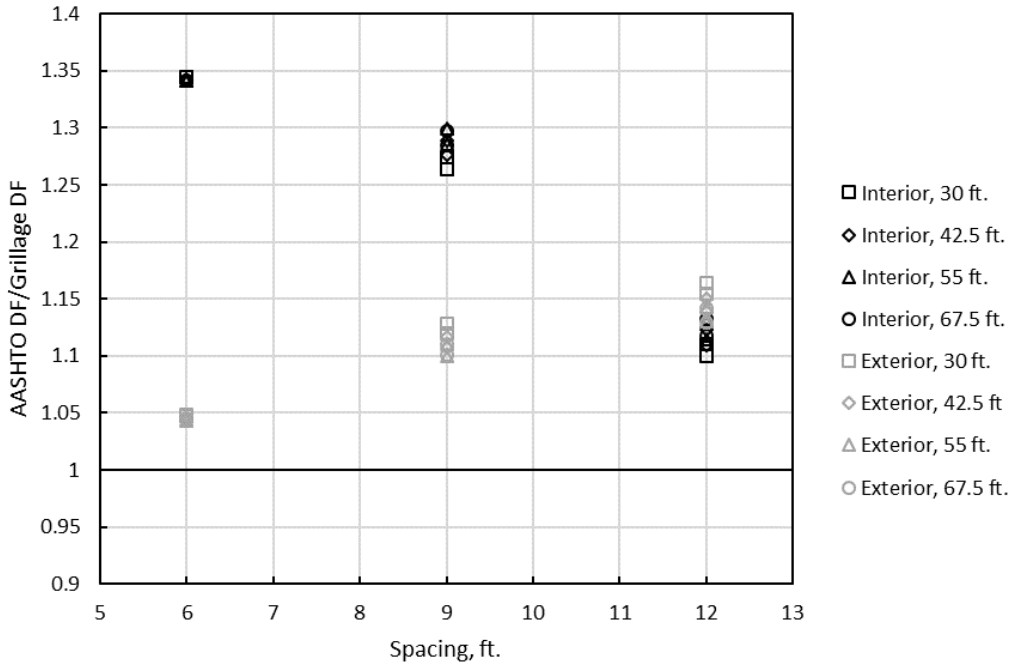

Figure 2.28. Potential conservativism of distribution factors for each girder spacing examined with diaphragms

Figure 2.29 shows the same comparison described above but for bridges with no diaphragms. The same trends are generally apparent as in Figure 2.28; decreasing conservativism for increasing length in interior girders, and the opposite for exterior

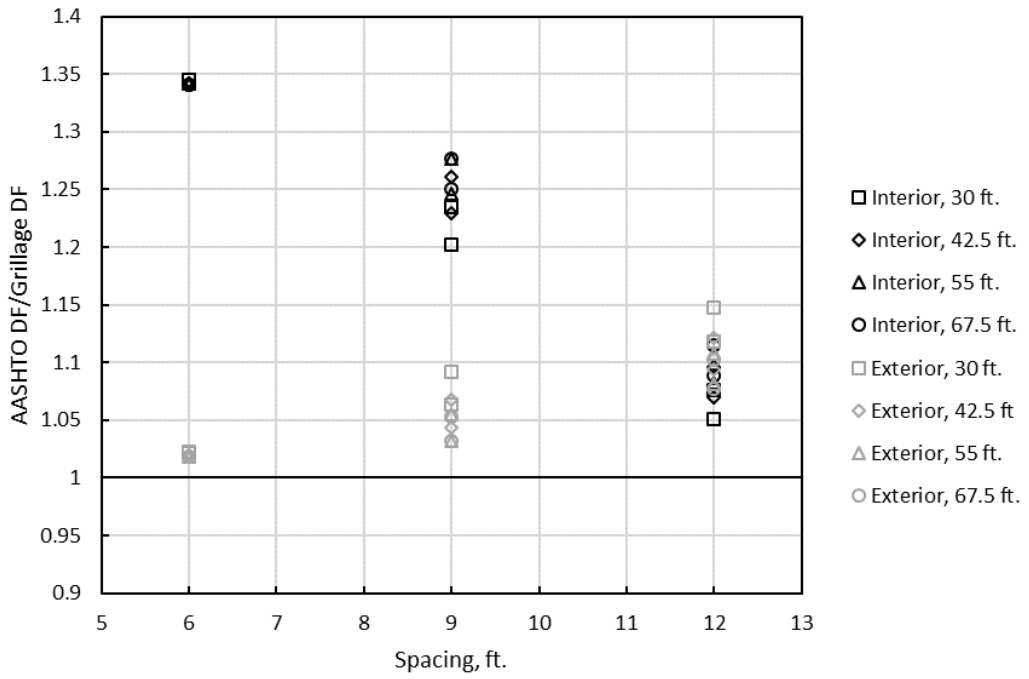

Figure 2.29. Potential conservativism of distribution factors for each girder spacing examined without diaphragms

girders. Distribution factors tend to be slightly less conservative across the board for bridges with no diaphragms. In particular, exterior girders in bridges with no diaphragms and a 6 ft girder spacing are predicted very closely (~1.02) by the code.

2.4.3 Effects of Diaphragms

Figure 2.30 shows the percent difference for interior girder grillage model distribution factors for situations with or without diaphragms (factors decrease when diaphragms are included). In this figure, the two markers at each span length relate to the different slab thicknesses. Smaller slab thicknesses had larger percent differences when diaphragms were included in the model. At a girder spacing of 6 ft, diaphragms do not affect load distribution. A trend is similar for the 9 ft and 12 ft girder spacings, where the factors differ most for shorter span lengths. Factors are larger when diaphragms are not present in all cases. At its largest, the difference is 4.9% (s=9 ft, t_s= 7 in., L=30 ft), which would correspond to a decrease in shear of about 2.4 kips for the design truck. The AASHTO distribution factors are the same in this case whether diaphragms are present or not.

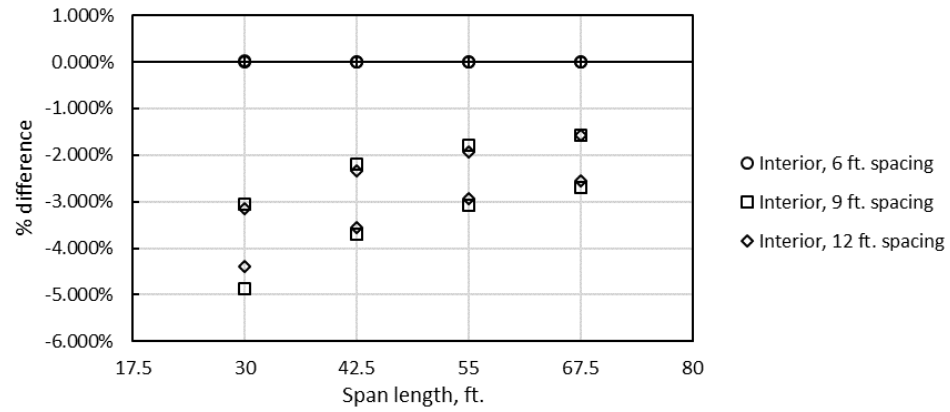

Figure 2.30. Difference in distribution factors for diaphragm versus no diaphragm for interior girders

Figure 2.31 shows percent difference for exterior girder grillage model distribution factors for situations with or without diaphragms. The code accounts for diaphragms for exterior girders, unlike for interior girders (aforementioned “special analysis”). The opposite trend appears in this figure compared to Figure 2.30. Diaphragms increase distribution factors for exterior girders by almost the same degree as they decrease for interior girders. This effect is most apparent at shorter span lengths and larger girder spacings. Additionally, the difference is greater for 7 in. slabs than for 9 in. slabs at a given girder spacing and span length. Again, at shorter girder spacings (6 ft), diaphragms do not appear to affect load distribution.

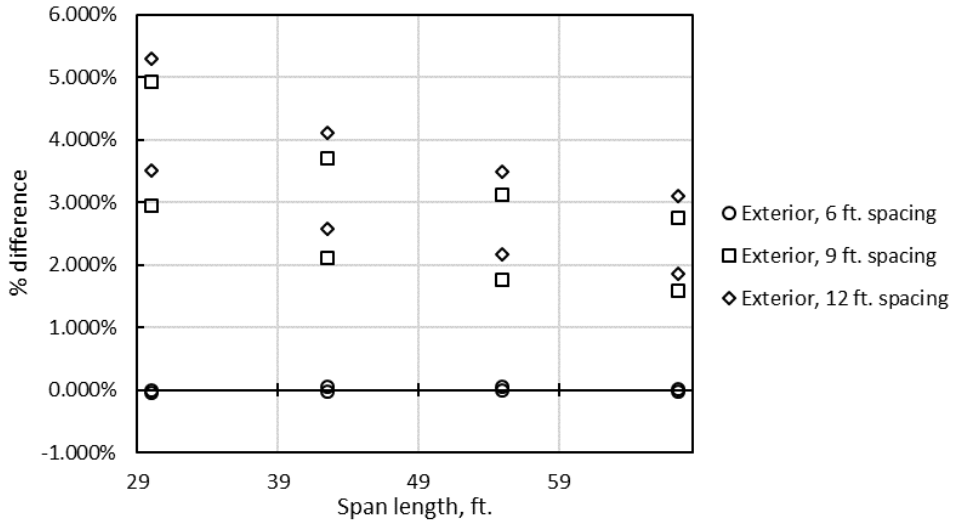

Figure 2.31. Difference in Distribution factors for diaphragm versus no diaphragm for exterior girders

2.4.4 Effects of Deck Thickness

Slab thickness also affects the conservativism of the code factors compared to those derived using the grillage models, although to a lesser degree than spacing and span length. Interestingly, interior and exterior girders had alternate trends in the effects of slab thickness. For interior girders, increasing slab thickness increased conservativism; for exterior girders the opposite is true. The differences between AASHTO and grillage model distribution factors with varying slab thickness are very small however, so slab thickness does not affect load distribution as much as span length or spacing. Table 2.12 shows this comparison. The numbers in the table represent the average of the AASHTO factors for varying lengths for the lengths divided by the grillage derived distribution factors for the corresponding variables. Span length did not appear to alter the effects of slab thickness on load distribution.

Table 2.12. Conservativism of AASHTO LRFD code for varying slab thickness

s (ft)	t_s (in.)	Int. Diaphragm	Ext. Diaphragm	Int. No Diaphragm	Ext. No Diaphragm
6	7	1.342	1.045	1.342	1.020
6	9	1.342	1.046	1.343	1.020
9	7	1.278	1.116	1.232	1.070
9	9	1.290	1.107	1.262	1.043
12	7	1.110	1.150	1.073	1.120
12	9	1.124	1.138	1.099	1.093

2.4.5 Effects of Span Length

The influence of span length on distribution was examined by plotting the distribution factors against span length for each girder spacing. Note that the following figures have variable scales on the ordinate to better show the differences. Figure 2.32 shows the distribution factors for interior girders spaced at 6 ft for the case of one lane loaded. AASHTO distribution factors were conservative for this case, becoming more conservative for longer span lengths. For the 67.5 ft span length, distribution factors determined using the grillage models were approximately 0.1 less than the AASHTO predictions.

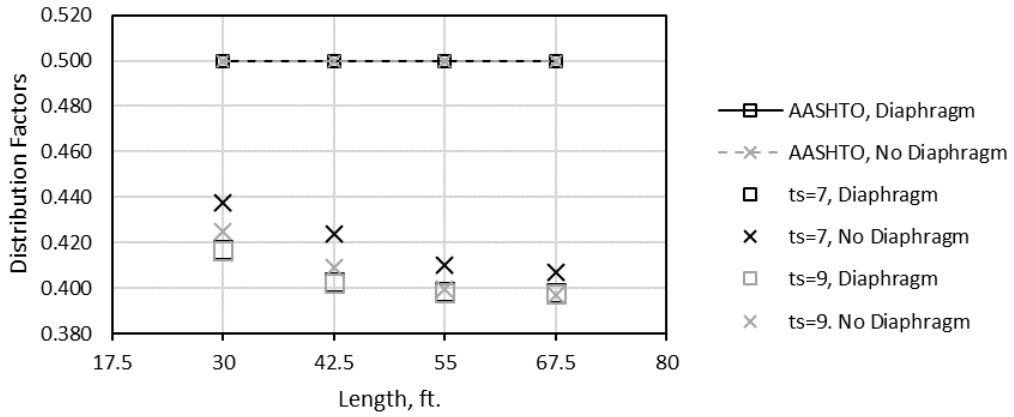

Figure 2.32. Distribution factors for interior girders with one lane loaded, 6 ft girder spacing

Figure 2.33 shows the distribution factors for interior girders spaced at 9 ft with one lane loaded. There is a larger spread of distribution factors for this wider spacing, the difference between a given DF for lengths of 30 ft to 67.5 ft was 0.05 on average. The distribution factors from the AASHTO LRFD code are generally conservative, though less so for shorter spans. The grillage model derived distribution factor for the case of a 30 ft span length with a 7 in. deck and no diaphragm exceeds the AASHTO factors by 0.015 (1.5% more shear).

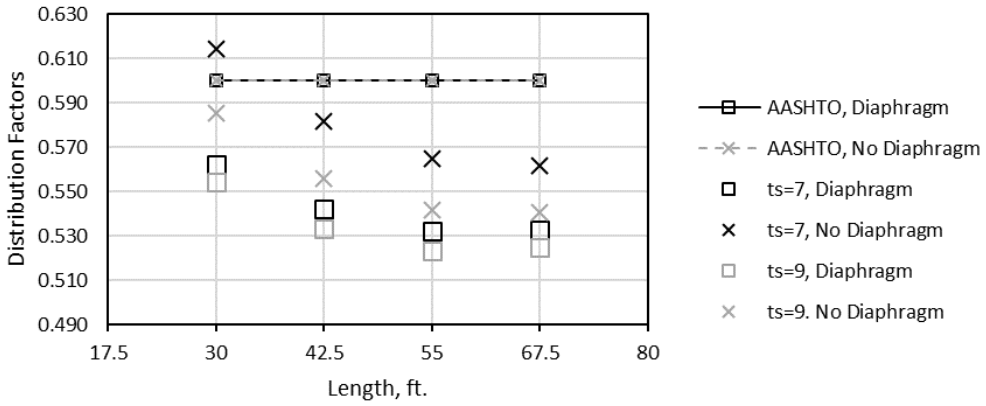

Figure 2.33. Distribution factors for interior girders with one lane loaded, 9 ft girder spacing

Finally, the case of 12 ft spacing is given in Figure 2.34. There is a general trend of decreasing distribution factors with length, as seen in the other figures. The code

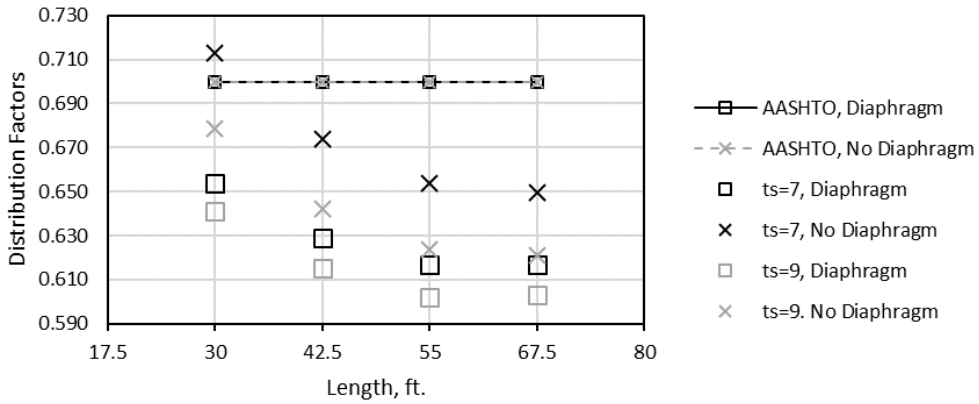

Figure 2.34. Distribution factors for interior girders with one lane loaded, 12 ft girder spacing

distribution factors are conservative except for 7 in. deck thickness with no diaphragms for shorter span lengths (i.e. < 42.5 ft) and 6 ft girder spacing. For these unconservative cases, the code equations are at most unconservative by 0.01. For deck thickness of 9 in. with diaphragms, the code distribution factors are greater than the grillage values by as much as 0.1 for the 67.5 ft span length. The effects of diaphragms and slab thickness appear to be more pronounced for larger spacings.

The same variables were considered for the case for 2+ lanes loaded for each girder spacing. Figure 2.35 shows the distribution factors for interior girders at a spacing of 6 ft. Regardless of deck thickness or diaphragms or length, the distribution factors are basically unchanged. The code is conservative for this case, producing distribution

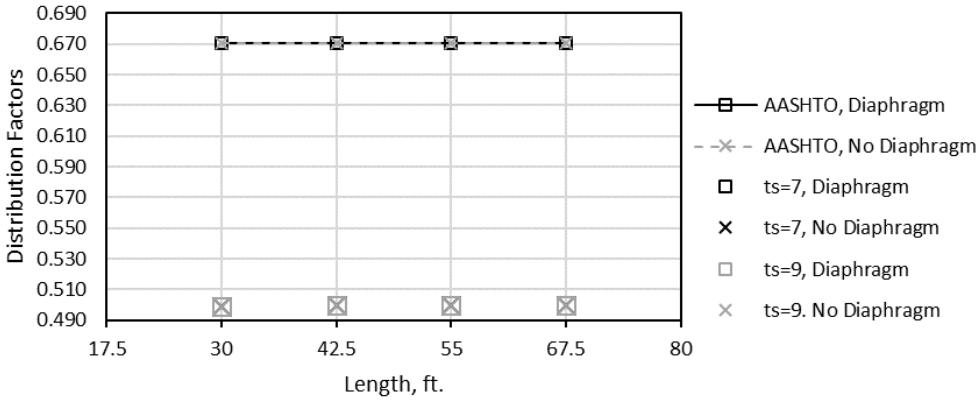

Figure 2.35. Distribution factors for interior girders with 2+ lanes loaded, 6 ft girder spacing

factors larger than those derived from the grillage models by 0.15. For this small spacing, the end of the bridge appears to be very stiff.

When the spacing was increased to 9 ft (Figure 2.36), distribution factors tend to decrease with increasing length. The AASHTO conservative equations are generally for longer lengths at the 9 ft girder spacing.

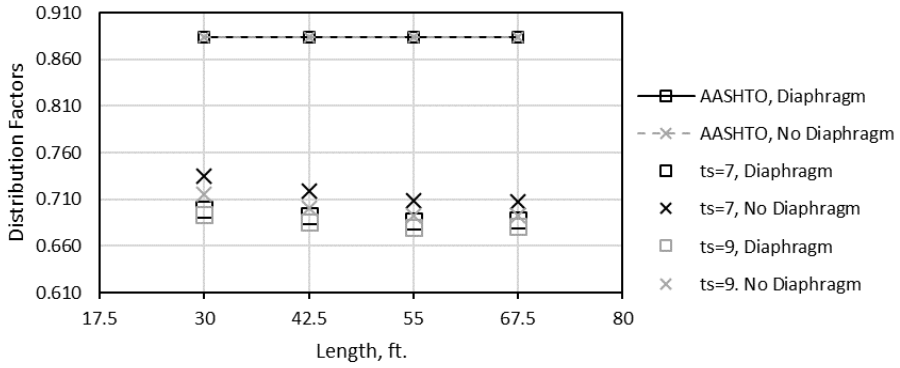

Figure 2.36. Distribution factors for interior girders with 2+ lanes loaded, 9 ft girder spacing

Finally, Figure 2.37 shows the distribution factors for interior girders at a spacing of 12 ft. Again, the AASHTO distribution factors become more conservative for longer span lengths, and the conservativism is greater for 12 ft spacing compared to 9 ft spacing. The code equations are generally conservative. At their most conservative they differ from the grillage model derived factors by 0.204 (20.4% of the total shear at 9 ft spacing, 55 ft length, 9 in. deck thickness, with no diaphragms).

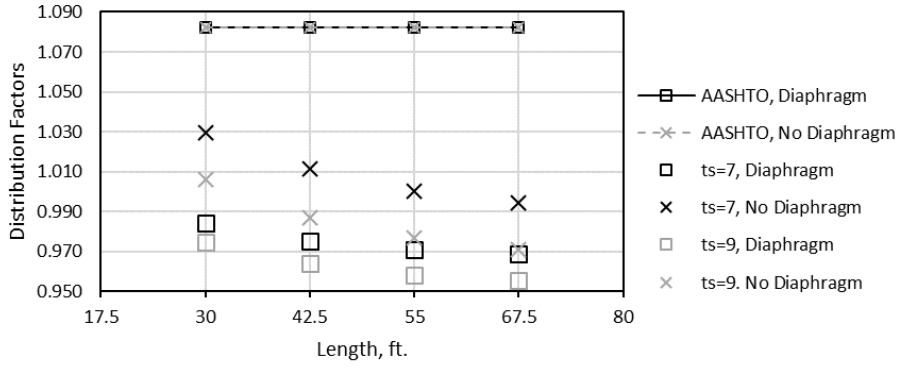

Figure 2.37. Distribution factors for interior girders with 2+ lanes loaded, 12 ft girder spacing

The previous six figures compared distribution factors for interior girders by length for one and two or more lanes loaded. The next six compare the same factors for exterior girders. For exterior girders, the distribution factors for 6, 9, and 12 ft spacings with one lane loaded are given in Figure 2.38, Figure 2.39, and Figure 2.40, respectively. For a spacing of 6 ft, the grillage models showed very little change with increasing slab thickness or with the presence of diaphragms. If the special analysis is not used (diaphragms not present), the code under predicts distribution by about 0.025. On the other hand, when the rigid section special analysis is used the code overpredicts distribution factors by the same margin.

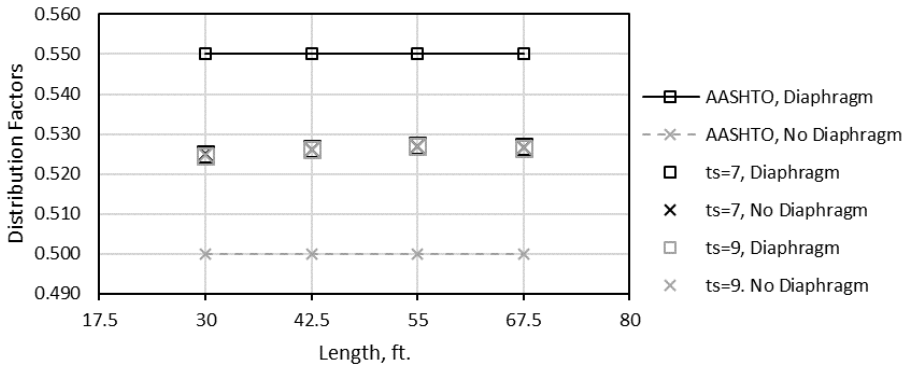

Figure 2.38. Distribution factors for exterior girders with one lane loaded, 6 ft spacing

For the 9 ft girder spacing (Figure 2.39), the code distribution factors are conservative at every span length. The code factors differ from the grillage factors by about 0.04 on average, so the difference is relatively small.

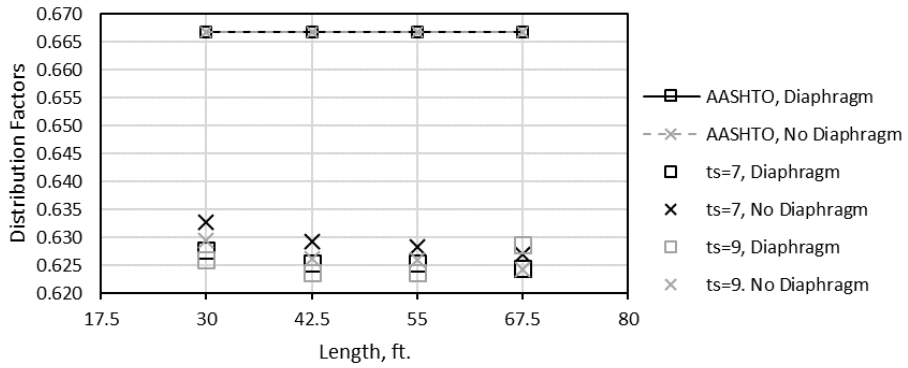

Figure 2.39. Distribution factors for exterior girders with one lane loaded, 9 ft spacing

The trend for the 12 ft girder spacing (Figure 2.40) is similar to that observed for the 9 ft girder spacing. On average, the code distribution factors differ from the model derived values by about 0.048. Distribution factors tend to decrease for longer spans for both 9 ft and 12 ft girder spacings.

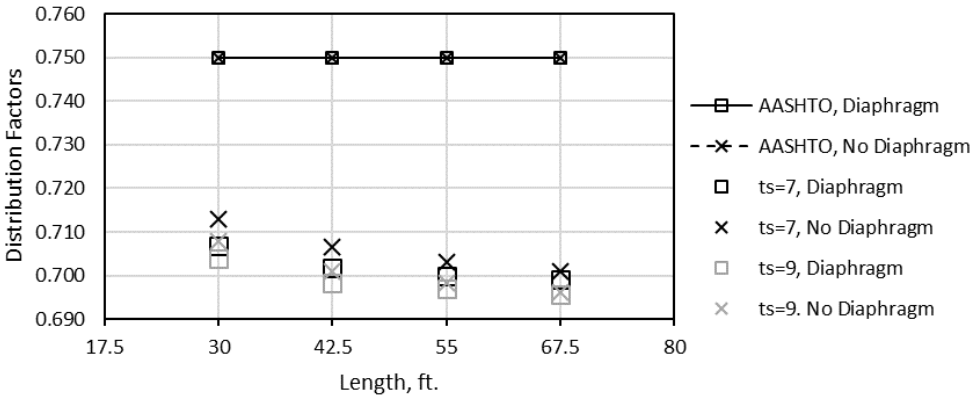

Figure 2.40. Distribution factors for exterior girders with one lane loaded, 12 ft spacing

Next, distribution factors were compared for exterior girders with two or more lanes loaded. Figure 2.41 shows the distribution factors for 6 ft girder spacing. There is a general trend of decreasing distribution factor with span length. The magnitude of the change with length is small for this spacing, and the code and grillage derived factors agree reasonably well (decrease of 0.035 for 67.5 ft as opposed to 30 ft).

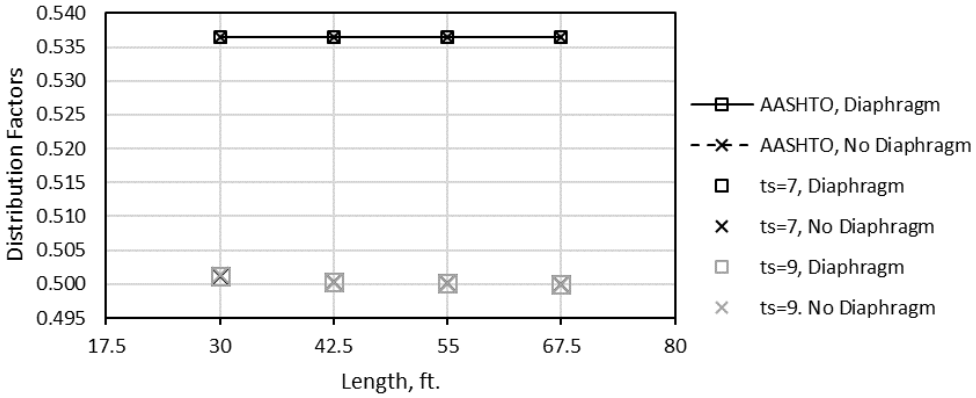

Figure 2.41. Distribution factors for exterior girders with 2+ lane loaded, 6 ft spacing

Figure 2.42 shows the distribution factors for 9 ft girder spacing and a trend of increasing distribution factors with length is present. This trend seems to diminish after

a 55 ft span length. The different code distribution factors (diaphragm versus no diaphragm) are a result of the “special analysis” used when diaphragms are present in exterior girders. Where diaphragms are accounted for (solid lines), the code is more conservative for all span lengths. Otherwise, the code is less conservative, particularly at longer spans.

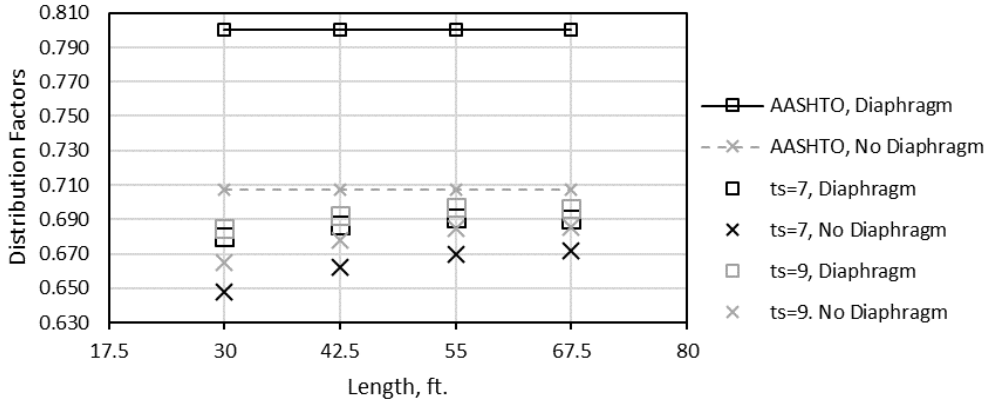

Figure 2.42. Distribution factors for exterior girders with 2+ lane loaded, 9 ft spacing

Finally, Figure 2.43 shows the distribution factor comparison for 12 ft girder spacing. For the cases considered with this spacing, the code is conservative, more so if the “special analysis” is used (diaphragms accounted for). For short span lengths where diaphragms are present, the code can be increasingly conservative (0.155 greater than the grillage model).

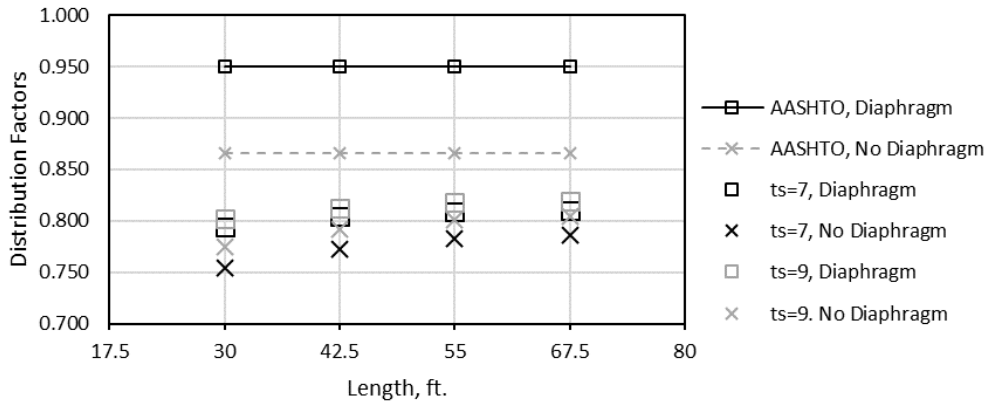

Figure 2.43. Distribution factors for exterior girders with 2+ lane loaded, 12 ft spacing

2.5 Type III Girder Model Results

2.5.1 Overview

For the Type II girder results the difference in distribution factor was taken as an absolute value of percentage of total shear distributed to the individual girder. For the remaining girder types, the percentage difference between the distribution factor calculated using the AASHTO LRFD equation and the distribution factor determined from the grillage model was calculated for the different models using Equation 2.1.

$$Percentage\ Difference = \frac{x_{AASHTO} - x_{grillage}}{x_{AASHTO}} \quad (2.1)$$

where:

X_{AASHTO} = Distribution factor calculated using AASHTO equations

$X_{grillage}$ = Distribution factor determined using grillage models

All resulting distribution factors were compared with the load distribution factors calculated using equations available in AASHTO LRFD. All of these distribution factor equations already include the multiple presence factor. Therefore, all the results obtained from AASHTO LRFD equations were divided by the respective multiple presence factor to ensure the correct comparison with the grillage models. It was determined that grillage models produced smaller load distribution factors than the AASHTO equations for most cases. However, in few of the cases the load distribution factor from the model was found to be greater than the value given by the AASHTO LRFD equations. Specifically for Type-III girders, when the bridge was loaded with two trucks on either end of the bridge in the transverse direction with minimum spacing of 4 ft between the trucks, the grillage models gave a larger distribution factor than the AASHTO LRFD equations for the 6 ft girder spacing. However, these differences were by a maximum of only 4% for all configurations considered for Type-III girders.

2.5.2 Effects of Girder Spacing

Girder spacing is the most important factor influencing the load distribution factor based on previous research and the results of this study. Figures 2.44-2.46, 2.47-2.49, 2.50-2.52 and 2.53-2.55 compare the load distribution factors calculated from the AASHTO LRFD equations and those determined from grillage models for Type-III

girders. Each group of three figures covers three different span lengths and there are four sets of figures, as comparisons were made between one and two lanes load cases for the interior and exterior girders. It is obvious from Figures 2.44-2.55 that the load distribution factor increased with an increase in girder spacing for all cases examined. The distribution factor calculated using the AASHTO LRFD equations for each case showed good agreement with the parametric models examined. It can also be noticed that trends of distribution factor given by the AASHTO LRFD equations are linear for interior girders and are not linear for exterior girders, whereas, all the results from grillage models have a nonlinear trend.

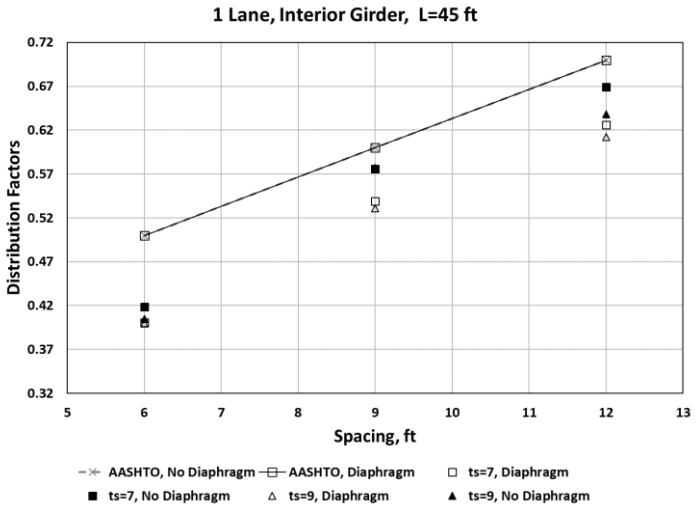

Figure 2.44. Grillage model and AASHTO load distribution factors for 45 ft span interior Type-III girders, one lane loaded case versus girder spacing

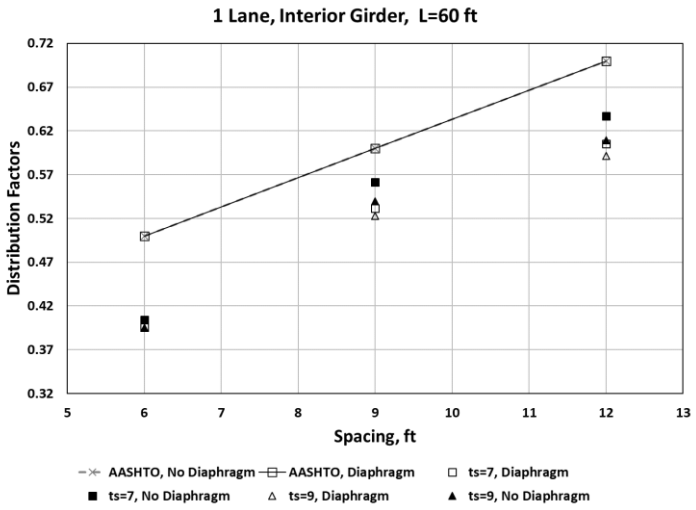

Figure 2.45. Grillage model and AASHTO load distribution factors for 60 ft span interior Type-III girders, one lane loaded case versus girder spacing

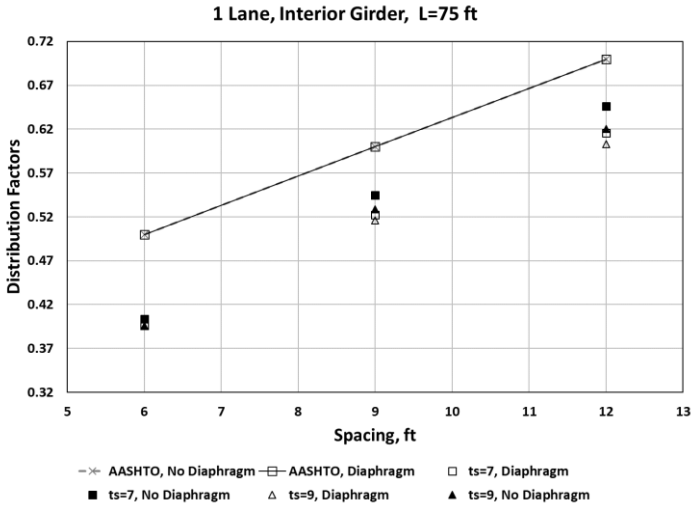

Figure 2.46. Grillage model and AASHTO load distribution factors for 75 ft span interior Type-III girders, one lane loaded case versus girder spacing

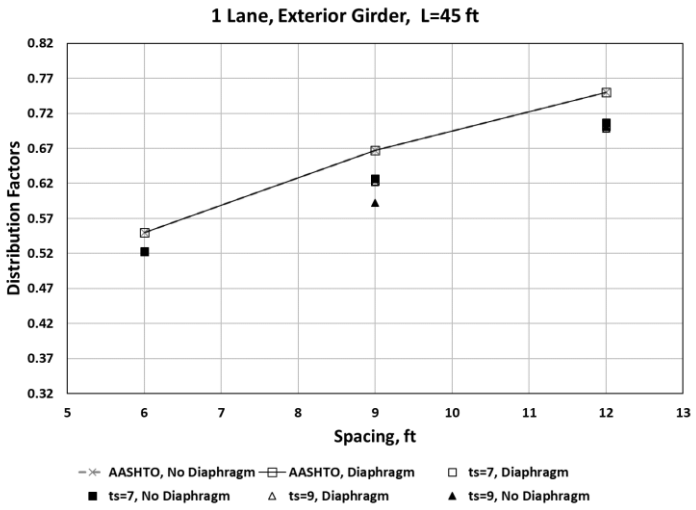

Figure 2.47. Grillage model and AASHTO load distribution factors for 45 ft span exterior Type-III girders, one lane loaded case versus girder spacing

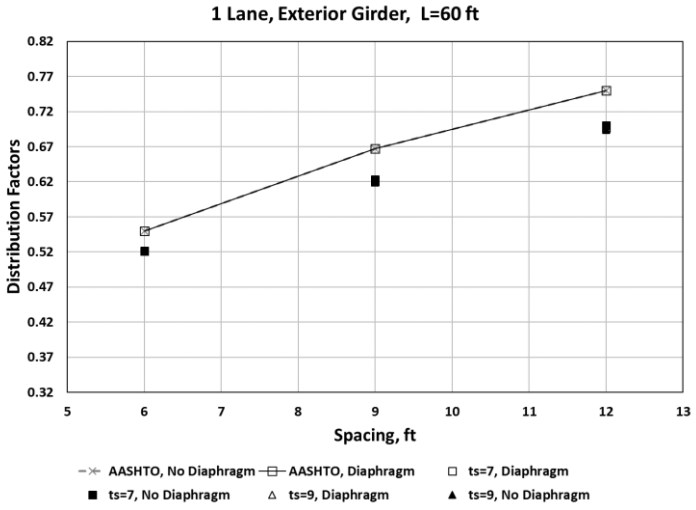

Figure 2.48. Grillage model and AASHTO load distribution factors for 60 ft span exterior Type-III girders, one lane loaded case versus girder spacing

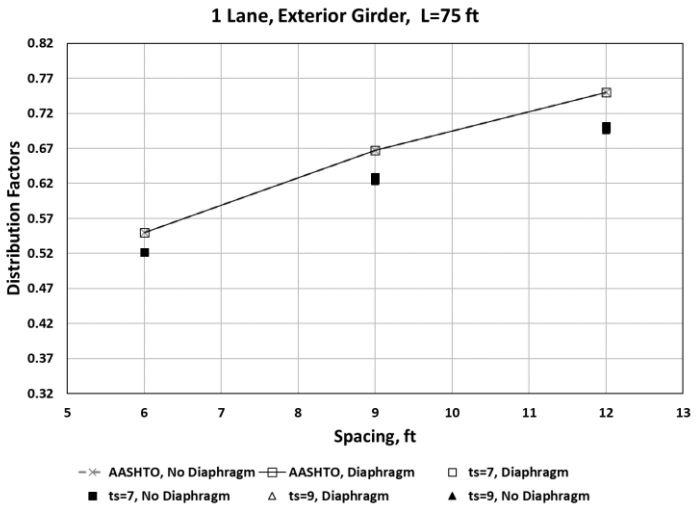

Figure 2.49. Grillage model and AASHTO load distribution factors for 75 ft span exterior Type-III girders, one lane loaded case versus girder spacing

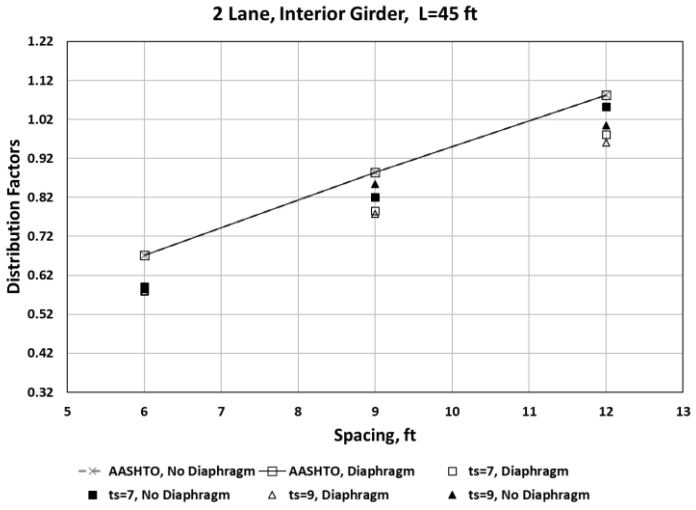

Figure 2.50. Grillage model and AASHTO load distribution factors for 45 ft span interior Type-III girders, two lanes loaded case versus girder spacing

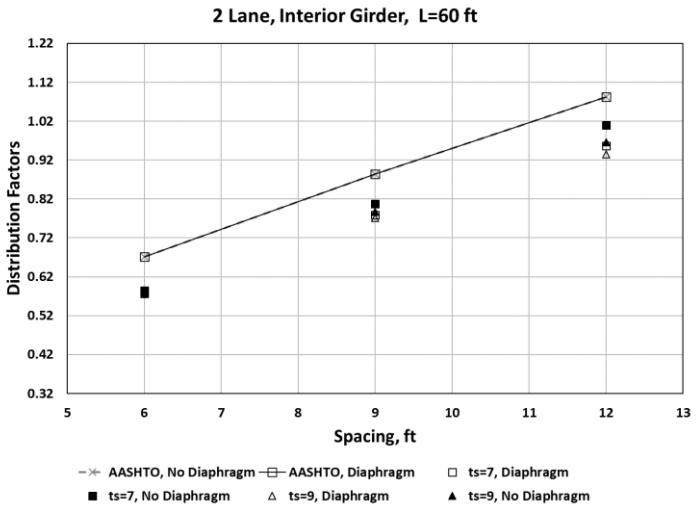

Figure 2.51. Grillage model and AASHTO load distribution factors for 60 ft span interior Type-III girders, two lanes loaded case versus girder spacing

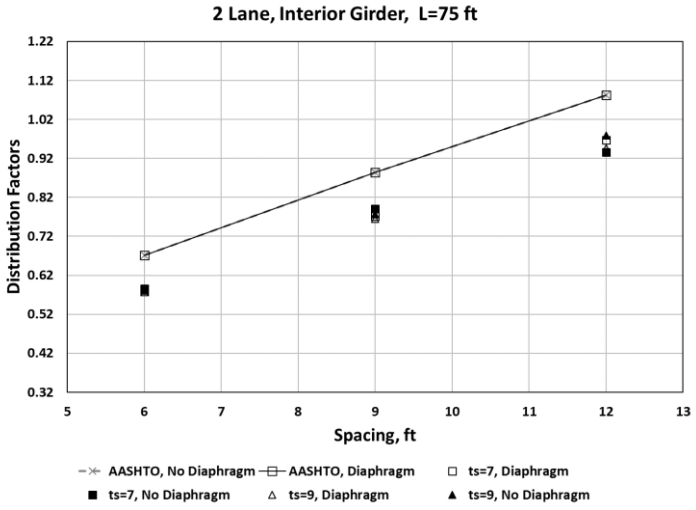

Figure 2.52. Grillage model and AASHTO load distribution factors for 75 ft span interior Type-III girders, two lanes loaded case versus girder spacing

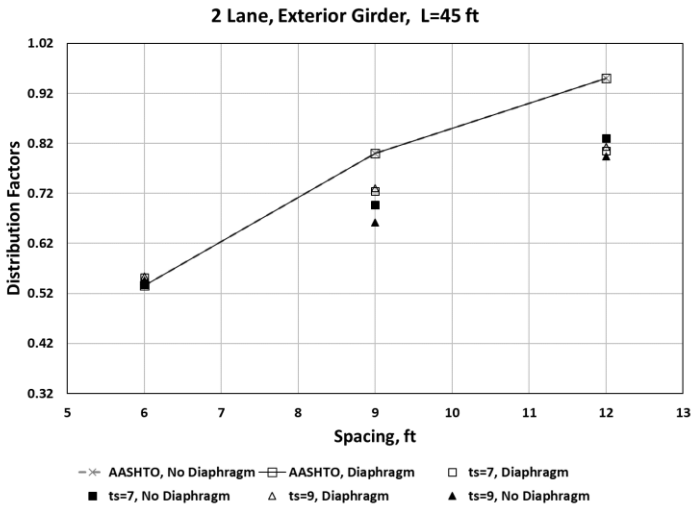

Figure 2.53. Grillage model and AASHTO load distribution factors for 45 ft span exterior Type-III girders, two lanes loaded case versus girder spacing

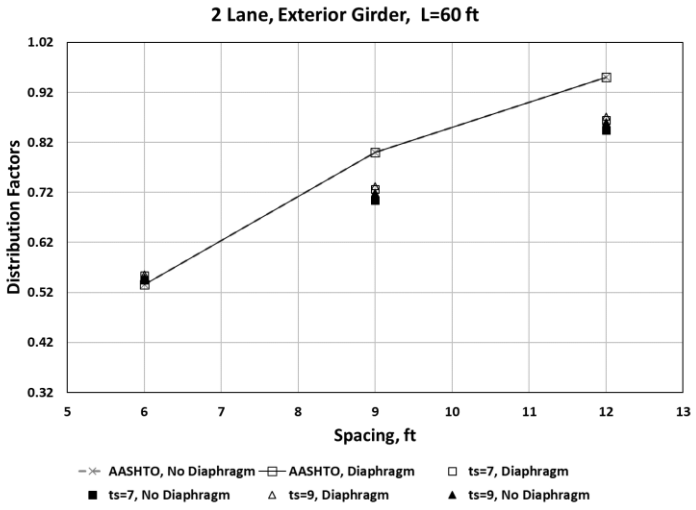

Figure 2.54. Grillage model and AASHTO load distribution factors for 60 ft span exterior Type-III girders, two lanes loaded case versus girder spacing

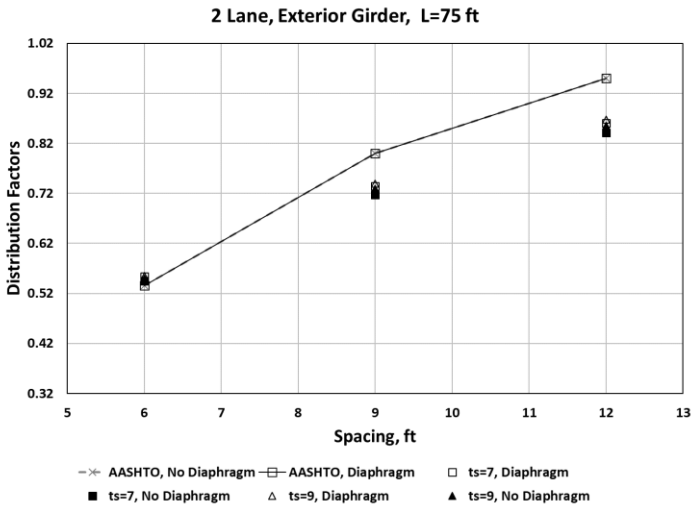

Figure 2.55. Grillage model and AASHTO load distribution factors for 75 ft span exterior Type-III girders, two lanes loaded case versus girder spacing

Figures 2.56-2.67 show the difference between the AASHTO LRFD distribution factors and those determined from the grillage models. These figures show that the AASHTO LRFD equations produce larger distribution factors compared to the grillage models for all cases. For the one lane loaded interior girder case it can be seen in Figures 2.56-2.58 that the AASHTO LRFD equation gives 16.3% to 21% higher distribution factors than the grillage model when girders are spaced at 6 ft. For the 9 ft and 12 ft girder spacing the difference between AASHTO LRFD equations and grillage model reduces to about 3.8% to 15.5% for all configurations considered for the Type-III girder. It can be seen from Figures 2.59-2.61 that for the exterior girder with one lane loaded case the AASHTO LRFD equations result in 4.9% to 11.2% higher load distribution factors than the grillage models for all configurations considered. Specifically, for the 6 ft, 9 ft, and 12 ft spacings the range is 4.9% to 5.3%, 5.7% to 11.2% and 5.8% to 7.5%, respectively.

Similarly, the case when two lanes are loaded for interior girders (Figure 2.62-2.64) the AASHTO LRFD equations give distribution factors 3.8% to 15.5% higher than the grillage models for 9 ft and 12 ft girder spacing, but for 6 ft girder spacing the AASHTO LRFD equation factors were larger by 11.9% to 14.2%. The difference between the AASHTO LRFD equation and grillage model factors for the two lanes loaded cases can be seen for interior and exterior girders in Figures 2.62-2.64 and 2.65-

2.67 respectively. For most cases considered, the AASHTO LRFD factors were larger than those from the grillage models. It should be noted that the when the bridge was loaded with two trucks on either end of the bridge in the transverse direction with minimum spacing of 4 ft between the trucks, the grillage models gave a larger distribution factor than the AASHTO LRFD equations for the 6 ft girder spacing. However, these differences were by a maximum of only 4% for all configurations considered for Type-III girders as shown in Figures 2.65-2.67.

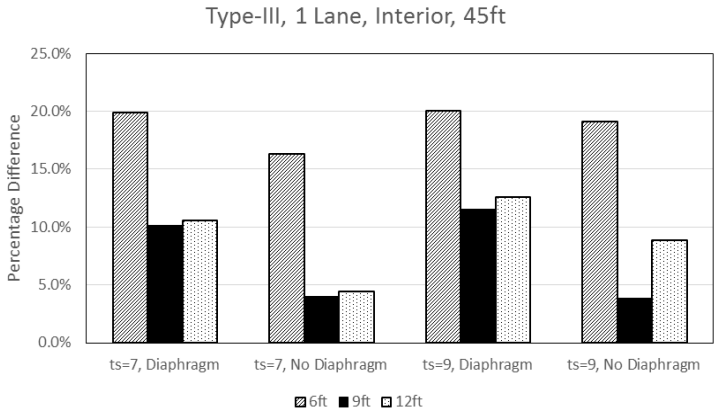

Figure 2.56. Percentage difference between AASHTO equations and grillage model derived load distribution factors for 45 ft span Type-III interior girders, one lane loaded case

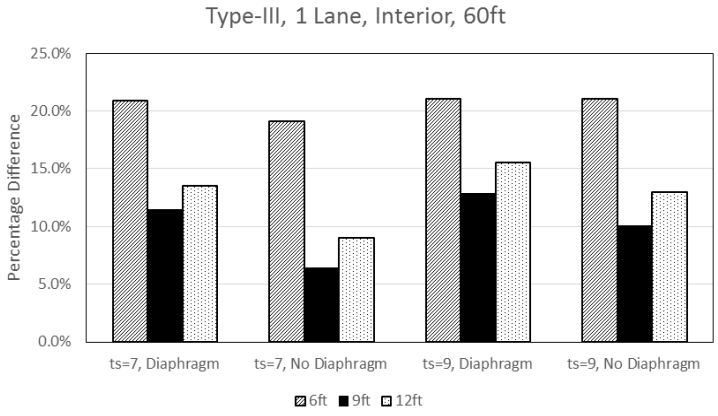

Figure 2.57. Percentage difference between AASHTO equations and grillage model derived load distribution factors for 60 ft span Type-III interior girders, one lane loaded case

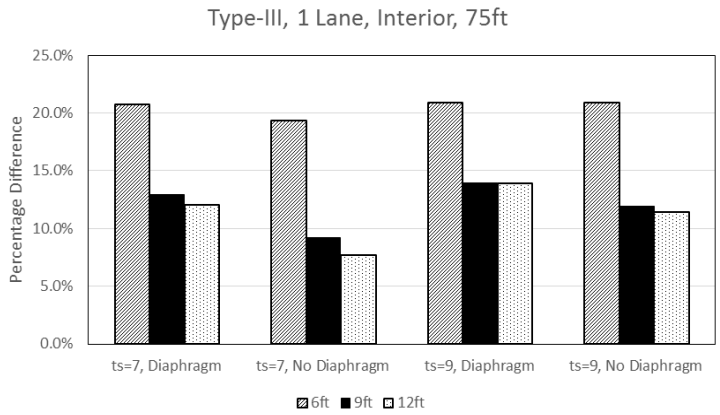

Figure 2.58. Percentage difference between AASHTO equations and grillage model derived load distribution factors for 75 ft span Type-III interior girders, one lane loaded case

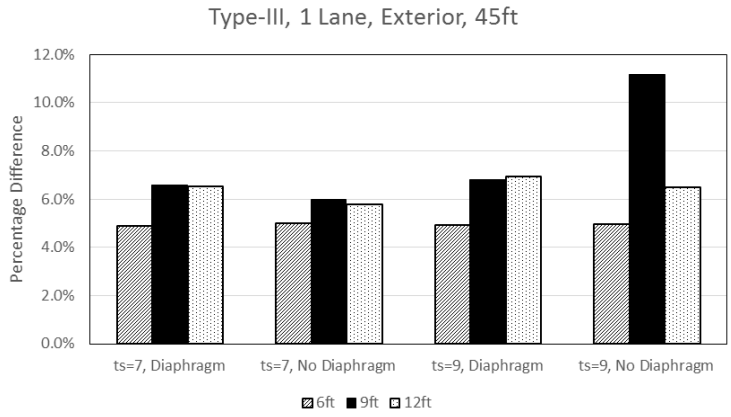

Figure 2.59. Percentage difference between AASHTO equations and grillage model derived load distribution factors for 45 ft span Type-III interior girders, two lanes loaded case

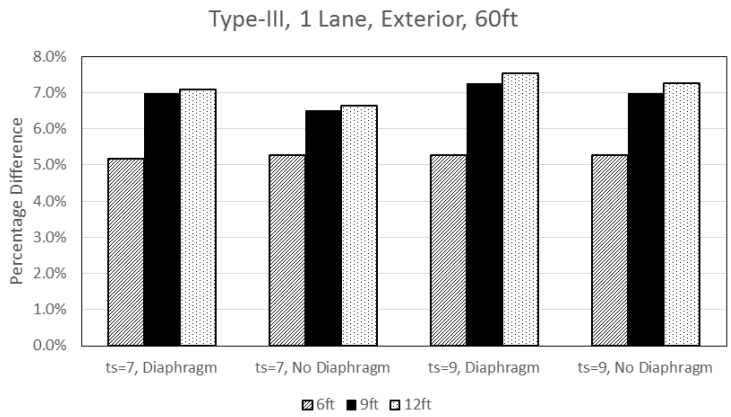

Figure 2.60. Percentage difference between AASHTO equations and grillage model derived load distribution factors for 60 ft span Type-III interior girders, two lanes loaded case

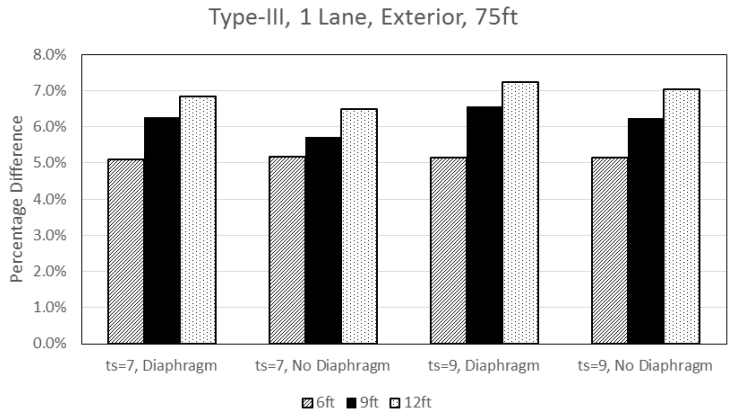

Figure 2.61. Percentage difference between AASHTO equations and grillage model derived load distribution factors for 75 ft span Type-III interior girders, two lanes loaded case

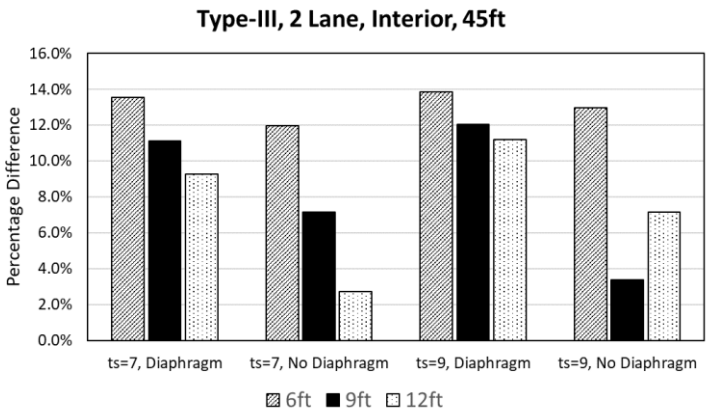

Figure 2.62. Percentage difference between AASHTO equations and grillage model derived load distribution factors for 45 ft span Type-III interior girders, two lanes loaded case

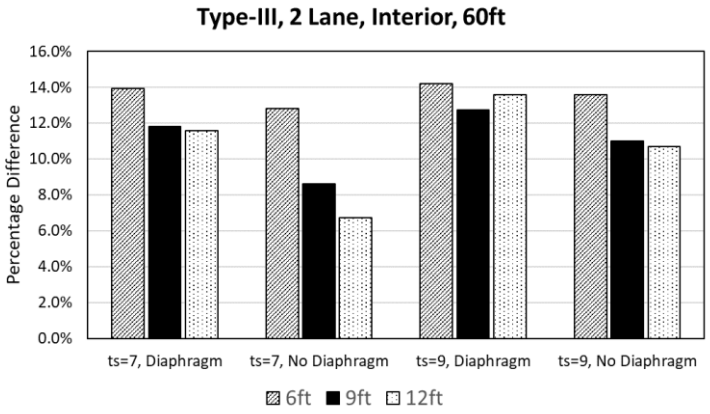

Figure 2.63. Percentage difference between AASHTO equations and grillage model derived load distribution factors for 60 ft span Type-III interior girders, two lanes loaded case

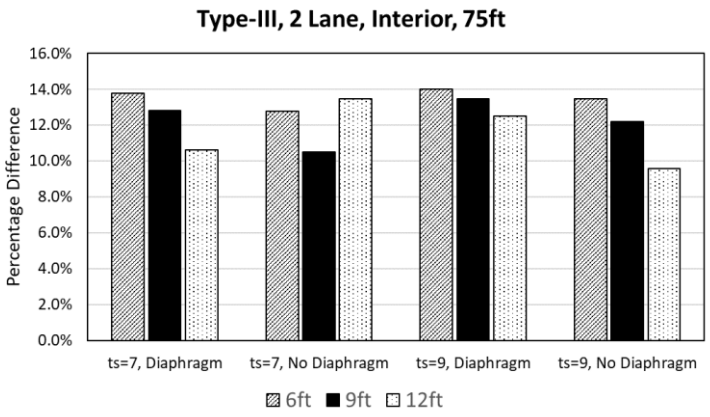

Figure 2.64. Percentage difference between AASHTO equations and grillage model derived load distribution factors for 75 ft span Type-III interior girders, two lanes loaded case

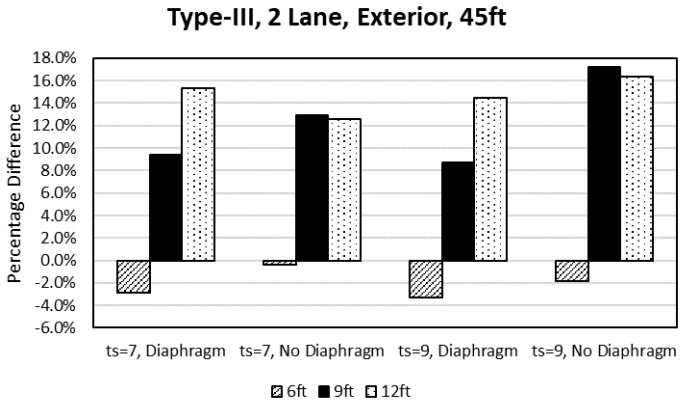

Figure 2.65. Percentage difference between AASHTO equations and grillage model derived load distribution factors for 45 ft span Type-III exterior girders, two lanes loaded case

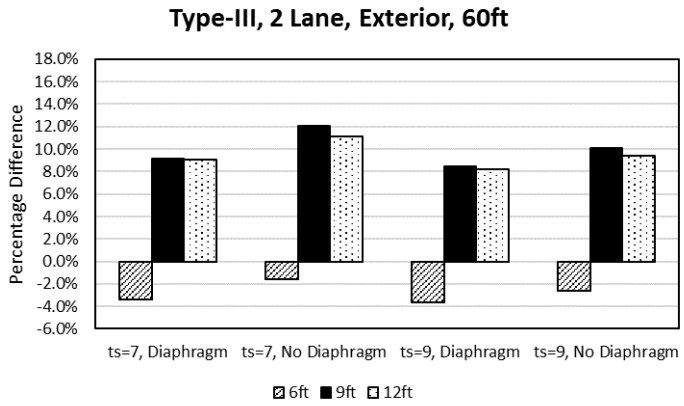

Figure 2.66. Percentage difference between AASHTO equations and grillage model derived load distribution factors for 60 ft span Type-III exterior girders, two lanes loaded case

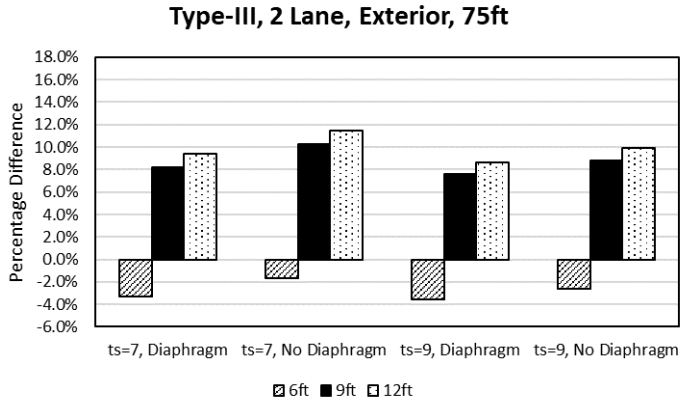

Figure 2.67. Percentage difference between AASHTO equations and grillage model derived load distribution factors for 75 ft span Type-III exterior girders, two lanes loaded case

2.5.3 Effects of Diaphragms

The AASHTO LRFD equations do not take the effect of the presence of transverse diaphragms into account directly. In general, the grillage models show that the effect of diaphragms is not significant. Nevertheless, the grillage models showed that diaphragms help in transfer of load to the adjacent girders. The load case for calculating maximum load distribution for exterior girders and one lane loaded is shown in Figure 2.68. This was the critical case for all the Type-III girder bridge configurations for exterior girders and the one lane loaded condition. It was observed that the reaction at the support of the interior girder was slightly higher when an end diaphragm was

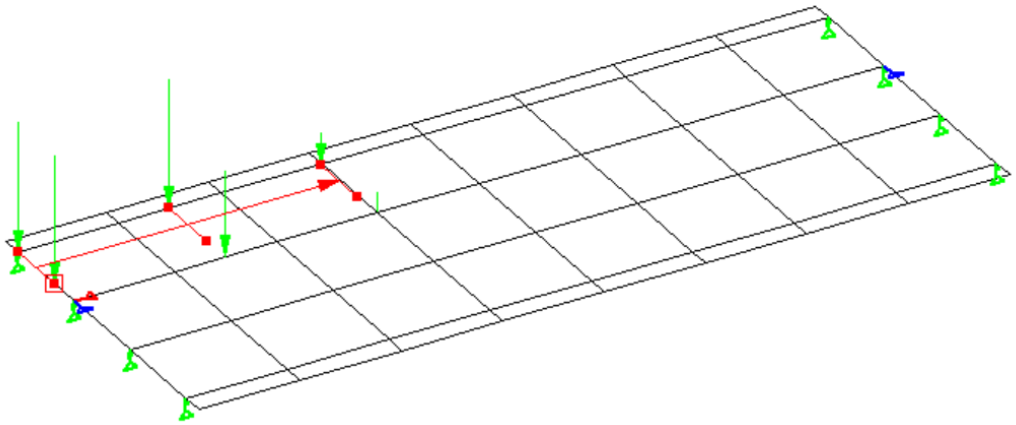

Figure 2.68. Grillage model showing the critical load case for exterior girder one lane loaded condition

present and less when there was no diaphragm for all the models. This behavior was more evident in plate models. This resulted in a smaller distribution factor for the exterior girder when a diaphragm was included. The difference between the reactions in cases of diaphragm and no diaphragm was small, which is why the effects cannot be seen clearly in graphs where comparisons are made. Similar trends can be seen in Figures 2.56-2.67 that the percentage difference between the AASHTO LRFD and grillage model distribution factors for no diaphragm cases are smaller than for the diaphragm cases. This is because of the better transfer of load to adjacent girders with end diaphragms. It should be noted that a higher percentage difference shows that the load distribution factor determined using grillage model was smaller than the AASHTO LRFD factor and vice versa.

2.5.4 Effects of Deck Thickness

The grillage model results showed that for the values examined, deck thickness had very little effect on load distribution. Some of the results given in Figures 2.56 to 2.67 are so close that it is difficult to differentiate between them visually. Generally, it was observed that the 9 in. thick deck resulted in slightly higher distribution factors than the 7 in. thick deck. For all of the models of Type-III girders examined, the distribution factor for the 9 in. thick deck cases was 2% - 4% higher than the load distribution factor for the 7 in. deck.

2.5.5 Effects of Span Length

The effect of span length for all the configurations considered can be divided into two types. The first type is bridges without diaphragms. The grillage model results for bridges without diaphragms show little or no effect of span length on the load distribution factor. The support reactions increased with an increase in span length, as expected, since the loads are placed close to one end of the bridge span such that with a longer span the other end of the bridge takes a smaller portion of the total truck load. However, the load distribution factors remained relatively constant since the load distribution factor is a ratio of the force taken by an individual girder to that of the entire reaction.

The second type is bridges with diaphragms. All the models with diaphragms had three diaphragms: one at the center of the span and one at each end. It was observed that shorter spans, which have less distance between the end and intermediate diaphragm, gave slightly better load distribution (smaller distribution factors) than for the bridges with the longer spans in which the distance between the intermediate and the end diaphragm is much greater. This was more evident for larger girder spacings. It can be observed from Figures 2.56-2.58 where, if the bars for the 12 ft spacing are compared with one another, it can be seen that percentage difference is higher for the 45 ft span and reduces for the 60 ft and 75 ft spans.

2.5.6 Quantitative Comparison of Load Distribution Factors

Figures 2.69-2.72 show linear trendlines for Type-III girder distribution factors relative to girder spacing for the four different load cases. All the variations investigated for each load case for Type-III girders are merged in one graph. For the interior girder one lane loaded case, shown in Figure 2.69, the AASHTO LRFD equation is linear with a slope of 0.0333, therefore, the coefficient of determination for the linear fit of the AASHTO distribution factors is 1.0. A linear trendline plotted for the different variations examined with grillage models gave a coefficient of determination 0.9454, indicating that a linear trend was an appropriate model. The AASHTO LRFD equation for an interior girder with two lanes loaded, is a quadratic. However, the slope of the quadratic is very small and linear trendline resulted in a reasonable coefficient of determination. The

same is true for the exterior girder with two lanes loaded since the distribution factor is based on the interior girder case. For all cases, a linear trendline gave a good fit of the data and the lowest coefficient of determination was 0.9454, indicating that spacing has a significant impact on load distribution factors. For all the cases, the grillage model gave less steep trendlines than the AASHTO LRFD equations except for the one lane loaded interior girder case where the slopes for AASHTO LRFD and grillage models were 0.0333 and 0.0371, respectively. The highest percentage difference in slope of

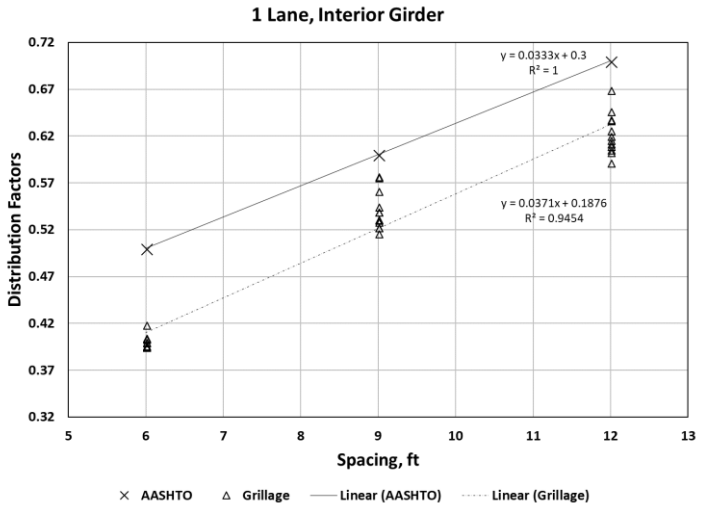

Figure 2.69. Linear trendlines for effect of girder spacing on distribution factors for interior Type-III girders, one lane loaded case

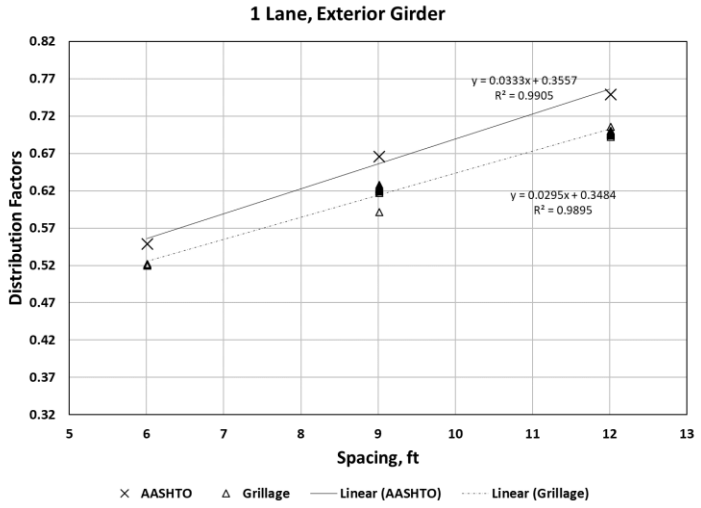

Figure 2.70. Linear trendlines for effect of girder spacing on distribution factors for exterior Type-III girders, one lane loaded case

29.4% was found for the two lanes loaded exterior girder case. The cases where the slope of the trendline for the grillage model data was less than for the AASHTO equations indicates that spacing has less of an impact on grillage model load distribution factors than for AASHTO LRFD distribution factors, even though spacing is still the primary variable.

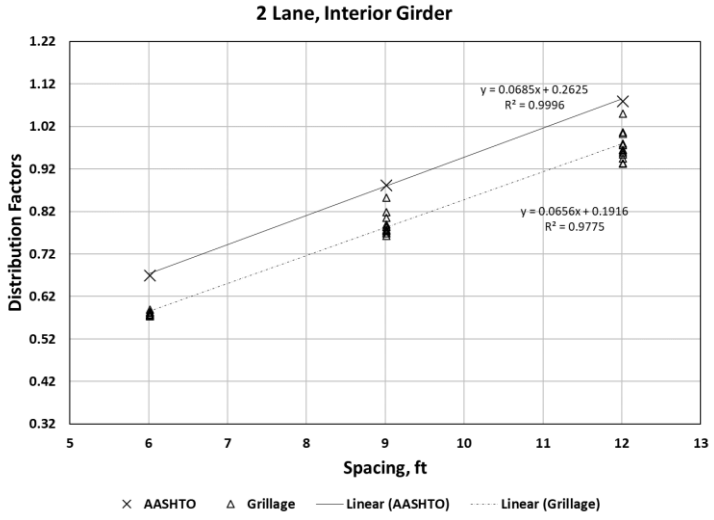

Figure 2.71. Linear trendlines for effect of girder spacing on distribution factors for interior Type-III girders, two lanes loaded case

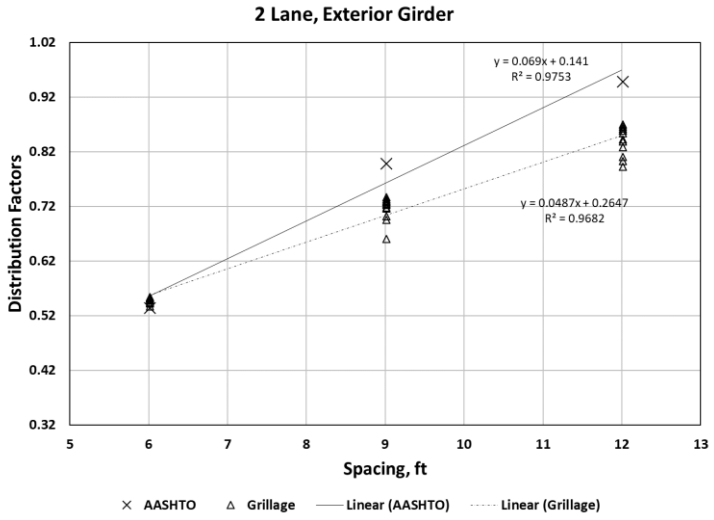

Figure 2.72. Linear trendlines for effect of girder spacing on distribution factors for exterior Type-III girders, two lanes loaded case

2.6 Summary of Grillage Parametric Study

It should be noted immediately that the equations in AASHTO were developed for much wider range of bridges than what was considered in this study and are only dependent on the spacing of girders unless the lever rule is applied or a special analysis is considered for the case of exterior girders and diaphragms. This could be the reason behind the larger load distribution factors for the AASHTO equations compared to the grillage models.

Table 2.13 presents a summary of the ranges of difference between the AASHTO LRFD distribution factors and the grillage model derived factors for all the configurations considered in this study. The major variable that controls the load distribution factor is the girder spacing, which is why Table 2.13 is arranged by spacing. This table can be interpreted using as an example when the one lane loaded case is

Table 2.13. Range of difference between AASHTO and grillage distribution factors (%)

Girder Type	Location	Load Case	6 ft Min	6 ft Max	9 ft Min	9 ft Max	12 ft Min	12 ft Max
Type-II	Interior	One Lane	14.4	25.9	-2.4	14.7	-1.8	16.3
Type-II	Interior	Two Lane	34.2	34.5	20.3	30.0	5.0	13.2
Type-II	Exterior	One Lane	-5.1	4.8	5.3	6.8	5.2	7.8
Type-II	Exterior	Two Lane	7.0	7.2	3.2	17.6	7.7	19.5
Type-III	Interior	One Lane	16.3	21.0	3.8	14.0	4.4	15.5
Type-III	Interior	Two Lane	11.9	14.2	3.4	13.5	2.7	13.6
Type-III	Exterior	One Lane	4.9	5.3	5.7	11.2	5.8	7.5
Type-III	Exterior	Two Lane	-0.4	-3.6	7.6	17.2	8.2	16.4
Type-IV	Interior	One Lane	18.2	21.6	9.6	21.4	8.6	16.0
Type-IV	Interior	Two Lane	12.3	14.7	10.9	13.9	7.0	14.0
Type-IV	Exterior	One Lane	5.3	6.4	6.4	7.3	6.4	7.8
Type-IV	Exterior	Two Lane	-0.6	-3.2	8.0	10.7	7.7	11.3
BT-63	Interior	One Lane	21.5	22.5	13.5	16.1	14.7	18.0
BT-63	Interior	Two Lane	14.0	15.1	13.8	15.5	1.9	15.9
BT-63	Exterior	One Lane	10.0	11.1	10.9	12.3	10.4	11.8
BT-63	Exterior	Two Lane	-0.7	-2.2	11.3	12.5	11.1	12.1
BT-72	Interior	One Lane	20.6	22.4	12.2	16.1	12.3	18.0
BT-72	Interior	Two Lane	13.5	14.8	13.3	15.5	12.6	15.7
BT-72	Exterior	One Lane	11.0	11.1	11.3	12.3	7.1	11.8
BT-72	Exterior	Two Lane	-0.4	-1.5	11.6	12.9	10.4	12.2

considered for Type III girders with a 6 ft spacing and interior girder the range of difference between the AASHTO LRFD and grillage mode load distribution factors is 16.3% to 21.0%. It should be noted that this range includes the effects of variations in the other three parameters considered, i.e. deck thickness, span length, and presence of diaphragms. Considering that both the AASHTO equations and grillage models are allowed for analysis of load distribution, Table 2.13 can be used to identify situations where use of grillage models may be beneficial for load rating.

Table 2.14 summarizes the slopes of trendlines for distribution factors relative to girder spacing plotted for AASHTO LRFD equations and the grillage model results. For all of the cases, except for the one lane loaded interior girder case of Type-III girders, the AASHTO LRFD equations produce a steeper slope than grillage models. The largest deviation among slopes can be observed for the two lanes loaded exterior case for all of the girder types. The comparison of slopes indicates that the effect of girder spacing on distribution factors determined using grillage models was generally similar to or less than for the AASHTO equations.

Table 2.14. Summary of distribution factor vs spacing trendline slopes

Girder Type	Load Case	Location	AASHTO	Grillage Models	% Difference
Type-III	One Lane	Interior	0.0333	0.0371	-11.4
Type-III	One Lane	Exterior	0.0333	0.0295	11.4
Type-III	Two Lanes	Interior	0.0685	0.0656	4.2
Type-III	Two Lanes	Exterior	0.0690	0.0487	29.4
Type-IV	One Lane	Interior	0.0333	0.0329	1.2
Type-IV	One Lane	Exterior	0.0333	0.0299	10.2
Type-IV	Two Lanes	Interior	0.0685	0.0629	8.2
Type-IV	Two Lanes	Exterior	0.0690	0.0518	24.9
BT-63	One Lane	Interior	0.0333	0.0324	2.7
BT-63	One Lane	Exterior	0.0333	0.0293	12.0
BT-63	Two Lanes	Interior	0.0685	0.0568	17.1
BT-63	Two Lanes	Exterior	0.0690	0.0496	28.1
BT-72	One Lane	Interior	0.0333	0.0332	0.3
BT-72	One Lane	Exterior	0.0333	0.0300	9.9
BT-72	Two Lanes	Interior	0.0685	0.0583	14.9
BT-72	Two Lanes	Exterior	0.0690	0.0498	27.8

Several items can be identified from the results of the parametric study. The potential conservativism of the code distribution factors is primarily affected by girder spacing. For interior girders, smaller girder spacings (6 ft) result in more conservative distribution factors, while the widest spacings (12 ft) are still potentially conservative, although to a lesser degree. The opposite trend was apparent for exterior girders, where a larger spacing resulted in a larger level of conservativism. When comparing the effects of girder spacing on distribution factors determined from grillage models and the AASHTO equations, a linear fit of the grillage derived data resulted in a shallower slope than for the AASHTO equation. In general, based on the results of this study the code distribution factors are less conservative for exterior girders than interior girders except at larger girder spacings.

For interior girders, longer spans tended to result in more conservative AASHTO Distribution factors compared to those determined using grillage models. For exterior girders on the other hand, shorter spans resulted in more conservative distribution factors when other variables were equal. Span length has more of an effect on load distribution for larger girder spacings. Shorter span lengths lead to less conservative distribution factors for interior girders, and more conservative distribution factors for exterior girders. The effect of span length on shear load distribution also reduces with increases in span length. A minimum span length of 30 ft and maximum of 150 ft were used in this study. When the models with span lengths of 45 ft and 60 ft were compared with all other remaining parameters remaining identical, the range of change in load distribution factor determined using grillage models was 0.2% to 7.6%. When the spans lengths of 135 ft and 150 ft were considered the percentage change was only 0% to 3.6%.

Deck slab thickness had the smallest effect on distribution of all the factors examined. The deck thickness did not substantially affect load distribution for the two thicknesses modeled. The change in load distribution factors, determined using grillage model, when the deck thickness was changed from 7 in to 9 in for a given set of conditions was 0% to 6% for Type-III and Type-IV girders. The change was 0% to 3% for Type II, BT-63 and BT-72 girders for all the cases. In one odd case of BT-63 girder bridge configurations the percentage change was 8.1%.

The presence of diaphragms appears to cause the opposite effects for interior and exterior girders; diaphragms decrease distribution factors for interior girders and increase distribution factors for exterior girders. The code accounts for this behavior for exterior girders, but not for interior girders. In general, the code factors are less conservative for interior and exterior girders without diaphragms than with diaphragms. Span length and slab thickness affect the conservativism of the code factors more when diaphragms are not present than when they are present. The effect of intermediate diaphragms on shear load distribution reduces with increases in span length. It should be noted that there was only one intermediate diaphragm provided for each span length, therefore with an increase in span length the distance between end and intermediate diaphragms also increased.

The shear load distribution factors calculated using the AASHTO LRFD equations were greater than grillage model results for all but a handful of cases. For the one lane and two lanes loaded case for interior girders, the AASHTO LRFD equation shear load distribution factors were found to be -2.4% to 25.9% and 1.9% to 34.5%, respectively, greater than the corresponding grillage model derived factors. For the exterior girder one lane loaded case the AASHTO LRFD equation shear load distribution factors were -5.1% to 12.3% greater than those determined using the grillage model. For the exterior girder two lanes loaded case with 6 ft spacing the grillage models gave greater shear load distribution factors than the AASHTO LRFD equation by a maximum of 3.6% and for other spacings the distribution factors calculated using the AASHTO LRFD equation were greater than those derived from the grillage models by a maximum of 17.2%. It should be noted that the ranges given here include influence of all the parameters considered.

2.7 Comparison of Plate and Grillage Models

For the comparison of grillage models with plate models only Type-III and BT-72 girders along with the smallest and largest girder spacing were considered for comparison. This was intended to bracket the possible results for girder type and girder spacing. Even though the results for the grillage and plate models presented in Table 2.4 are almost identical and validate the modeling paradigm, they are still not conclusive

because of the smaller size of the bridge. The differences can be analyzed in a better way by comparing models of real bridges. Tables 2.15 and 2.16 summarize the models considered for this comparison.

Table 2.15. Type III girder bridge plate models (deck thickness in in. on interior of table)

Spacing (ft)	45 ft Span	45 ft Span	75 ft Span	75 ft Span	Presence of Diaphragms
6	7	9	7	9	Diaphragm
6	7	9	7	9	No Diaphragm
12	7	9	7	9	Diaphragm
12	7	9	7	9	No Diaphragm

Table 2.16. BT-72 girder bridge plate models (deck thickness in in. on interior of table)

Spacing (ft)	120 ft Span	120 ft Span	150 ft Span	150 ft Span	Presence of Diaphragms
6	7	9	7	9	Diaphragm
6	7	9	7	9	No Diaphragm
12	7	9	7	9	Diaphragm
12	7	9	7	9	No Diaphragm

Figures 7.73 – 7.80 present comparisons of the load distribution factors determined using plate and grillage models. These figures not only compare the grillage and plate model results, but also show the impact of the diaphragms, girder spacing and deck thickness. When the Type-III and BT-72 girders are compared, the bars representing load distribution factors follow the same pattern for most cases. To simplify the situation, the comparisons are divided into eight sets of graphs. For the 12 ft spacing and two lanes loaded case, as shown in Figures 2.73 – 2.76, the plate model gives larger load distribution factors than grillage model for the exterior girder and vice versa for the interior girder. For the one lane loaded case and 12 ft spacing the behavior is opposite that of two lanes loaded case as shown in Figures 2.77 – 2.80.

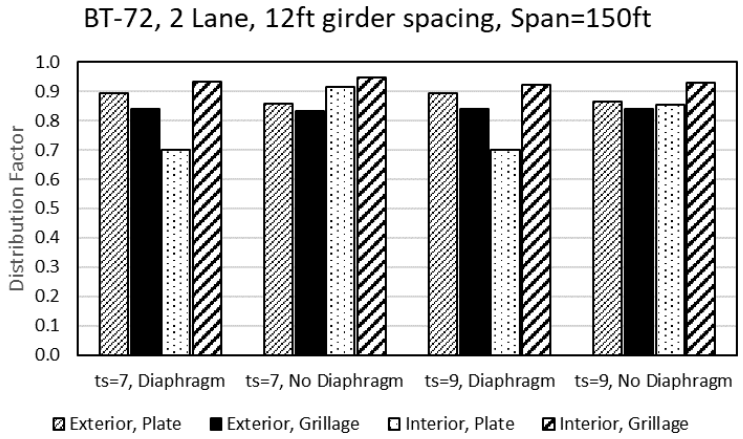

Figure 2.73. Comparison of plate and grillage models for 12 ft spacing and 2 lanes loaded case for BT-72 girders with 150 ft span

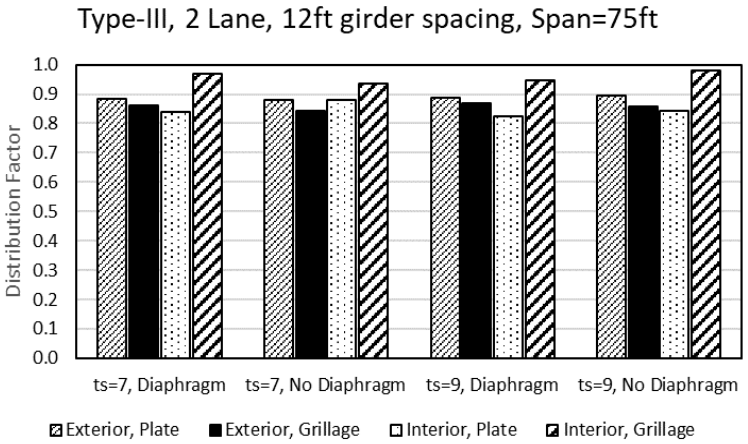

Figure 2.74. Comparison of plate and grillage models for 12 ft spacing and 2 lanes loaded case for Type III girders with 75 ft span

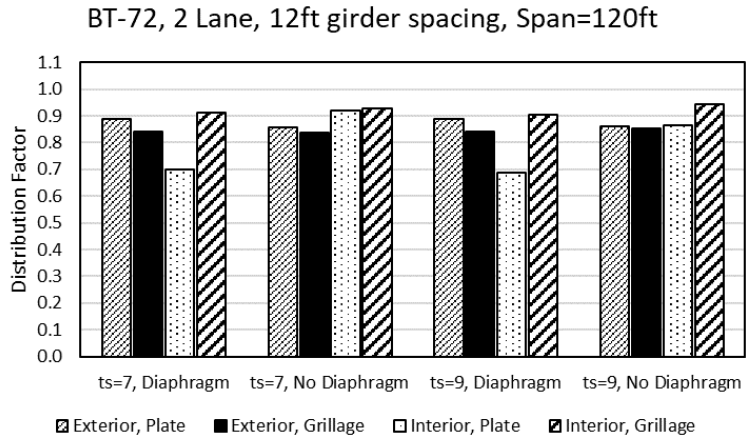

Figure 2.75. Comparison of plate and grillage models for 12 ft spacing and 2 lanes loaded case for BT-72 girders with 120 ft span

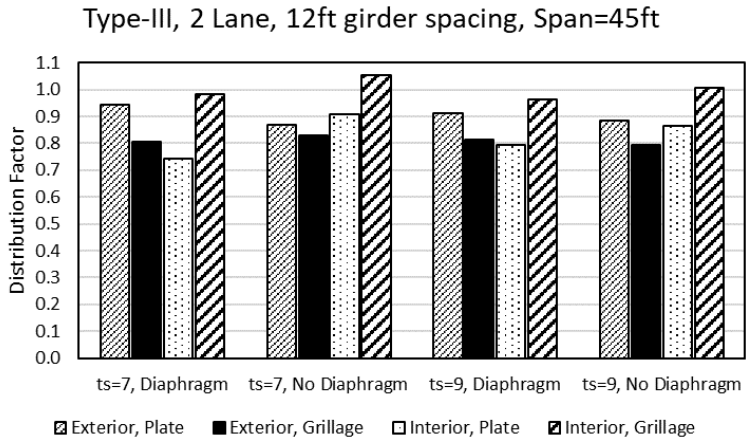

Figure 2.76. Comparison of plate and grillage models for 12 ft spacing and 2 lanes loaded case for Type-III girders with 45 ft span

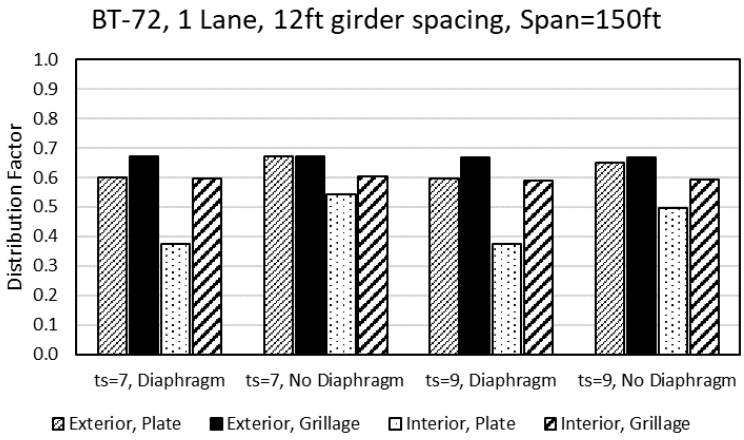

Figure 2.77. Comparison of plate and grillage models for 12 ft spacing and 1 lane loaded case for BT-72 girders with 150 ft span

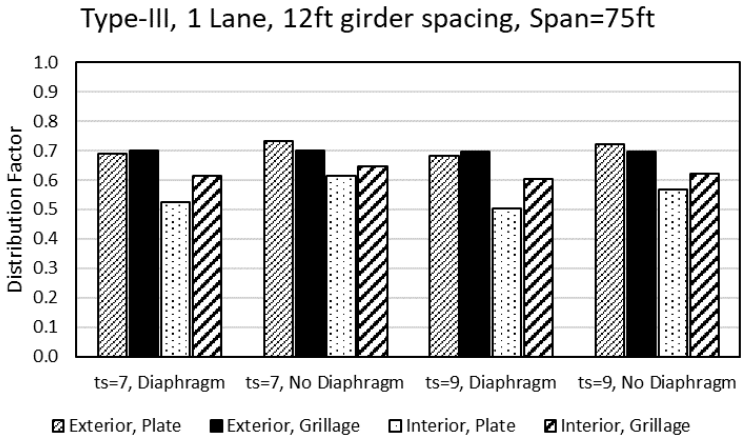

Figure 2.78. Comparison of plate and grillage models for 12 ft spacing and 1 lane loaded case for Type-III girders with 75 ft span

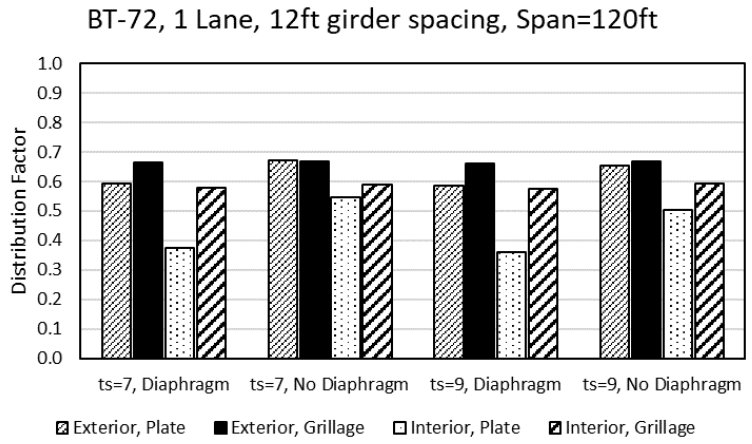

Figure 2.79. Comparison of plate and grillage model for 12 ft spacing and 1 lane loaded case for BT-72 girders with 120 ft span

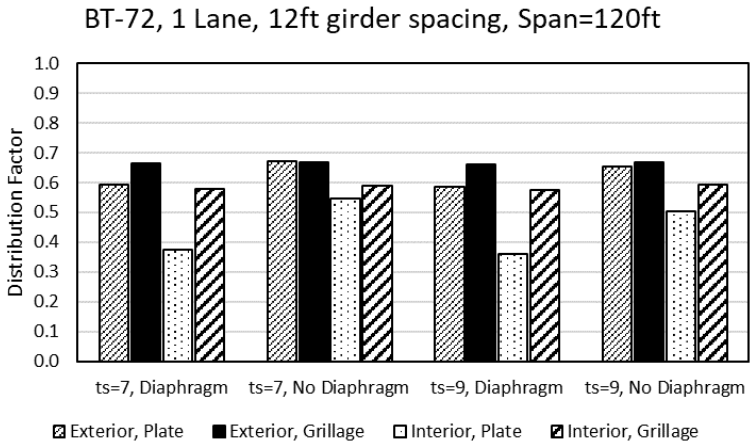

Figure 2.80. Comparison of plate and grillage model for 12 ft spacing and 1 lane loaded case for Type-III girders with 45 ft span

When the spacing of the girders is 6 ft and two lanes are loaded, the pattern is the same as 12 ft spacing and two lanes loaded as shown in Figures 2.81 – 2.84. For the one lane loaded case with 6 ft spacing the pattern is different for the different types of girder. For Type-III girders, plate models give greater load distribution factors for exterior girders and grillage models give greater load distribution factors for interior girders. The results are opposite in case of BT-72 girders as shown in Figures 2.85 – 2.88. The governing load cases should also be kept in mind (discussed in section 2.2.2) to better understand of these patterns because these graphs are based on multiple load cases. It can be observed from Figures 2.77 and 2.78 and 2.81 and 2.82 that

diaphragms had a negligible impact on load distribution factor when grillage models were used for these configurations. The plate models, however, exhibited larger effects from the presence of diaphragms. To determine the maximum load distribution factor for the interior beam, the center of the 6 ft wide HS-20 truck was placed over the interior beam. Since plate models have better lateral load distribution than the grillage models, the plate models always had a smaller load distribution factor for interior beams than the grillage models.

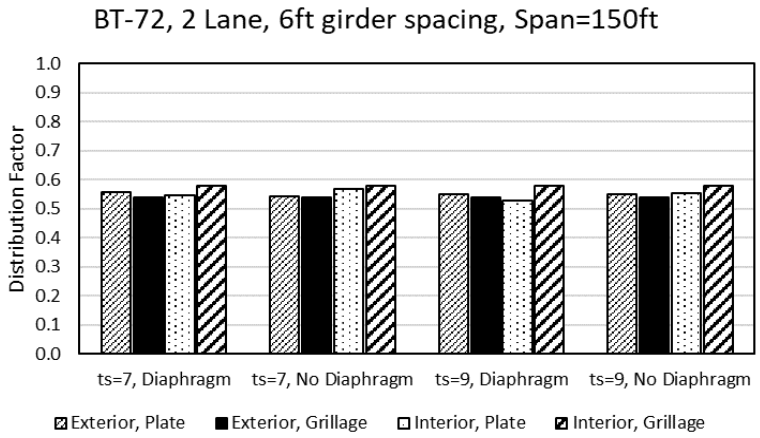

Figure 2.81. Comparison of plate and grillage model for 6 ft spacing and 2 lanes loaded case for BT-72 girders with 150 ft span

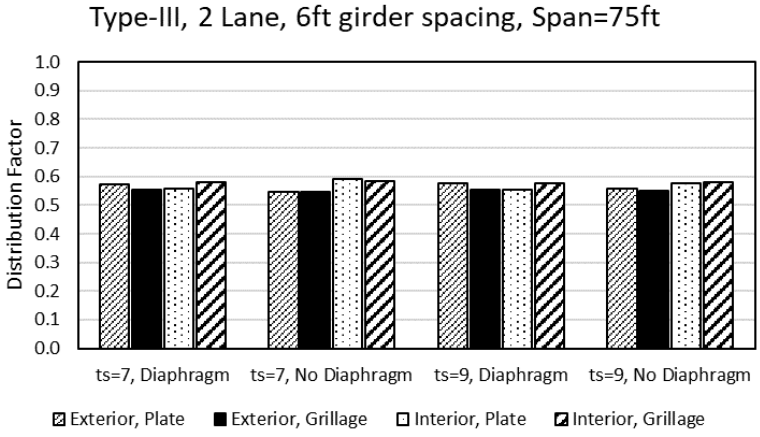

Figure 2.82. Comparison of plate and grillage model for 6 ft spacing and 2 lanes loaded case for Type-III girders with 75 ft span

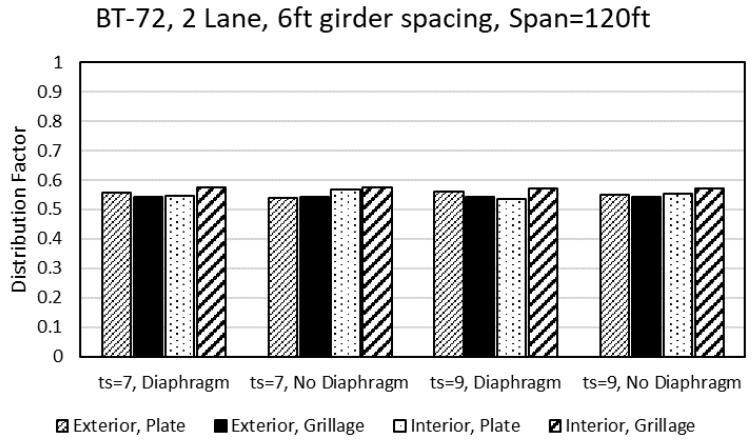

Figure 2.83. Comparison of plate and grillage models for 6 ft spacing and 2 lanes loaded case for BT-72 girders with 120 ft span

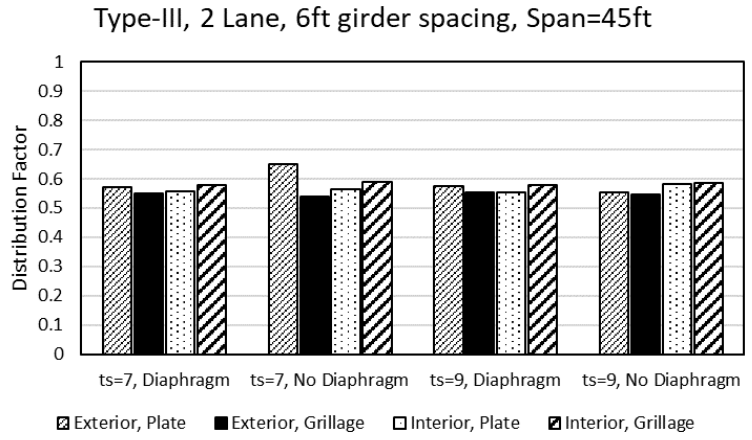

Figure 2.84. Comparison of plate and grillage models for 6 ft spacing and 2 lanes loaded case for Type III girders with 45 ft span

A variation in load distribution factor for interior and exterior girders is noticeable when diaphragm and no diaphragm cases are compared for plate models. This variation is not significant in grillage models. Figures 2.81 – 2.84 present the 2 lanes loaded case with 6 ft girder spacing. All the load distribution factors shown in Figures 2.81 – 2.84 are almost the same. Only four girders are used for all the models. Therefore, for a 6 ft girder spacing, the width of the deck is 22 ft if a 2 ft overhang is included on each side and the distance from first girder to the last is 18 ft. When two HS-20 are placed on this bridge configuration, most of the bridge deck is loaded and it is difficult to determine the impact of different parameters, including the use of a plate for the deck. Figures 2.85 –

2.88 show the load distribution factors for the 6 ft girder spacing and one lane loaded case. In this case, there is not much impact visible from the diaphragms because of the small girder spacing. The results show that diaphragms only impact the distribution factors when the spacing is higher than 6 ft. It can be noticed that the load distribution factor for the Type-III exterior girder is higher than the load distribution factor for the BT-72 exterior girder. It could have been due to the span length, which changes the distance between end and intermediate diaphragms. When only the section properties of Type-III girder were changed to BT-72, the lateral distribution improved, and the exterior girder attracts less force thus resulting in a smaller load distribution factor. It can therefore be said that lateral distribution is better with the stiffer girders.

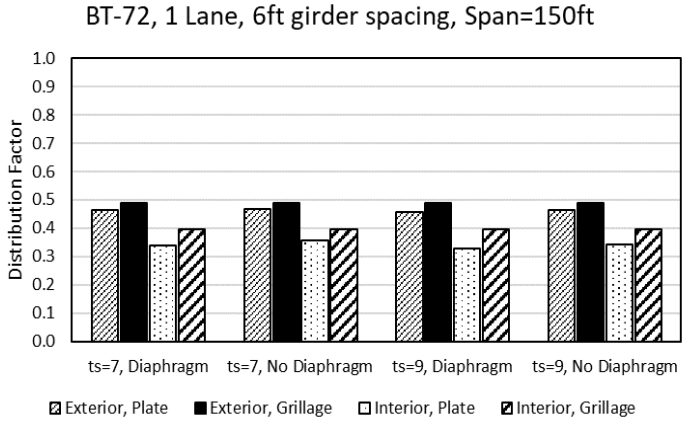

Figure 2.85. Comparison of plate and grillage models for 6 ft spacing and 1 lane loaded case for BT-72 girders with 150 ft span

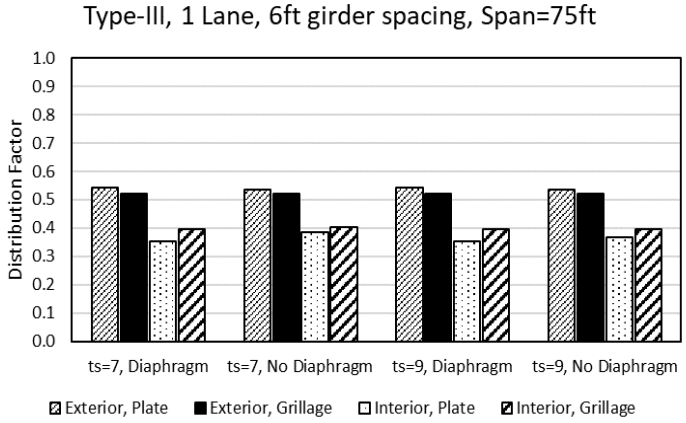

Figure 2.86. Comparison of plate and grillage models for 6 ft spacing and 1 lane loaded case for Type-III girders with 75 ft span

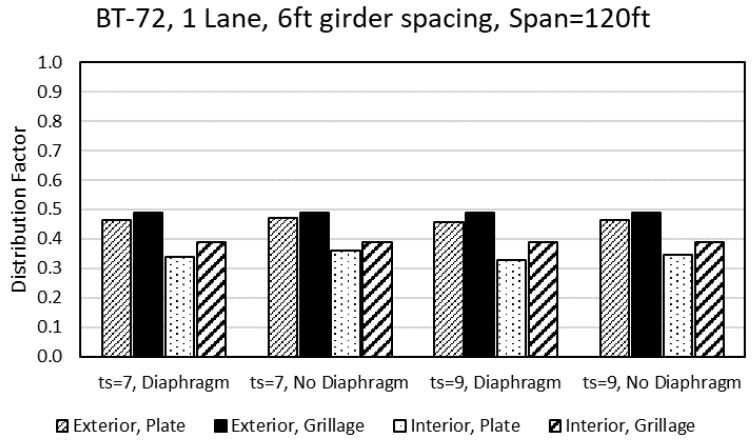

Figure 2.87. Comparison of plate and grillage models for 6 ft spacing and 1 lane loaded case for BT-72 girders with 120 ft span

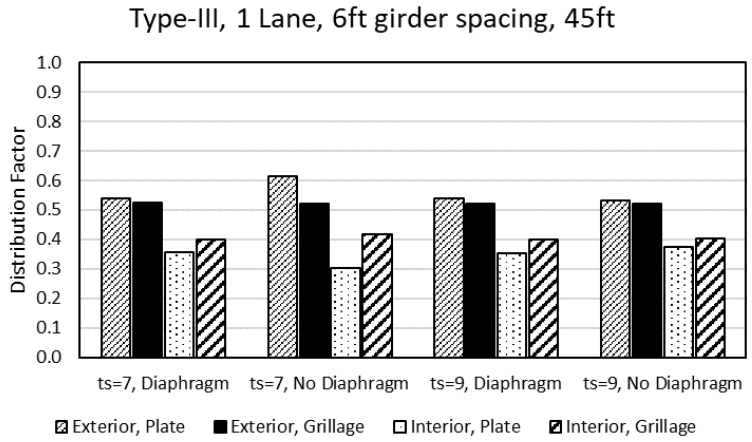

Figure 2.88. Comparison of plate and grillage models for 6 ft spacing and 1 lane loaded case for Type-III girders with 45 ft span

The plate model and grillage model results were quite comparable. A deviation was observed when the spacing between the girders increased. The impact of diaphragms on load distribution was more evident for plate models than grillage models particularly when the girder spacing was high.

2.8 Collection of Previous Experimental Results

Data from experimental shear testing available in the literature including girder type, bridge configuration, experimental capacity, and calculated capacity was collected. The focus of this endeavor was on AASHTO Type II and Type III girders since these are

the most likely to be affected by the previous codes. This included information from previous tests conducted at OU sponsored by ODOT (Floyd et al. 2016), work sponsored by the Florida Department of Transportation (Shahawy et al. 1993), large projects performed at the University of Texas focused on creating a shear database (Nakamura 2011), and other smaller testing programs performed across the country (Osborn et al. 2012, Ross et al. 2011). More information on the projects from which the data were taken is provided in Section 1.5. Other data were identified for larger girders, but these were not included in the summary data. The data collected includes more than 70 tests of AASHTO Type II girders of various ages.

All data were compiled into a spreadsheet including girder type, design drawings where available, concrete compressive strength, loading configuration, ultimate measured applied shear, calculated shear capacity, ratio of applied to calculated shear capacity and relationship of applied moment to flexural capacity of the member. This information can be used to inform capacity calculations for in-service members.

A comparison of the ratio of maximum experimental shear to calculated shear capacity using the AASHTO LRFD (2007) modified compression field theory (MCFT) method for the AASHTO Type II girders tested in previous research sponsored by ODOT (Floyd et al. 2016) based on *a*/*d* ratio is shown in Figure 2.89. It can be seen that

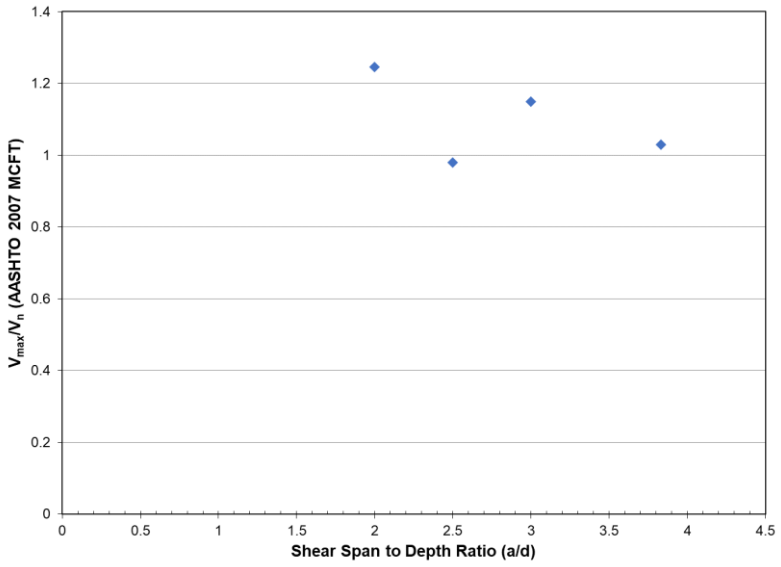

Figure 2.89. Comparison of experimental shear to calculated capacity for girders tested by Floyd et al. (2016) relative to a/d ratio

in general the calculated capacity was more conservative for smaller *a*/*d* ratios. The exception tested at an *a*/*d* ratio of 2.5 exhibited strand slip due to strand corrosion.

A similar comparison is shown in Figure 2.90 for failure type based on the AASHTO Standard Specifications used for original design of the girders.

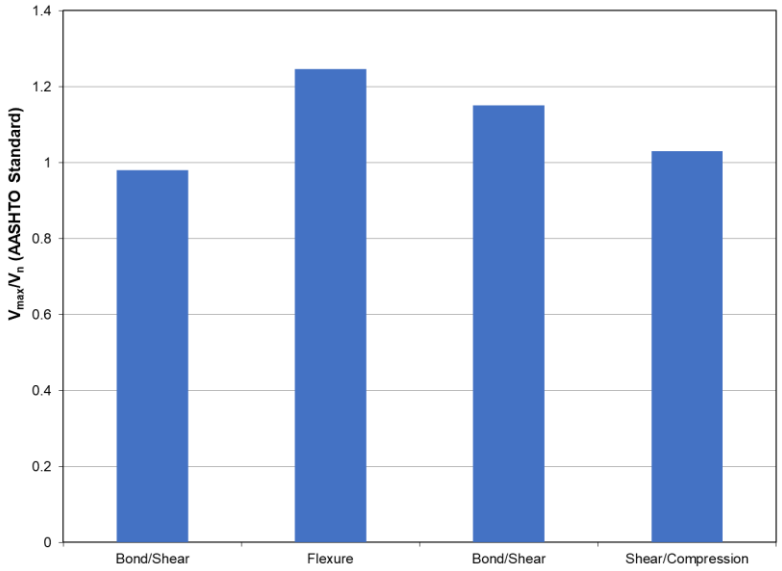

Figure 2.90. Comparison of experimental shear to calculated capacity for girders tested by Floyd et al. (2016) relative to failure type

Seven girders from a 42-year-old bridge in Utah were obtained to determine effective prestress force and ultimate shear capacity. The shear tests were performed at *a*/*d* = 1.5 using a single point load for two of the girders. The authors found that the code equations were conservative for the failure loads observed in testing. The research showed that STM was more accurate for loads near a discontinuity and a finite element model showed that concrete compressive strength had a larger effect on shear capacity than stirrup spacing (Osborn et al. 2012).

A comparison of the ratio of maximum experimental shear to calculated shear capacity using the AASHTO LRFD (2009) MCFT method for the AASHTO Type II girders tested by Osborn et al. (2012) based on *a*/*d* ratio is shown in Figure 2.91. These girders were tested at a small *a*/*d* ratio of 1.5, and in both cases the MCFT method produced a conservative prediction of capacity. A similar comparison is shown in Figure 2.92 for failure type based on the AASHTO LRFD (2009) MCFT.

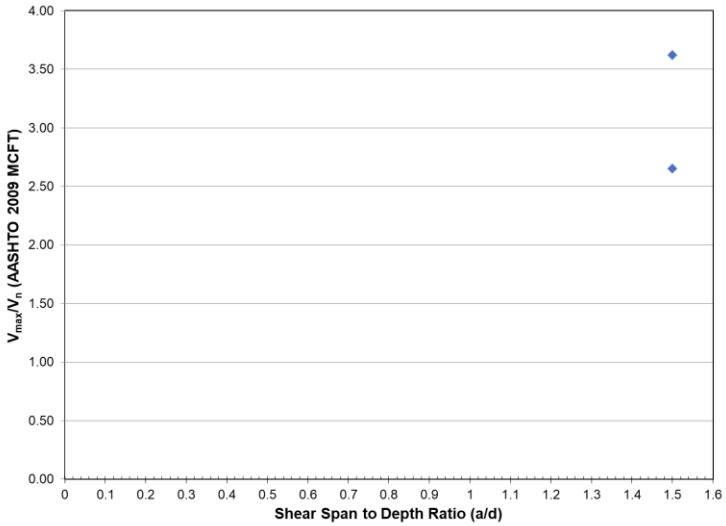

Figure 2.91. Comparison of experimental shear to calculated capacity for girders tested by Osborn et al. (2012) relative to a/d ratio

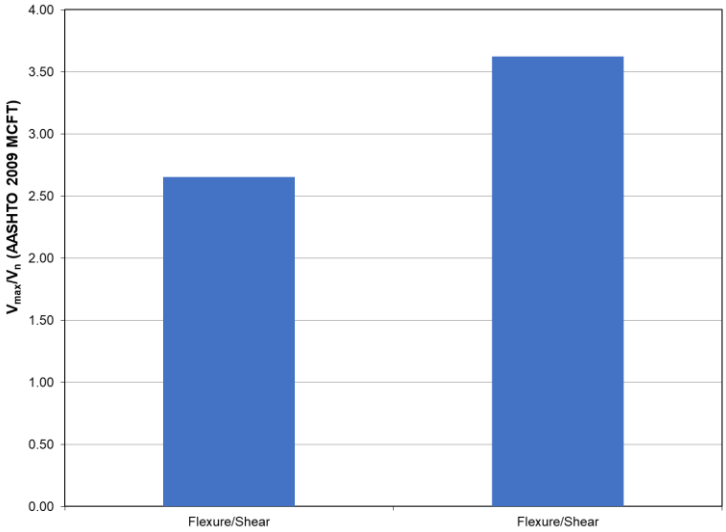

Figure 2.92. Comparison of experimental shear to calculated capacity for girders tested by Osborn et al. (2012) relative to failure type

Shahawy et al. (1993) performed 64 tests of AASHTO Type II girders constructed specifically for testing. However, tests exhibiting pure flexural failure were not included in the following discussion. A comparison of the ratio of maximum experimental shear to calculated shear capacity using the AASHTO Standard Specifications method for the AASHTO Type II girders tested by Shahawy et al. (1993) based on *a*/*d* ratio is shown in Figure 2.93. A number of shear tests exhibited non-conservative results. The capacity calculated with the AASHTO Standard method tends to overestimate steel capacity due

to the use of a small shear crack angle and tends to underestimate concrete capacity due to a low maximum compressive strength. A similar comparison is shown in Figure 2.94 for failure type. This figure indicates that all tests with non-conservative predicted capacities exhibited some type of bond failure that is not explicitly considered by the AASHTO Standard method for shear capacity.

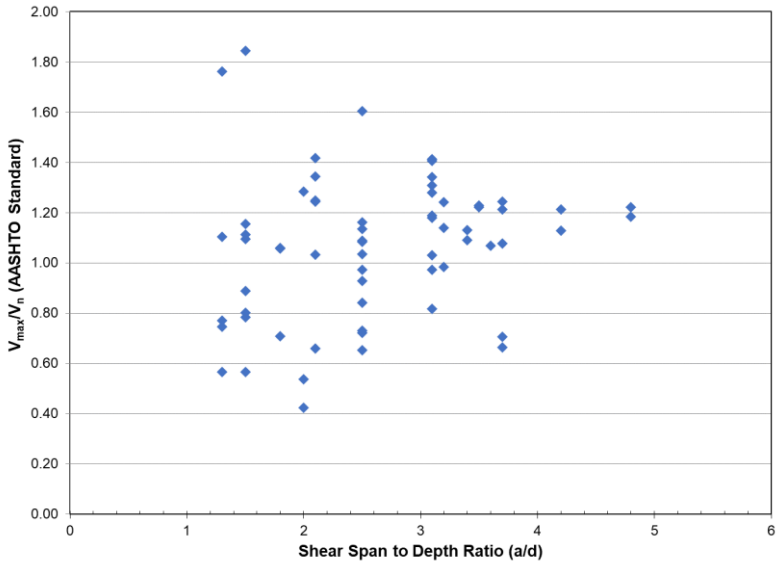

Figure 2.93. Comparison of experimental shear to calculated capacity for girders tested by Shahawy et al. (1993) relative to a/d ratio

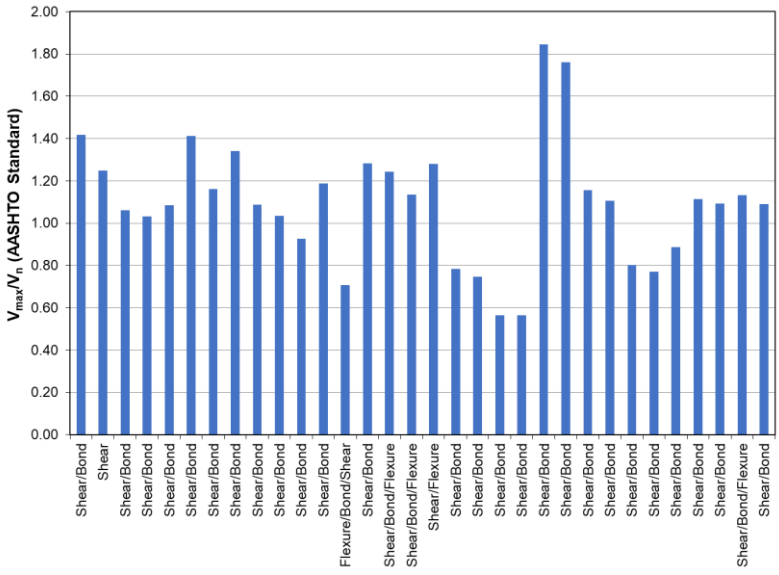

Figure 2.94. Comparison of experimental shear to calculated capacity for girders tested by Shahawy et al. (1993) relative to failure type

A comparison of the ratio of maximum experimental shear to calculated shear capacity using the AASHTO LRFD (2007) MCFT method for the AASHTO Type III girders tested by Ross et al. (2011) based on *a*/*d* ratio is shown in Figure 2.95. The AASHTO MCFT method provided an accurate prediction of shear strength for *a/d* greater than 2.0, and a conservative prediction for *a*/*d* smaller than 3.0. A similar comparison is shown in Figure 2.96 for failure type based on the AASHTO LRFD (2007) MCFT method. The AASHTO MCFT method provided conservative failure values for situations with bond-shear failures, which are not explicitly accounted for by these methods (Ross et al. 2011).

A comparison of the ratio of maximum experimental shear to calculated shear capacity for all the specimens examined using the AASHTO LRFD MCFT method based on *a*/*d* ratio is shown in Figure 2.97. The AASHTO MCFT method provided an accurate prediction of shear strength for *a/d* greater than 2.0, a generally conservative prediction for *a*/*d* smaller than 3.0, and a conservative prediction for *a*/*d* less than 2.0. A similar comparison is shown in Figure 2.98 for failure type based on the AASHTO LRFD MCFT method. The only ratios less than 1.0 were for either bond shear failures or failures due to flexure.

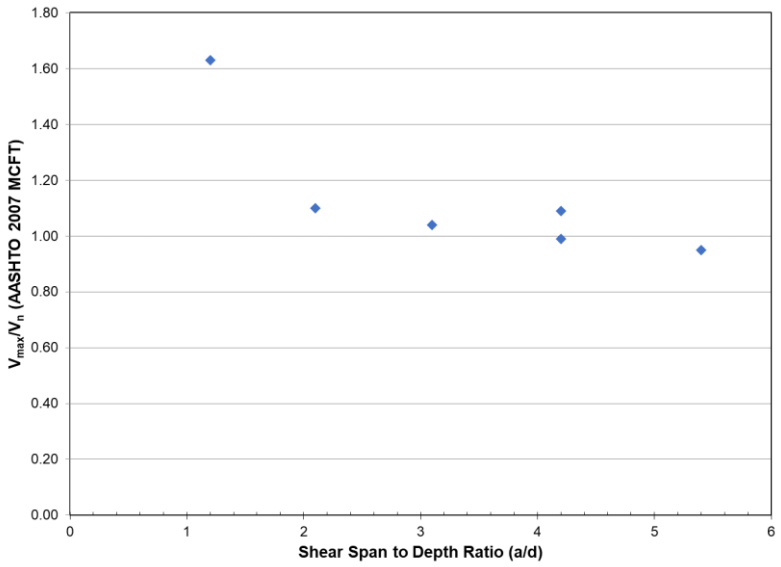

Figure 2.95. Comparison of experimental shear to calculated capacity for girders tested by Ross et al. (2011) relative to a/d ratio

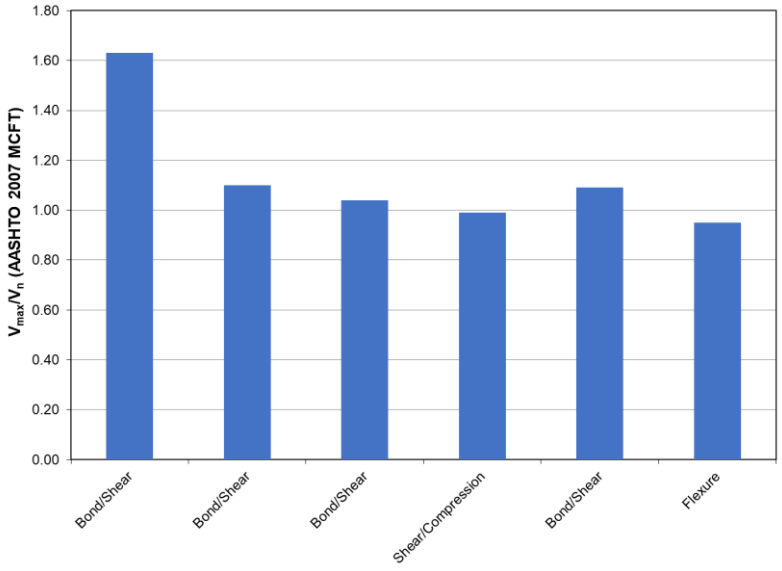

Figure 2.96. Comparison of experimental shear to calculated capacity for girders tested by Ross et al. (2016) relative to failure type

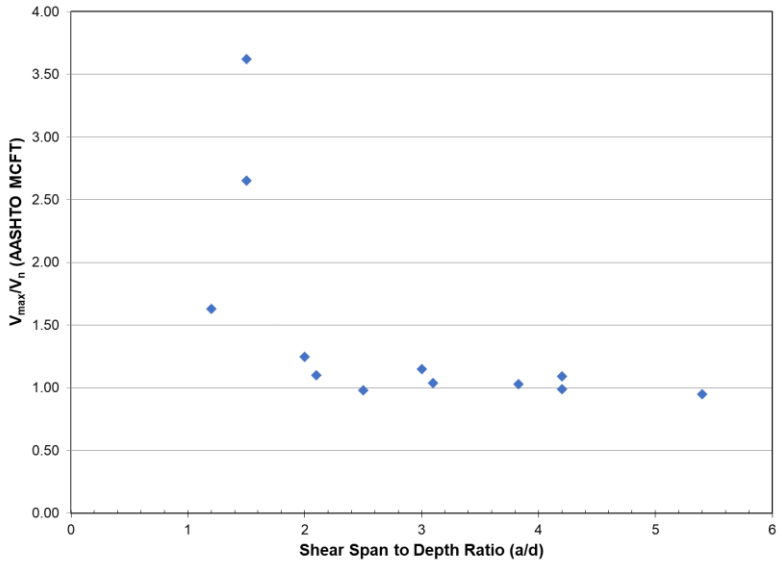

Figure 2.97. Comparison of experimental shear to calculated capacity for girders tested by Floyd et al. (2016), Osborn et al (2012). and Ross et al. (2011) relative to a/d ratio

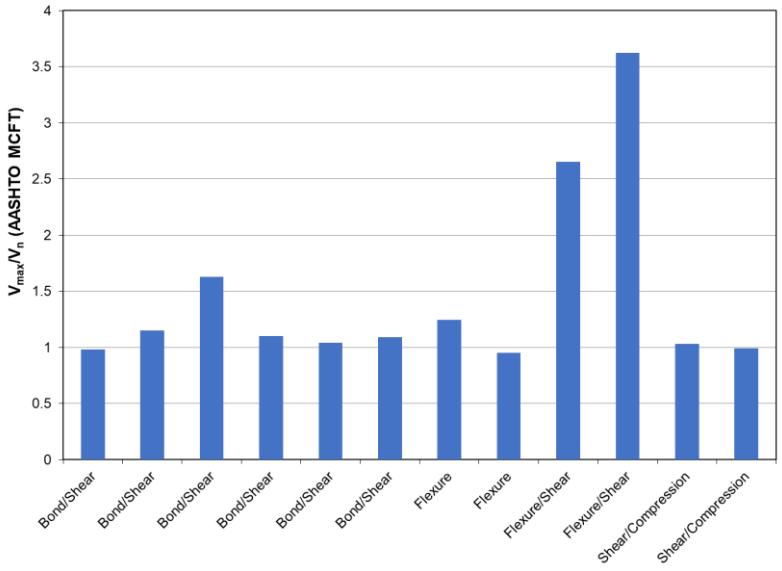

Figure 2.98. Comparison of experimental shear to calculated capacity for girders tested by Floyd et al. (2016), Osborn et al (2012). and Ross et al. (2011) relative to failure type

2.9 End Region Corrosion

As described in Sections 1.5 and 2.8, previous research by Floyd et al. (2016) on AASHTO Type II girders indicated that even minor corrosion damage at the very end regions of the girder can affect the shear failure mechanism even if the ultimate capacity is not reduced. Work by Mayhorn et al. (2017) on half-scale AASHTO Type II girders with varying levels of end region corrosion showed mixed results. All specimens exhibited experimental shear capacities less than capacity calculated using the AASHTO LRFD (2007) and ACI (2014) methods when tested at an *a*/*d* ratio of 2.0. Specimen ends with corrosion resulting from up to 6 months of exposure to a 5% chloride solution exhibited higher experimental shear capacities than the corresponding control specimen ends. All specimens exhibited some measure of bond failure, either bond-shear or bond-shear/flexure, which explains the inaccuracy of the AASHTO and ACI predictions which do not account for these mechanisms. However, corroded end specimens exhibited strand slip before shear cracking occurred while control specimens exhibited shear cracking before strand slip occurred. This cracking behavior further supports that minor strand corrosion can affect failure mechanism while not reducing overall capacity.

Site visits conducted by Mayhorn et al (2017) on 19 Oklahoma bridges constructed between 1960 and 1979 indicated that several end region deterioration characteristics were present at multiple bridges. Those deterioration characteristics included: corroded bearing plates; corroded anchor bolts and nuts; spalling of the girder concrete above the support; exposed rebar and prestressing strands; diagonal cracking of the back corner of the girder; vertical cracking along the girder and diaphragm interface; diagonal cracking originating from the top flange and web interface; and diaphragm deterioration. These observations included corrosion similar to and worse than present on the beams previously tested by Floyd et al. (2016).

2.10 Inspection Data Interpretation

Several sample inspection reports were collected and examined to determine available information useful to estimating shear capacity based on condition of the bridge and identifying items that should be considered for inspection. The overall objective was to provide guidance on how to effectively capture the information relevant to shear behavior during the limited time available during an inspection. Several sample inspection reports were collected from ODOT by the OU research team and reviewed to identify information useful to identifying characteristics and items relevant to accurately rating bridges vulnerable to shear based on the items identified in Sections 2.4-2.9. The inspection reports examined were for the bridges listed in Table 2.17. For a given bridge under consideration, information on the bridge itself should be available from sources other than the inspection report, but in this section all items will be discussed.

Table 2.17. List of Sample Inspection Reports Examined

NBI No.	Facility Carried	Feature Intersected	County	Division	Identified Vulnerable to Shear
19101	U.S. 412	Verdigris River O-Flow	Rogers	8	Yes
19276	S.H. 3E	N. Canadian River	Pottawatomie	3	No
19257	U.S. 70	Little River O-Flow	McCurtain	2	Yes
19269	U.S. 70	Little River O-Flow	McCurtain	2	Yes

Bridge span length is an important characteristic for determining vulnerability to shear and both the span length and number of spans are included in the bridge description portion of the inspection report and as items 48 and 244 in the inspection

report. The main span material and design type (item 43) are critical considerations in that only prestressed concrete stringer/girder systems are of interest. However, more information is needed due to the fact that different girder types may have different characteristics relative to shear behavior. The year built (item 27) is an important consideration as it may be used to identify the potential design code used to design the girders which can identify the design method (e.g. whether the Standard Specifications and “quarter-point rule” were used for design. Figures 2.99 to 2.101show portions of an inspection report for the U.S. 412 over Verdigris River Overflow (NBI 19101).

The deck type (item 107 shown in Figure 2.99) is important for modeling load transfer between the girders. The width curb to curb (item 51) and width out to out (item 52) are important considerations for determining the number of design lanes that can fit on the bridge. These items (shown in Figure 2.101) may also be combined with information on girder spacing/number of girders (item 243 shown in Figure 2.100) to determined load transfer to the individual girders.

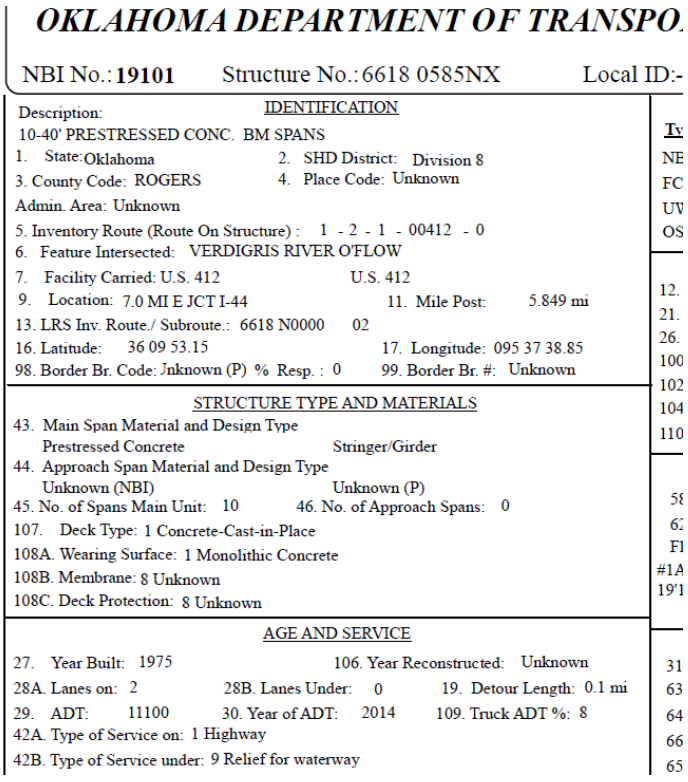

OKLAHOMA DEPARTMENT OF TRANSPO

NBI No.: **19101** Structure No.: 6618 0585NX Local ID:-

IDENTIFICATION

Description:
10-40' PRESTRESSED CONC. BM SPANS
1. State: Oklahoma 2. SHD District: Division 8
3. County Code: ROGERS 4. Place Code: Unknown
Admin. Area: Unknown
5. Inventory Route (Route On Structure) : 1 - 2 - 1 - 00412 - 0
6. Feature Intersected: VERDIGRIS RIVER O'FLOW
7. Facility Carried: U.S. 412 U.S. 412
9. Location: 7.0 MI E JCT I-44 11. Mile Post: 5.849 mi
13. LRS Inv. Route./ Subroute.: 6618 N0000 02
16. Latitude: 36 09 53.15 17. Longitude: 095 37 38.85
98. Border Br. Code: Unknown (P) % Resp. : 0 99. Border Br. #: Unknown

STRUCTURE TYPE AND MATERIALS

43. Main Span Material and Design Type
Prestressed Concrete Stringer/Girder
44. Approach Span Material and Design Type
Unknown (NBI) Unknown (P)
45. No. of Spans Main Unit: 10 46. No. of Approach Spans: 0
107. Deck Type: 1 Concrete-Cast-in-Place
108A. Wearing Surface: 1 Monolithic Concrete
108B. Membrane: 8 Unknown
108C. Deck Protection: 8 Unknown

AGE AND SERVICE

27. Year Built: 1975 106. Year Reconstructed: Unknown
28A. Lanes on: 2 28B. Lanes Under: 0 19. Detour Length: 0.1 mi
29. ADT: 11100 30. Year of ADT: 2014 109. Truck ADT %: 8
42A. Type of Service on: 1 Highway
42B. Type of Service under: 9 Relief for waterway

Figure 2.99. Section of sample inspection report showing Main Span Material and Design Type (item 43) and Year Built (item 27)

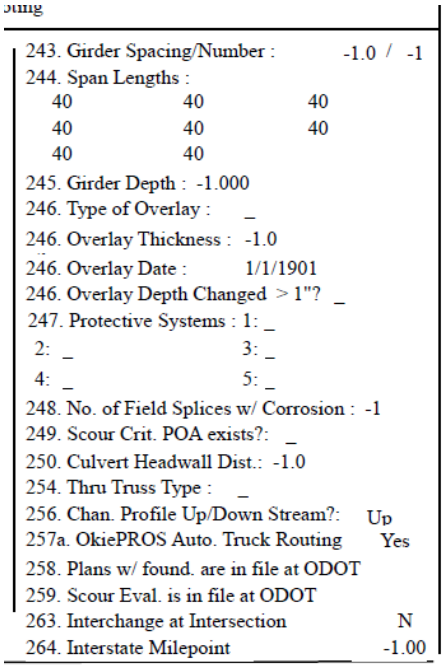

243. Girder Spacing/Number : -1.0 / -1
244. Span Lengths :
40 40 40
40 40 40
40 40
245. Girder Depth : -1.000
246. Type of Overlay : _
246. Overlay Thickness : -1.0
246. Overlay Date : 1/1/1901
246. Overlay Depth Changed > 1"? _
247. Protective Systems : 1: _
2: _ 3: _
4: _ 5: _
248. No. of Field Splices w/ Corrosion : -1
249. Scour Crit. POA exists?: _
250. Culvert Headwall Dist.: -1.0
254. Thru Truss Type : _
256. Chan. Profile Up/Down Stream?: Up
257a. OkiePROS Auto. Truck Routing Yes
258. Plans w/ found. are in file at ODOT
259. Scour Eval. is in file at ODOT
263. Interchange at Intersection N
264. Interstate Milepoint -1.00

Figure 2.100. Section of sample inspection report showing Girder Spacing/Number (item 243) and Span Lengths (item 244)

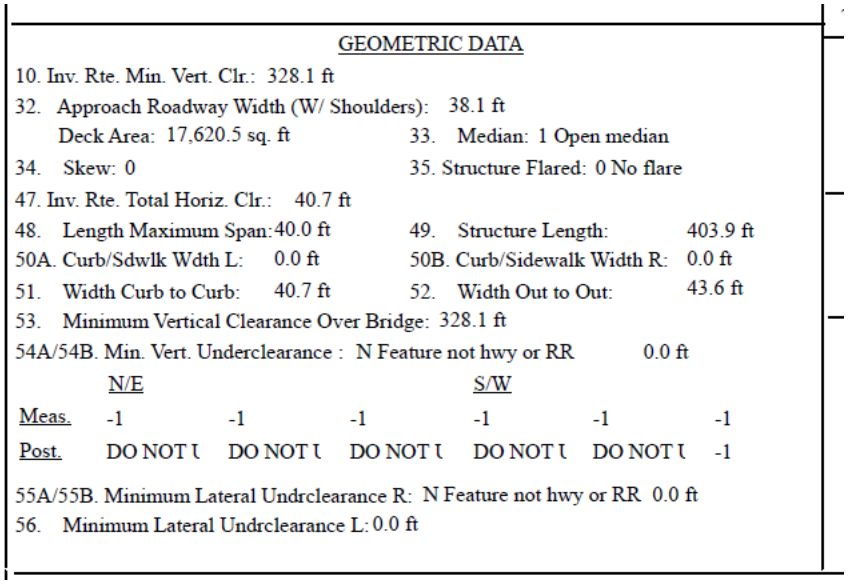

GEOMETRIC DATA

10. Inv. Rte. Min. Vert. Clr.: 328.1 ft
32. Approach Roadway Width (W/ Shoulders): 38.1 ft
Deck Area: 17,620.5 sq. ft 33. Median: 1 Open median
34. Skew: 0 35. Structure Flared: 0 No flare
47. Inv. Rte. Total Horiz. Clr.: 40.7 ft
48. Length Maximum Span: 40.0 ft 49. Structure Length: 403.9 ft
50A. Curb/Sdwlk Wdth L: 0.0 ft 50B. Curb/Sidewalk Width R: 0.0 ft
51. Width Curb to Curb: 40.7 ft 52. Width Out to Out: 43.6 ft
53. Minimum Vertical Clearance Over Bridge: 328.1 ft
54A/54B. Min. Vert. Underclearance : N Feature not hwy or RR 0.0 ft

	N/E			S/W		
Meas.	-1	-1	-1	-1	-1	-1
Post.	DO NOT U	DO NOT U	DO NOT U	DO NOT U	DO NOT U	-1

55A/55B. Minimum Lateral Undrclearance R: N Feature not hwy or RR 0.0 ft
56. Minimum Lateral Undrclearance L: 0.0 ft

Figure 2.101. Section of sample inspection report showing Width Curb to Curb (item 51) and Width Out to Out (item 52)

Overlay type, thickness, and age (items 246 shown in Figure 2.100) may be important items for consideration of failure mode based on the failures observed in

previous research at OU (Floyd et al. 2016). Bonded concrete overlays resulted in premature girder failure for some of the configurations tested.

Bridge Element Condition States and Element Notes included in a typical inspection report can provide valuable information on condition at the end regions that may affect shear behavior and capacity. The following bridge elements may be indicators of corrosion damage at the girder ends that can lead to a bond failure mechanism and potentially reduced capacity: Element 109, Prestressed Concrete Girder/Beam, Element 819, P/S concrete open girder/beam end (5 ft), and Element 916, Steel Bearing Assembly. Exposed prestressing and condition state 3 or 4 may indicate end region deterioration that can affect shear behavior for both Elements 109 and 819. Corrosion of steel bearing plates, which may be included in the element notes, often can contribute to deterioration of the prestressed concrete girder ends. In general, element notes may be of use for finding additional information. For example, in the U.S. 412 over Verdigris Overflow inspection report the following note is included for Element 916 Steel Bearing Assembly: “Bearing Plates Moderate to Severe Corrosion @ Abut’s”. Even if these bearing plates are repaired and/or coated, the corrosion may have already spread to the beam ends, which could in the future affect end region/shear capacity. A similar note is included for Element 916 on the inspection report for the S.H. 3E bridge over the North Canadian River (Figure 2.102), which also indicates that 20% of the beam ends (Element 719) exhibit condition state 3 (Figure 2.103) and notes cracking, spalling, and staining of the beam ends (Element 719 in Figure 2.102). Figure 2.104 shows a photo of one of these locations on the S.H. 3E bridge, which exhibits spalling at the beam end similar to the beams tested in previous research (Floyd et al. 2016).

The quantities for individual elements, especially prestressed girder/beam ends combined with the percentage of the total quantity in each condition state may be useful for making an engineering judgment on the potential impact of end region deterioration on shear capacity. For example, identification of end region deterioration may require additional analysis methods accounting for bond loss when considering girder capacity.

Elem.	Element Notes (Include Size and Location of Deterioration
12	< none >
109	FX - 3 BEAMS @ 3RD,4TH, 5TH & 6TH SPAN FROM W. CTR BEAM W. SPAN HAVE UP TO 4" DIAM BY 3/4" DEEP SPALLS - PROBABLY DONE DURING CONSTRUCTION, SOME CRACKING & SPALLING TO CONCRETE END TREATMENTS W/ STAINS. LIGHT CRACKS (SOME HAVE LEACHING & STAINS STARTING @ THE TOP)
205	NOTE:SUBSTR. WORK COMPLETED ON CONTRACT. CONCRETE FOOTINGS EXPOSED AT PIERS 1,2,3,4,5 AND 7 BOTH COLUMNS EACH ALSO PIER 6 JUST THE NORTH COLUMN.
210	< none >
215	NOTE:THIS WAS REPAIRED ON CONTRACT.
234	< none >
301	< none >
310	FX:MINOR DEFROMATION IN A FEW PADS.
321	NOTE:SLABS HAVE HAD APPR 2" LEVELUP, FX:E. SLAB HAS BROKEN TRANSVERSELY @ END OF BRIDGE
331	FX - MINOR SPALLS W/ EXP REBAR. HEAVY SCALING TO SOME SECTIONS.
358	< none >
361	< none >
510	< none >
659	< none >
719	FX:See note for elem. # 109.
909	NOTE:NEW JTS. DONE ON CONTRACT. A FEW AREAS ARE STARTING TO TEAR
916	FX:MOD/SEV. SECT/LOSS TO BRG.PLATES & BOLTS.(SEE PHOTOS)

Figure 2.102. Section of sample inspection report showing Element Notes for Beam Ends (Element 719) and Steel Bearing Assembly (Element 916)

Structure / Inspection Notes

CONTRACTORS FIXED ALL JTS AND SUBSTR. REHAB DONE 2011.

NOTE:INSP.W/SNOOPER.

Elm.	Env.	Description	Un.	Qty.	Qty.St. 1	% 1	Qty.St. 2	% 2	Qty.St. 3	% 3	Qty.St. 4	% 4	Qty.St. 5	% 5
12	4	Reinforced Concrete Deck	(SF)	37,488	33,739	90 %	3,749	10 %	0	0 %	0	0 %	0	0 %
109	4	P/S Conc Open Girder/Beam	(LF)	4,431	4,254	96 %	133	3 %	44	1 %	0	0 %	0	0 %
205	4	Reinforced Conc Column or Pile Extension	(EA)	16	0	0 %	16	100 %	0	0 %	0	0 %	0	0 %
210	4	Reinforced Conc Pier Wall	(LF)	240	0	0 %	240	100 %	0	0 %	0	0 %	0	0 %
215	4	Reinforced Conc Abutment	(LF)	105	1	1 %	104	99 %	0	0 %	0	0 %	0	0 %
234	4	Reinforced Conc Cap	(LF)	397	0	0 %	397	100 %	0	0 %	0	0 %	0	0 %
301	4	Pourable Joint Seal	(EA)	136	136	100 %	0	0 %	0	0 %	0	0 %	0	0 %
310	4	Elastomeric Bearing	(EA)	104	0	0 %	104	100 %	0	0 %	0	0 %	0	0 %
321	4	Reinforced Conc Approach Slab w/ or w/o AC O	(EA)	2	0	0 %	1	50 %	1	50 %	0	0 %	0	0 %
331	4	Reinforced Conc Bridge Railing	(LF)	1,704	0	0 %	1,671	98 %	33	2 %	0	0 %	0	0 %
358	4	Concrete Cracking	(EA)	1	0	0 %	1	100 %	0	0 %	0	0 %	0	0 %
361	4	Scour	(EA)	1	0	0 %	1	100 %	0	0 %	0	0 %	0	0 %
510	4	Wearing Surfaces	(SF)	37,488	0	0 %	37,488	100 %	0	0 %	0	0 %	0	0 %
659	4	Soffit of Concrete Decks and Slabs	(EA)	1	0	0 %	1	100 %	0	0 %	0	0 %	0	0 %
719	4	P/S Concrete Open Girder/Beam End (5 Ft.)	(LF)	520	260	50 %	156	30 %	104	20 %	0	0 %	0	0 %
909	4	Pourable Fixed Joint Seal	(EA)	45	45	100 %	0	0 %	0	0 %	0	0 %	0	0 %
916	4	Steel Bearing Assembly	(EA)	104	0	0 %	50	48 %	54	52 %	0	0 %	0	0 %

Figure 2.103. Section of sample inspection report showing Element Condition States for Beam Ends (Element 719) and Steel Bearing Assembly (Element 916)

Figure 2.104. Bearing plate corrosion and spalling at the prestressed beam end

3.0 Methods for Assessing Condition of Aged Girders

3.1 Overview

Previous research focused on two methods of determining in-service properties of prestressed girders critical to accurate characterization of girder strength and performance was conducted as part of previous projects sponsored by ODOT (Pei et. al., 2008; Floyd et al., 2016). The power of these techniques is rooted in the following:

i) These are physics-based modeling techniques designated for prestressed concrete girders. Their direct results include remaining prestress force, concrete surface strain, and flexural stiffness of sections of a girder. These are physical quantities affecting the bond transfer and shear capacity of the girder ends.

ii) These are techniques for processing properly collected field data from either long- or short-term monitoring/testing. Unlike commonly used finite-element modeling, these techniques fundamentally do not make gross assumptions on critical parameter values used in modeling. Rather, these critical parameter values are obtained from processing measured real-world data. These techniques are thus a more rational path to estimating the remaining shear capability of aged real-world girders.

iii) These techniques are characterized by directly modeling time-dependent behavior of concrete and variability of section properties (e.g., due to corrosion) of real-world prestressed concrete girders. They are built on rigorous mathematical formulation, engineering mechanics, and data processing principles.

3.2 Technique #1: Bond Transfer Inverse Modeling Using Draw-In Data

3.2.1 Introduction

Time evolution of prestress loss and bond transfer length holds vital information concerning long-term performance of pretensioned prestressed concrete. To extract this time-varying information, a method was developed utilizing long-term measurements of strand draw-in to evaluate these properties (Floyd et al. 2018). Draw-in measurements can be more effectively obtained than concrete or strand surface strain measurements. Theoretical investigations combined with numerical studies of experimental data were carried out for this purpose. The work described by Floyd et al. (2018) builds on a boundary value problem (BVP) model which quantifies draw-in for instantaneous elastic response. A one-dimensional linear viscoelastic standard solid model is employed to model concrete creep, which is a simple but effective model of the time-dependent response of concrete. Guyon's BVP model (Guyon 1953) is generalized to include time dependence and then combined with an existing initial value problem (IVP) model for post-tensioned concrete leading to a new mixed model for time-dependent prestress loss and bond transfer in pretensioned concrete.

In addition to Guyon (1953), a report by Fédération International de la Précontrainte (FIP) (1982) is another source for mathematical modeling of bond transfer in pretensioned concrete. Other relevant publications include Balázs (1993); Baxi (2005); Oh et al. (2006); Ayoub and Filippou (2010); Beńıtz and Gálvez (2011); Geßner and Henne (2016). Analysis was undertaken in Floyd et al. (2018) to:

i) quantify long-term prestress loss and bond-transfer behaviors by applying the proposed model and directly utilizing measured draw-in time history data, and
ii) validate the proposed quantitative analysis by using scaled pretensioned concrete beams with different types of aggregates and strengths of concrete – among other factors.

The model is based on using Guyon's Figures 11 and 13 (replotted and presented in Figure 3.1), which allows the displacements at each end of an infinitesimal element to be defined before "the total strain" is obtained.

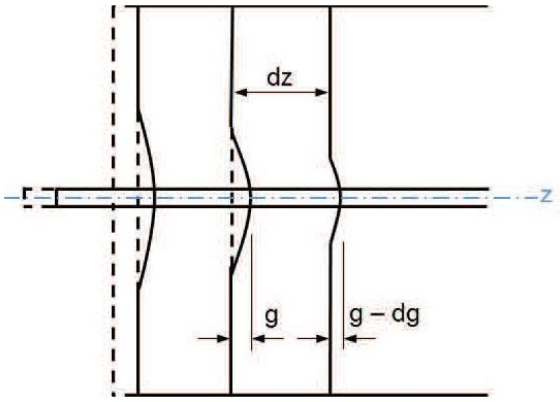

Figure 3.1. Displacements of the strand and concrete at the end of a prestressed concrete beam, following Figures 11 and 13 in Chapter VII of Guyon (1953) but with a minor correction on both the concrete and strand ends.

Hooke's law is then applied to connect the total strain to the stress, from which an ordinary differential equation is finally obtained to solve the wire stress *f* in section 5 of Guyon (1953), shown in Equation 3.1.

$$f = \frac{f_{si}}{1+mp} - \frac{E_{ps}}{1+mp} \cdot \frac{dg}{dz} \tag{3.1}$$

where $\frac{E_{ps}}{E_c} \triangleq m$ and $\frac{A_s}{A_c} \triangleq p$. Equation (3.1) captures the stress-strain behavior of the strand as a function of z (a coordinate along the strand). Floyd et al. (2018) extends the key deformation compatibility equation in Guyon (1953) from $t = 0$ to $t > 0$ with the estimation formula given in Equation 3.2:

$$\underbrace{g(0,t)}_{draw-in} = \underbrace{\int_0^{\frac{L}{2}} \left[\frac{P_i - P(z,t)}{A_s E_{ps}}\right] dz}_{from\ strand\ relaxation} - \underbrace{\int_0^{\frac{L}{2}} \varepsilon_c(z,t) dz}_{from\ concrete\ creep} \tag{3.2}$$

where the creep of concrete is evaluated using a standard solid model. The estimated draw-in is compared with measured draw-in, and a normalized root-mean-squared (NRMS) error is calculated as a measure to evaluate the performance of the model.

Key assumptions made in Floyd et al. (2018) are as follows:

(i) 1-D analysis only – A zone characterized by z, which goes along a strand and the concrete bonded in its vicinity is examined. While the strand is linear elastic, the concrete is linear viscoelastic. Specifically, a standard solid model is adopted.

Stress-strain behavior of each material is assumed to be uniaxial, considering normal stresses only.

(ii) No drying shrinkage of concrete is considered – This introduces an inherently unmodeled error.

(iii) A perfectly bonded core in the mid-section of a beam is considered – This core is equivalent to a post-tensioned concrete beam.

(iv) No plastic/friction bond considered – An exponential stress distribution for elastic bond is considered for both strand and concrete at any time instance.

Existing laboratory measurements were used to validate the technique. A brief description of test setup and procedure for obtaining those data can be seen in Dang et al. (2016). The prestress loss determined using the model for selected specimens is presented in Figure 3.2.

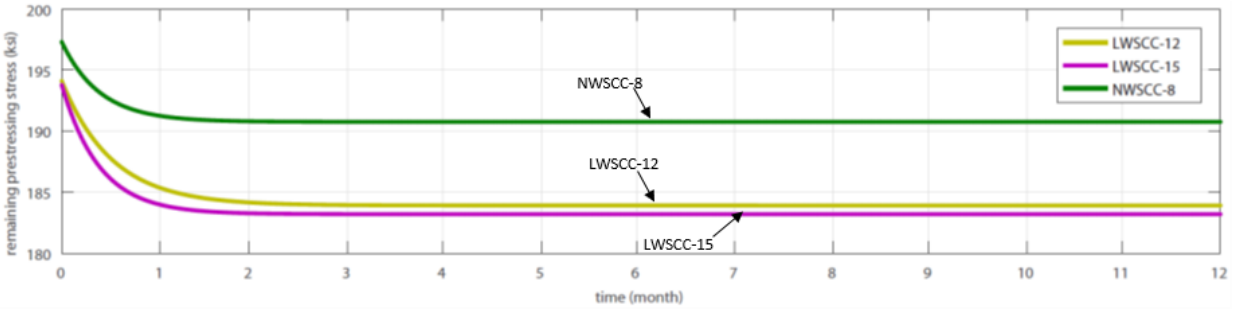

Figure 3.2. One-year prestress loss for selected normal- and lightweight self-consolidating concrete beam specimens by assuming the ultimate creep coefficient to be 2.35

Figure 3.3 indicates that, even though the measured draw-in time histories come in different forms, the proposed method can: (i) reproduce a draw-in time history similar to the measured one, and (ii) reproduce both strand and concrete movement time histories at the beam end that cannot be measured. The strand and concrete movement histories seem rational because their difference is reasonable compared to the measured values of end slip which are a measure of the relative motion. Similarly, Figure 3.4 presents the promising prediction capability of the method as presented in Floyd et al. (2018).

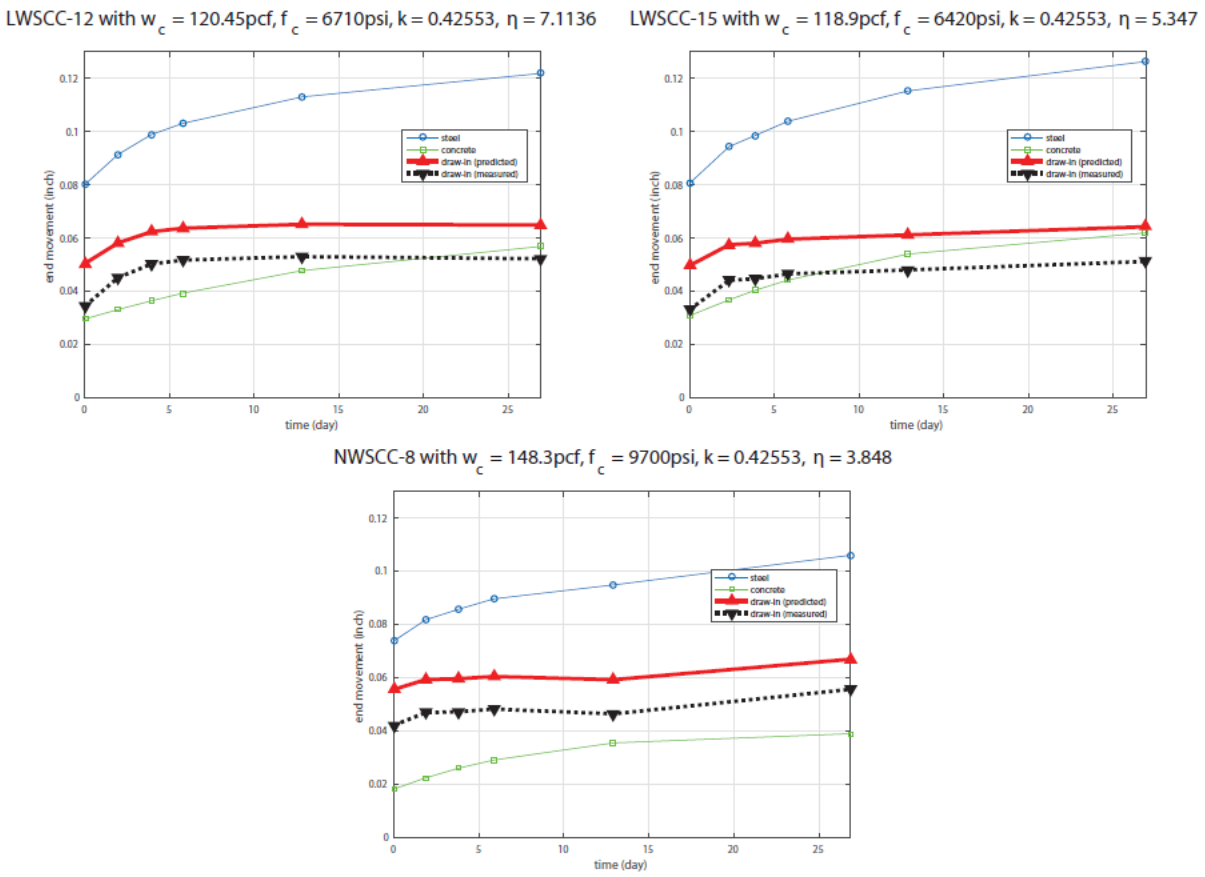

Figure 3.3. Measured vs. predicted strand draw-in, and predicted end movement of strand and concrete for two LWSCC and one NWSCC specimen.

While promising, the initially developed method had several limitations. Additional draw-in data from specimens more accurately representing field conditions and varying types of concrete were needed to better evaluate the accuracy of the model. The model did not include the effects of concrete shrinkage and consideration of available theoretical and empirical concrete shrinkage prediction models was needed to identify the best method for inclusion in the model. Additional consideration of input parameter values and error propagation was also needed.

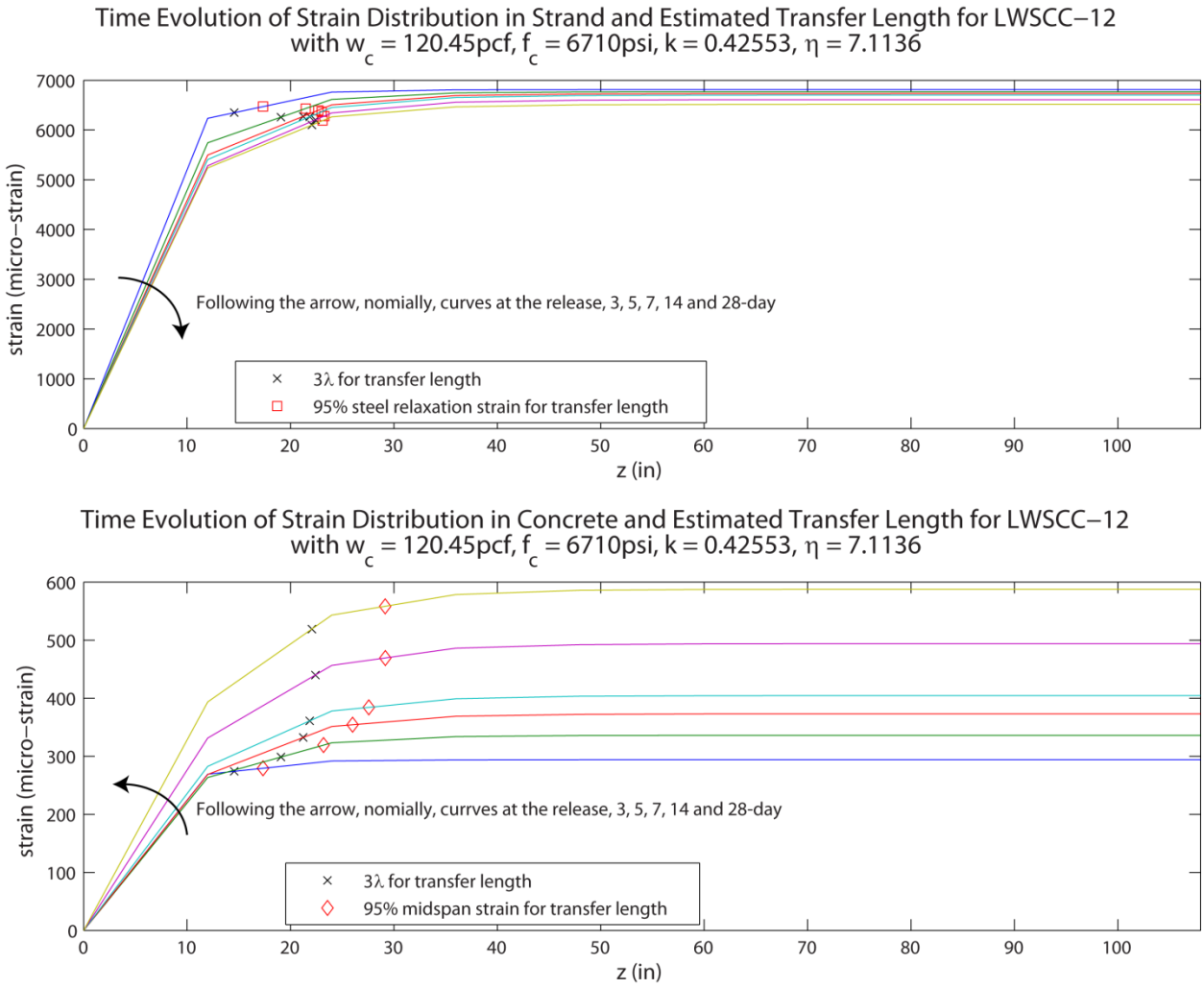

Figure 3.4. Time evolution of strain distribution for both strand and concrete and estimated transfer length in comparison with 3λ for a lightweight self-consolidating concrete beam specimen LWSCC-12 with $w_c = 120.45$ pcf, $f'_c = 6700$ psi, $k = 1/2.35$, and $\eta = 7.114$ day. Only the left half is presented due to symmetry.

3.2.2 Strand Draw-in Data Collection

Strand draw-in measurements were conducted on the twelve prestressed beam specimens cast as part of work on ODOT project SPR 2276 conducted at the same time as the research described in this report. These beams are approximately ½ scale AASHTO Type II girders similar to those used in the completed ODOT SPR project 2256 (Floyd et al. 2016). The details of the beam specimens are shown in Figure 3.5. Strand draw-in was measured using steel block clamps attached to the exposed strands and a micrometer. These draw-in data were combined with existing data for use in

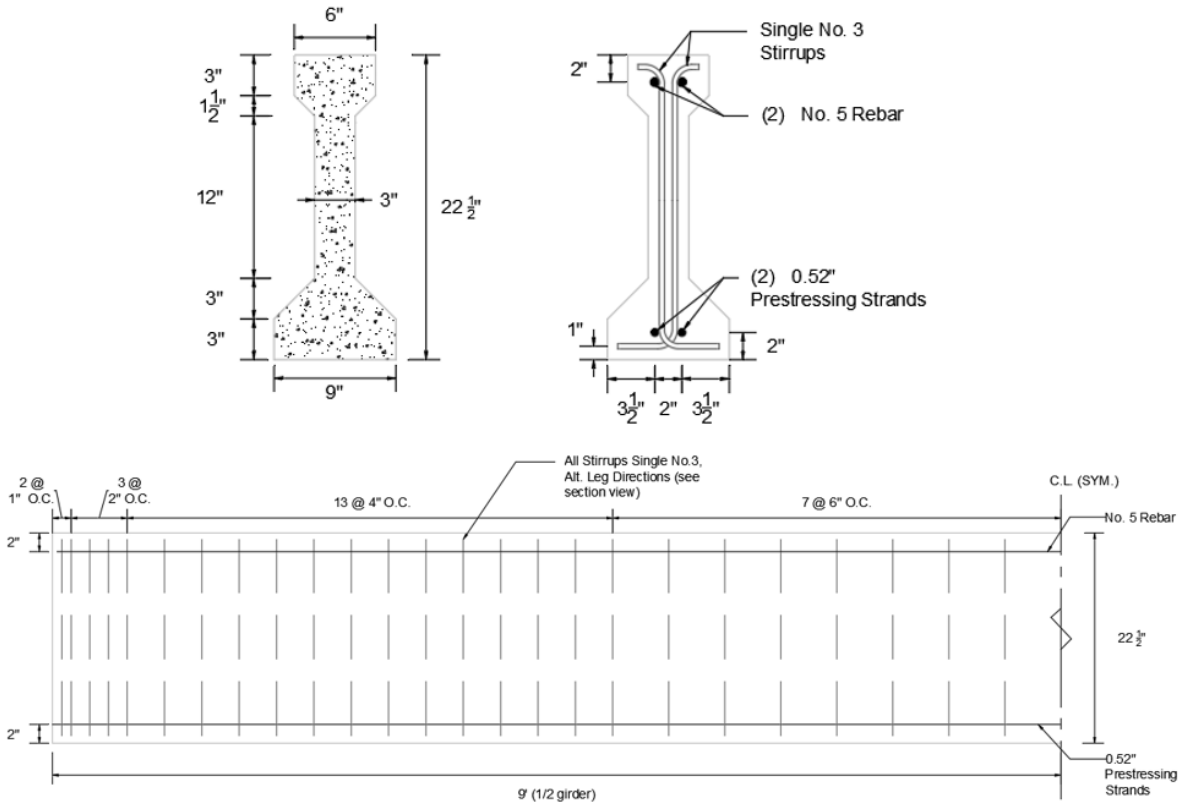

Figure 3.5. Prestressed beam specimen cross-section and elevation

developing and validating the bond transfer model. A sample time history of the strand draw-in measurements from these beam specimens is presented in Figure 3.6 and a summary of the remaining measurements is provided in Appendix C.

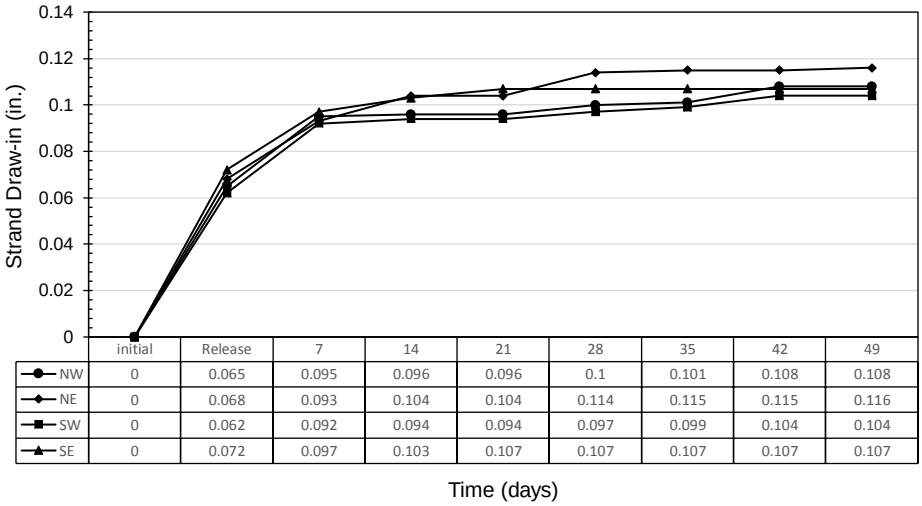

	initial	Release	7	14	21	28	35	42	49
NW	0	0.065	0.095	0.096	0.096	0.1	0.101	0.108	0.108
NE	0	0.068	0.093	0.104	0.104	0.114	0.115	0.115	0.116
SW	0	0.062	0.092	0.094	0.094	0.097	0.099	0.104	0.104
SE	0	0.072	0.097	0.103	0.107	0.107	0.107	0.107	0.107

Figure 3.6. Sample strand draw-in time history measured for prestressed beam specimen PC11

A single prestressed beam with the same design as those used for SPR 2276 and the draw-in data collection was cast in mid-May 2018 as part of a project sponsored by the Southern Plains Transportation Center (SPTC). It was instrumented with surface mounted DEMEC gage points, thirteen internal vibrating wire strain gages, and thirty fiber optic strain sensors to measure transfer length, in addition to clamps for measuring strand draw-in. The locations of the internal sensors along the beam length are shown in Figure 3.7. These sensors are able to collect very accurate concrete strain data. Data were collected at increments until an age of 28 days was reached. A summary of the strain data collected from this beam is shown in Figure 3.8. The strain data collected using the internal vibrating wire strain gages and the fiber optic strain sensors are a valuable addition for validating the predictions of concrete creep and shrinkage.

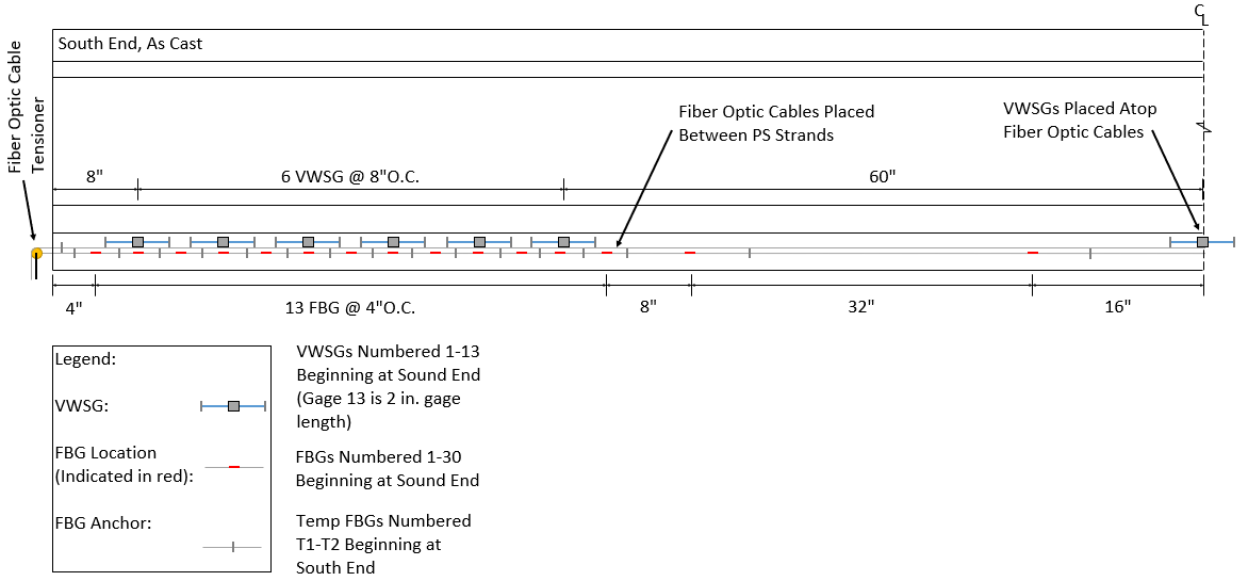

Figure 3.7. Internal instrumentation plan for SPTC prestressed beam

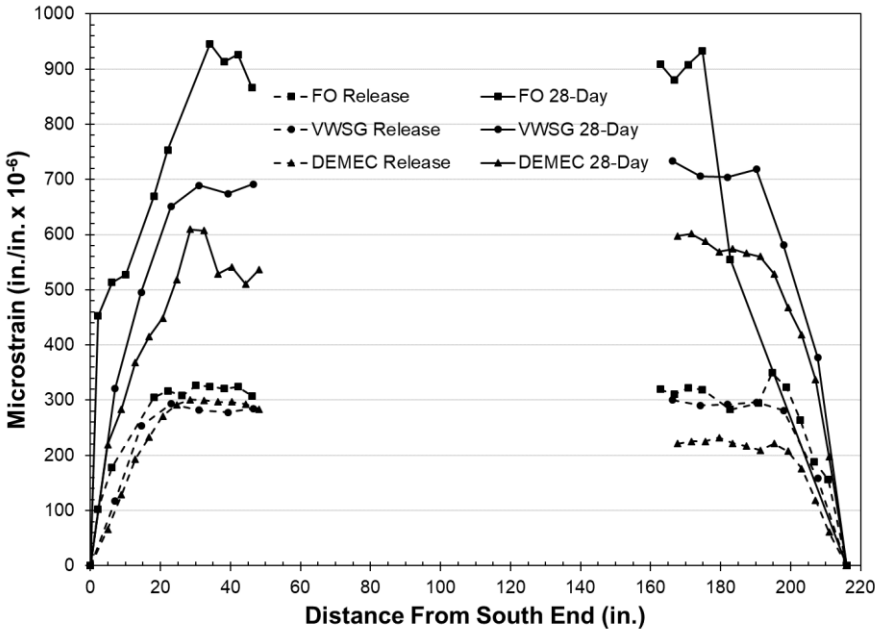

Figure 3.8. Plot of strain measured along the length of the beam using DEMEC surface gages, internal VSWGs, and fiber optic sensors at 1 and 28 days of age

3.2.3 Improving Model in Floyd et al. (2018)

In Floyd et al. (2018), normalized root-mean-squared errors of the inverse model are summarized in Tables 4 and 5 of the paper for LWSCC and NWSCC, respectively. The estimated draw-in time histories are always significantly over-predicting with an average of 15.9% for LWSCC and 12.1% for NWSCC. Figure 3 there (Figure 3.3 in this report) shows results for the first 28 days. The measured and predicted draw-in curves in this figure are parallel with the discrepancy between the two starting at Day-1. This difference is the limitation intended to be addressed in the study described in this report.

3.2.3.1 Shrinkage effect

A substantial literature review of shrinkage prediction methods was conducted and the different procedures evaluated for inclusion in the bond transfer model. However, if the initial prediction is not correct, continuing the prediction in time is not reasonable. The cause of the initial error must be identified. Bazant and Xi (1994) focuses on creep during the first year. According to Digler (1982), shrinkage modeled via “age-adjusted effective modulus” (Eq. (1) there) could be significant during the first 28 days. In most cases shrinkage takes a longer time than 28 days to be significant,

which does not explain the initial discrepancy. Additionally, if only increasing concrete shrinkage, it seems that the predicted draw-in would increase (not decrease). In light of this discovery, other factors involved in the prediction were investigated.

3.2.3.2 Re-examining the values for A_s and A_c

In the initial model (Floyd et al. 2018), the following values were used:

- A_s = 0.434 in^2: This is the area of the two 0.6 in. diameter prestressing strands used in the test specimens
- A = 80.6 in^2: This is the average gross cross-sectional area of test specimens
- $A_c = A - A_s$: This is the actual area of concrete in the cross-section obtained by subtracting the area of the steel strands

Instead of these existing values, the following values were examined:

- A_s = 0.283 in^2: This is the area of one strand including concrete surrounding the individual wires to create a circular section.
- A = 12.5 in^2: The 1-D Guyon model (Guyon (1953)) and the Thick-Wall Cylinder model (e.g., Ramirez-Garcia et al. (2017)) are conceptually equivalent. Figure 2 in Ramirez-Garcia et al. (2017) leads to a suggestion that the area, A, surrounding one strand is a circle with a diameter no more than 4 in.

The values A_s = 0.283 in^2 and A = 12.5 in^2 were then used in the computation with little improvement in the prediction results.

It makes sense to use the effective value for the outer diameter of the cylinder similar to Figure 9 in Ramirez-Garcia et al. (2017) for closely spaced strands. Since the two strands in the test specimens considered in the current model were spaced at 2 in. on center and were located 2 in. from the bottom of the beam to strand center the effective distance from the edge of the strand to the edge of the thick-walled cylinder, C_{eff}, would be 1.6 in. resulting in a cylinder with outer radius of 1.9 in. An area between 11.3 in^2 and 12.5 in^2 therefore makes sense for interaction between the strand and concrete. However, for consideration of creep effects it makes sense to consider the full dimension of the beams and actual area of strands for calculating overall compressive

stress leading to creep and for shrinkage effects to consider the full dimensions of the beams for volume effects.

3.2.3.3 Study of rate of convergence for predicted end movement

Eventually, calculations indicated that 10 subdivisions along the length as in Floyd et al. (2018) was not enough. Taking specimen LWSCC-12 as an example, a parametric study regarding the number of subdivisions was carried out to determine the rate of convergence for the predicted end movement. It can be seen from Table 3.1 that a much higher number of subdivisions, e.g., 320, should be adopted. The improved prediction compared to agreement shown in Figure 3.3 is clearly seen in Figure 3.9. These results indicate that this correction significantly improves the performance of the inverse bond transfer model reported in Floyd et al. (2018).

Table 3.1. Study of rate of convergence for predicted end movement using LWSCC-12

Number of subdivisions	Predicted end movement (in.)
20	0.0685
40	0.0657
80	0.0650
160	0.0649
320	0.0648
640	0.0648

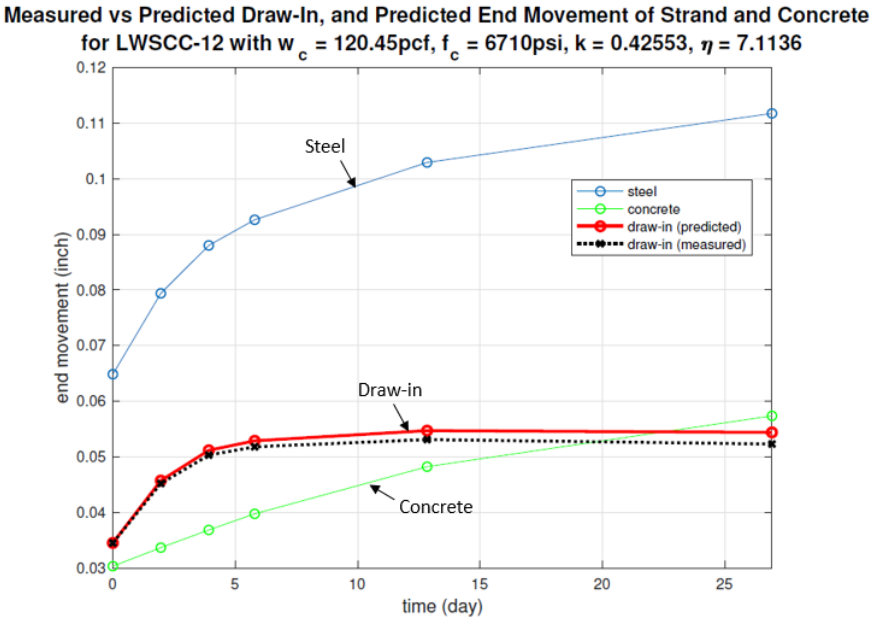

Figure 3.9. An example of significantly improved results of predicted draw-in for specimen LWSCC-12

3.2.4 Other Literature Review

Multiple models for shrinkage prediction were considered including all of those in ACI 209.2R (2008). The promising methods for inclusion in the bond transfer model were based on the efforts of Dr. Zdenek Bazant and his colleagues regarding aging and drying concrete, which also would be helpful to future work on this topic. Initially, “Model B3 Creep Design Aid Program”, available on Dr. Bazant’s website (http://www.civil.northwestern.edu/people/bazant/), was considered. B3 and B4 are the two most recent iterations of a model aimed at accounting for long-term (multi-decade) creep and shrinkage effects in concrete. B4 is the latest model. The creep design aid (CDA) program should make it easier to utilize the information contained in the extensive database collected over many years by Bazant and co-workers. Yu et al. (2012), and Bazant et al. (2012), which describe the logarithmic time-scale FEM technique, show promise for future work to implement Bazant’s analysis method for long-term creep data. Bazant and Jirasek (2018) is the latest comprehensive recent book by Bazant.

3.3 Technique #2: Piecewise EI Identification

3.3.1 Introduction

3.3.1.1 Background of Current Research

Research carried out by Pei et al. (2008) initiated the effort to study methods of rating precast prestressed concrete bridges, a typical design in Oklahoma, for their shear capacities in order to aid Oklahoma Department of Transportation (ODOT) engineers on recommendations of load postings and/or retrofitting. As part of the research, Pei et al. (2008) details the construction of an inverse problem based on mechanics and real-world measurements to estimate the flexural stiffness distribution along the length of a prestressed girder, which was assumed to be piecewise constant to simplify the effect of the aging of the girder as well as a glass fiber reinforced polymer (GFRP) retrofitted end. Measurements from flexural stiffness (load-deflection) testing were adopted.

In later research by Floyd et al. (2016) the flexural stiffness identification process was revisited for improvement through two different girders, dubbed “A” and “C” obtained from the eastbound side of the same bridge as in Pei et al. (2008) when the bridge was demolished in 2013. The recovered girders were subjected to both flexural stiffness and other destructive testing to identify their system properties. Concerns regarding the inverse problem formulation in Pei et al. (2008) were raised and suggestions for improvement were included.

3.3.1.2 Intended Contributions

The problem formulation in Pei et al. (2008) was revamped by using the state-of-the-art Bayesian analysis (Huang et al. 2019) and datasets collected from Floyd et al. (2016). This study vividly demonstrates the usefulness of Bayesian analysis in contrast with a linear least-squares method for the identified problem, which is typical for structural health monitoring (SHM) of pretensioned precast concrete bridge girders. In particular, the use of Bayesian analysis completely eliminates the possibility of obtaining negative flexural stiffness values. User-defined parameter values in Bayesian analysis were perturbed and studied systematically.

The methodology was coded in a comprehensive MATLAB file suite for analysis and illustration of identification results. Validation of the Bayesian analysis method was done using data was simulated with theoretical beam models and Gaussian noise added to the data. Real-world laboratory data collected from Girder A described in Floyd et al. (2016) were analyzed systematically. Experimental variability (Roy and Oberkampf 2011) was also considered in the analysis. Extensive parametric studies were carried out numerically and identification results were compared with stiffness values for Girder A taken from various sources.

3.3.1.3 Brief Literature Review

3.3.1.3.1 Research with similar focus

The following list summaries the literature with a similar research focus/application to the current study.

- **Kato and Shimada (1986)**
    - Ambient Vibration Testing (AVT) – Comparing modal parameters before and after bridge failure
    - Static loading
    - Assumed time-dependent effects of concrete had taken maximum toll in 5 years
    - Digital signal processing
    - Damage detection difficulty if prestressed tendons did not yield
- **Maeck et al. (2000)**
    - Finite element updating - Monitoring changes in Young's Modulus for stiffness reduction
    - Assuming symmetrical damage patterns
    - Not accounting for time-dependent effects of concrete
    - Direct stiffness calculation (DSC) – Quantification of damage using mode shapes
    - Best damage detection requires a dense measurement grid
- **Huth et al. (2005)**
    - Not accounting for time-dependent effects of concrete
    - Output-only system identification algorithms – Comparing modal parameters before and after bridge failure
    - Modeling dynamics of physical system and relating outputs to state variables of system
    - 8 month monitoring of ambient temperature
    - Modal assurance criterion (MAC) – Measuring correlation between two mode shapes
    - Mode shape area index – Monitoring mode shape areas for change between damage steps
    - Bridge partitioned into several spans for analysis
    - Flexibility difference – Comparing changes in flexibility matrices of a healthy and damaged structure
    - Localized damage detection

    - Finite element updating – Monitoring changes in Young's Modulus for stiffness reduction
    - Ambiguous damage localization and quantification caused by ill-conditioned methodology
    - Direct stiffness calculation (DSC) – Quantification of damage using mode shapes
    - Ambiguous damage related results attributed to modal estimation errors
- **Unger et al. (2006)**
    - Not accounting for time-dependent effects of concrete
    - FE updating – Monitoring changes in Young's Modulus for stiffness reduction
    - Non-linear least-squares optimization
    - Weighting modal parameters
    - Clear damage localization and quantification at 80% failure load
- **Song et al. (2007)**
    - Sensing crack formation at concrete surface
    - Cannot offer detailed crack information (location, width, length, orientation)
- **Pei et al. (2008)**
    - Inverse problem – Using physical measurements to identify piecewise constant stiffness
    - Static loading
    - Significant influence from time-dependent effects of concrete on results
    - Linear least-squares optimization
    - Non-unique solutions inherent to inverse problem
    - Not accounting for time-dependent effects of concrete
- **Impollonia et al. (2016)**
    - FE updating - Monitoring changes in Young's Modulus for stiffness reduction
    - Not accounting for time-dependent effects of concrete
    - Methodology not applied to physical experiments
    - Questionable damage detection based on threshold stiffness value

- **Floyd et al. (2016)**
    - Flexural stiffness identification process revisited Concerns and suggestions:
    - Necessity of double regression's effect on validity of study
    - Time-dependent effects of concrete
    - Contradiction in original problem formulation

3.3.1.3.2 Application of Bayesian analysis

Quoting "Nonlinear System Identification in Structural Dynamics:10 More Years of Progress" by Noel and Kerschen (2017): "An important change of paradigm has blossomed over the past few years in the third step of this process, as researchers have progressively recognized the importance of quantifying uncertainties in nonlinear system identification. This has given rise to methods estimating parameters together with, e.g., confidence bounds or distributions. In this context, the Bayesian framework put forward by Jim Beck and his collaborators is currently drawing noticeable attention in the community." Similarly, in Green and Worden (2015), it says "To date, the most systematic and extensive development of Bayesian SI is the result of the work of James Beck and his various collaborators." Here, Professor Beck directly contributed to this project for a linear system identification problem. Indeed, there is a huge body of literature contributing to applying Bayesian analysis in structural health monitoring. The latest literature review is entitled "State-of-the-art review on Bayesian inference in structural system identification and damage assessment" in Huang et al. (2019).

3.3.2 Methodology and Coding

3.3.2.1 Modeling: Illustrated

The assumption of a constant flexural rigidity (*EI*) across the beam does not hold for the given real-world girder(s) due to strand harping, varying reinforcement layouts, and unknown damage, therefore it is reasonable to divide the span of the beam into *N* smaller segments imparting a piecewise flexural rigidity along the length of the beam. The nature of the problem of identifying the assumed piecewise flexural rigidities requires an inverse approach.

The following aspects are involved in this study, however only the first aspect is illustrated in this section:

1. Formulation of Response Function **H**
2. Formulation of Measured Deflection Matrix with Rigid Body Motion Correction
3. Least-squares Solution
4. Bayesian Solution

To achieve a thorough understanding of the problem formulation, a specific example is given in the following sections where $N = 3$, $J = 4$ and $K = 1$ meaning that three piecewise values for EI (over L_1, L_2 and L_3) are assumed (N), deflection measurements from four active linear voltage differential transformers (LVDTs) are used (J), and the data of only one time step (K) (incremental load) is considered. Figure 3.10 illustrates the example.

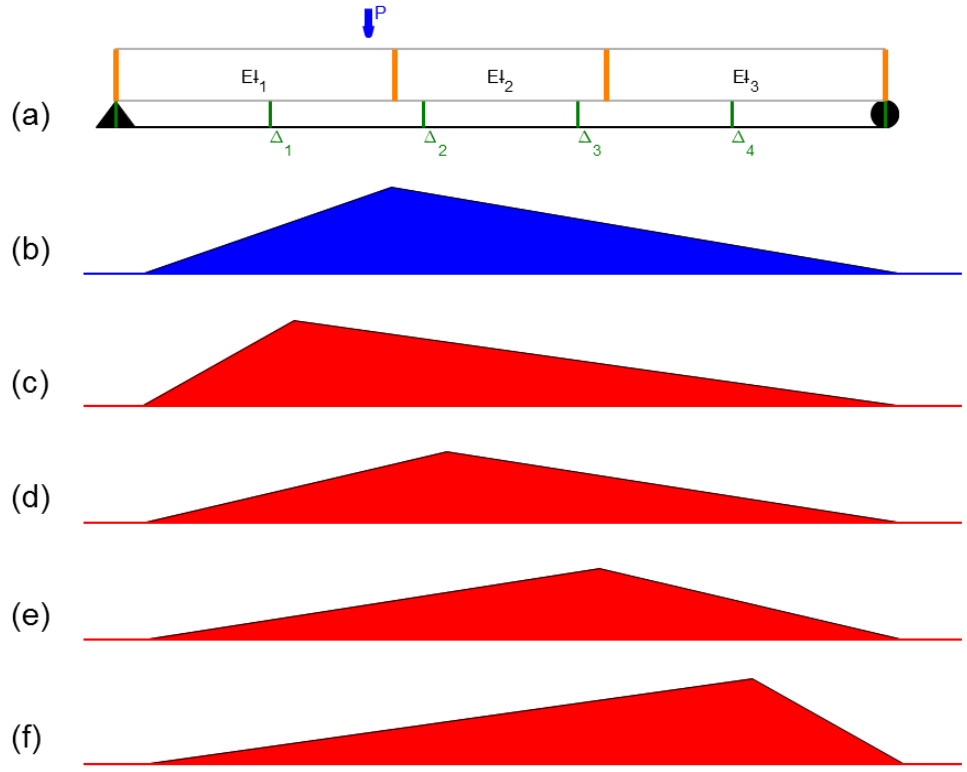

Figure 3.10. An illustrative example using $N = 3$, $J = 4$ and $K = 1$: (a) test setup and (b) real and (c) – (f) virtual bending moment diagrams utilized in the MATLAB code Leastsquares.m

For the case of a simply supported beam, the bending moment diagrams can be constructed through Equation 3.3 in response to a generically applied point load as in Figure 3.10. The blue moment distribution (b) signifies the real bending moment diagram produced by a unit point load whereas the red bending moment diagrams (c-f) signify those produced by unit virtual loads. The principle of virtual work is well established as follows:

$$\Delta = \int_L \frac{Mm}{EI} dx \tag{3.3}$$

where Δ is the deflection of the beam at the point of interest, *M* refers to the real bending moment diagram caused by the application of the physical load and *m* refers to the virtual bending moment diagram caused by the application of a virtual load.

Utilizing the bending moment diagrams in Figure 3.10 theoretical expressions for the deflections, by Equation 3.3, experienced at the active LVDTs are:

$$\Delta_1 = \int_{L1} \frac{Mm_1}{EI_1} dx + \int_{L2} \frac{Mm_1}{EI_2} dx + \int_{L3} \frac{Mm_1}{EI_3} dx \tag{3.4}$$

$$\Delta_2 = \int_{L1} \frac{Mm_2}{EI_1} dx + \int_{L2} \frac{Mm_2}{EI_2} dx + \int_{L3} \frac{Mm_2}{EI_3} dx \tag{3.5}$$

$$\Delta_3 = \int_{L1} \frac{Mm_3}{EI_1} dx + \int_{L2} \frac{Mm_3}{EI_2} dx + \int_{L3} \frac{Mm_3}{EI_3} dx \tag{3.6}$$

$$\Delta_4 = \int_{L1} \frac{Mm_4}{EI_1} dx + \int_{L2} \frac{Mm_4}{EI_2} dx + \int_{L3} \frac{Mm_4}{EI_3} dx \tag{3.7}$$

where Equations 3.4 to 3.7 can be manipulated through the use of vector inner product (dot product) as:

$$\Delta_1 = \begin{bmatrix} \int_{L1} M\, m_1 dx & \int_{L2} M\, m_1 dx & \int_{L3} M\, m_1 dx \end{bmatrix} \begin{bmatrix} \frac{1}{EI_1} \\ \frac{1}{EI_2} \\ \frac{1}{EI_3} \end{bmatrix} \tag{3.8}$$

$$\Delta_2 = \begin{bmatrix} \int_{L1} M\, m_2 dx & \int_{L2} M m_2 dx & \int_{L3} M m_2 dx \end{bmatrix} \begin{bmatrix} \frac{1}{EI_1} \\ \frac{1}{EI_2} \\ \frac{1}{EI_3} \end{bmatrix} \tag{3.9}$$

$$\Delta_3 = \begin{bmatrix} \int_{L1} M m_3 dx & \int_{L2} M m_3 dx & \int_{L3} M m_3 dx \end{bmatrix} \begin{bmatrix} \frac{1}{EI_1} \\ \frac{1}{EI_2} \\ \frac{1}{EI_3} \end{bmatrix} \tag{3.10}$$

$$\Delta_4 = \begin{bmatrix} \int_{L1} M m_4 dx & \int_{L2} M m_4 dx & \int_{L3} M m_4 dx \end{bmatrix} \begin{bmatrix} \frac{1}{EI_1} \\ \frac{1}{EI_2} \\ \frac{1}{EI_3} \end{bmatrix} \tag{3.11}$$

where the row vectors containing the products of the integrations of the real and virtual bending moment diagrams are the unit response functions. Combining these four equations into a linear system of equations produces:

$$\begin{bmatrix} \Delta_1 \\ \Delta_2 \\ \Delta_3 \\ \Delta_4 \end{bmatrix} = \begin{bmatrix} \int_{L1} M m_1 dx & \int_{L2} M m_1 dx & \int_{L3} M m_1 dx \\ \int_{L1} M m_2 dx & \int_{L2} M m_2 dx & \int_{L3} M m_2 dx \\ \int_{L1} M m_3 dx & \int_{L2} M m_3 dx & \int_{L3} M m_3 dx \\ \int_{L1} M m_4 dx & \int_{L2} M m_4 dx & \int_{L3} M m_4 dx \end{bmatrix} \begin{bmatrix} \frac{1}{EI_1} \\ \frac{1}{EI_2} \\ \frac{1}{EI_3} \end{bmatrix} \tag{3.12}$$

Normalization by EI_0 so that $\frac{EI_0}{EI_i} \approx 1 \text{ for } i = 1,2,3$ is then introduced to obtain a better numerical performance:

$$\begin{bmatrix} \Delta_1 \\ \Delta_2 \\ \Delta_3 \\ \Delta_4 \end{bmatrix} = \frac{1}{EI_0} \begin{bmatrix} \int_{L1} M m_1 dx & \int_{L2} M m_1 dx & \int_{L3} M m_1 dx \\ \int_{L1} M m_2 dx & \int_{L2} M m_2 dx & \int_{L3} M m_2 dx \\ \int_{L1} M m_3 dx & \int_{L2} M m_3 dx & \int_{L3} M m_3 dx \\ \int_{L1} M m_4 dx & \int_{L2} M m_4 dx & \int_{L3} M m_4 dx \end{bmatrix} \begin{bmatrix} \frac{EI_0}{EI_1} \\ \frac{EI_0}{EI_2} \\ \frac{EI_0}{EI_3} \end{bmatrix} \tag{3.13}$$

Equation 3.13 is for one generic time step. To utilize data of multiple time steps:

$$\begin{bmatrix} \Delta_{1k} \\ \Delta_{2k} \\ \Delta_{3k} \\ \Delta_{4k} \end{bmatrix} = \frac{1}{EI_0} \begin{bmatrix} \int_{L1} M_k m_1 dx & \int_{L2} M_k m_1 dx & \int_{L3} M_k m_1 dx \\ \int_{L1} M_k m_2 dx & \int_{L2} M_k m_2 dx & \int_{L3} M_k m_2 dx \\ \int_{L1} M_k m_3 dx & \int_{L2} M_k m_3 dx & \int_{L3} M_k m_3 dx \\ \int_{L1} M_k m_4 dx & \int_{L2} M_k m_4 dx & \int_{L3} M_k m_4 dx \end{bmatrix} \begin{bmatrix} \frac{EI_0}{EI_1} \\ \frac{EI_0}{EI_2} \\ \frac{EI_0}{EI_3} \end{bmatrix} \tag{3.14}$$

Generalizing Equation 3.14 to multiple loading steps, for example, considering $N = 3$, $J = 4$, and $K = 2$:

$$\begin{bmatrix} \Delta_{11} \\ \Delta_{21} \\ \Delta_{31} \\ \Delta_{41} \\ \Delta_{12} \\ \Delta_{22} \\ \Delta_{32} \\ \Delta_{42} \end{bmatrix} = \frac{1}{EI_0} \begin{bmatrix} \int_{L1} M_1 m_1\, dx & \int_{L2} M_1 m_1 dx & \int_{L3} M_1 m_1 dx \\ \int_{L1} M_1 m_2\, dx & \int_{L2} M_1 m_2\, dx & \int_{L3} M_1 m_2\, dx \\ \int_{L1} M_1 m_3 dx & \int_{L2} M_1 m_3\, dx & \int_{L3} M_1 m_3 dx \\ \int_{L1} M_1 m_4\, dx & \int_{L2} M_1 m_4\, dx & \int_{L3} M_1 m_4\, dx \\ \int_{L1} M_2 m_1\, dx & \int_{L2} M_2 m_1 dx & \int_{L3} M_2 m_1 dx \\ \int_{L1} M_2 m_2\, dx & \int_{L2} M_2 m_2\, dx & \int_{L3} M_2 m_2\, dx \\ \int_{L1} M_2 m_3 dx & \int_{L2} M_2 m_3 dx & \int_{L3} M_2 m_3 dx \\ \int_{L1} M_2 m_4\, dx & \int_{L2} M_2 m_4\, dx & \int_{L3} M_2 m_4\, dx \end{bmatrix} \begin{bmatrix} \frac{EI_0}{EI_1} \\ \frac{EI_0}{EI_2} \\ \frac{EI_0}{EI_3} \end{bmatrix} \tag{3.15}$$

Despite multiple time steps, the bending moment response does not change in shape, only magnitude. Given the fact that $M_k = M_0 P_k$, where M_0 is the moment response of the beam under a unit load and P_k is the scaling time step, and after applying vectorization in coding for computational efficiency:

$$HP = \underbrace{\begin{bmatrix} h_{11}^{(1)} & h_{11}^{(2)} & h_{11}^{(3)} & h_{21}^{(1)} & h_{21}^{(2)} & h_{21}^{(3)} & \cdots & h_{32}^{(1)} & h_{32}^{(2)} & h_{32}^{(3)} & h_{42}^{(1)} & h_{42}^{(2)} & h_{42}^{(3)} \\ P_1 & P_1 & P_1 & P_1 & P_1 & P_1 & \cdots & P_2 & P_2 & P_2 & P_2 & P_2 & P_2 \end{bmatrix}^T}_{1\ x\ JKN} \tag{3.16}$$

Reshaping and transposing Equation 3.16 and normalizing this scaled up response function matrix by EI_0 results in the matrix **H** to be introduced in the following.

3.3.2.2 Modeling: Mathematical Overview

Utilizing the system's response to *K* applied loading schemes, the measured deflections across *J* active degrees of freedom can be formulated into a math problem to solve for system stiffness through the equation:

$$\underbrace{\boldsymbol{\Delta}}_{JK\ x\ 1} = \underbrace{\boldsymbol{H}}_{JK\ x\ N}\ \underbrace{\boldsymbol{\theta}}_{N\ x\ 1} \tag{3.17}$$

where Δ is a column vector of length *JK* housing the elastic deflections that are induced by an incremental loading scheme, illustrated previously. Next, **H** is a *JK* × *N* matrix of the response function that is scaled up and normalized by EI_0, also illustrated previously. Lastly, θ is the least-squares solution to Equation 3.17 consisting of *N* elements each representing a piecewise segment of the beam. For each piecewise

segment the value of θ is to be approximately equal to 1 through the ratio EI_0/E_i as illustrated previously.

Bayesian analysis starts with accounting for stochastic forward model prediction errors through the inclusion of $\boldsymbol{\varepsilon}$ using:

$$\boldsymbol{\Delta} = \widehat{\boldsymbol{H}}\,\boldsymbol{\theta} + \boldsymbol{\varepsilon} \tag{3.18}$$

where the Gaussian $\boldsymbol{\varepsilon}$ represents *a priori* modeling uncertainty and measurement uncertainty. This term is modeled through maximum Shannon entropy to return maximum uncertainty subject to statistical moment constraints of zero mean and covariance matrix $\sigma^2 I_{JK}$, where σ^2 is the prediction error variance whose value is uncertain and must be learned from the data. A Gaussian prior σ_0^2, is also required to quantify the *a priori* uncertainty about the values of the parameters to be identified, θ.

The Bayesian solution in this study is derived analytically involving an optimization with respect to σ^2. In short, calculation starts with priors and ends with posteriors. First, the posterior covariance is:

$$\boldsymbol{S} = \left[\sigma_0^{-2}\,\boldsymbol{I}_N + \sigma^{-2}\,\widehat{\boldsymbol{H}}^{\boldsymbol{T}}\widehat{\boldsymbol{H}}\right]^{-1} \in \mathbb{R}^{N\,x\,N} \tag{3.19}$$

which is a square matrix of $N \times N$ dimensions, where N is the number of the parameters to be identified. The posterior mean is the most probable values of the parameters to be identified is given as:

$$\overline{\boldsymbol{\theta}} = \sigma^{-2}\boldsymbol{S}\,\widehat{\boldsymbol{H}}^{\boldsymbol{T}}\widehat{\boldsymbol{\Delta}} + \sigma_0^{-2}\boldsymbol{S}\boldsymbol{\theta}_{\boldsymbol{0}} \in \mathbb{R}^N \tag{3.20}$$

A parametric study regarding the choice of σ_0^2 and the initial value for σ_0^2 in the optimization are extensively studied in Toshima (2019). A brief summary of the study is provided in Section 3.3.

3.3.2.3 Coding: Organization

The solution to the inverse problem was automated through a suite of files constructed in MATLAB; the individual files will be referred to as *m-files* hereafter due to their naming (filename.m). The processes of the m-files run by MATLAB in this study

are separated into two unique parts: Main and Preprocessing. All components of the suite are given as follows:

Preprocessing: Real-world data preprocessing

- Data truncation
- High frequency noise filtering
- Data quality check
- Data reduction

Main: Ordinary least-squares solution

- Rigid body motion correction
- Unit response function construction
- Scaling and normalization
- Ordinary least-squares regression
- Pseudo-inverse algorithm application

Main: Bayesian solution

- Introduction of uncertainty to problem formulation
- Maximizing objective function
- Parametric study tuning prior
- Identifying most probable solution

Utilities:

- Specifying test configuration
- Specifying identification substructure
- Saving results
- Plotting results

The flowchart in Figure 3.11 illustrates the interactions of all m-files created for this study. The flowcharts in Figures 3.11 and 3.12 illustrate the interactions of all m-

files created for this study for stiffness identification and data preprocessing, respectively. Detailed descriptions of the coding of the m-files can be found in Toshima (2019). The code is extensively and intensively validated.

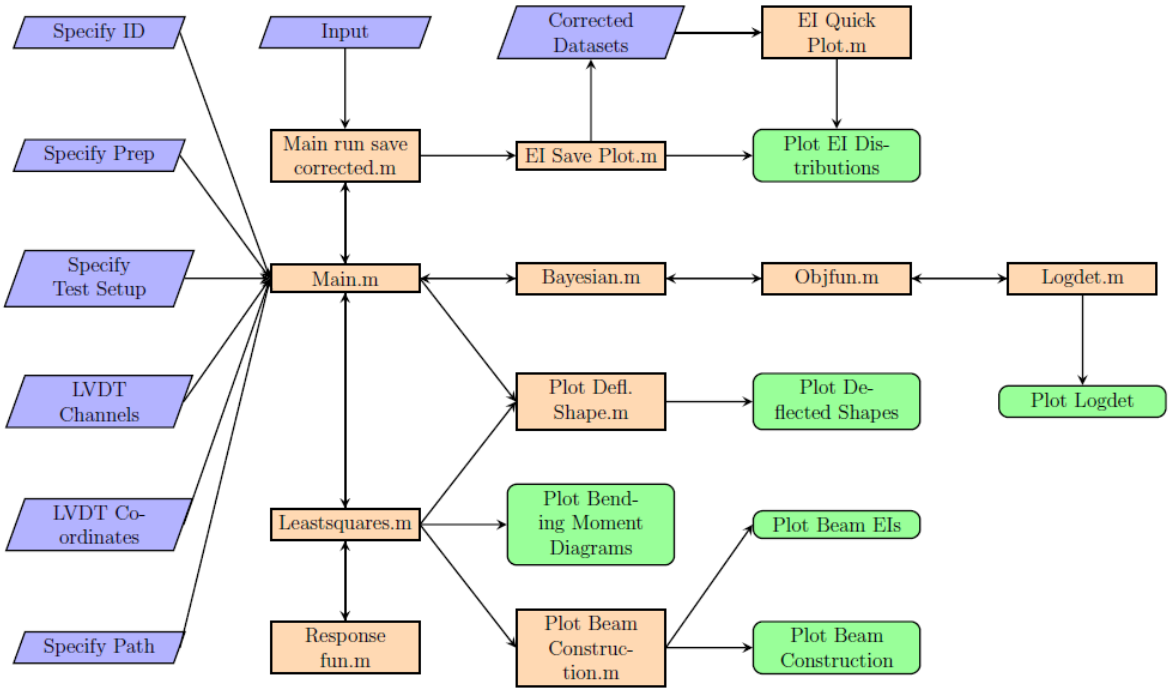

Figure 3.11. A flowchart of the developed code for piecewise EI identification

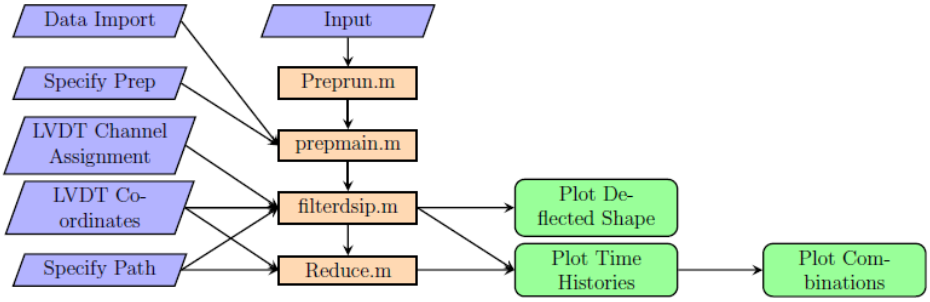

Figure 3.12. A flowchart of the involved additional preprocessing

3.3.2.4 Coding: Preprocessing

A total of 27 datasets were obtained from Girder A as in Floyd et al. (2016), which were stored as Excel (.csv) files. The datasets encompass the 17 testing configurations conducted by Floyd et al. (2016) and shown in Appendix D of Cranor (2015). Tests where data acquisition issues were suspected to have occurred warranted

additional testing and are distinguished by letters “a” and “b” following the test configuration number.

The Preprocessing code was looped for the 27 datasets to automate filtering and truncation for data cleansing and reduction, respectively. A typical raw dataset is presented in Figure 3.13.

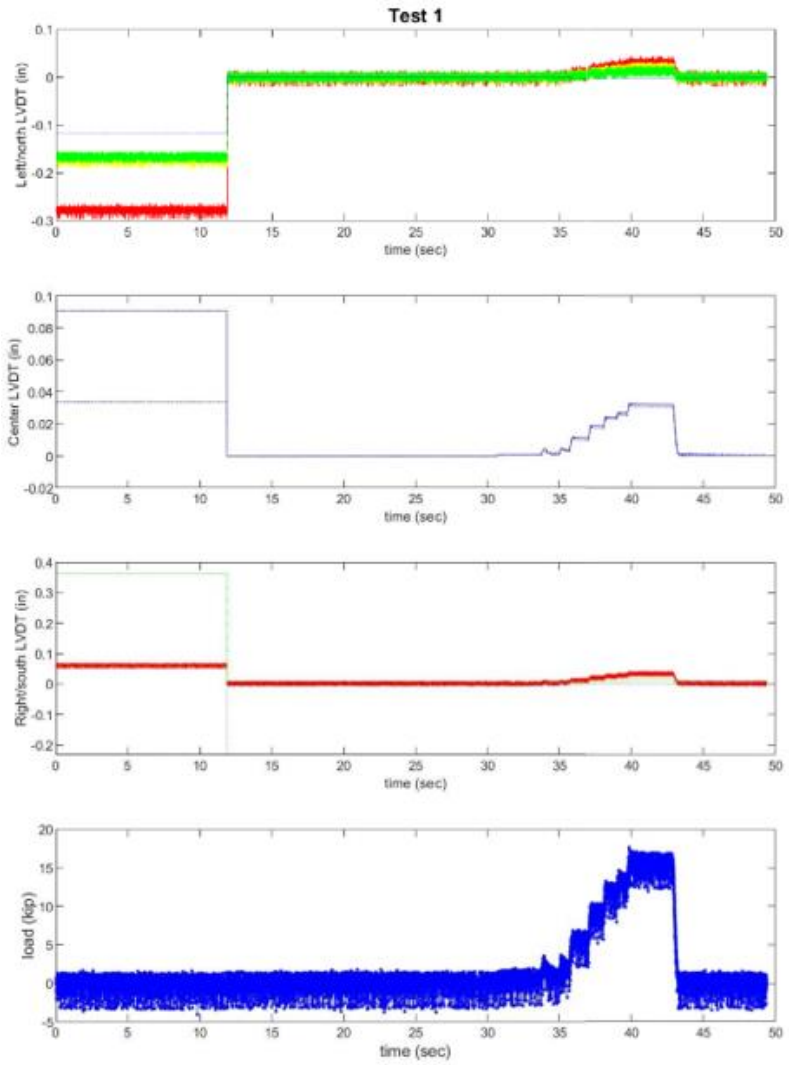

Figure 3.13. Raw load and displacement time histories of a typical test including irrelevant data

The deflection dataset’s time histories were first truncated to remove the irrelevant data before testing commenced. The high frequency noise visible in Figure 3.13 was then filtered utilizing MATLAB’s butter and filter commands, where a second-

order Butterworth digital filter was used with a cutoff frequency of 0.01. Load-deflection graphs for all LVDTs were then produced. Next, the load-deflection datasets were reduced to include only the data points (denoted by the circle markers in Figure 3.14)

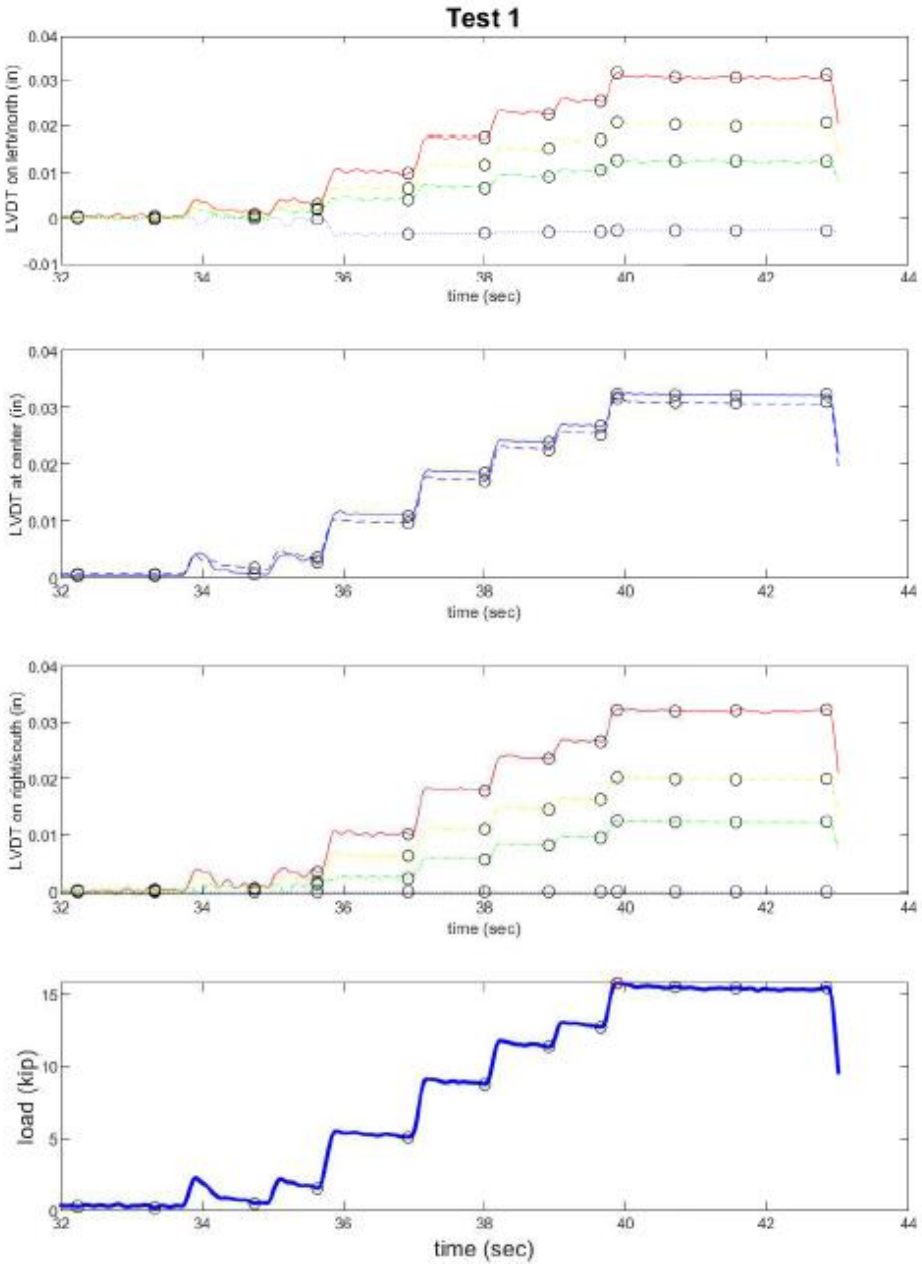

Figure 3.14. Filtered (with a low-pass filter) and reduced (as shown in circles) multi-channel data measurements for further analysis

3.2.2.5 Coding: Validation

Validation of both the model and code was necessary. The validation datasets used were load-deflection datasets simulated using beam theory and matrix structural analysis (MSA), where the parameter values were assumed/known. The validation cases mirrored the 17 testing configurations of Girder A characterized into three conditions: a simply supported beam without overhanging spans, a simply supported beam with an overhang on the left/north side of the beam, and a simply supported beam with an overhang on the right/south side of the beam. The MSA beam datasets contained various piecewise *EI* scenarios.

These simulated datasets with additional added noise were processed using the developed code. Typical results given in Figures 3.15 to 3.17 and Tables 3.2 to 3.4 indicate that the proposed method and developed code are able to successfully identify piecewise constant *EI* values and perform better than the least-squares method that was previously adopted.

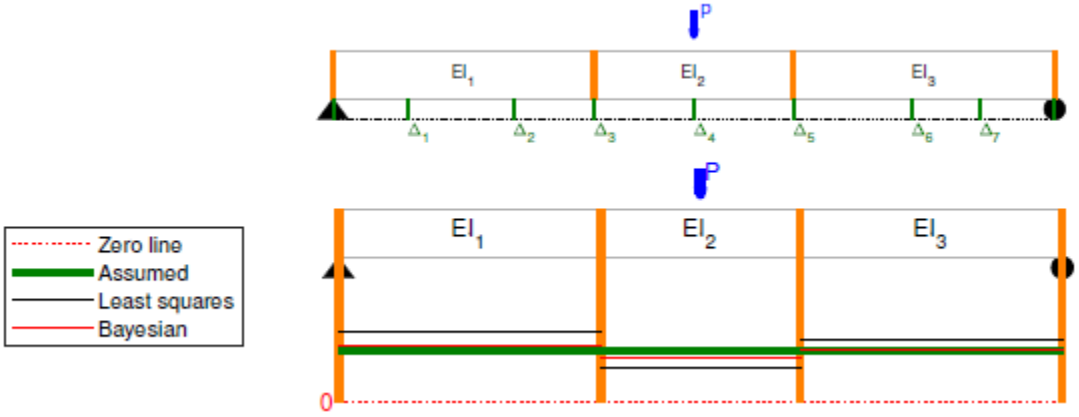

Figure 3.15. Visual representation of validation of the least-squares and Bayesian methodologies using a simple beam - with uniform EIs, for the test 1 setup

Table 3.2. Results from validation of the least-squares and Bayesian methodologies using a simple beam – with uniform EIs, for the test 1 setup

Result	**EI_1**	**EI_2**	**EI_3**
Anticipated θ	1.00	1.00	1.00
Least Squares θ	0.81	1.19	0.88
Bayesian θ	0.96	1.08	1.00
Anticipated EI ($x10^8$ kip-in^2)	3.50	3.50	3.50
Least Squares EI ($x10^8$ kip-in^2)	4.34	2.95	3.96
Bayesian EI ($x10^8$ kip-in^2)	3.65	3.23	3.49

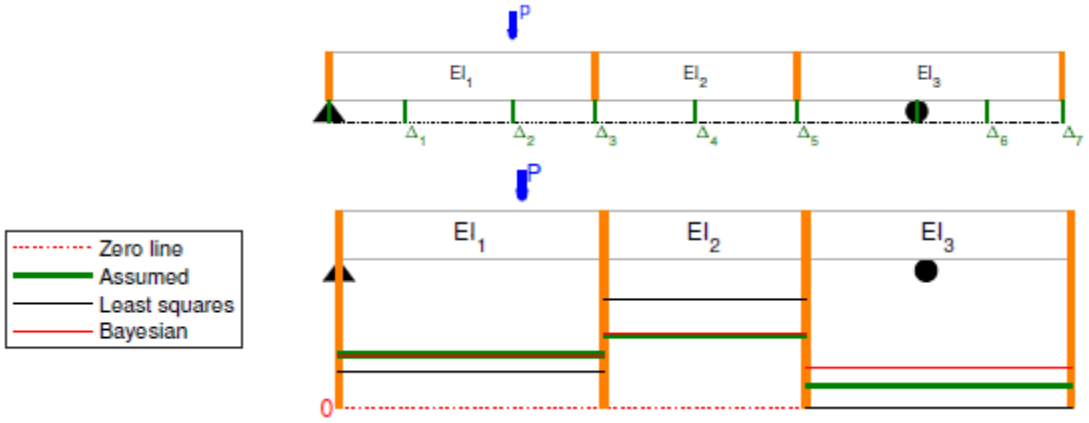

Figure 3.16. Validation of the least-squares and Bayesian methodologies using a simple beam - with varying piecewise constant EIs, for the test 10 setup

Table 3.3. Results from validation of the least-squares and Bayesian methodologies using a simple beam – with varying piecewise constant EIs, for the test 10 setup

Result	**EI_1**	**EI_2**	**EI_3**
Anticipated θ	1.00	0.80	1.33
Least Squares θ	1.17	0.42	2.74
Bayesian θ	1.00	0.78	1.14
Anticipated EI ($x10^8$ kip-in^2)	4.00	4.00	4.00
Least Squares EI ($x10^8$ kip-in^2)	3.41	9.42	1.46
Bayesian EI ($x10^8$ kip-in^2)	3.99	5.11	3.52

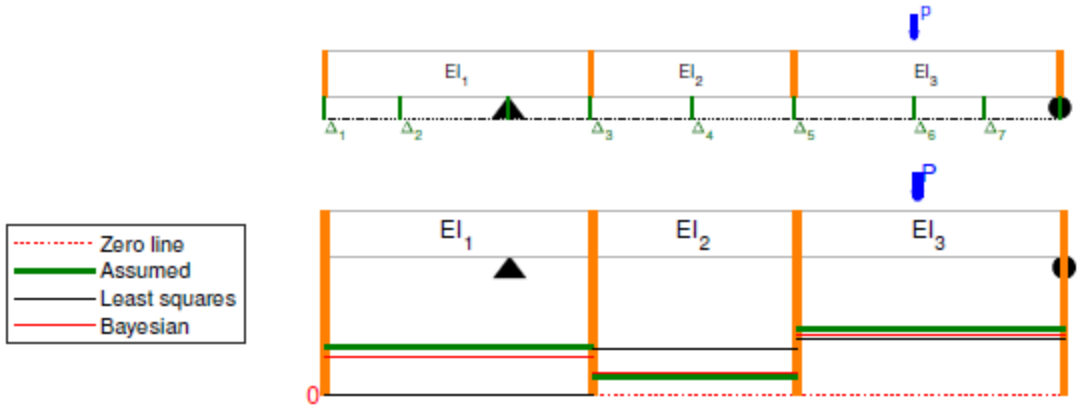

Figure 3.17. Validation of the least-squares and Bayesian methodologies using a simple beam - with varying piecewise constant EIs, for the test 15 setup

Table 3.4. Results from validation of the least-squares and Bayesian methodologies using a simple beam - with varying piecewise constant EIs, for the test 15 setup

Result	**EI_1**	**EI_2**	**EI_3**
Anticipated θ	1.00	1.33	0.80
Least Squares θ	4.14	1.01	0.91
Bayesian θ	1.12	1.29	0.86
Anticipated EI ($x10^8$ kip-in^2)	4.00	4.00	4.00
Least Squares EI ($x10^8$ kip-in^2)	0.966	3.95	4.39
Bayesian EI ($x10^8$ kip-in^2)	3.58	3.11	4.67

3.3.3 Analysis, Results and Discussion

3.3.3.1 "Good" and "Bad" Data

A total of 27 tests, with 17 different loading and support configurations, were conducted on Girder A. The quality and condition of some of the measurement devices were questioned when the data was collected. For example, even if an LVDT was functioning properly even after calibration and examinations this suspicion was the rationale for repeated testing on most of the configurations. In this study, the preprocessed data was first examined in terms of time histories, force-displacement and deflected shape plots regarding measurements by all LVDTs in all tests. Quality of measurements from a few LVDTs was in question from time to time. A discussion of LVDT L1, meaning the first LVDT left to the center of the span, is included here to illustrate the challenge. Figure 3.18 shows the measured deflections along the length of

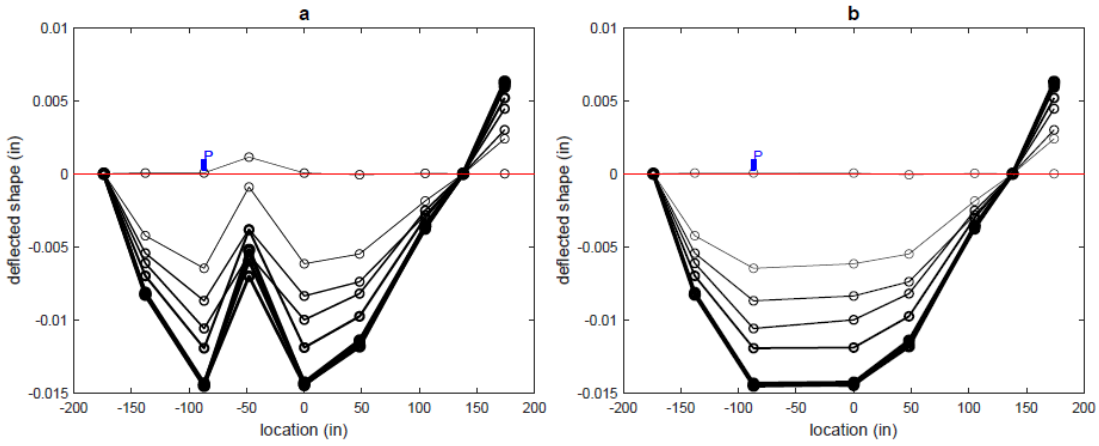

Figure 3.18. Panel (a) shows a typical test result involving a potentially malfunctioning LVDT L1 (located approximately 50 in. left of the beam centerline). Panel (b) shows the strategy adopted to remove all readings from the possibly unreliable LVDT L1

the girder at several different load levels. LVDT L1 appears to provide results that do not make sense relative to the expected behavior and the effects of rigid body motion were corrected resulting in elastic curves.

In principle, an elastic curve is obtained through the so-called double-integration of *M(x)/EI(x)*. It is known that *M*(*x*) is piecewise linear, and it was assumed that *EI*(*x*) is piecewise constant. Since the piecewise constant *EI* is not anticipated to drastically differ between segments, the elastic curve should not differ fundamentally from the counterpart of one constant *EI* value, which is known based on structural analysis. For the test configuration shown in Figure 3.18, no inflection points were anticipated between supports. With this said, the “spikes” caused by LVDT L1 were questionable. This difference from the anticipated behavior raised concern of whether and how much the readings of a suspicious LVDT(s) would impact the identified piecewise *EI* values.

Carefully examining the elastic curves led to the conclusion that not all LVDTs performed reasonably at all times. In other words, some elastic curves were deemed reasonable relative to the loading and support configurations, while others were not. Confirming that some LVDT readings were questionable, for example LVDT L1 in Figure 3.18, it was necessary to remove the data associated with the specific malfunctioning LVDT so that the identification results were not corrupted. Panel B of Figure 3.18 shows the removal of L1 from all loading history associated with the test resulting in a smoother curve. In this instance, the malfunctioning LVDT was seemingly obvious to identify. In other cases it was increasingly difficult to identify a malfunctioning LVDT(s). A consistent method is required to determine which tests were affected by possible malfunctions. For this purpose, Relative Entropy (Kullback-Leibler (KL) Distance), a concept from Computer Science (Bishop 2006), of each realization (of the identified results) was calculated to quantify LVDT L1’s effect, as documented in detail in Toshima (2019).

3.3.3.2 Uncertainties in Measurements and Modeling

More generally, uncertainties can be attributed to the problem at hand under the following non-exhaustive categories:

- **Category 1: Environmental** - Effects stemming from ambient conditions such as temperature or humidity;
- **Category 2: Material Properties** - Variations in second moment of inertia (I) along the length of the girder as well as those in Young's Modulus (E_c) along both span and depth of the member, (time-effects considered accordingly), and prior damage and testing damage experienced by Girder A in terms of steel debonding and crack formations between tests;
- **Category 3: Experimental** - Variability in data acquisition capabilities by the load cell or LVDTs as discussed previously;
- **Category 4: Modeling** - Numerical uncertainties and model-form uncertainties including technical details concerning Bayesian analysis used in this study.

The discussion in this section intends to shed light on the potential impacts stemming from the uncertainty in these categories on stiffness identification.

Not accounting for the curing of the concrete in any harsh conditions, focus is shifted to the effects of Category 1 on flexural testing. A vast amount of literature exists on temperature and moisture effects on the curing of concrete however, relatively little exists (or is available) in terms of their effects on flexural testing. Shoukry et al. (2009) determined an inverse correlation in both concrete strength and Young's Modulus related to temperature and moisture content. Testing of Girder A occurred at Fears Structural Engineering Lab at The University of Oklahoma during the summer season, over the course of several days. The testing of Girder A in a laboratory setting allows for minimal effects in concrete strength reduction in terms of the research by Shoukry et al. (2009), who tested their specimens at upwards of 90 percent moisture content and 38 °C (100 °F). Though not a direct comparison to flexural testing, it is assumed that perhaps the impacts of ambient conditions are negligible and their minimal effects may be encompassed by the chosen prior standard deviation accounting for uncertainties in other categories.

Regarding Category 2, a brief investigation of the variation of I along Girder A's length in Toshima (2019) indicates insignificant variation in I due to strand harping. The value of Young's Modulus as determined by Cranor (2015) encompasses the variability

of E_c to describe the beam. Two determinations of Young's Modulus were conducted for Girder A by Cranor (2015): through concrete cores and flexural stiffness testing. The concrete cores were taken at varying depths and span locations to find an average E_c. Of the cores taken, only 6 samples were retained due to sampling issues, however, spread is still seen in the determination of Young's Modulus for the cores. The spread in determined results can also be attributed to time-dependent decreases, such as creep, after Girder A's 40 years of service. Though cores represent discrete points along the length and depth of Girder A with some variation, the average E_c from flexural stiffness testing has a higher potential for fluctuation between tests based on procedure and measurement errors. The largest value of Young's Modulus from flexural stiffness testing may best represent variations with respect to creep effects as it is smaller than the average E_c measured from the cores and the calculated E_c using the ACI (2014) equation. Thus, the representative E_c for Girder A, based on the largest value of E_c from flexural stiffness testing, 4150 ksi, was used.

Issues related to data acquisition errors were discussed in Section 3.3.3.1 and are grouped into Category 3. High resolution measurements were made for loading and deflection by the load cell and LVDTs utilized in testing. Error is inherent to the measurements taken despite the accuracy of these instruments. The Interface model 1252 load cell's static error band (maximum error) is ±0.10 % Full Scale. Meanwhile, the LVDTs were able to accurately detect changes of approximately 0.001 in. with typical errors on the order of 0.5 percent when compared to a calibrated micrometer.

Another potential source of error in experimental measurements may be attributed to possible imperfections in vertical alignment of the LVDTs. The testing of Girder A was conducted over the course of several days and repeated for certain tests where data quality was questioned by the researchers conducting the tests. When set for testing, the LVDTs should contact the underside of the girder at a perpendicular angle - otherwise, measurement errors may arise due to the angle of contact. Instruments utilized were calibrated for each non-repeated test but repositioning of the LVDTs was necessary between tests with different test configurations and those tests with questionable data quality, denoted by "a" and "b" in the test name. Repositioning the LVDTs on the underside of Girder A was found to be difficult at times. Of the

instruments used in experimental data collection, the LVDT readings are thought to be most influenced by uncertainties. Uncertainties and their impact through the act of flexural testing and test setup must be learned through the data learning process from Bayesian analysis viewpoint (e.g., Huang et al. 2019).

Under Category 4, uncertainties in modeling are based mostly on the assumptions in the problem formulation (model-form uncertainty) as well as observed numerical performance. An assumption made in the problem formulation includes the piecewise constant nature of stiffness that is to be identified. Built on the foundations of beam theory and applied to numerous substructures, this assumption holds only for linear-elastic beam behavior. Hence, it is possible to inversely identify *EI* through deflections and loading. For sections of the beam having pre-existing damage (e.g. end regions with strands debonded due to corrosion), it is difficult to quantify the effects of this damage on collected data without an undamaged dataset for comparison. Through piecewise constant stiffness it is expected to see localizations of damage in the form of reduced stiffness, but functional threshold(s) of stiffness must first be assumed to properly characterize what is considered “damage”.

The issue of numerical uncertainties was addressed through the verification and validation process. Verification is the determination of whether the mathematical model is correctly solved and validation is the assessment of accuracy of the model simulation for its application domain. Roache (1998) simplifies these definitions as “solving the equations right” and “solv[ing] the right equations”. Freitas (2002) further expands on validation to “solving the right model equations with the right methods” to disassociate numerical errors that arise between a given model and methodology to arrive at a solution. In this study, the model and code was validated extensively through sets of problems with known solutions.

Carrying out the Bayesian analysis outlined in Section 3.3.2 was a sequential operation starting by specifying a σ_0 value and then an initial value for numerically optimizing the σ value. The systematic approach was detailed with reasons and limitations in Toshima (2019). Beyond the results that have been obtained and will be

presented herein, a novel alternative approach to improve both the efficiency and insight - built on what we have accomplished – is currently being pursued.

3.3.3.3 EI Distributions

Different piecewise divisions (substructures) were explored to determine possible idealizations of *EI* distribution and efficacy of the model. Idealized distributions consist of a small number of piecewise constant *EI* substructures required for consistency in identification. For example, a beam segmented into three substructures will return three *EI* values. The three substructures are then further subdivided into six substructures to examine if the *EI*s obtained are consistent with those of the three substructure beam. An illustration of different piecewise divisions is shown in Figure 3.19. It is important to note that these divisions are not exhaustive but an initial exercise.

The following *EI* division substructures were used as shown in Figure 3.19:

A. “One substructure”: no division in the beam with one uniform value of *EI* throughout,
B. “Three substructures”: three divisions with separation at the harp points (approximately 4 ft from centerline),
C. “Six substructures”: subdivisions are made to see if the results are consistent with those under “B”,
D. “Nine substructures”: further divisions made to see if the results are consistent with those under “C”,
E. “Ten substructure”: division of the beam into ten segments for damage detection localization,
F. “Arbitrary substructure”: one realization of an arbitrary segmentation of the beam to explore robustness of model (a minimum span of 3ft is specified for identification clarity).

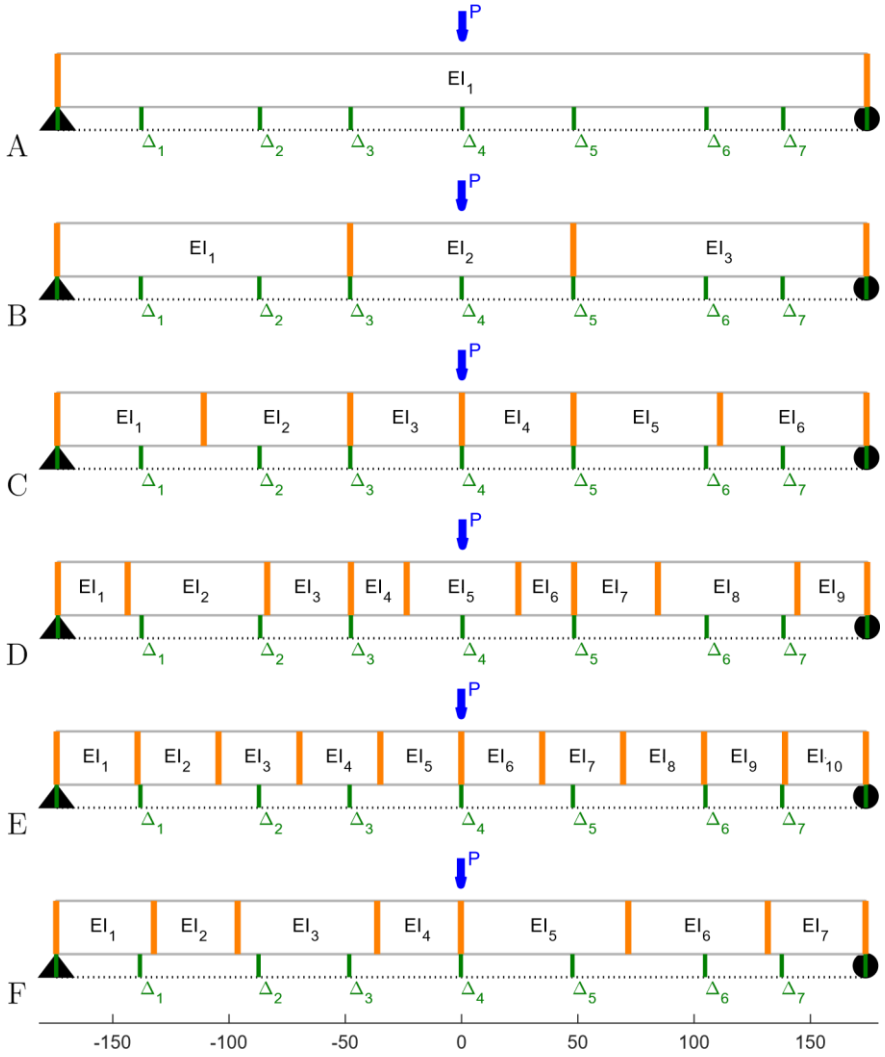

Figure 3.19. 1, 3, 6, 9, 10, and example arbitrary substructure divisions applied to a simulated Girder A

Substructure idealizations are subsequently referred to as lower or higher-order based on the number of substructures utilized. For example, case “A” is a lower-order substructure when compared to “B”, which in this instance would be a higher-order substructure.

3.3.3.4 Identified Results of EI

Using least-squares analysis can from time to time lead to individual negative *EI* values. The mean values are thus strongly tinted by the negative *EI* values in identification making the mean values untrustworthy. Conceptually, this is because the least-squares method only focuses on fitting the data not considering prior knowledge

(e.g., all *EI* values must be positive). Therefore, no results obtained using the least squares method are presented herein.

3.3.3.4.1 Identified results from specific tests

Results presented are for the *EI* divisions of the data categories listed:

Category A "Uncorrected": All LVDT readings were used,

Category B "L1 Corrected": All L1 readings were removed,

Category C: "L1-KL Corrected": Relative Entropy (Kullback-Leibler Distance) was used as criteria in removing some L1 readings.

Individual results were first obtained and plotted on a test-by-test basis for each category to determine if consistency existed in identification between higher and lower-order substructures. Test 1 is used as an example, shown in Figures 3.20 to 3.22. The constant stiffness value of $3.88\times10^8\ kip{-}in^2$ shown as a dotted line in Figures 3.20 to 3.22 was determined from a battery of flexural stiffness tests conducted in prior research by Cranor (2015). The constant stiffness value of $4.12 \times 10^8\ kip{-}in^2$ shown as a dashed line in Figures 3.20 to 3.22 represents the value calculated using the transformed second moment of inertia I_{tr} determined from MATLAB programming, its calculation is discussed in Toshima (2019).

It can be seen in Figure 3.20 that the lower-order substructure *EI*s - if simplified as averages of the higher-order, show agreement in identification between substructures for the "Uncorrected" data. True averages are not obtained as this simplification ignores the fitting of data within individual substructures; higher-order substructure cases partition data into smaller sections, affecting data fit and producing localized increases/decreases in stiffness. Furthermore, higher-order substructures' standard deviations encompass lower-order identifications. These trends are also exhibited in Figures 3.21 and 3.22 when the identification was carried out with either full or partial removal of the readings from LVDT L1. Figure 3.21 shows that the lower-order substructure EIs - if simplified as averages of the higher-order, show agreement in identification between substructures for the "L1 Corrected" data. Figure 3.22 shows that

the lower-order substructure EIs - if simplified as averages of the higher-order, show agreement in identification between substructures for the “L1-KL Corrected” data.

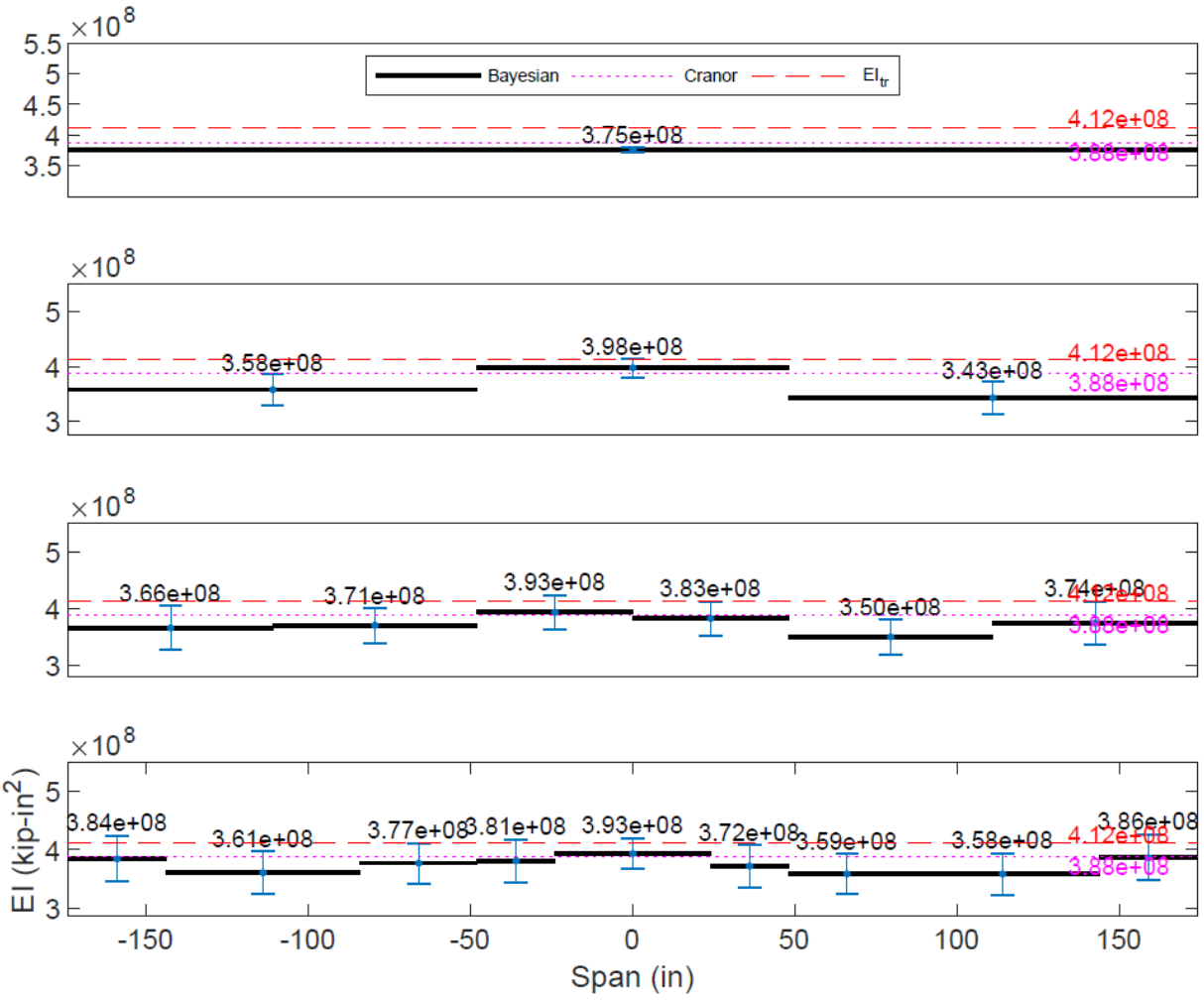

Figure 3.20. Test 1 “Uncorrected” identification for 1 (top), 3, 6, and 9 (bottom) substructure divisions

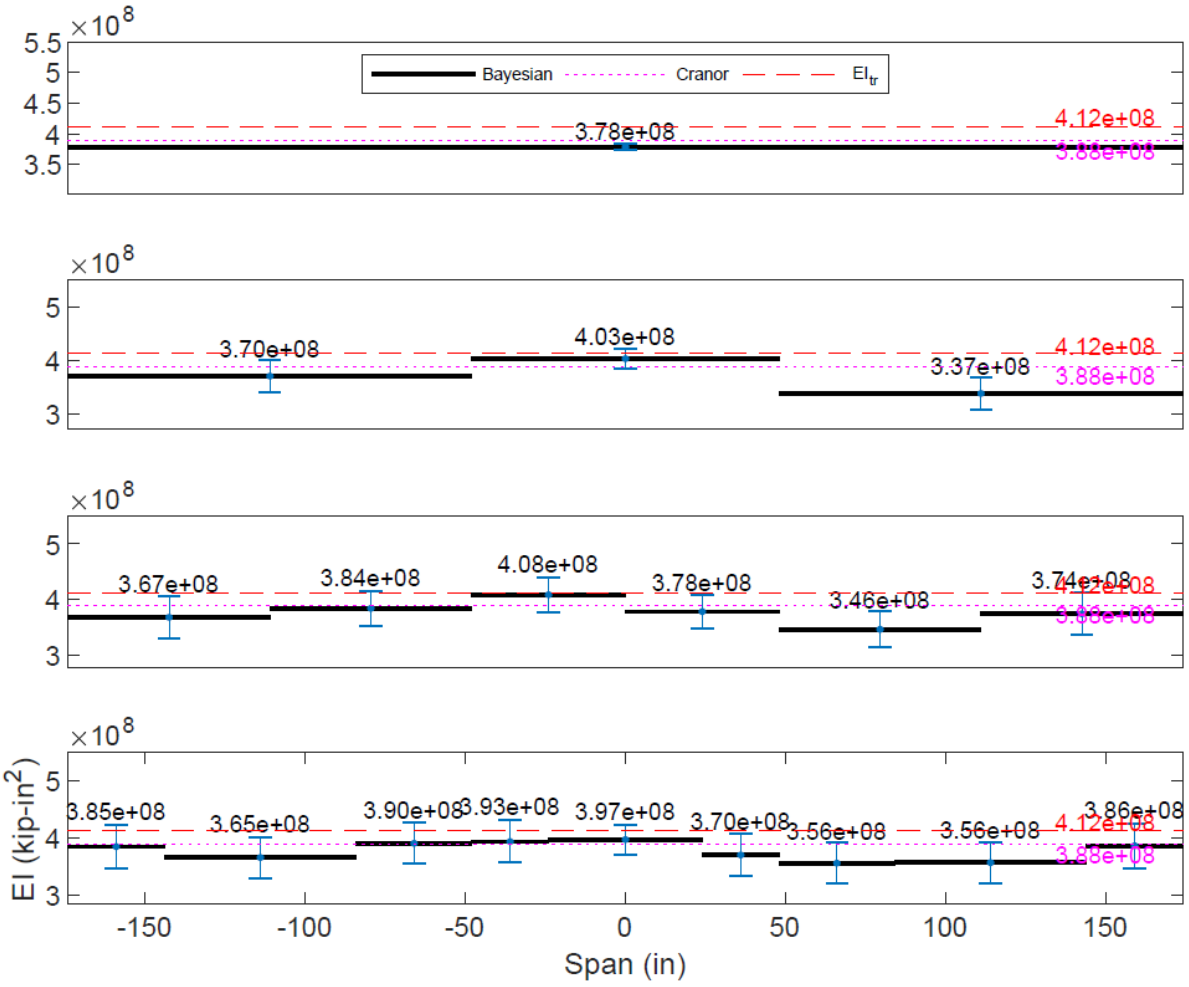

Figure 3.21. Test 1 “L1 Corrected” identification for 1 (top), 3, 6, and 9 (bottom) substructure divisions

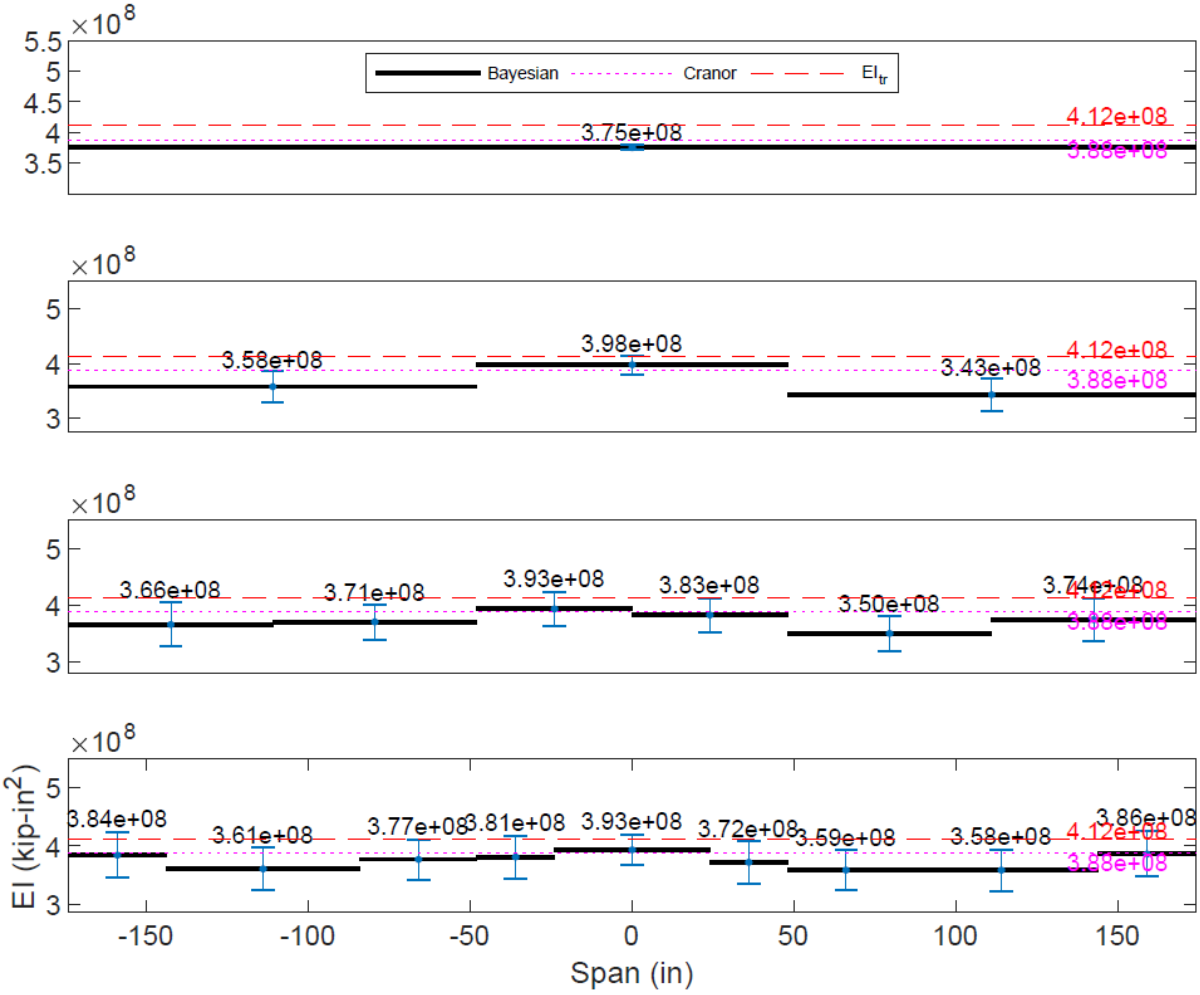

Figure 3.22. Test 1 “L1-KL Corrected” identification for 1 (top), 3, 6, and 9 (bottom) substructure divisions

3.3.3.4.2 Mean identified results from all tests

Figure 3.23 shows all three data categories plotted for each test according to testing day for the one substructure *EI* identification using Bayesian analysis. Each test day is denoted by a grey-scale section with chronological test progression from left to right. Each category’s respective mean and standard deviation are shown below the corresponding data marker in the legend. It must be noted that a few results were suspected of being unreliable and are intentionally left blank (e.g., test 5b across all substructure cases, test 4b in the six and higher-order substructure cases, and test 14b in the arbitrary substructure case). The identified results in test 14b are unusually high, the reason for which is still to be understood.

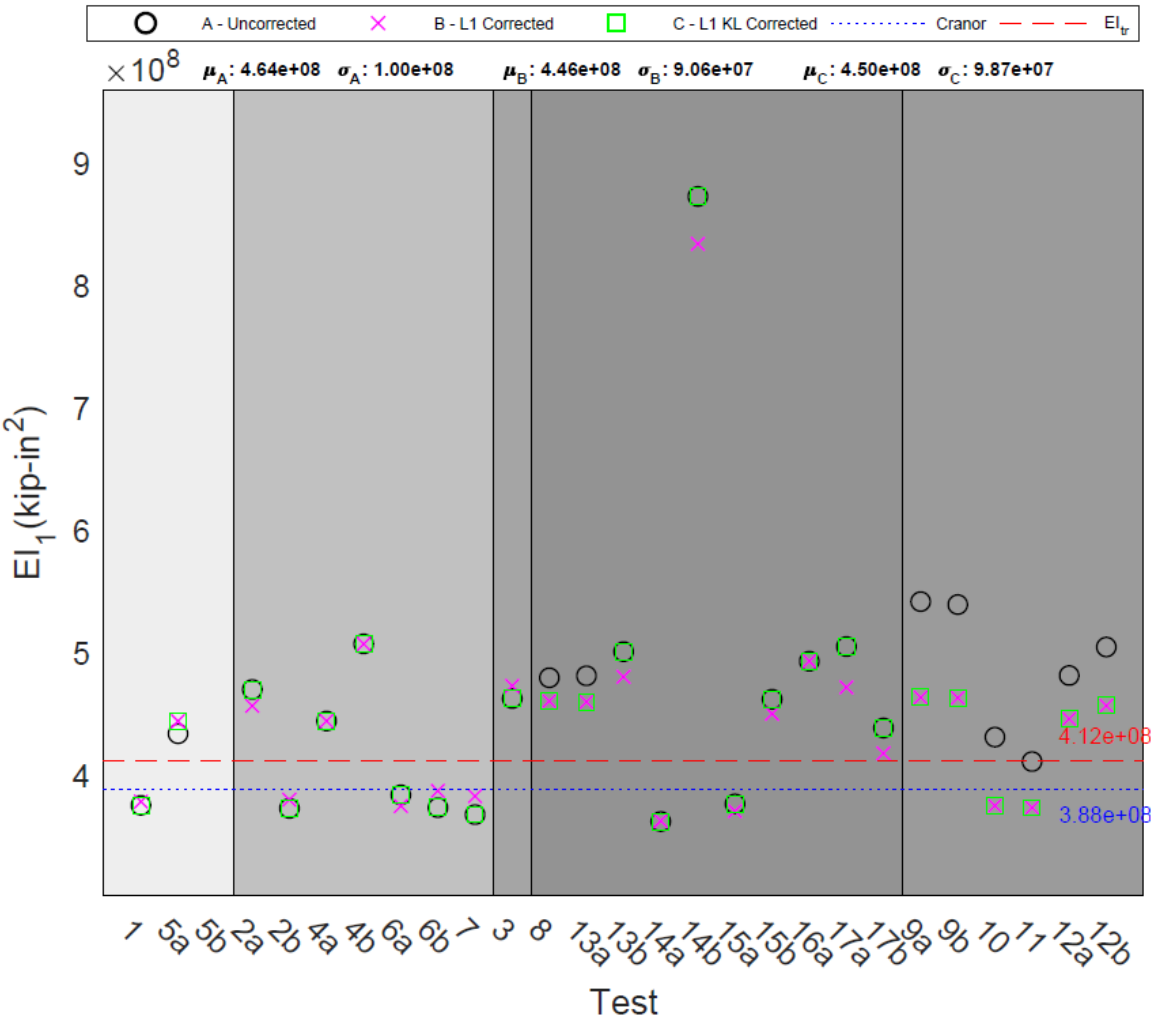

Figure 3.23. One EI value for Girder A when Bayesian analysis was applied to the one substructure case: distribution of EI identification for each test is based on data category

Comparing the location of the markers between categories, it is evident that measurements from LVDT L1 indeed affected *EI* identification, especially for those tests encompassed in the last day of testing. It should be noted that most tests in the "L1 Corrected" and "L1-KL Corrected" categories suffered a reduction in stiffness for the one substructure case, and less so for other substructures, nonetheless, the mean values of *EI* decreased minimally while reducing the standard deviations. Figure 3.23 illustrates that the partial removal of L1 mentioned in Section 3.3.3.1 may not always work more accurately, taking test 5a of the one substructure case, for example.

The effects of measurements from LVDT L1 are again seen in the plotting of the three substructure identification using Bayesian analysis in Figure 3.24. Each panel describes a substructure of the beam and the three categories are plotted for each substructure. Mixed results are evident when comparing LVDT L1's effects on each substructure. For the first substructure (EI_1), trends in mean and standard deviation between categories are found resembling the one substructure identification, which t also holds for the second substructure. The third substructure, however, displays improved identification after the removal of measurements from LVDT L1 with an increase in standard deviation for category "L1 Corrected" and the opposite for "L1-KL Corrected".

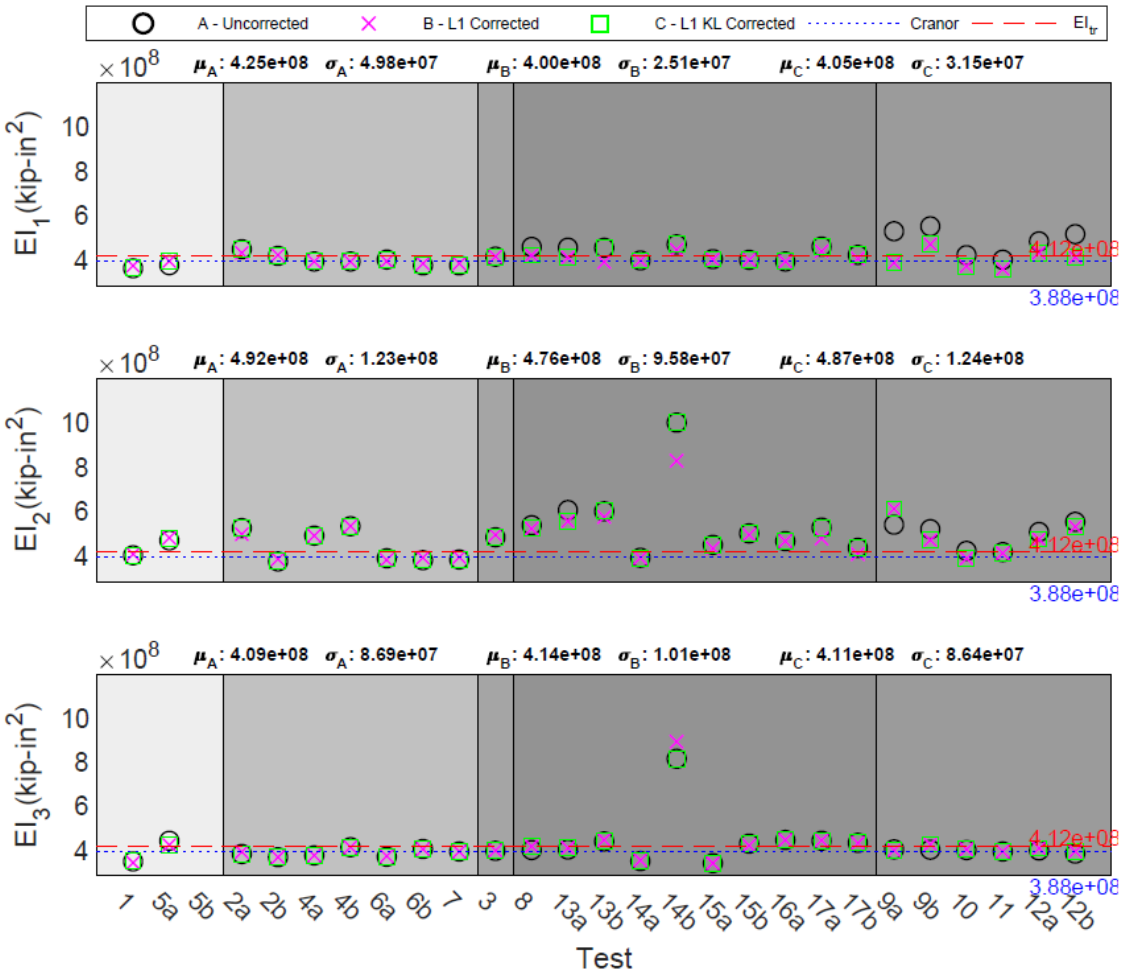

Figure 3.24. Three EI values for Girder A when Bayesian analysis was applied to the three substructure case: distribution of EI identification for each test is based on data category

The results from the six substructure case are consistent with results for the three and one substructure cases. With increasing substructures, such as to ten in Figure 3.25, the effects of removing measurements from LVDT L1 are increasingly pronounced in the substructures immediately surrounding L1. By segmenting the beam into smaller sections minuscule changes in mean identification in substructures further from L1 are visible across all categories, even with L1 removal.

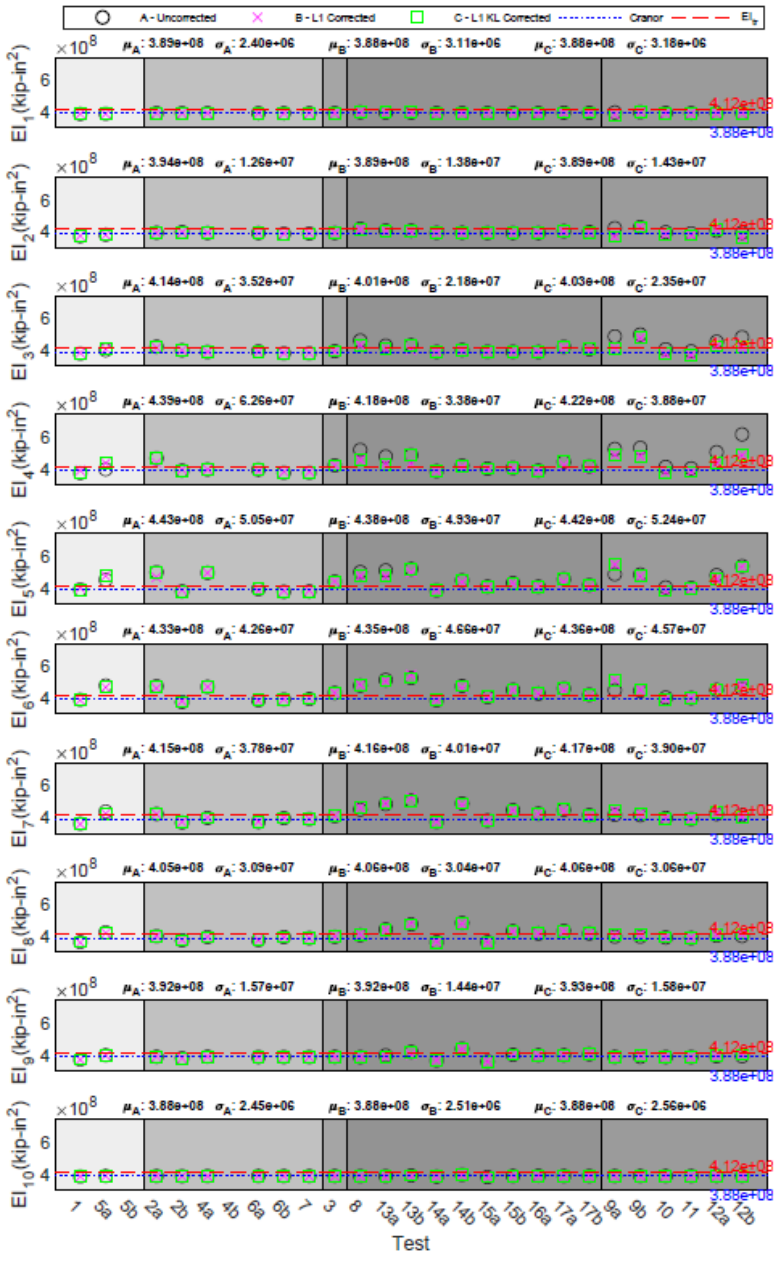

Figure 3.25. Ten EI values for Girder A when Bayesian analysis was applied to the ten substructure case: distribution of EI identification for each test is based on data category

3.3.4 Summary

Across both validation cases and actual experimental data analysis, inconsistent (zero or negative) identified flexural stiffness valued were obtained using the linear least-squares method manifesting a serious limitation, which is now well-known to structural health monitoring community. As a remedy, the Bayesian analysis method exercised in this study can lead to reasonable identified results - if how the method works is clearly understood and how to tune the involved parameters in a systematic manner is known. There is a nontrivial learning curve for Bayesian analysis, however it is a rewarding effort. Not only were meaningful initial results gained, but this method directly facilitated an improved implementation with better efficiency and more insights, which is still being pursued further.

Observations from the exercises carried out indicate that higher-order substructures, specifically the ten substructure case, return the most consistent identified results, even with LVDT malfunction(s). The higher-order, ten substructure case holds the potential for improved damage identification. The ten substructure case resulted in approximately 3 ft per substructure and smaller substructures could perhaps be utilized in future studies for this purpose.

The constant EI determined by Cranor (2015) best characterizes the beam at the two end spans (EI_1 and EI_{10}) using the ten substructure case. The reduced stiffness values at the end regions are roughly 94 percent of the conservative value of EI_{tr} with EIs larger than EI_{tr} identified at midspan. It is thus evident that Girder A has lost stiffness over the course of its 40+ years of service-life based on a conservative upper-bound stiffness given by EI_{tr}. This itself also justifies the usefulness of Bayesian analysis as expected reductions in EI are seen near the end regions of Girder A where corrosion was evident.

4.0 Examination of Sample Oklahoma Bridges

4.1 Selected Oklahoma Bridges

Originally, three actual Oklahoma bridges were modeled: the I-244 spans from which girders A and C came (deconstructed in 2013), and the Little River Overflow

bridge on Oklahoma Highway 70 (NBI # 19269, still in service). The two spans from I-244 (I-244A and I-244C) were modeled to compare with full-scale girder test results. These bridges consisted of seven longitudinal Type-II girders spaced at 7 ft 8 in. with end and middle diaphragms and a 7 in. deck (when tested in the lab these girders included a 2 in. wearing surface as well). The two spans considered were 32 ft and 46 ft for I-244A and I-244C respectively. The Little River Overflow (LRO) is also composed of Type-II girders and was an interesting case presented by ODOT engineers. This bridge has a relatively short span (35 ft) and a wide girder spacing (11 ft 9 in.). Another interesting aspect of the LRO was a relatively large deck overhang at the exterior girders (4 ft 3 in.). This increased load distribution to the exterior girders. The LRO also had a larger deck thickness as designed (9 in.) and a uniform shear reinforcement spacing of 10.5 in. These cases were examples of specific bridges modeled based on the original drawings. The other cases tested in the parametric study performed in this research were based on common dimensions found in the bridge inventory. Since the real-world bridges were cases found in Oklahoma, and since two girders from these bridges were tested in this study, the grillage models were compared to the load ratings for the bridges as well as to the results of the lab tests. Load ratings were carried out using LEAP Concrete Bridge, a commercial bridge design software by Bentley (Bentley Systems, Inc. 2016). Comparing actual tests of older girders to load ratings and finally comparing code distribution factors to grillage model derived load distribution provides a more complete view of the behavior of an in-service bridge that is not often found in the literature.

4.2 Results of Oklahoma Bridge Models

The same processes were used for these models as for the models of the scale bridge and the parametric bridge models discussed in previous sections. Section properties used in the models are given in Appendix B.

The distribution factors for the three bridges modeled are given in Table 4.1. These factors include the distribution factors from grillage modeling and the AASHTO LRFD code for interior and exterior girders with one and two or more (2+) lanes loaded.

This information is displayed graphically in Figure 4.1 to show the differences between the factors amongst the bridges and compared to the AASHTO distribution factors.

Table 4.1. Shear distribution factors for selected Oklahoma bridges

Bridge	AASHTO LRFD Ext. 1 Lane	Grillage Ex. 1 Lane	AASHTO LRFD Ext. 2+ Lanes	Grillage Ext. 2+ Lanes	AASHTO LRFD Int. 1 Lane	Grillage Int. 1 Lane	AASHTO LRFD Int. 2+ Lanes	Grillage Int. 2+ Lanes
LRO	0.823	0.760	0.951	0.854	0.692	0.632	1.066	1.000
I244 A	0.478	0.467	0.649	0.497	0.556	0.402	0.791	0.688
I244 C	0.478	0.496	0.649	0.513	0.556	0.519	0.791	0.657

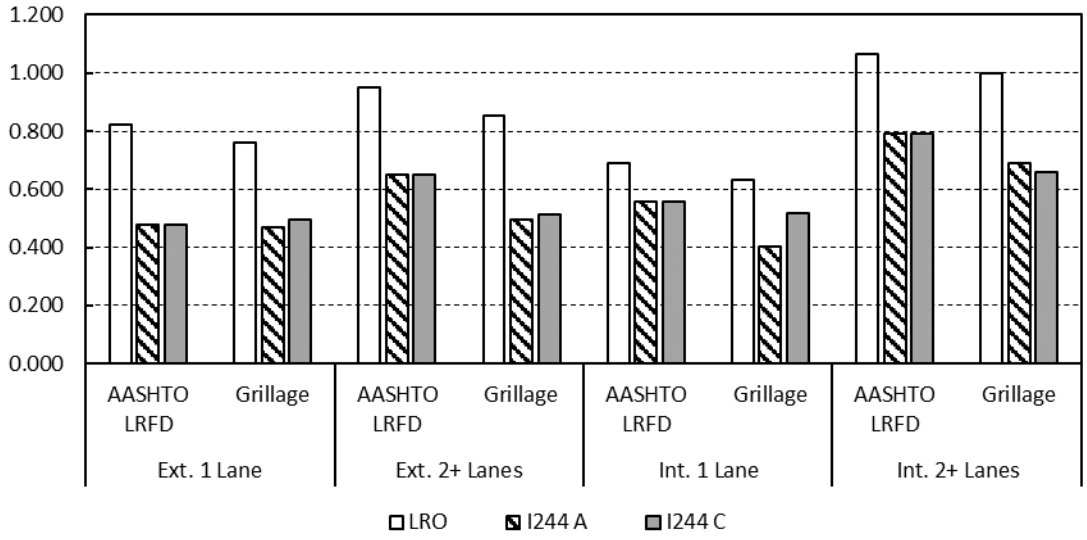

Figure 4.1. Comparison of distribution factors for selected Oklahoma bridges

Because the two spans of the I-244 bridge have the same girder spacing and the same edge distances, they have the same distribution factors according the AASHTO LRFD code. The grillage model shows that I-244C tends to have larger distribution factors than I-244A for most load cases except for interior girders loaded with two or more lanes loaded. In some cases, the AASHTO LRFD distribution factors appear to be overly conservative for the I-244 spans (for two or more lanes loaded). On the other hand, there is agreement between the AASHTO LRFD code and grillage derived distribution factors for the LRO bridge. These results are examined further in the discussion included in Section 4.3.

4.3 Discussion of Oklahoma Bridge Models

First, the Oklahoma bridge grillage models are compared with the AASHTO LRFD distribution factors to determine how well the code matched these particular cases. The distribution factors for both cases were given in Section 4.2, but Figure 4.2 shows the ratio of AASHTO distribution factor to grillage model distribution factor (note: the multiple presence factor was removed from the one lane loaded AASHTO LRFD code distribution factors). Compared this way, a number greater than 1.0 indicates a potentially conservative estimate of load distribution, and a number less than one indicates the distribution factor is underestimated by AASHTO LRFD compared to the grillage model. For the I-244C bridge span, the distribution factors are governed by the two or more lanes loaded case for both exterior and interior girders. For these cases, AASHTO LRFD is conservative relative to grillage model distribution factors by 0.265 and 0.204, respectively (26.5% and 20.4% more shear), based on the governing distribution factors. For the I-244A span, the distribution is governed by the two or more lanes loaded case for exterior girders and interior girders. For these cases, the code is conservative by a factor of 0.305 and 0.150, respectively. This results in an increase in shear demand of 30.5% for exterior girders and 15.0% for interior girders. This difference represents an added degree of conservativism to an already conservative process of rating bridges for shear.

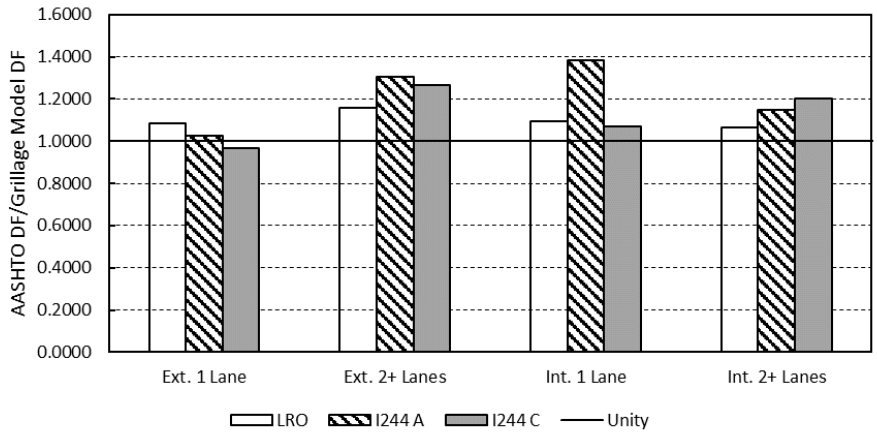

Figure 4.2. Distribution factor ratios for specific Oklahoma bridges

The AASHTO LRFD code predicts distribution factors for the LRO bridge relatively more accurately. The LRO bridge distribution factors are governed by the two or more lanes loaded case for both exterior and interior girders. These factors differ from the code factors by 13.0% and 6.7% (corresponding to the same increase in shear), respectively. The distribution factors for the LRO bridge are larger than those for the I-244 bridge, so as Figure 4.2 shows, these differences are proportionally less than for the spans of the I-244 bridge.

The conservativism of the governing AASHTO LRFD distribution factors for each case is shown in Figure 4.3. The trends in this figure conform to the observations made in the parametric study discussed in Section 2. For the two spans of the I-244 bridge, longer spans tend to increase conservativism for interior girders and decrease it for exterior girders. On the other hand, the distribution factors for the LRO bridge are the least conservative of the three bridges. Since this bridge had the largest girder spacing, less conservative distribution factors were expected based on the parametric modeling. For these real Oklahoma bridges, the results of the parametric model study are confirmed.

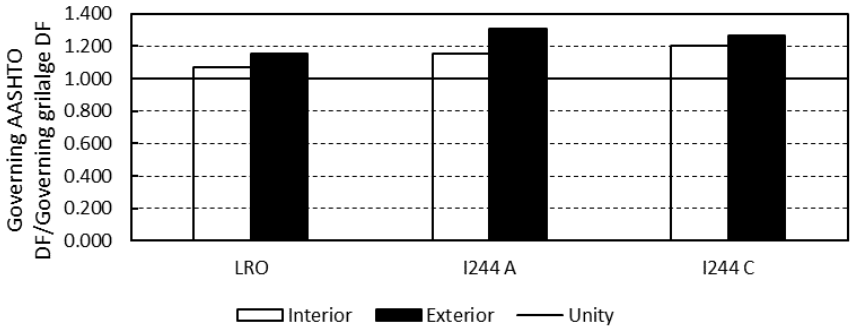

Figure 4.3. AASHTO DF/Grillage model DF for Oklahoma bridges

Grillage models can be used to provide better information on the load rating of bridges (Dymond et al. 2016). In the hands of an experienced modeler grillages are simple to create and provide a more realistic prediction of load distribution. These three Oklahoma bridges were load rated in LEAP Concrete Bridge against the HL-93 load and the results of this rating are given in Table 4.2. These ratings are developed based on the AASHTO LRFD code distribution factor equations. In general, the girders rate well

for shear. The only case where the rating is relatively low is for the LRO bridge interior girders at the inventory rating. The rating factors determined using grillage distribution factors for these bridges are shown in Table 4.3. Across the board, the ratings increase when grillage models are used to evaluate distribution factors. For these bridges, some of the increases are significant.

Table 4.2. Shear load ratings for the three Oklahoma bridges of interest (using AASHTO distribution factors)

Ratings (HL-93)	Inventory Exterior	Inventory Interior	Operating Exterior	Operating Interior
LRO	1.60	1.45	2.10	1.90
I244 A	3.97	2.26	5.15	4.08
I244 C	2.83	2.08	3.70	2.98

Table 4.3. Shear load ratings for the three Oklahoma bridges of interest (using grillage derived distribution factors)

Ratings (HL93)	Inventory Exterior	Inventory Interior	Operating Exterior	Operating Interior
LRO	1.86	1.55	2.43	2.03
I244 A	5.20	3.64	6.74	4.85
I244 C	3.59	2.64	4.70	3.60

Figure 4.4 shows the ratio of grillage model rating factor to AASHTO LRFD rating factor. A rating factor greater than unity indicates the bridge is capable of carrying current design loads. Larger numbers would mean a greater factor of safety compared to current demands. The AASHTO LRFD code distribution factors result in a particularly conservative rating for the I-244A bridge span. The smaller girder spacings of I-244A and C result in more conservative AASHTO distribution factors as explained in Section 4.2. The LRO bridge rating is still greater than one, though by a smaller margin. This conforms to the trend observed in the parametric study (Section 2.4) of decreasing conservativism with increasing girder spacing for interior girders. The I-244A bridge rating was more conservative than the rating for I-244C span, which was a result of the differing lengths of the two spans. Because the spans were the same in terms of number of girders and spacing, the distribution factors were the same according to the AASHTO LRFD code.

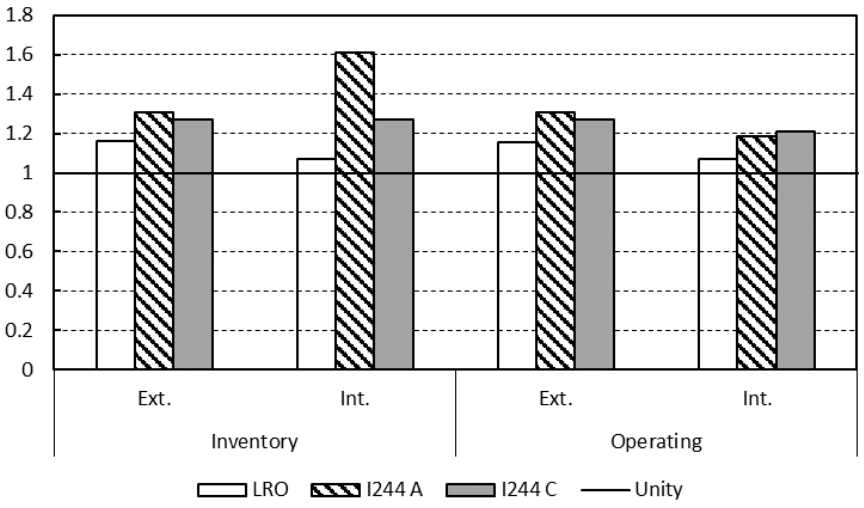

Figure 4.4. Grillage derived rating factors/AASHTO LRFD rating factors for Oklahoma bridges of interest

In summary, for these selected Oklahoma bridges, the distribution factors provided by grillage models would increase the rating factors, allowing for larger permit loads and potentially increasing the life of the bridges. While these particular bridges rated well for shear, there may be examples of bridges that have rating factors closer to unity but whose distribution factors are overly conservative. In these cases, a grillage model could decrease distribution factors and increase the usable life of the bridge, saving time, money, and lost productivity upon replacing the bridge without compromising safety. For the bridges modeled in this study, the rating factors are increased with the use of grillage model derived distribution factors, allowing larger permit vehicles and giving a potentially truer picture of the distribution behavior of the bridges.

5.0 Recommendations for Identifying and Rating Bridges Susceptible to Shear

5.1 Overview

Information presented in the first five sections of this report, including data from experimental testing, analytical investigation, and the literature, was synthesized to produce concrete recommendations for quickly identifying bridges potentially vulnerable to shear and accurately assessing bridge shear capacity. These recommendations are presented in the following sections along with a procedure for examining bridges

potentially vulnerable to shear. The overall procedure consists of five steps outlined visually in Figure 5.1.

1. Examine available information (Inspection Reports/NBI) to determine if bridge may be vulnerable to shear.
2. Collect additional information required to analyze the bridge from bridge plans and/or a site visit.
3. Use tables produced by the parametric study described in Sections 2.3-2.6 to identify what benefit grillage model derived distribution factors may have for analysis.
4. Rate bridge for shear using AASHTO LRFD MCFT and selected distribution factors.
5. If deficient, check database of experimental data to determine if the bridge configuration may have additional residual capacity.

Additional methods of assessing bridge condition such as those described in Section 3 may be considered if data are available or if the analysis indicates a more detailed assessment of the bridge is warranted. However, the recommendations in this section are intended to produce a relatively simple, but accurate, procedure with some

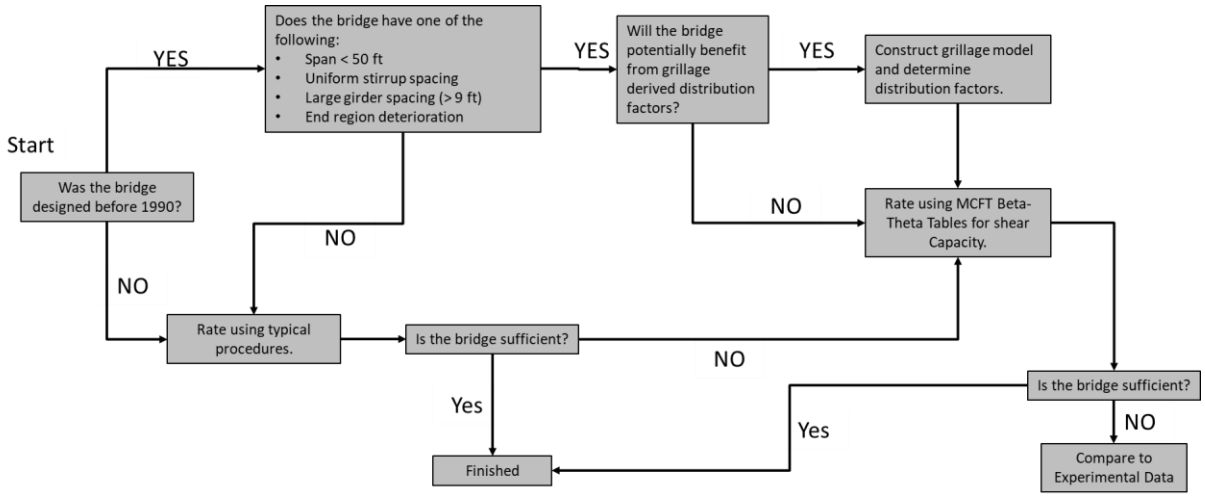

Figure 5.1. Flow chart of suggested procedures for examining bridges potentially susceptible to shear.

analysis when rating bridges, while this procedure describes general options based on the findings of the research described in this report.

5.2 Procedure

5.2.1 Step 1: Identifying Bridges Vulnerable to Shear

As described in Section 1.10, for the case of shear the AASHTO Manual for Bridge Evaluation (AASHTO 2011) does not require shear checks for design or legal loads if a concrete bridge does not show signs of shear distress. It should be checked for permit loads in all cases. However, current demands may be higher than when a particular bridge's girders were designed and shear capacity calculations have changed over the years. The current study indicates that shear performance may be a concern if the bridge was designed and put into service before 1990 and one of the following conditions is met:

- Short span length, set here as 50 ft or less,
- Uniform shear stirrup spacing along the length of the prestressed girders,
- Larger girder spacing, set here as 9 ft or greater,
- End region corrosion damage is visible, either existing or repaired.

If the bridge falls into one of the categories, the assessment should move to the next step. Sufficient information can typically be found in the bridge inspection report to make this initial assessment as described in Section 2.10. If the bridge was built after 1990 or does not exhibit any of the four conditions it should be rated using typical procedures.

5.2.2 Step 2: Collect Additional Information

Bridge plans should be obtained for a bridge identified as potentially vulnerable to shear. While necessary for accurately modeling and analyzing a bridge, these plans can also provide shear stirrup spacing, which can be useful to identify a bridge as susceptible to shear. If bridge plans are not available, measurements should be made in the field to identify bridge and girder geometry and rebar location technology should be used to provide an estimate of girder reinforcement.

5.2.3 Step 3: Determine if a Grillage Model May be Beneficial

A grillage model may provide a more accurate representation of load distribution within a bridge than the AASHTO LRFD equations for shear load distribution factor depending on the bridge characteristics. Table 2.11 presented in Section 2.6 (and reproduced here for convenience as Table 5.1) can be used to determine if a grillage model may less conservatively estimate the shear demand on the bridge girders. Positive values in the table indicate instances where the AASHTO LRFD equations provide larger values of load distribution to an individual girder relative to grillage model derived load distribution factors. Negative values indicated that the grillage model produces load distribution greater than that produced by the AASHTO LRFD equations. If the bridge under consideration has a girder type and girder spacing resulting in a substantially large positive number in Table 5.1, a grillage model may provide beneficial values for shear rating compared to what was done in the original design. It should be

Table 5.1. Range of difference between AASHTO and grillage distribution factors (%)

Girder Type	Location	Load Case	6 ft Min	6 ft Max	9 ft Min	9 ft Max	12 ft Min	12 ft Max
Type-II	Interior	One Lane	14.4	25.9	-2.4	14.7	-1.8	16.3
Type-II	Interior	Two Lane	34.2	34.5	20.3	30.0	5.0	13.2
Type-II	Exterior	One Lane	-5.1	4.8	5.3	6.8	5.2	7.8
Type-II	Exterior	Two Lane	7.0	7.2	3.2	17.6	7.7	19.5
Type-III	Interior	One Lane	16.3	21.0	3.8	14.0	4.4	15.5
Type-III	Interior	Two Lane	11.9	14.2	3.4	13.5	2.7	13.6
Type-III	Exterior	One Lane	4.9	5.3	5.7	11.2	5.8	7.5
Type-III	Exterior	Two Lane	-0.4	-3.6	7.6	17.2	8.2	16.4
Type-IV	Interior	One Lane	18.2	21.6	9.6	21.4	8.6	16.0
Type-IV	Interior	Two Lane	12.3	14.7	10.9	13.9	7.0	14.0
Type-IV	Exterior	One Lane	5.3	6.4	6.4	7.3	6.4	7.8
Type-IV	Exterior	Two Lane	-0.6	-3.2	8.0	10.7	7.7	11.3
BT-63	Interior	One Lane	21.5	22.5	13.5	16.1	14.7	18.0
BT-63	Interior	Two Lane	14.0	15.1	13.8	15.5	1.9	15.9
BT-63	Exterior	One Lane	10.0	11.1	10.9	12.3	10.4	11.8
BT-63	Exterior	Two Lane	-0.7	-2.2	11.3	12.5	11.1	12.1
BT-72	Interior	One Lane	20.6	22.4	12.2	16.1	12.3	18.0
BT-72	Interior	Two Lane	13.5	14.8	13.3	15.5	12.6	15.7
BT-72	Exterior	One Lane	11.0	11.1	11.3	12.3	7.1	11.8
BT-72	Exterior	Two Lane	-0.4	-1.5	11.6	12.9	10.4	12.2

noted that the ranges in this table include the effects of variations in the other three parameters considered in the study, i.e. deck thickness, span length, and presence of diaphragms and not all bridges in the overall girder category will realize potential benefits.

5.2.4 Step 4: Rate Bridge for Shear

If the bridge is identified as having a potential vulnerability to shear, a shear rating should be carried out using the AASHTO Manual for Bridge Evaluation (AASHTO 2018), or the current procedures specified by ODOT. Either the AASHTO load distribution factors or a grillage model should be used for determining shear demand on individual girders. Grillage model analysis is often included as a feature of bridge analysis programs and is typically used by ODOT for bridge rating. If a grillage model is identified as beneficial in Step 3, this option should be chosen in the program used for structural analysis. Whether the program includes grillage models as a feature, or if a grillage model is developed by the engineer, the procedures and references described in Section 2.2 of this report should be used as guidance in developing the model.

When determining shear capacity of the girders, the methods of AASHTO LRFD modified compression field theory using the tabular method, as described in Section 1.4.3 of this report and in Section 5.8.3.4.2 and Appendix B5 of the AASHTO LRFD Specifications (2015), should be used. If corrosion damage is identified near the support in Step 1, capacity of the end region should be assessed considering the possibility of a bond-shear failure as described in Section 1.4.6 of this report and Ross and Naji (2014).

5.2.5 Step 5: Examine Available Experimental Data

If during the rating process performed in Step 4 the girders are identified as deficient relative to shear, the experimental data described in Section 2.8 can be consulted to identify cases of experimental tests with similar girders. These data can be used to identify potential residual strength beyond what is calculated using the AASHTO LRFD methods. Cases of the same girder type and similar shear reinforcement should be used for comparison if possible. It should be noted that differences in girder design and condition will affect actual behavior of a given girder. It is at the engineer’s

discretion as to how these data are used in evaluating sufficiency of a given bridge and Section 2 of this report can be used as guidance in interpreting specific conditions.

5.3 Example: U.S. 412 over Verdigris River O'Flow (NBI 19101)

This section considers an example of following the procedure described in Section 6.2 considering the U.S. 412 bridge over the Verdigris River O'Flow (NBI 19101) in Rogers county, part of ODOT Division 8.

Step 1: Identifying Bridges Vulnerable to Shear

The inspection report for this bridge provides the following information relevant to determining whether the bridge may be vulnerable to shear:

- The bridge is a prestressed concrete bridge of stringer/girder construction (Item 43, Figure 5.2),
- The bridge was built in 1975 (Item 27, Figure 5.2),
- The bridge spans all have a 40 ft span length (Item 244, Figure 5.3),
- The girder spacing/number of girders is not provided (Item 243, Figure 5.3),
- Beam ends are not identified as having corrosion damage (Element 819, Figure 5.4),
- Steel bearing plates are identified as having corrosion damage (Element 916, Figure 5.4).

The year built (before 1990) and span length (less than 50 ft) indicate potential vulnerability when rating for shear and additional consideration should be made for this bridge.

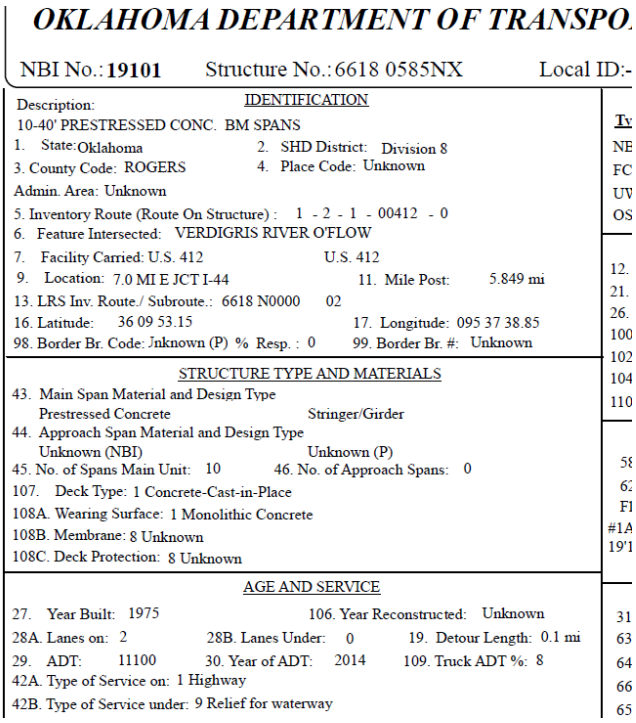

OKLAHOMA DEPARTMENT OF TRANSPO

NBI No.: **19101** Structure No.: 6618 0585NX Local ID:-

Description: IDENTIFICATION

10-40' PRESTRESSED CONC. BM SPANS

1. State: Oklahoma 2. SHD District: Division 8

3. County Code: ROGERS 4. Place Code: Unknown

Admin. Area: Unknown

5. Inventory Route (Route On Structure) : 1 - 2 - 1 - 00412 - 0

6. Feature Intersected: VERDIGRIS RIVER O'FLOW

7. Facility Carried: U.S. 412 U.S. 412

9. Location: 7.0 MI E JCT I-44 11. Mile Post: 5.849 mi

13. LRS Inv. Route./ Subroute.: 6618 N0000 02

16. Latitude: 36 09 53.15 17. Longitude: 095 37 38.85

98. Border Br. Code: Jnknown (P) % Resp. : 0 99. Border Br. #: Unknown

STRUCTURE TYPE AND MATERIALS

43. Main Span Material and Design Type

Prestressed Concrete Stringer/Girder

44. Approach Span Material and Design Type

Unknown (NBI) Unknown (P)

45. No. of Spans Main Unit: 10 46. No. of Approach Spans: 0

107. Deck Type: 1 Concrete-Cast-in-Place

108A. Wearing Surface: 1 Monolithic Concrete

108B. Membrane: 8 Unknown

108C. Deck Protection: 8 Unknown

AGE AND SERVICE

27. Year Built: 1975 106. Year Reconstructed: Unknown

28A. Lanes on: 2 28B. Lanes Under: 0 19. Detour Length: 0.1 mi

29. ADT: 11100 30. Year of ADT: 2014 109. Truck ADT %: 8

42A. Type of Service on: 1 Highway

42B. Type of Service under: 9 Relief for waterway

Figure 5.2. Portion of inspection report for the U.S. 412 Bridge over Verdigris River O'Flow (NBI 19101) showing span type and year built

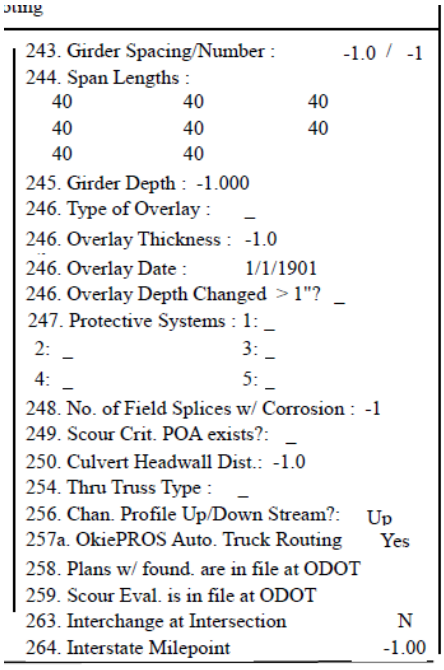

243. Girder Spacing/Number : -1.0 / -1

244. Span Lengths :

40 40 40

40 40 40

40 40

245. Girder Depth : -1.000

246. Type of Overlay : _

246. Overlay Thickness : -1.0

246. Overlay Date : 1/1/1901

246. Overlay Depth Changed > 1"? _

247. Protective Systems : 1: _

2: _ 3: _

4: _ 5: _

248. No. of Field Splices w/ Corrosion : -1

249. Scour Crit. POA exists?: _

250. Culvert Headwall Dist.: -1.0

254. Thru Truss Type : _

256. Chan. Profile Up/Down Stream?: Up

257a. OkiePROS Auto. Truck Routing Yes

258. Plans w/ found. are in file at ODOT

259. Scour Eval. is in file at ODOT

263. Interchange at Intersection N

264. Interstate Milepoint -1.00

Figure 5.3. Portion of inspection report for the U.S. 412 Bridge over Verdigris River O'Flow (NBI 19101) showing span lengths and girder spacing

Elem.	Element Notes (Include Size and Location of Deterioration
12	FX: MINOR SPALLS ,POTHOLES, SEVERAL PATCHED AREAS,IMPENDING SPALLS, & MINOR CRACKS.CLEAN DECK.
109	< none >
202	< none >
215	< none >
234	FX:#3&6 PIER CAP SPALLS W/ EXPOSED REBAR @ ENDS & MINOR CRACKS W/EFFLOR.
301	PX:EXP.JTS.FAILED.
310	< none >
321	FX:SEAL N.E.COR.
331	< none >
819	< none >
859	NOTE:SOFFIT MINOR EFFLOR. & PATCHED AREAS.
916	FX:BEARING PLATES MODERATE to SEVERE CORROSSION @ ABUT'S.
918	< none >
958	

Figure 5.4. Portion of inspection report for the U.S. 412 Bridge over Verdigris River O'Flow (NBI 19101) showing Element Notes

Step 2: Collect Additional Information

Bridge plans (or field measurements in lieu of bridge plans) are needed to perform proper analysis and rating of the bridge. Additionally, shear stirrup spacing and girder spacing are useful pieces of information to further define the potential vulnerability to shear for this bridge. In inspecting the bridge plans provided for this bridge the following items are of note:

- AASHTO Type II girders,
- Girder spacing of 9 ft – 0 in.,
- Shear reinforcement spacing of 12 in. along entire girder length.

The girder type, spacing, and shear reinforcement spacing further indicate that the bridge is potentially vulnerable to shear and should be considered for shear rating.

Step 3: Determine if a Grillage Model May be Beneficial

Considering the difference in AASHTO LRFD distribution factors and grillage model derived distribution factors for a Type-II girder with a 9 ft girder spacing in Table 5.2, there is substantial potential conservatism for the interior girder two or more lanes loaded case (minimum 20% to maximum 30%). Other load cases also have potential for

Table 5.2. Difference between AASHTO and grillage distribution factors (%) for Type II girders

Location	Load Case	6 ft Min	6 ft Max	9 ft Min	9 ft Max	12 ft Min	12 ft Max
Interior	One Lane	14.4	25.9	-2.4	14.7	-1.8	16.3
Interior	Two Lane	34.2	34.5	20.3	30.0	5.0	13.2
Exterior	One Lane	-5.1	4.8	5.3	6.8	5.2	7.8
Exterior	Two Lane	7.0	7.2	3.2	17.6	7.7	19.5

reduced conservatism indicating that a grillage model may be beneficial for rating this bridge. For the interior girder one lane loaded case AASHTO factors ranged from 2.4% less than grillage model derived factors to 15% greater than grillage model derived factors. For the exterior girder one lane loaded case the AASHTO factors were 5.3% to 6.8% larger than grillage model derived factors and for the exterior girder two lanes loaded case the AASHTO factors were 3.2% to 17.6% larger than grillage model derived factors.

Step 4: Rate Bridge for Shear

Design demand was determined for both interior and exterior girders using LEAP Concrete Bridge and the HL-93 loading with AASHTO distribution factors. The capacity of the individual girders was calculated using the AASHTO LRFD modified compression field theory method. Rating factors determined using the AASHTO Manual for Bridge Evaluation (AASHTO 2018) as described in Sections 1.10 and 5 of this report are presented in Table 5.3. For these calculations the condition factor (ϕ_c) and the system factor (ϕ_s) were taken as 1.0 and the comparison was made at *h*/*2* and a distance of 10% of the span from the support. The Inventory Rating is close to, but greater than 1.0 further indicating that a grillage model analysis may be beneficial for this bridge and that permit loads in excess of HL-93 may be problematic relative to shear. It should also be

Table 5.3. Shear load rating using AASHTO distribution factors

Rating (HL-93) Along Span	Inventory Exterior	Inventory Interior	Operating Exterior	Operating Interior
h/2	1.07	1.04	1.38	1.35
0.10L	1.23	1.20	1.59	1.55

noted that a more detailed analysis of the beam end may produce different results at *h*/2 from the support, with is in the beam discontinuity region.

Step 5: Examine Available Experimental Data

Similar AASHTO Type II girders were tested by Shahawy et al. (1993), Osborn et al. (2012), and Floyd et al. (2016). Data from Floyd et al. (2016) and Osborn et al. (2012) indicate experimental shear capacity generally 5 percent to 20 percent greater than predicted by AASHTO LRFD for *a*/*d* ratios between 1.5 and 4.0 unless bond shear was the controlling failure mechanism. At an *a*/*d* ratio of 1.5 the experimental capacity was much higher, but this is not necessarily an accurate assessment of the AASHTO LRFD shear method, since this location is within the discontinuity region of the girder. Shahawy et al. (1993) observed bond failures for most of the girders tested, and only observed experimental capacities less than predicted for girders that exhibited bond failures. It should be noted that the comparisons by Shahawy et al. (1993) were done using the AASHTO Standard Specifications.

6.0 Summary and Conclusions

6.1 Summary

In light of changes to the AASHTO Bridge Design Specifications since many older prestressed concrete bridge girders were designed and constructed, accurate load rating of bridges for shear is important to prevent adequate bridges from being rated deficient. This is especially true for the case of overloaded trucks or when there is some end region damage due to corrosion. This report documents a study of the factors affecting shear capacity and subsequent load rating, two potential methods for assessing condition of in-service prestressed concrete bridge girders, and a simple methodology for assessing whether a bridge should be rated for shear and how to carry out that rating. The following sections provide conclusions, recommendations, and limitations of this work.

6.2 Conclusions

6.2.1 Factors Affecting Shear Capacity and Load Rating.

Experimental test results from previous research compiled as part of this study indicates that aged girders in good condition typically possess residual capacity beyond expected design values. However, girder end region corrosion can affect the shear failure mechanism and accuracy of girder shear capacity calculations. The AASHTO LRFD modified compression field theory (MCFT) shear capacity beta-theta equations were the most conservative estimators of shear strength in previous research while the MCFT shear beta-theta tables provided the best estimation of experimental shear capacity and are the best option for shear capacity rating. The MCFT accurately predicted capacities for failures exhibiting strand slip, but a strut and tie model or end region equilibrium should be considered for areas with small *a*/*d* ratio (< 2.0, i.e. girder ends) and exhibiting corrosion. The shear capacity methods in the AASHTO 1973 Standard Specifications and the AASHTO LRFD simplified methods underestimated capacity in a number of cases found in the literature.

The 2 in. bonded concrete deck overlays present on girders tested by Floyd et al. (2016) delaminated and caused premature failure of all specimens tested. Presence of similar overlays may a cause for concern if a shear rating factor is very low. Corrosion cracking at girder ends led to bearing issues (cracking/spalling) even at service level loads. Full-depth diaphragms can change failure mechanisms and provide load transfer after girder failure.

Grillage models were shown to accurately predict load transfer in the scale bridge examined by Floyd et al. (2016) and Murray (2017). In the same research it was shown that elastic level distribution factors closely predicted ultimate load behavior of the scale bridge girders. Distribution factors from grillage models can accurately relate the expected capacity of a single bridge girder to the expected capacity of the entire bridge section. The grillage modeling method discussed in this report was shown to be easily implemented using typical structural analysis software. These grillage models are a promising alternative to the shear distribution factor equations in the AASHTO LRFD code for more accurate prediction of behavior. A detailed parametric study was

conducted comparing grillage models and AASHTO shear distribution factors. AASHTO shear distribution factors were generally found to be conservative (relative to the grillage models) for the bridges modeled, by a varying degree depending on the parameters in question. Longer spans resulted in more conservative distribution factors for interior girders but less conservative distribution factors for exterior girders compared to factors calculated using the AASHTO LRFD equations. As expected, girder spacing most influenced the level of distribution factor conservativism. Distribution factors for interior girders tended to be most conservative at small girder spacings and distribution factors for exterior girders were less conservative at small girder spacings. In general, interior girders had distribution factors roughly as conservative as for exterior girders. The presence of diaphragms was less influential on shear distribution factors than girder spacing and span length, but diaphragms changed distribution factors by as much as 7 percent. Diaphragm effects were greater for shorter spans and larger girder spacings. Diaphragms also distributed more load with thinner slabs for the two slab thicknesses examined, but slab thickness in general had less of an effect on shear distribution factors than other variables examined.

The most important result is that AASHTO factors are nearly always conservative when compared to the results of grillage models presented in this report. A result of this finding is that if older bridges being load rated are modeled, their rating factors can be increased if grillage models are used to determine the distribution factors instead of the code equations. This procedure is allowed by the AASHTO Specifications. This does not result in a decrease in known safety level, but may rather result in the elimination of an unnecessary level of conservativism. This finding was supported by the ratings of the selected Oklahoma bridges modeled and load rated in Section 4. It was seen that the most conservative rating factors (in relation to the grillage derived rating factors) will be found in short bridges with smaller girder spacings (I-244A). These bridges will be less of a concern at the load rating stage as they will tend to have conservative ratings (the demands will be artificially higher due to larger distribution factors from the code). On the other hand, less conservative ratings would be expected for long bridges (I-244C) or those with wide girder spacings (LRO).

Most Oklahoma bridges that should be considered for shear rating can be identified through a set of simple characteristics. These bridges will have a short span length, set here as 50 ft or less. They likely have a uniform shear stirrup spacing along the length of the prestressed girders. These bridges have larger girder spacing, set here as 9 ft or greater. If end region corrosion damage is visible, either existing or repaired, the girders are more likely to exhibit bond-shear failures, which should be considered in rating.

6.2.2 Conclusions on Methods for Assessing Condition of Aged Girders

It was found for the bond transfer inverse modeling method that only the influence area around the strand considering a thick-walled cylinder model should be considered and that calculations based on 10 subdivisions along the length as in Floyd et al. (2018) was not enough. The parametric study regarding the number of subdivisions carried out to determine the rate of convergence for the predicted end movement indicated that a much higher number of subdivisions, e.g., 320, should be adopted. These items improved the performance of the inverse bond transfer model reported in Floyd et al. (2018).

Validation cases and actual experimental data analysis for the piecewise EI identification resulted in inconsistent (zero or negative) identified flexural stiffness values using the linear least-squares method, manifesting a serious limitation. As a remedy, the Bayesian analysis method presented in this report can lead to reasonable identified results. There is a nontrivial learning curve for Bayesian analysis, however it produces improved results. This method also directly facilitated an improved implementation with better efficiency and more insights, which is being pursued further.

Observations from the exercises carried out indicate that higher-order substructures, specifically the ten substructure case, return the most consistent identified results. The higher-order, ten substructure case holds the potential for improved damage identification. Reduced stiffness values identified at the end regions of the girder tested were roughly 94 percent of the conservative value of EI_{tr} (based on the girder section properties and estimated Young's modulus) with EIs larger than EI_{tr} identified at midspan. It is thus evident that the girder lost stiffness over the course of its

40+ years of service-life based on a conservative upper-bound stiffness given by EI_{tr}. This also justifies the usefulness of Bayesian analysis as expected reductions in EI are seen near the end regions of the girder where corrosion was evident.

6.2.3 Overall Conclusions

A procedure for identifying and rating bridge that may be vulnerable to shear is described in this report. When rating older AASHTO I-girder bridges, it should be understood that the AASHTO distribution factors may add more conservativism to an already conservative process. Replacing the code distribution factors with grillage model derived distribution factors for load rating these types of bridges may be beneficial. Using a grillage model can increase load ratings, reducing the potential need to take some bridges out of service without sacrificing accuracy and safety. The girders examined in this study mostly reached expected capacities despite differences in the code at the time they were designed. The AASHTO MCFT methods are the best for use in rating older girders due to their balance of accuracy and conservativism. End region corrosion visible in the tested girders was not seen to affect ultimate capacity, but potentially led to strand slip and influenced the failure mechanism. Based on the results of previous shear testing and the findings of the grillage models, there may be conservativism built in when AASHTO distribution factors and the MCFT methods are used that leaves open the possibility of increased load ratings for some older bridges.

6.3 Limitations

Several limitations of the work described in this report should be considered when using these results in practice. Shear behavior in beam tests is known to be highly variable, limiting the scope of the conclusions drawn from individual tests. The results presented this report should be considered in conjunction with other similar shear tests of older girders. Consideration was not made for skewed bridges in the models developed for this report and the results should not be considered directly applicable to skewed bridges. Experimental results were only available for girders with minimal corrosion damage and the effects of large amounts of corrosion may cause differing behavior. Results from load testing of full-scale composite bridges is lacking and applicability of the models presented in this report is based on limited data. The full-

scale bridges modeled represented bridges falling into the categories potentially vulnerable to shear, but more critical cases should be examined.

6.4 Suggestions for Future Research

The grillage models reported in the parametric study were verified based on testing of a single scale bridge. Ideally these should be checked against factors for real-world bridges. A study which compared this modeling paradigm with results from field tests would be valuable in confirming the methods (although grillage models have been verified in some past research explained in the literature review). A study comparing the results of grillage models to bridges with skew, multiple interior diaphragms, and varying geometry would be useful in particular. Additional scale bridge testing with varying spacings and lengths of bridges would also be useful. In order to more fully understand the impact of corrosion on older girders it would be ideal to test several similar girders with varying levels of corrosion and compare results. Finally, this study made recommendations related to load rating of bridges, including which shear methods are more conservative and how grillage model derived distribution factors can increase load ratings. These findings should be confirmed against some bridges that rate closer to unity for shear, or that rate poorly.

References

AASHTO (1973) *Standard Specifications for Highway Bridges*, American Association of State Highway and Transportation Officials, Washington, D.C.

AASHTO (2002) *Standard Specifications for Highway Bridges*, American Association of State Highway and Transportation Officials, Washington, D.C.

AASHTO (2007) *LRFD Bridge Design Specifications Customary U.S. Units 4th Edition*, American Association of State Highway and Transportation Officials, Washington, D.C.

AASHTO (2011) *Manual for Bridge Evaluation*, American Association of State Highway and Transportation Officials, Washington, D.C.

AASHTO (2015) *AASHTO LRFD Bridge Design Specifications* (7th ed.), American Association of State Highway and Transportation Officials, Washington, D.C.

AASHTO (2018) *Manual for Bridge Evaluation 3rd Edition*, American Association of State Highway and Transportation Officials, Washington, D.C.

ACI Committee 318 (2014) *Building Code Requirements for Structural Concrete (ACI 318-14) and Commentary*, American Concrete Institute.

Alshegeir, A., and Ramirez, J. A. (1992) Strut-Tie Approach in Prestressed Deep Beams, *ACI Structural Journal*, 89(3): 296-304.

Altay, A. K., Arabbo, D. S., Corwin, E. B., Dexter, R. J., & French, C. E. (2003). *Effects of Increasing Truck Weight on Steel and Prestressed Bridges*. St. Paul, MN: Minnesota Department of Transportation.

ACI Committee 209 (2008) "Guide for Modeling and Calculating Shrinkage and Creep in Hardened Concrete (ACI 209.2R-08)", American Concrete Institute, Farmington Hills, MI, 47 pp.

Avendaño, A. R., and Bayrak, O. (2008) Shear Strength and Behavior of Prestressed Concrete Beams, Technical Report: IAC-88-5DD1A003-3, Center for Transportation Research, the University of Texas, Austin, TX.

Ayoub, A. and Filippou, F. C. (2010) "Finite-element Model for Pretensioned Prestressed Concrete Girders," *ASCE Journal of Structural Engineering*, 136(4): 401–409.

Balazs, G. L. (1993) "Transfer Length of Prestressing Strand as a Function of Draw-in and Initial Prestress," *PCI Journal* 38(2): 86–93.

Barr, P. J., Eberhard, M. O., and Stanton, J. F. (2001) "Live-Load Distribution Factors in Prestressed Concrete Girder Bridges," *Journal of Bridge Engineering*, 5(5): 298-306.

Baxi, A. N. (2005) "Analytical modeling of fully bonded and debonded pre-tensioned prestressed concrete members," Ph.D. Thesis, The University of Texas, Austin, TX.

Bazant, Z.P. and Jirasek, M. (2018) *Creep and Hygrothermal Effects in Concrete Structures*, Springer.

Bazant, Z.P. and Xi, Y. (1994) "Drying creep of concrete: constitutive model and new experiments separating its mechanisms," *Materials and Structures*, 27: 3–14.

Bazant, Z.P., Yu, Q., and Li, G.H. (2012) “Excessive long-time deflections of prestressed box girders. I: Record-span bridge in Palau and other paradigms,” *ASCE Journal of Structural Engineering*, 138: 676–696.

Bechtel, A., McConnell, J., and Chajes, M. (2011) “Ultimate Capacity Destructive Testing and Finite-Element Analysis of Steel I-Girder Bridges,” *Journal of Bridge Engineering*, 16(2): 197-206.

Bennett, E. W., and Balasooriya, B. M. A. (1971) “Shear Strength of Prestressed Beams with Thin Webs Failing in Inclined Compression,” *ACI Journal*, 68(3): 204-212.

Bentley Systems, Inc. (2016). LEAP Bridge Concrete CONNECT Edition. (16.00.00.24).

Benítz, J. M., Gálvez, J. C. (2011) “Bond modelling of prestressed concrete during the prestressing force release,” *Materials and Structures*, 44: 263–278.

Bentz, E. C., Vecchio, F. J., and Collins, M. P. (2006) “Simplified Modified Compression Field Theory for Calculating Shear Strength of Reinforced Concrete Elements,” *ACI Structural Journal*, 103(4): 614-624.

Bishop, C.M. (2006) *Pattern Recognition and Machine Learning*, Springer.

Burdette, E. G. and Goodpasture, D. W. (1973) “Tests of four highway bridges to failure,” *Journal of the Structural Division*, 99(3): 335-348.

Choulli, Y., Mari, A. R., and Cladera, A. (2008) “Shear Behaviour of Full-Scale Prestressed I-Beams Made with Self Compacting Concrete,” *Materials and Structures*, 41(1): 131-141.

Cranor, B. N. (2015). “Analysis and Experimental Testing for Shear Behavior of an AASHTO Type II Girder in Service for Several Decades,” M.S. Thesis, The University of Oklahoma, Norman, OK.

Cross, B., Vaughn, B., Panahshahi, N., Petermeier, D., Shuenn Siow, Y., and Domagalski, T. (2009) “Analytical and Experimental Investigation of Bridge Girder Shear Distribution Factors,” *Journal of Bridge Engineering*, 14(3): 154-163.

Dang, C. N., Floyd, R. W., Prinz, G. S., and Hale, W. M. (2016) “Determination of the bond stress distribution coefficient by the maximum likelihood method,” *ASCE Journal of Structural Engineering*, 142(5).

Digler, W.H. (1982) “Creep analysis of prestressed concrete structures using creep-transformed section properties,” *PCI Journal*, 27(1): 98–119.

Dymond, B. Z., French, C. E., and Shield, C. K. (2016) *Investigation of Shear Distribution Factors in Prestressed Concrete Girder Bridges*, Report No. MN/RC 2016-32, Minnesota Department of Transportation, St. Paul, MN.

Eamon, D. C., Chehab, A. and Parra-Montesinos, G. (2016) “Field Tests of Two Prestressed-Concrete Girder Bridges for Live-Load Distribution and Moment Continuity,” *Journal of Bridge Engineering*, 21(5): 1-12, 10.1061/(ASCE)BE.1943-5592.0000859

Eby, C. C., Kulicki, J.M., and Kostem, C. N. (1973) “The evaluation of St. Venant torsional constant for prestressed concrete I-beam.” Fritz Engineering Laboratory Rep. No. 400.12, Lehigh Univ., Bethlehem, Pa.

Elzanaty, A. H, Nilson, A. H., and Slate, F. O. (1987) “Shear Capacity of Prestressed Concrete Beams Using High-Strength Concrete,” *ACI Structural Journal*, 83(2): 359-368.

FDOT. (2013). *Florida Department of Transportation*. Retrieved from FDOT.com: http://www.fdot.gov/roadway/ds/14/ids/ids-20120.pdf

Federation International de la Precontrainte (FIP) (1982) “Report on Prestressing Steel: 7. Test for the determination of tendon transmission length under static conditions,” Technical report, Wexham Springs, U.K.

Floyd, R.W., Pei, J.S., and Wright, J.P. (2018) “Simple model for time-dependent bond transfer in pretensioned concrete using draw-in data,” *Engineering Structures*, 160: 546–554, Short Communication.

Floyd, R. W., Pei, J. S., Murray, C. D., Cranor, B., and Tang, P. F. (2016) *Understanding the Behavior of Prestressed Girders After Years of Service.* Report No. FHWA-OK-16-03, Oklahoma Department of Transportation, Oklahoma City, OK.

Freitas, C.J. (2002) “The Issue of Numerical Uncertainty,” Report. Southwest Research Institute.

Fu, G. (2013) *Bridge Design and Evaluation: LRFD and LRFR*, John Wiley and Sons, Hoboken, NJ.

Geßner, S. and Henne, M. (2016) “Bond behavior of indented wired in pretensioning,” Proceedings of the 2016 PCI Convention and National Bridge Conference, Nashville, TN, March 3-6.

Ghali, A. and Neville, A. M. (1997) *Structural analysis: a unified classical and matrix approach*, 7th Edition, CRC Press, Boca Raton, FL.

Green, P. L. and Worden, K. (2015) “Bayesian and markov chain monte carlo methods for identifying nonlinear systems in the presence of uncertainty,” *Philosophical Transactions of The Royal Society A*, 373(2051): https://doi.org/10.1098/rsta.2014.0405.

Guyon, Y. (1953) *Prestressed Concrete*, John Wiley.

Halsey, T. J., and Miller, R. (1996) “Destructive Testing of Two Forty-Year-Old Prestressed Concrete Bridge Beams,” *PCI Journal*, 41(5): 84-93.

Hambly, E. C. (1991) “Bridge Deck Behaviour (2nd Ed.)”. CRC Press, Boca Raton, FL.

Hamilton III, H. R., Llanos, G., and Ross, B. E. (2009) “Shear Performance of Existing Prestressed Concrete Bridge Girders,” Final Report, BD 545-56, University of Florida, Gainesville, FL.

Hanson, J. M. and Hulsbos, C. L. (1964) “Ultimate Shear Tests Of Prestressed Concrete I-Beams Under Concentrated And Uniform Loadings,” *PCI Journal*, 9(3): 15-28.

Hawkins, N. M., Kuchma, D. A., Mast, R. F., and Reineck, K.-H. (2005) *NCHRP 549: Simplified Shear Design of Concrete Members*. Transportation Research Board, Washington, D.C.

Huang, Y., Shao, C., Wu, B., Beck, J. L., Li, H. (2019) “State-of-the-art review on Bayesian inference in structural system identification and damage assessment,” *Advances in Structural Engineering*, 22: 1329–1351.

Huth, O., Feltrin, G., Maeck, J., Kilic, N. and Motavalli, M. (2005) “Damage identification using modal data: Experiences on a prestressed concrete bridge,” *Journal of Structural Engineering*, 131, doi:10.1061/(ASCE)0733-9445(2005)131:12(1898).

Impollonia, N., Failla, I. and Ricciardi, G. (2016) “Parametric statistical moment method for damage detection and health monitoring.” *ASCE-ASME Journal of Risk and Uncertainty in Engineering Systems, Part A: Civil Engineering*, 2(2), https://doi.org/10.1061/AJRUA6.0000863.

Jorgenson, J. L., and Lawson, W. (1972) “Field testing of a reinforced concrete highway bridge to collapse,”. *Transportation Research Record*, 607: 66-71.

Kato, M., and Shimada, S. (1986) “Vibration of pc bridge during failure process,” *Journal of Structural Engineering*, 112(7): 1692-1703, https://doi.org/10.1061/(ASCE)0733-9445(1986)112:7(1692).

Lightfoot, E., and Sawko, F. (1959) “Structural frame analysis by electronic computer: grid frameworks resolved by generalized slope deflection,” *Engineering*, 187: 18-20.

Maeck, J., Wahab, M. A., Peeters, B., Roeck, G.D., Visscher, J.D., Wilde, W. P. D., Ndambi, J. M., and Vantomme, J. (2000) “Damage identification in reinforced concrete structures by dynamic stiffness determination,” *Engineering Structures*, 22(10): 1339-1349, https://doi.org/10.1016/S0141-0296(99)00074-7.

MacGregor, J. G., and Hanson, J. M. (1969) “Proposed Changes in Shear Provisions for Reinforced and Prestressed Concrete Beams,” *ACI Journal*, 66(4): 276-288.

MacGregor, J. G., Sozen, M. A., and Siess, C. (1965) “Strength of Prestressed Concrete Beams with Web Reinforcement,” *ACI Journal Proceedings*, 62(12): 1503-1520.

Martin, R. D., Kang, T. H.-K., and Pei, J.-S. (2011), “Experimental and code analyses for shear design of AASHTO prestressed concrete girders,” *PCI Journal*, 56(1): 54-74.

Mertz, D. (2006) *NCHRP Report 592: Simplified Live Load Distribution Factor Equations*, Transportation Research Board, Washington, D.C.

Miller, R. A., Aktan, A. E., and Shahrooz, B. M. (1994) “Destructive Testing of Decommissioned Concrete Slab Bridge,” *Journal of Structural Engineering*, 120(7): 2176-2198.

Morcous, G., Hanna, K., and Tadros, M. K. (2011) “Use of 0.7-in.-diameter strands in pretensioned bridge girders,” *PCI Journal*, 56(4): 65-82.

Murray, C. D., (2017) “Understanding ultimate behavior of prestressed concrete girder bridges as a system through experimental testing and analytical methods,” Ph.D. Dissertation, The University of Oklahoma, Norman, OK.

Naji, B., Ross, B. E., and Floyd, R. W. (2017) “Characterization of bond-loss failures in pretensioned concrete girders (technical note),” *Journal of Bridge Engineering*, 22(4).

Nakamura, E. (2011) “Shear Database for Prestressed Concrete Members,” M.S. Thesis, The University of Texas at Austin, Austin, TX.

Nawy, E. G., (2009) *Prestressed Concrete: A Fundamental Approach (5th Ed.)*, Prentice Hall.

Newmark, N. M., Siess, C. P., and Peckham, R. R. (1946) *Studies of Slab and Beam Highway Bridges. Part I: Tests of Simple Span Highway Bridges*, University of Illinois, Urbana, IL.

Noel, J. P. and Kerschen, G., (2017) “Nonlinear system identification in structural dynamics: 10 more years of progress,” *Mechanical Systems and Signal Progressing*, 83: 2-35.

Nutt, R. V., Schamber, R. A., and Zokaie, T. (1988) *NCHRP 12-26: Distribution of Wheel Loads on Highway Bridges*, Transportation Research Board, Washington, D.C.

O'Brien, E. J., and Keogh, D. L. (1999) *Bridge deck analysis (1st ed.)*. CRC Press, Boca Raton, FL.

ODOT (2016) *Bridge Design Standards & Specifications*, Retrieved from Oklahoma Department of Transportation: http://www.okladot.state.ok.us/bridge/2009-sb/brd_std_2009-lrfd-sb-index.php

Oh, B. H., Kim, E. S., and Choi, Y. C. (2006) “Theoretical analysis of transfer lengths in pretensioned prestressed concrete members,” *ASCE Journal of Engineering Mechanics*, 132(10): 1057–1066.

Osborn, G. P. (2010) “Ultimate Shear Capacity and Residual Prestress Force of Full-Scale, Forty-One-Year-Old Prestressed-Concrete Girders,” M.S. Thesis, Utah State University, Logan, UT.

Osborn, G. P., Barr, P., Petty, D., Halling, M., and Brackus, T. (2012) “Residual Prestress Forces and Shear Capacity of Salvaged Prestressed Concrete Bridge Girders,” *Journal of Bridge Engineering*, 17(2): 302–309.

Patrick, M. D., Huo, X. S., Puckett, J. A., Jablin, M., and Mertz, D. (2006) “Sensitivity of Live Load Distribution Factors to Vehicle Spacing (technical note),” *Journal of Bridge Engineering*, 11(1): 131-134

Pei, J. S., Martin, R., Sandburg, C., Kang, T. H. K. (2008) “Rating Precast Prestressed Concrete Bridges for Shear,” Report No. FHWA-OK-08-08, Oklahoma Department of Transportation, Oklahoma City, OK.

Pessiki, S., Kaczinski, M., and Wescott, R. H. (1996) “Evaluation of Effective Prestress Force in 28-Year-Old Prestressed Concrete Bridge Beams, *PCI Journal*, 41(6): 78-89.

Peterman, R. J., Ramirez, J. A., and Olek, J. (2000) “Influence of flexure-shear cracking on strand development length in prestressed concrete members,” *PCI Journal*, 45(5): 76-94.

Petersen-Gauthier, J. (2013) “Application of the Grillage Methodology to Determine Load Distribution Factors for Spread Slab Beam Bridges,” M.S. Thesis, Texas A&M University, College Station, TX.

Pough, K., Mayhorn, D., Prinz, G. S., and Floyd, R. W. (2017) “Evaluation and Repair of Existing Bridges in Extreme Environments,” Report No. SPTC 14.1-58-F, Southern Plains Transportation Center, Norman, OK.

Ramirez-Garcia, A., Dang, C.N., Hale, W.M., Martí-Vargas, J.R. (2017) “A higher-order equation for modeling strand bond in pretensioned concrete beams,” *Engineering Structures*, 131: 345–361.

Roache, P. (1998) “Verification and Validation in Computational Science and Engineering,” Hermosa Publishing.

Ross, B. E., Ansley, M. H., and Hamilton III, H. R. (2011) “Load Testing of 30-Year-Old AASHTO Type III Highway Bridge Girders,” *PCI Journal*, 56(4): 152-163.

Ross, B. E. and Naji, B. (2014). “A model for nominal bond-shear capacity of pretensioned concrete girders,” *Transportation Research Record*, 2406(1): 79–86.

Roy, C.J. and Oberkampf, W.L. (2011) “A comprehensive framework for verification, validation, and uncertainty quantification in scientific computing,” *Computer Methods in Applied Mechanics and Engineering*, 200: 2131–2144.

Runzell, B., Shield, C., and French, C. (2007) *Shear Capacity of Prestressed Concrete Beams*, Report No. MN/RC 2007-47, Minnesota Department of Transportation, St. Paul, MN.

Sanayei, M., Reiff, A. J., Brenner, B. R., and Imbaro, G. R. (2015) “Load rating of a fully instrumented bridge: comparison of LRFR approaches,” *Journal of Performance of Constructed Facilities*, 30(2).

Schlaich, J., Schafer, K. and Jennewein, M. (1987) "Toward a Consistent Design of Structural Concrete," *PCI Journal,* 32(3), 74-150.

Shahawy, M., Robinson, B., Batchelor, B. deV. (1993) “An Investigation of Shear Strength of Prestressed Concrete AASHTO Type II Girders,” Florida Department of Transportation, Tallahassee, FL.

Shahawy, M. A., and Batchelor, B. (1996) “Shear Behavior of Full-Scale Prestressed Concrete Girders: Comparison Between AASHTO Specifications and LRFD Code,” *PCI Journal*, 41(3): 48-62.

Shenoy, C. V. and Frantz, G. C. (1991) “Structural Tests of 27-Year-Old Prestressed Concrete Bridge Beams. *PCI Journal*, 36(5): 80-90.

Shoukry, S., William, G. W., Riad, M. Y., and Downie, B., (2009) “Effect of Moisture and Temperature on the Mechanical Properties of Concrete,” Report. West Virginia University, Morgantown, WV.

Song, G., Gu, H., Mo, Y.L., Hsu, T.T.C., and Dhonde, H. (2007) “Concrete structural health monitoring using embedded piezoceramic transducers,” *Smart Materials and Structures*, 16(4).

Sotelino, E. D., Liu, J., Chung, W., and Phuvoravan, K. (2004) *Simplified Load Distribution Factor for Use in LRFD Design*, Report No. FHWA/IN/JTRP-2004/20, Indiana Department of Transportation, Indianapolis, IN.

Taly, N. (2014) *Highway bridge superstructure engineering: LRFD approaches to design and analysis*, CRC Press, Boca Raton, FL.

Toshima, J.M. (2019) “Identification of Piecewise Stiffness in Prestressed Concrete Bridge Girders,” M.S. Thesis, University of Oklahoma, Norman, OK.

Turer, A. and Shahrooz, B. M. (2011) “Load rating of concrete-deck-on-steel-stringer bridges using field-calibrated 2D-grid models,” Engineering Structures, 33: 1267-1276

Unger, J.F., Teughels, A., and Roeck, G.D. (2006) “System identification and damage detection of a prestressed concrete beam,” *Journal of Structural Engineering*, 132(11), doi:10.1061/(ASCE) 0733-9445(2006)132:11(1691).

Vecchio, F. J., and Collins, M. P. (1986) “The Modified Compression-Field Theory for Reinforced Concrete Elements Subjected to Shear,” *ACI Journal*, 83(2): 219-231.

Westergaard, H. M. (1930) “Computations of Stresses in Bridge Slabs Due to Wheel Loads,” *Public Roads, 11*(1): 1-23.

Yousif, Z. and Hindi, R. (2007) “AASHTO-LRFD Live Load Distribution for Beam-and-Slab Bridges: Limitation and Applicability,” *Journal of Bridge Engineering*, 12(6): 765-773.

Yu, Q., Bazant, Z. P., and Wender, R. (2012) “Improved algorithm for efficient and realistic creep analysis of large creep-sensitive concrete structures,” *ACI Structural Journal*, 109(5): 665-675.

Zokaie, T. (2000) “AASHTO-LRFD Live Load Distribution Specifications,” *Journal of Bridge Engineering*, 5(2): 131-138.

Zokaie, T., Osterkamp, T. A., and Imbsen, R. A. (1991a) *NCHRP report 12-2611: Distribution of wheel loads on highway bridges*, Transportation Research Board, Washington, D.C.

Zokaie, T., Imbsen, R. A., and Okstercamp, T. A. (1991b) “Distribution of wheel loads on highway bridges,” *Transportation Research Record*, 1290: 119-126, Transportation Research Board, Washington, D.C.

Zwoyer, E. M. and Siess, C. P. (1954) “Ultimate strength in shear of simply-supported prestressed concrete beams without web reinforcement,” *ACI Journal*, 51(10): 181-200.

Appendix A: Additional Parametric Study Results

A.1 Type-IV Girders

A.1.1 Effects of Girder Spacing

Figures A.1-A.3, A.4-A.6, A.7-A.9 and A.10-A.12 compare the load distribution factors calculated from the AASHTO LRFD equations and those determined from grillage models for Type-IV girders. Each set of three figures covers three different span lengths and there are four groups as comparisons are made for one and two lanes load cases for the interior and exterior girders. Figures A.13-A.15, A.16-A.18, A.19-A.21 and A.22.-A.24 show the difference between the AASHTO LRFD distribution factors and those determined from the grillage models. These figures show that the load distribution factors from the AASHTO LRFD equations are larger than the grillage model factors for all cases. For the one lane loaded interior girder case it can be seen in Figures A.13-A.15 that the AASHTO LRFD equation gives 18.2% to 21.6% higher distribution factor than the grillage model when girders are spaced at 6 ft. For the 9 ft and 12 ft girder spacing the difference between AASHTO LRFD equations and grillage models reduces to a range of 9.6% to 21.4% for all configurations considered for the Type-IV girder. It can be seen from Figures A.16-A.18 that for the exterior girder with one lane loaded case the AASHTO LRFD equations resulted in at least 5.3% higher load distribution factors than the grillage model for all configurations considered. Similarly, for the case when two lanes are loaded for interior girders, as shown in Figures A.19-A.21, the AASHTO LRFD equations give distribution factors 7.0% to 14.7% higher than the grillage models for the 6 ft, 9 ft and 12 ft girder spacings. The difference between the AASHTO LRFD equation and grillage model factors for the two lanes loaded case can be seen for exterior girders in Figures A.16-A.18. When comparison is made between Type-III and Type-IV girders, Type-IV girders had larger lower and upper limits for the range of difference from the AASHTO LRFD distribution factors for one lane loaded interior and two lanes load interior cases. The corresponding ranges are inconsistent for exterior girders except for when the girder spacing 6 ft and two lanes are loaded, the grillage models gave higher load distribution factor than the AASHTO LRFD equations.

A.1.2 Effects of Diaphragms

It is difficult to differentiate between the diaphragm or no diaphragm cases in Figures A.1-A.12. If Figures A.13-A.24 are considered, it can be seen that most of the cases have 1% to 2% difference in the percentage difference when diaphragm and no diaphragm are compared and there are some odd cases where the difference goes up to 6%.

A.1.3 Effects of Deck Thickness

Just like for diaphragms, the effects of deck thickness on distribution factors are difficult to determine as the distribution factors for these cases are plotted very close to each other on the graphs in Figures A.1-A.12. When the percentage differences were compared between the 7 in. and 9 in. thick deck cases, which is shown in Figure A.13-A.245, a difference of 2% was observed which is not significant.

A.1.4 Effects of Span Length

There is the variation of about 1% to 4% in the percentage difference between the AASHTO LRFD and grillage model load distribution factors when different spans were considered for the two lanes loaded exterior, two lanes loaded interior and one lane loaded exterior load cases in Figures A.16-A.18, A.19-A.21 and A.22-A.24. When the variation for the one lane loaded interior case is observed in Figure A.13-A.15, the variation of about 10% between span length of 75 ft, 90 ft, and 105 ft appears significant.

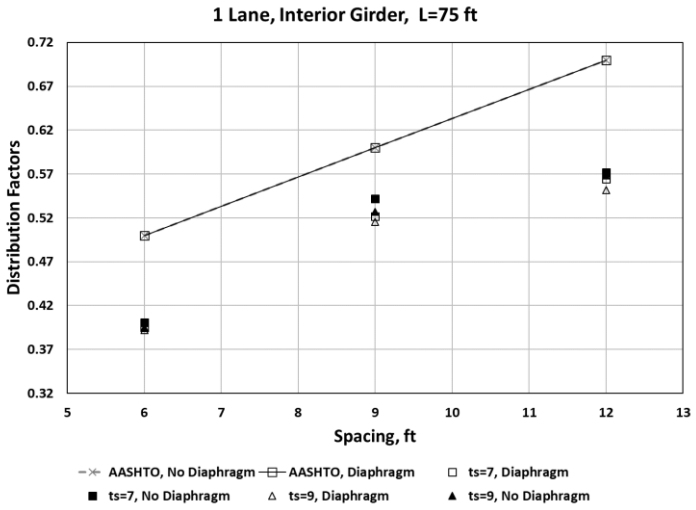

Figure A.1. Distribution factors for the interior girders, one lane loaded versus girder spacing, Type-IV with 75 ft span

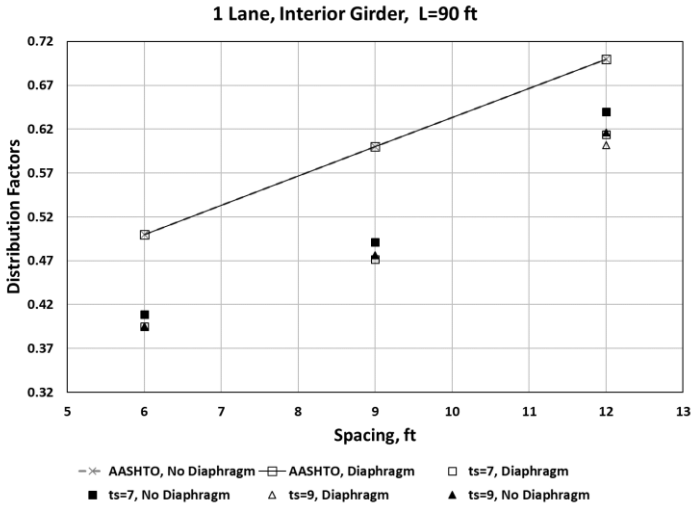

Figure A.2. Distribution factors for the interior girders, one lane loaded versus girder spacing, Type-IV with 90 ft span

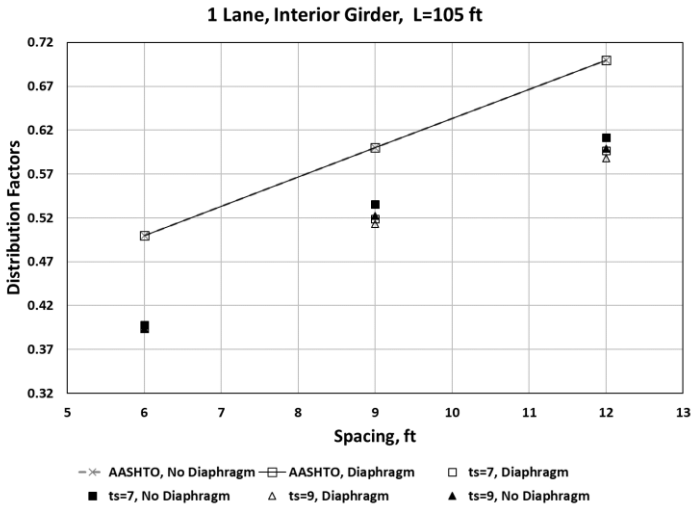

Figure A.3. Distribution factors for the interior girders, one lane loaded versus girder spacing, Type-IV with 105 ft span

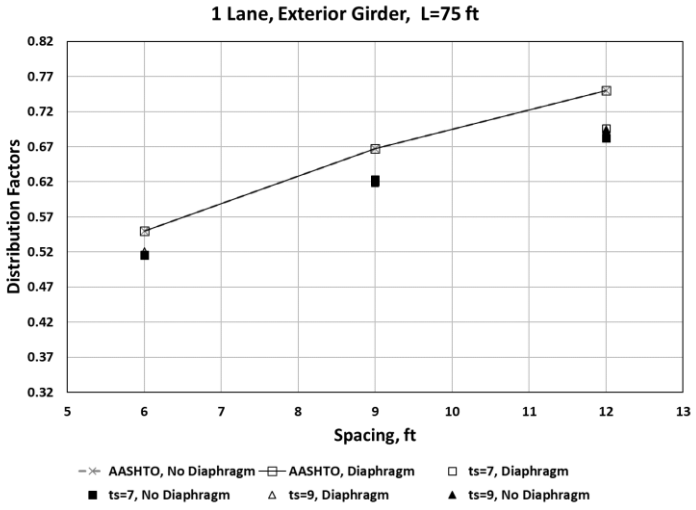

Figure A.4. Distribution factors for the exterior girders, one lane loaded versus girder spacing, Type-IV with 75 ft span

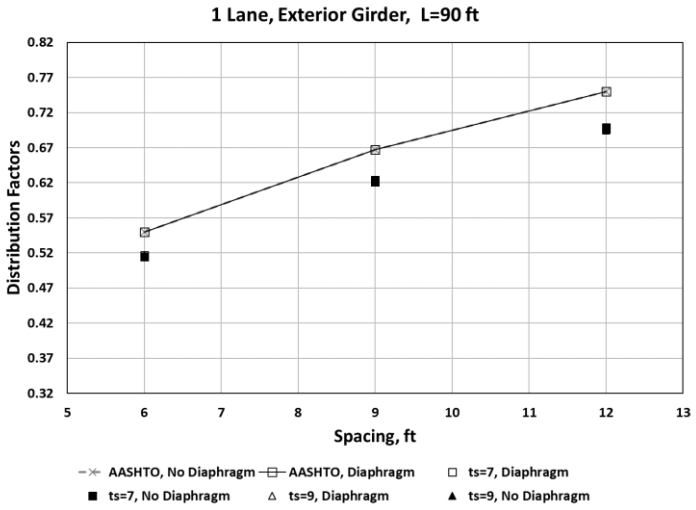

Figure A.5. Distribution factors for the exterior girders, one lane loaded versus girder spacing, Type-IV with 90 ft span

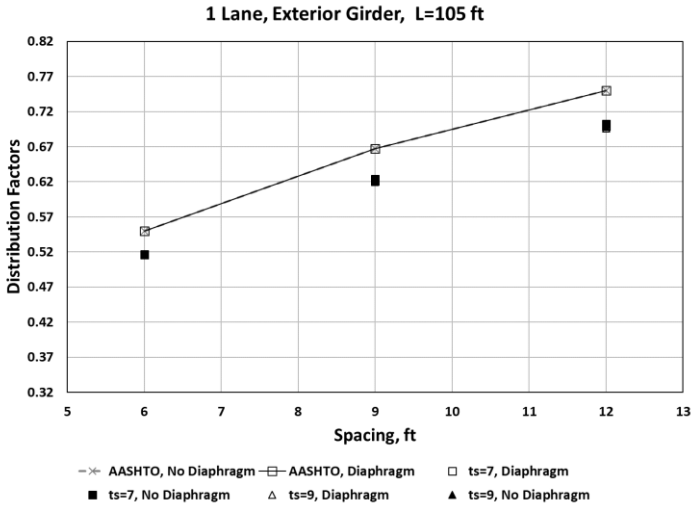

Figure A.6. Distribution factors for the exterior girders, one lane loaded versus girder spacing, Type-IV with 105 ft span

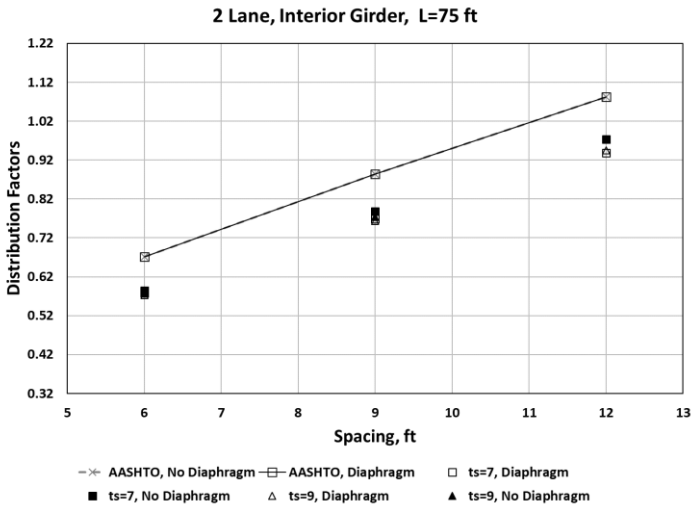

Figure A.7. Distribution factors for the interior girders, two lanes loaded versus girder spacing, Type-IV with 75 ft span

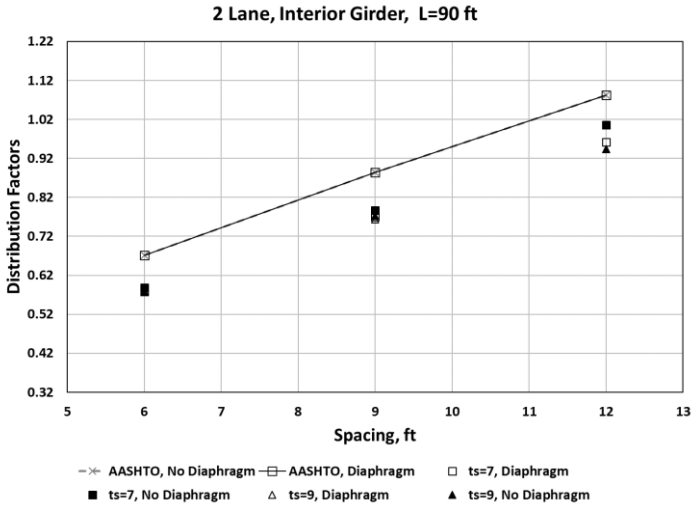

Figure A.8. Distribution factors for the interior girders, two lanes loaded versus girder spacing, Type-IV with 90 ft span

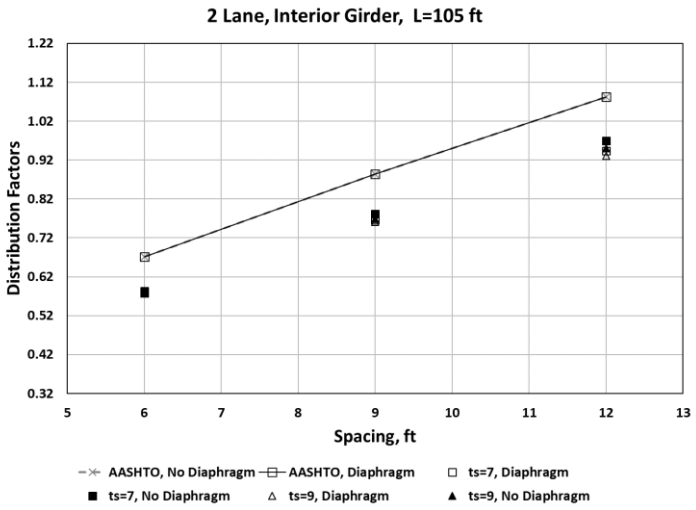

Figure A.9. Distribution factors for the interior girders, two lanes loaded versus girder spacing, Type-IV with 105 ft span

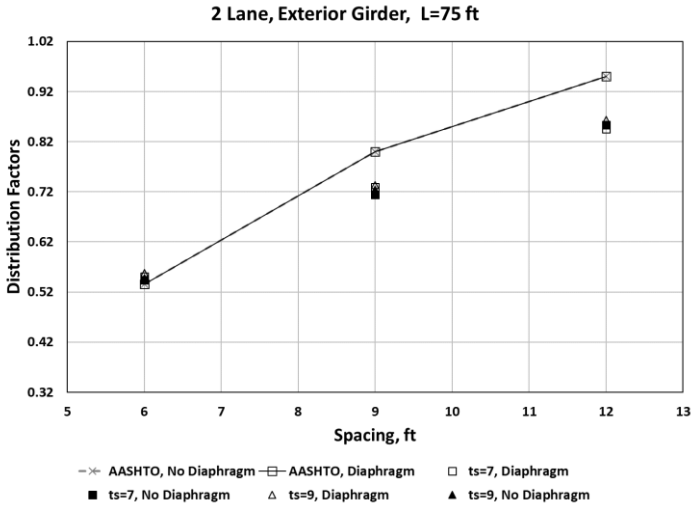

Figure A.10. Distribution factors for the exterior girders, two lanes loaded versus girder spacing, Type-IV with 75 ft span

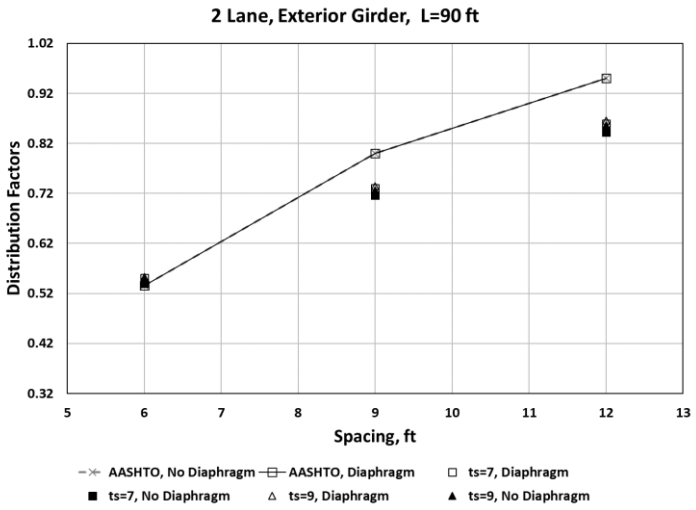

Figure A.11. Distribution factors for the exterior girders, two lanes loaded versus girder spacing, Type-IV with 90 ft span

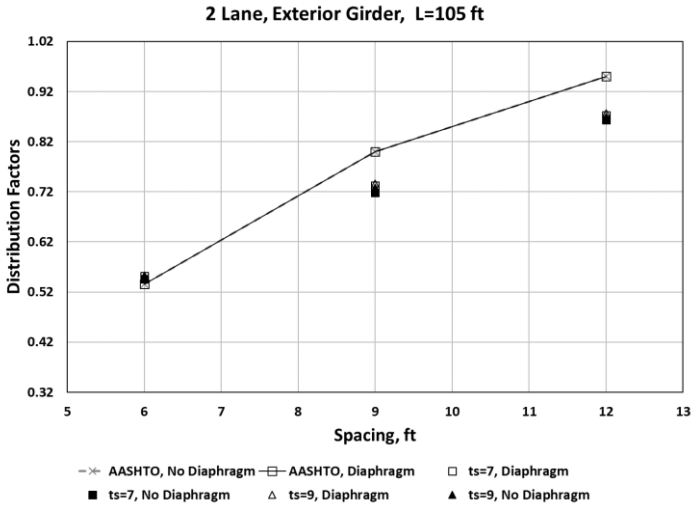

Figure A.12. Distribution factors for the exterior girders, two lanes loaded versus girder spacing, Type-IV with 105 ft span

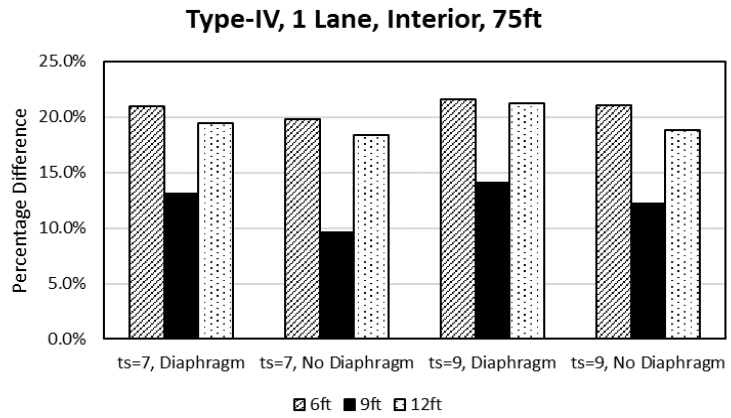

Figure A.13. Percentage difference between AASHTO equations and grillage models, for one lane loaded and interior girder, Type-IV with 75 ft span

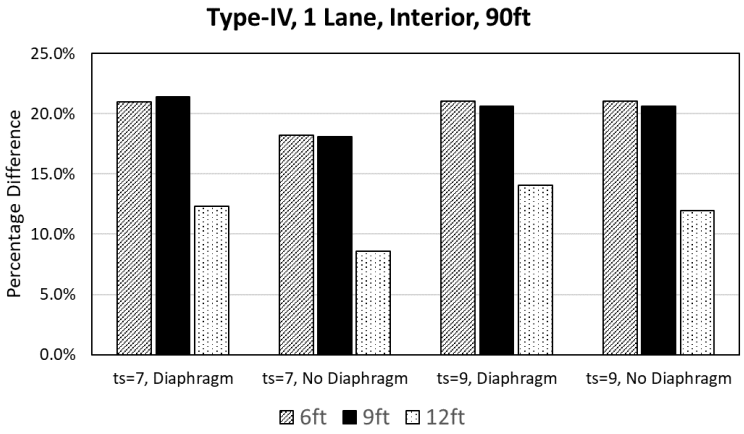

Figure A.14. Percentage difference between AASHTO equations and grillage models, for one lane loaded and interior girder, Type-IV with 90 ft span

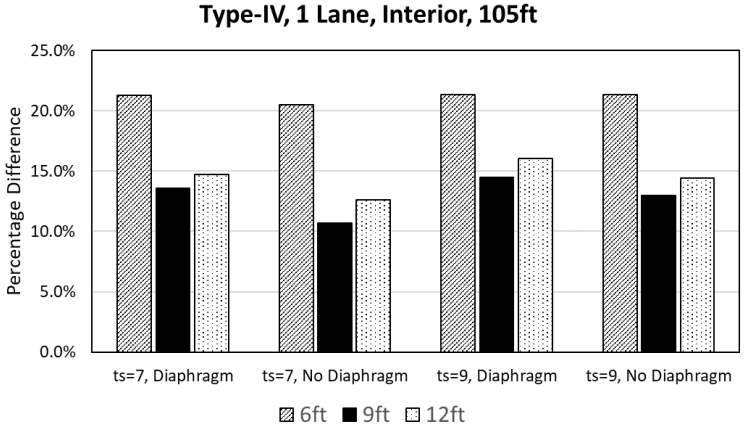

Figure A.15. Percentage difference between AASHTO equations and grillage models, for one lane loaded and interior girder, Type-IV with 105 ft span

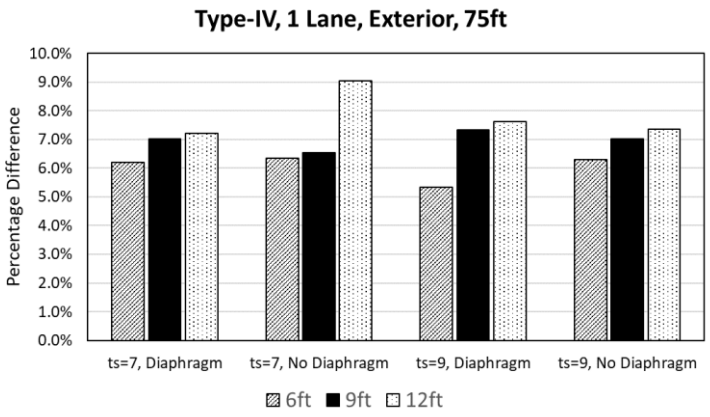

Figure A.16. Percentage difference between AASHTO equations and grillage models, for one lane loaded and exterior girder, Type-IV with 75 ft span

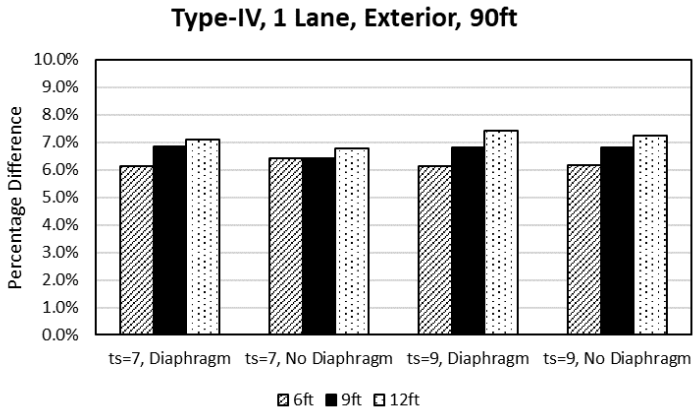

Figure A.17. Percentage difference between AASHTO equations and grillage models, for one lane loaded and exterior girder, Type-IV with 90 ft span

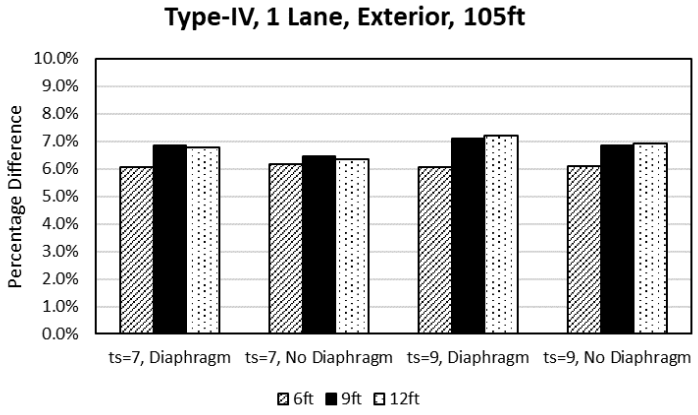

Figure A.18. Percentage difference between AASHTO equations and grillage models, for one lane loaded and exterior girder, Type-IV with 105 ft span

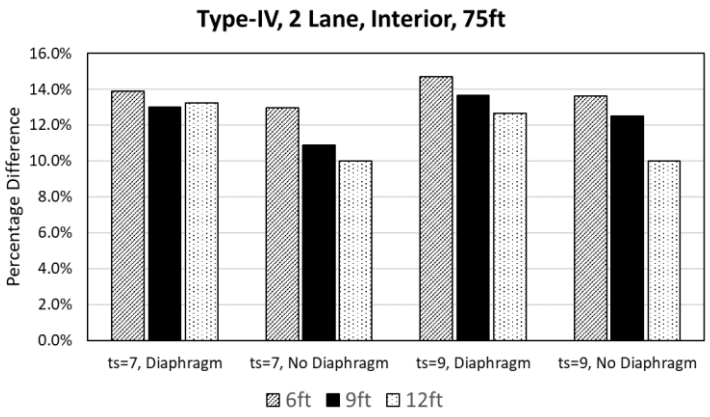

Figure A.19. Percentage difference between AASHTO equations and grillage models, for two lanes loaded and interior girder, Type-IV with 75 ft span

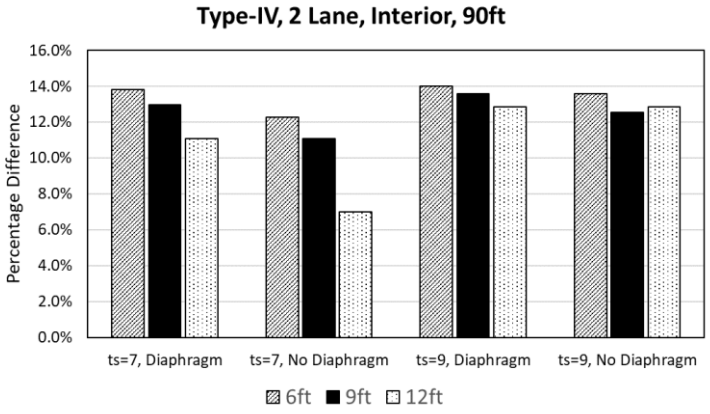

Figure A.20. Percentage difference between AASHTO equations and grillage models, for two lanes loaded and interior girder, Type-IV with 90 ft span

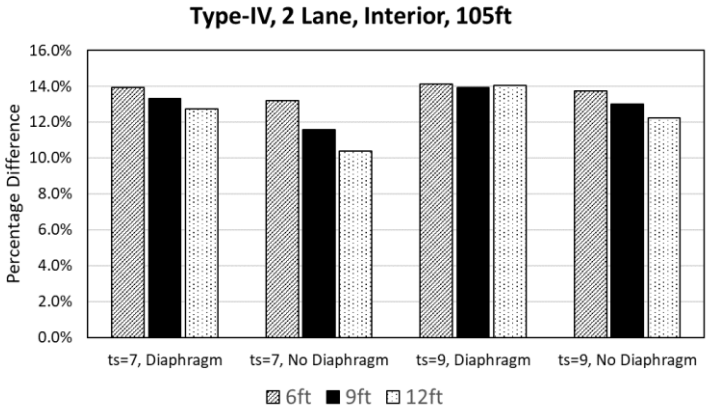

Figure A.21. Percentage difference between AASHTO equations and grillage models, for two lanes loaded and interior girder, Type-IV with 105 ft span

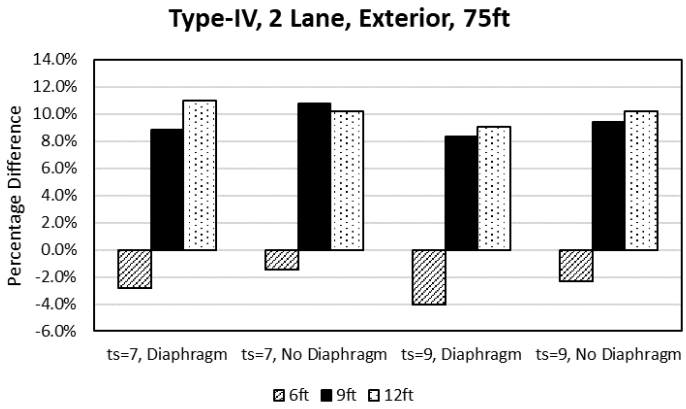

Figure A.22. Percentage difference between AASHTO equations and grillage models, for two lanes loaded and exterior girder, Type IV with 75 ft span

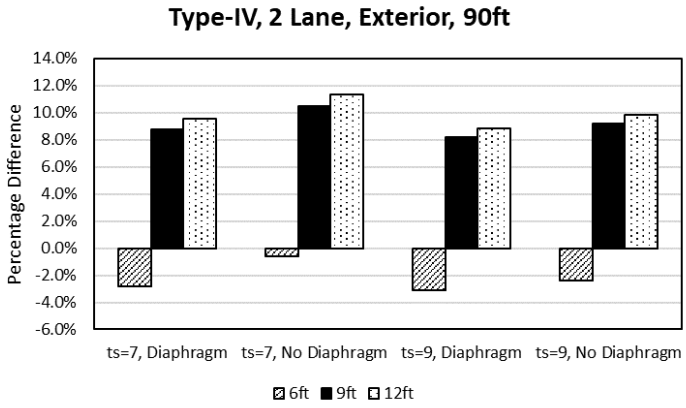

Figure A.23. Percentage difference between AASHTO equations and grillage models, for two lanes loaded and exterior girder, Type IV with 90 ft span

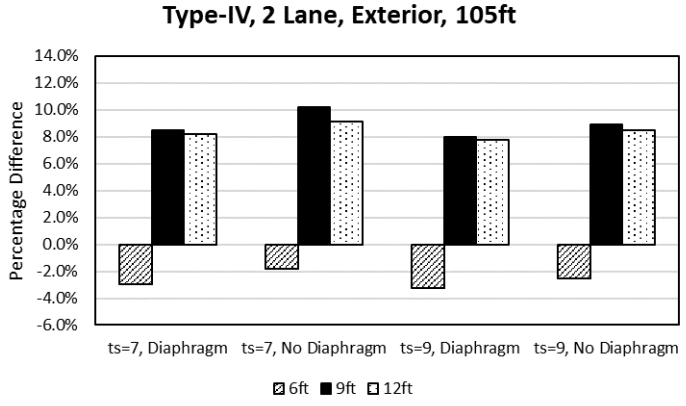

Figure A.24. Percentage difference between AASHTO equations and grillage models, for two lanes loaded and exterior girder, Type IV with 105 ft span

A.1.5 Quantitative Comparison of Load Distribution Factors

Figures A.25-A.28 show linear trendlines for load distribution factors determined from AASHTO LRFD equations and grillage models relative to girder spacing. Discussion on the use of a linear trendline for the quadratic AASHTO equation is provided in Section 2.5.6. For all of the cases examined for Type-IV girders, trendlines for load distribution factors determined from grillage models were less steep than all of the AASHTO LRFD equations. The maximum difference of slope was 25%, which was for two lanes exterior girder load case. The minimum coefficient of determination was for the one lane loaded interior girder case, but was still found to be 0.9373 indicating that a linear trend was an appropriate model for the data. These results indicate that girder spacing had a large impact on load distribution factors and that the effect was less for grillage models than for the AASHTO equations.

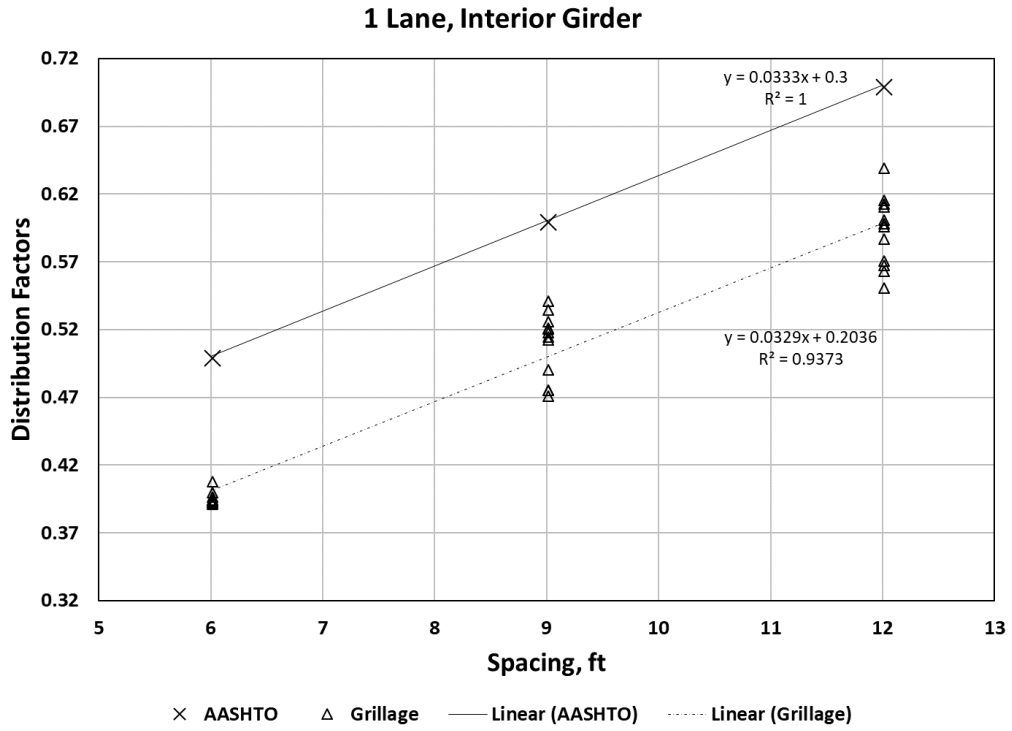

Figure A.25. Linear trendlines for effect of girder spacing on distribution factors for Type-IV girders, interior girder one lane loaded case

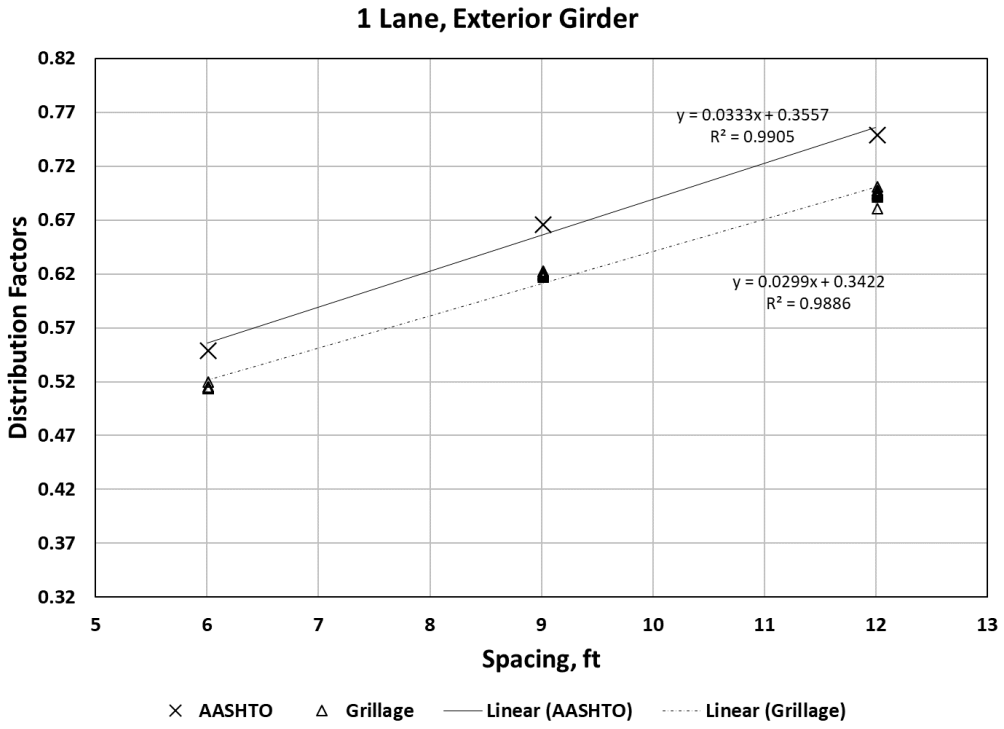

Figure A.26. Linear trendlines for effect of girder spacing on distribution factors for Type-IV girders, exterior girder one lane loaded case

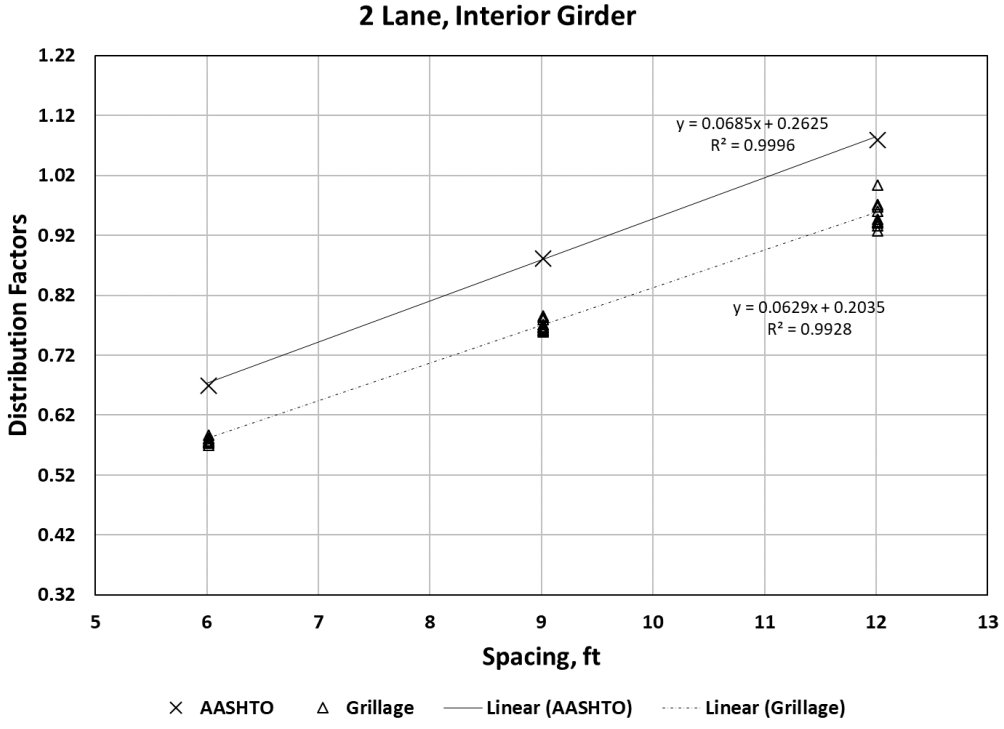

Figure A.27. Linear trendlines for effect of girder spacing on distribution factors for Type-IV girders, interior girder two lanes loaded case

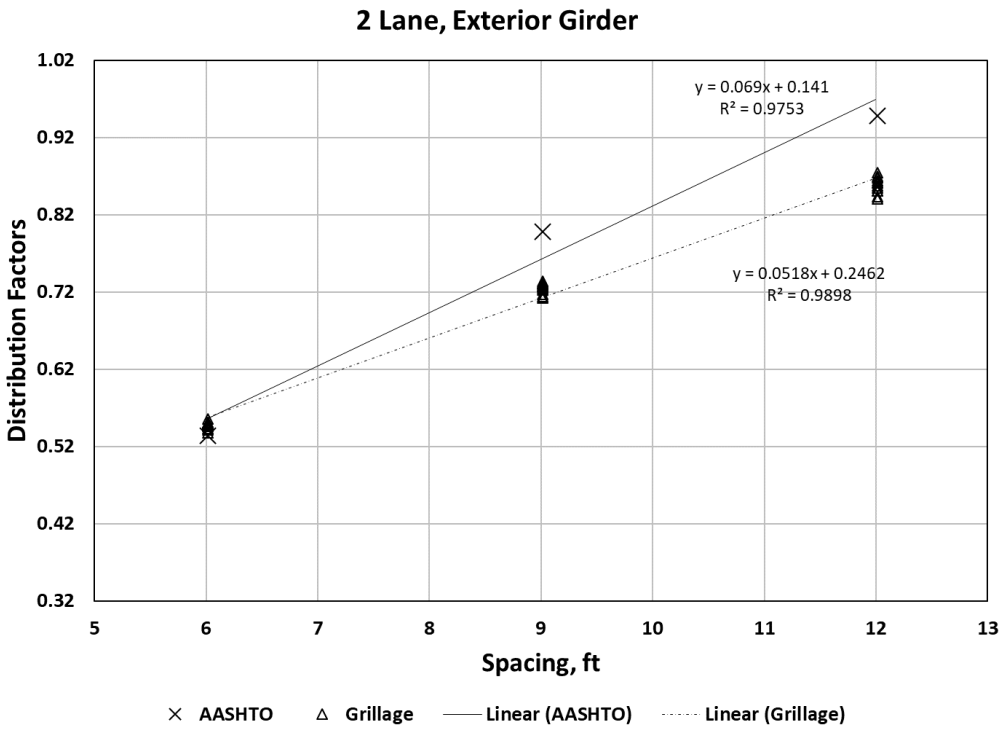

Figure A.28. Linear trendlines for effect of girder spacing on distribution factors for Type-IV girders, exterior girder two lanes loaded case

A.2 BT-63 Girders

A.2.1 Effects of Girder Spacing

Geometrically, the Bulb Tee (BT) sections are different than the AASHTO I-girders (Type I, Type-II, Type-III, etc.). The BT sections have a larger depth to weight ratio than the typical AASHTO beams. For instance, a BT-72 has a depth of 72 in. and weight of 0.799 kip/ft while a Type-VI beam which has the same depth of 72 in. but the weight is 1.13 kip/ft (Nawy, 2009). When Figures A.29-A.31, A.32-A.34, A.35-A.37 and A.38-A.40 showing the distribution factors from the AASHTO LRFD equations and grillage models are considered, it can be seen that the AASHTO LRFD equations give linearly related distribution factors for one lane and two lanes loaded interior girders and bilinearly related distribution factors for one lane and two lanes loaded exterior girders. The grillage models give bilinear relationships for all of the cases. The trends of spacing are different for the BT-63. The effect of girder spacing does not follow the same pattern as when Type-III and Type-IV girders are compared. In some cases, the 9 ft spacing

gives greater deviation from AASHTO equations and in some cases 6 ft or 12 ft for similar configurations of the different girder types. This difference in trends could be the function of girder stiffness or potentially span lengths since as with the depth of the girders the span lengths are increasing, and all other variables such as deck thickness, presence of diaphragm and girder spacing are the same.

A.2.2 Effects of Diaphragms

The effects of diaphragm are similar to what was observed for Type-III and Type-IV girders. A difference of about 1% to 2% is observed between the percentage differences between the grillage model and AASHTO distribution factors when the diaphragm and no diaphragm cases are compared as shown in Figures A.41-A.43, A.44-A.46, A.47-A.49 and A.50-A.52.

A.2.3 Effects of Deck Thickness

Similar to results observed for Type-III and Type-IV girders the effects of deck thickness are not noteworthy for BT-63 girders. Very little impact of about 1% to 2% is observed when the deck thickness is changed from 7 in. to 9 in.

A.2.4 Effects of Span Length

The percentage differences between the AASHTO and grillage model distribution factors, shown in Figures A.41-A.43, A.44-A.46, A.47-A.49 and A.50-A.52 suggest that there is only 1% to 2% change in the percentage difference when same configuration of bridge is compared with different span lengths. This difference could also be due to the change in location of intermediate diaphragm with change in span length, but a change in percentage difference can also be observed when different span lengths of no diaphragm cases are compared. Since the span lengths considered for BT-63 girders are very high compared to Type-III, the effect of intermediate diaphragm relative to span length observed for Type-III girders cannot be seen for BT-63 girders.

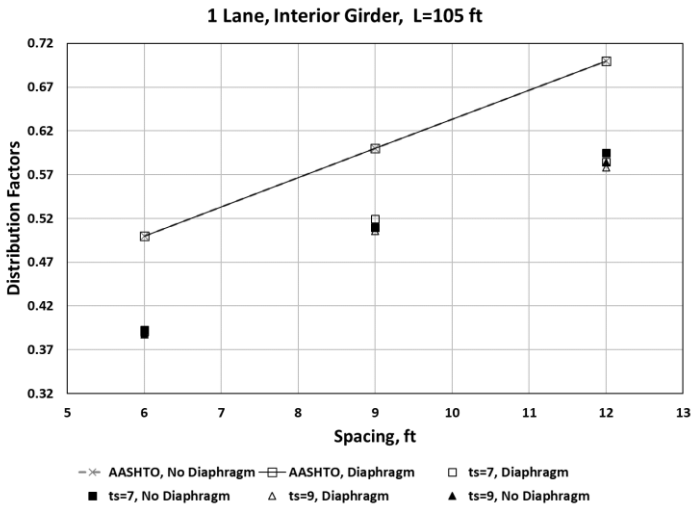

Figure A.29. Distribution factors for the interior girders, one lane loaded versus girder spacing, BT-63 with 105 ft span

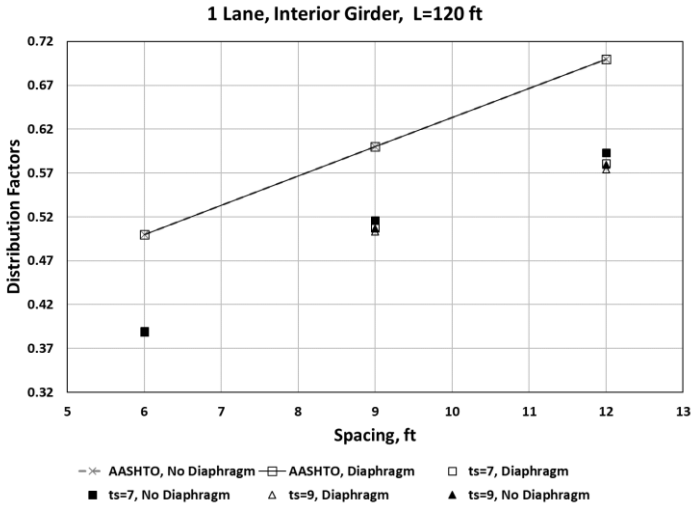

Figure A.30. Distribution factors for the interior girders, one lane loaded versus girder spacing, BT-63 with 120 ft span

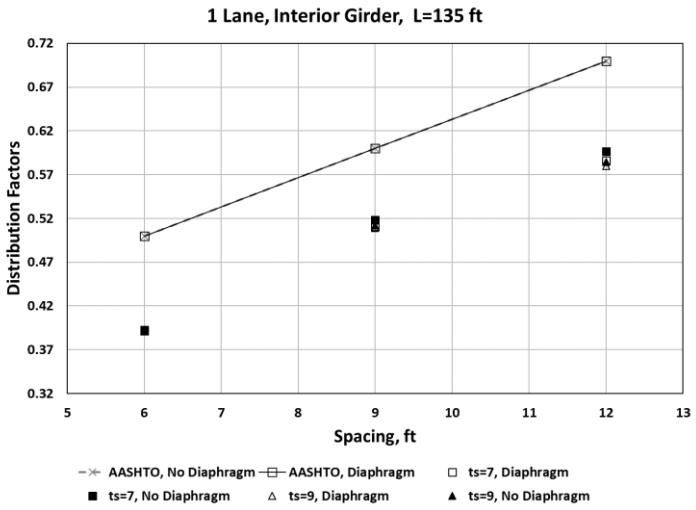

Figure A.31. Distribution factors for the interior girders, one lane loaded versus girder spacing, BT-63 with 135 ft span

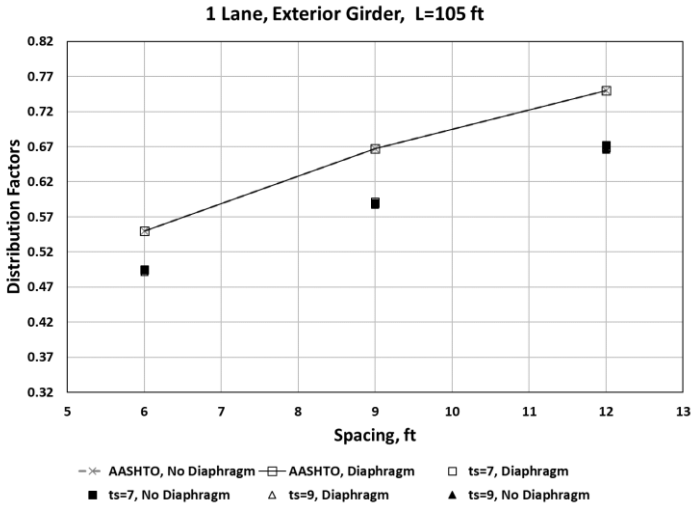

Figure A.32. Distribution factors for the exterior girders, one lane loaded versus girder spacing, BT-63 with 105 ft span

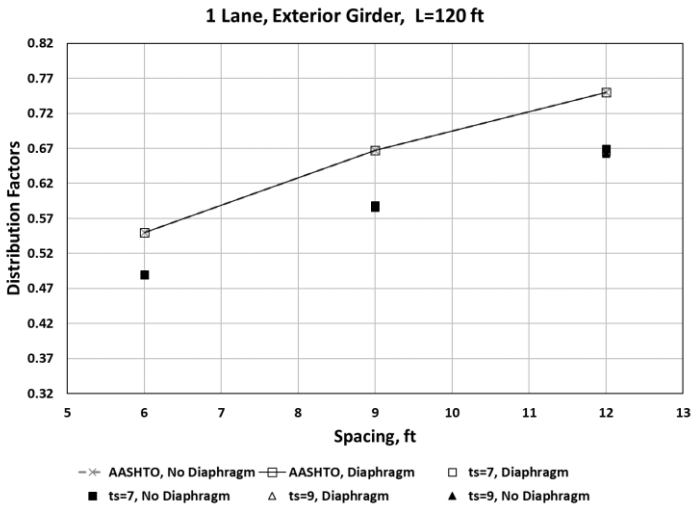

Figure A.33. Distribution factors for the exterior girders, one lane loaded versus girder spacing, BT-63 with 120 ft span

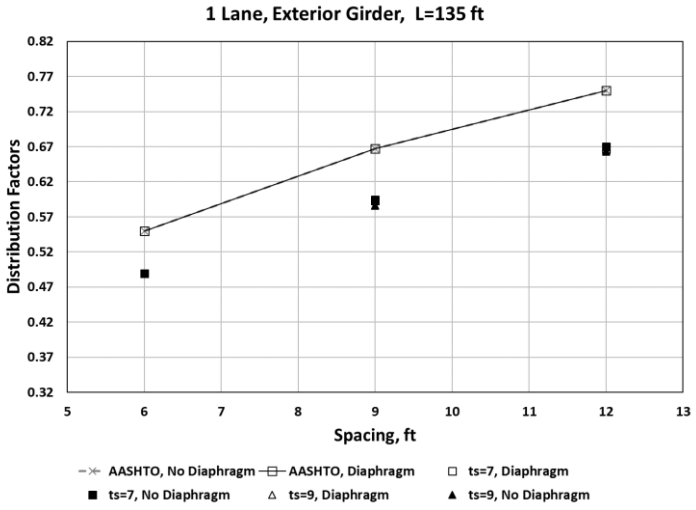

Figure A.34. Distribution factors for the exterior girders, one lane loaded versus girder spacing, BT-63 with 135 ft span

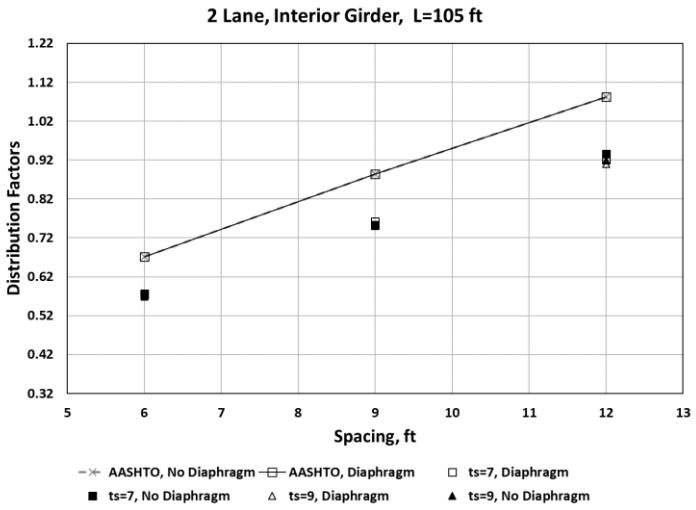

Figure A.35. Distribution factors for the interior girders, two lanes loaded versus girder spacing, BT-63 with 105 ft span

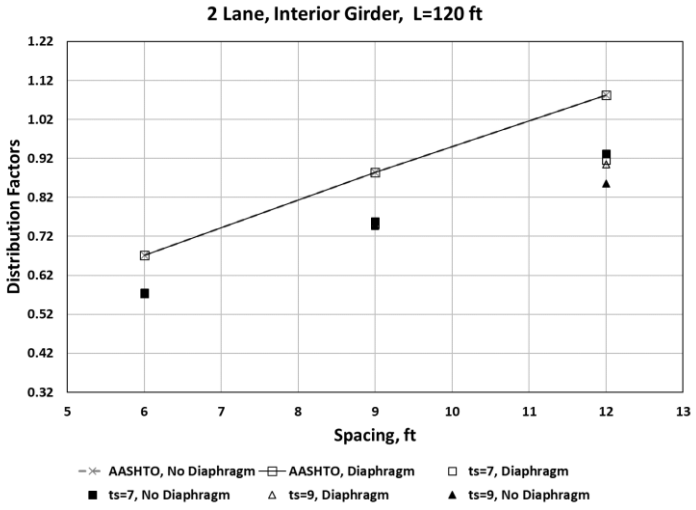

Figure A.36. Distribution factors for the interior girders, two lanes loaded versus girder spacing, BT-63 with 120 ft span

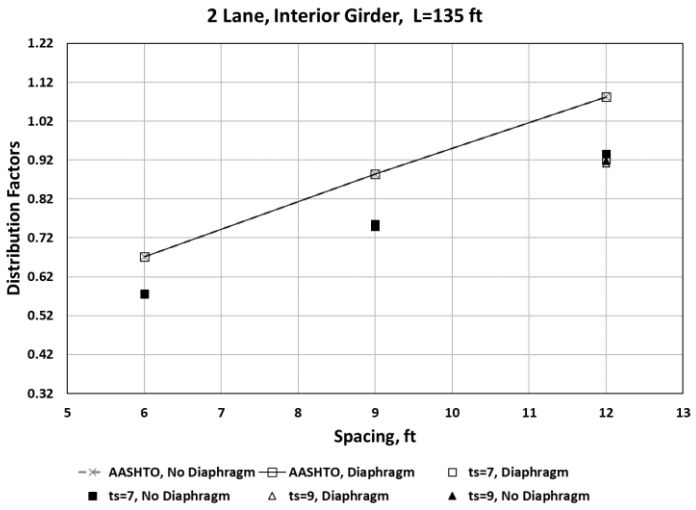

Figure A.37. Distribution factors for the interior girders, two lanes loaded versus girder spacing, BT-63 with 135 ft span

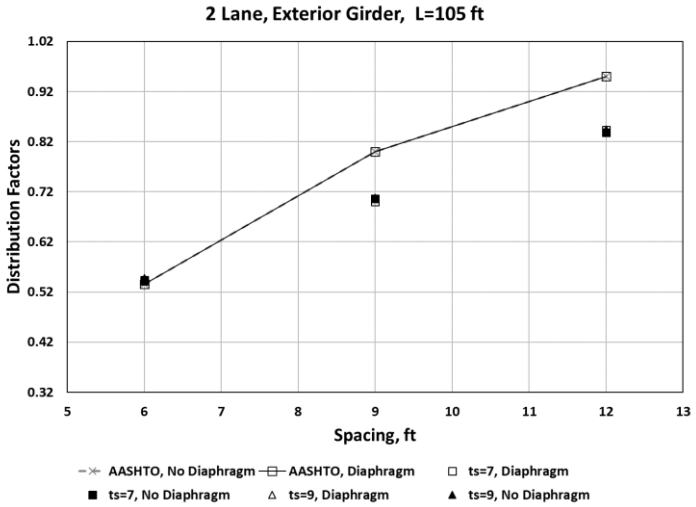

Figure A.38. Distribution factors for the exterior girders, two lanes loaded versus girder spacing, BT-63 with 105 ft span

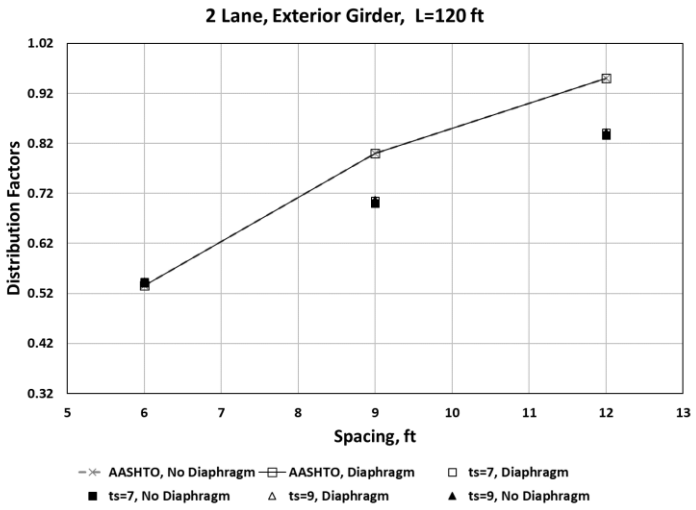

Figure A.39. Distribution factors for the exterior girders, two lanes loaded versus girder spacing, BT-63 with 120 ft span

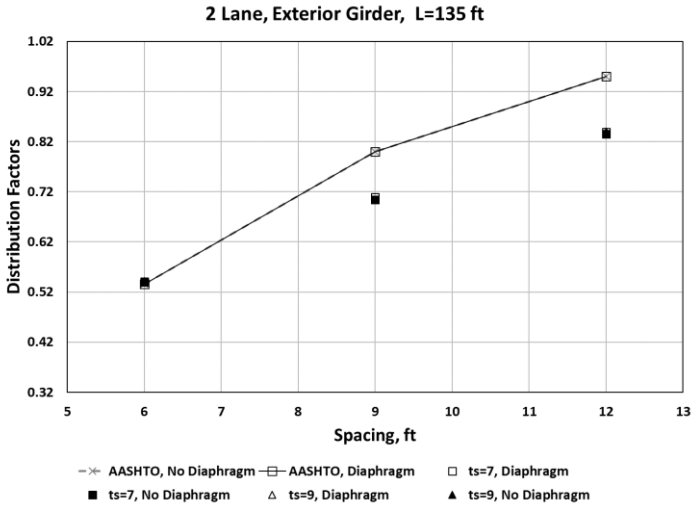

Figure A.40. Distribution factors for the exterior girders, two lanes loaded versus girder spacing, BT-63 with 135 ft span

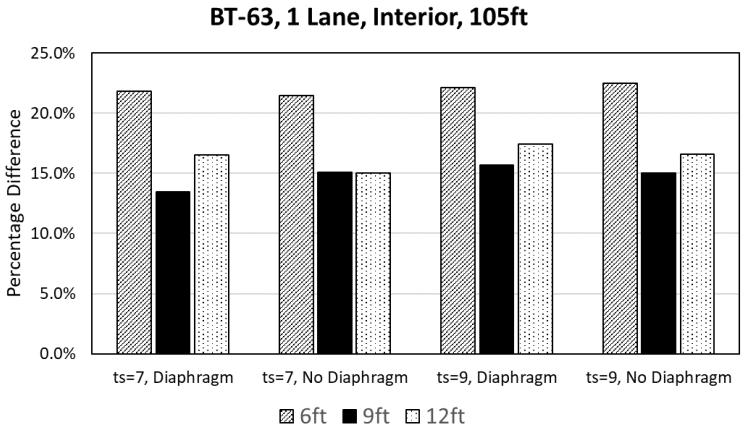

Figure A.41. Percentage difference between AASHTO equations and grillage models, for one lane loaded and interior girder, BT-63 with 105 ft span

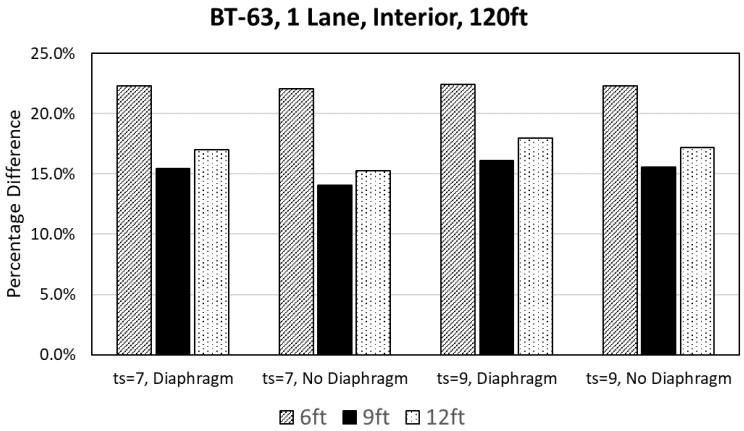

Figure A.42. Percentage difference between AASHTO equations and grillage models, for one lane loaded and interior girder, BT-63 with 120 ft span

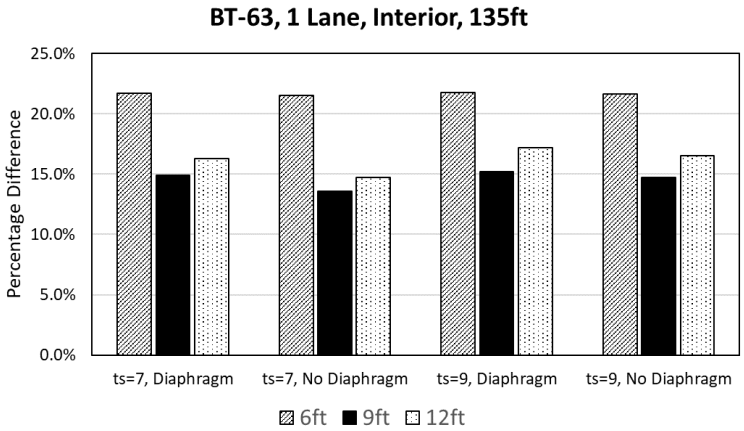

Figure A.43. Percentage difference between AASHTO equations and grillage models, for one lane loaded and interior girder, BT-63 with 135 ft span

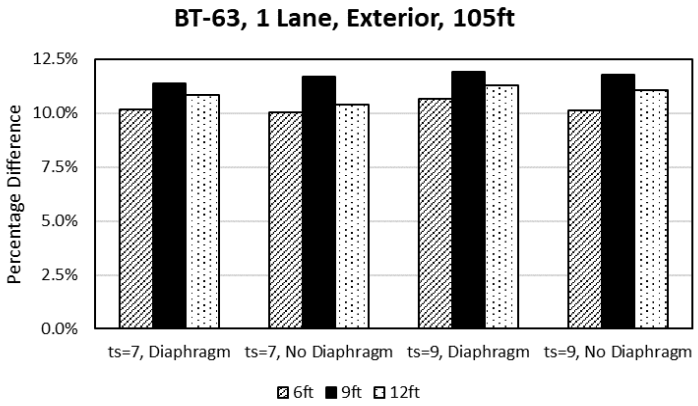

Figure A.44. Percentage difference between AASHTO equations and grillage models, for one lane loaded and exterior girder, BT-63 with 105 ft span

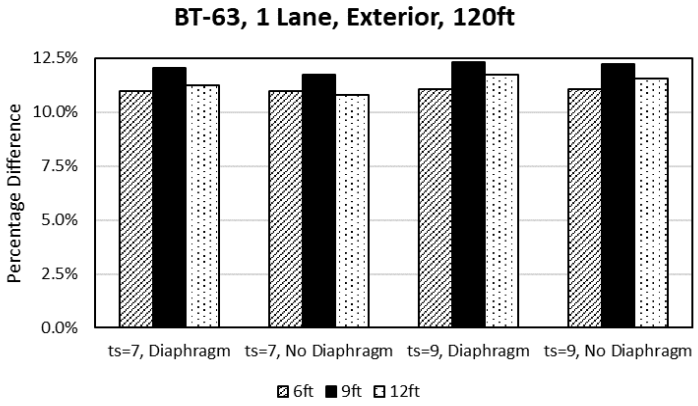

Figure A.45. Percentage difference between AASHTO equations and grillage models, for one lane loaded and exterior girder, BT-63 with 120 ft span

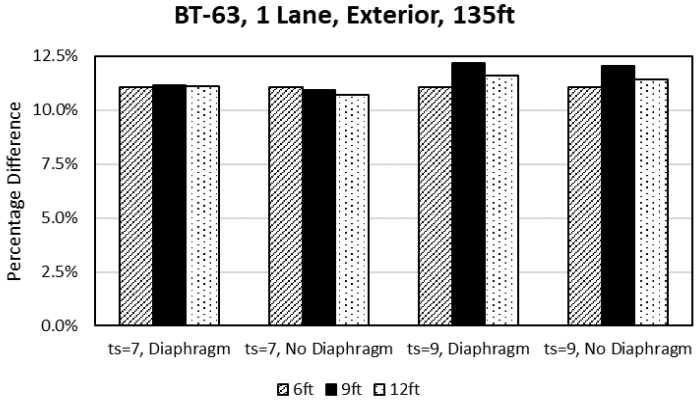

Figure A.46. Percentage difference between AASHTO equations and grillage models, for one lane loaded and exterior girder, BT-63 with 135 ft span

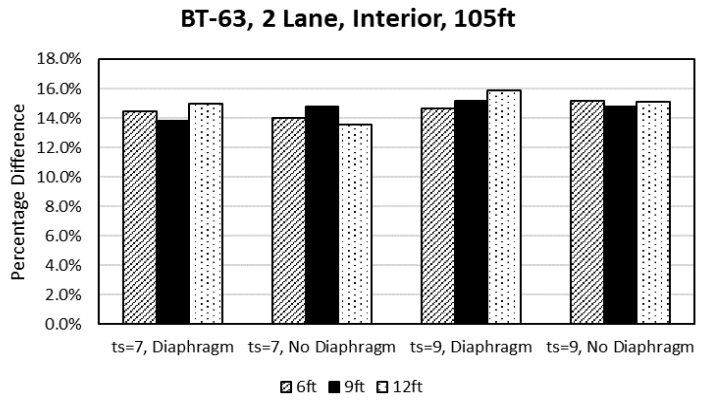

Figure A.47. Percentage difference between AASHTO equations and grillage models, for two lanes loaded and interior girder, BT-63 with 105 ft span

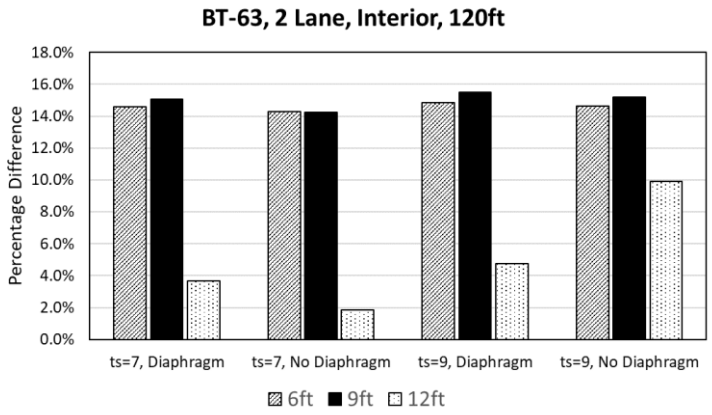

Figure A.48. Percentage difference between AASHTO equations and grillage models, for two lanes loaded and interior girder, BT-63 with 120 ft span

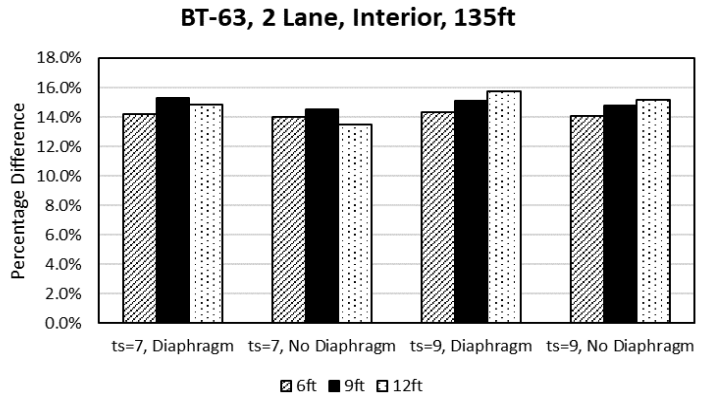

Figure A.49. Percentage difference between AASHTO equations and grillage models, for two lanes loaded and interior girder, BT-63 with 135 ft span

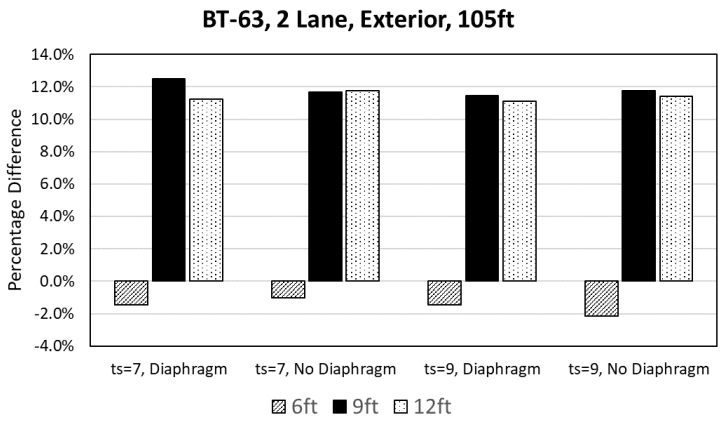

Figure A.50. Percentage difference between AASHTO equations and grillage models, for two lanes loaded and exterior girder, BT-63 with 105 ft span

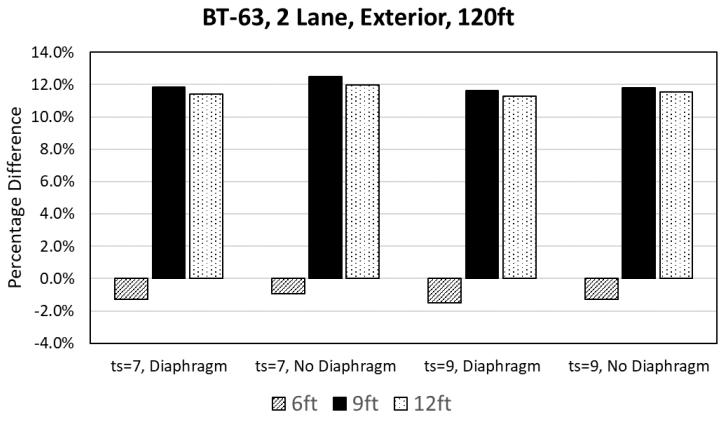

Figure A.51. Percentage difference between AASHTO equations and grillage models, for two lanes loaded and exterior girder, BT-63 with 120 ft span

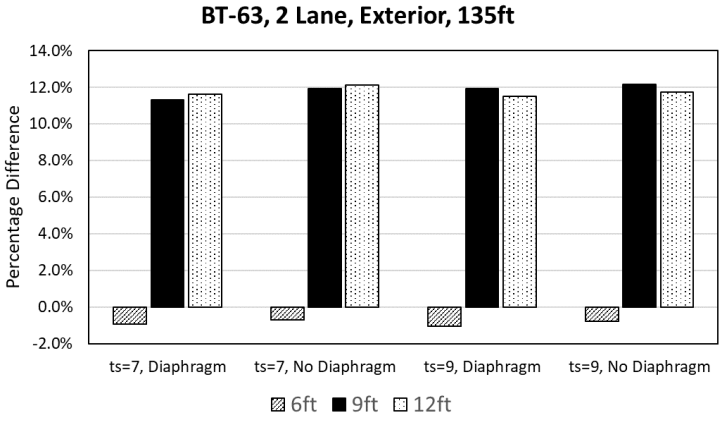

Figure A.52. Percentage difference between AASHTO equations and grillage models, for two lanes loaded and exterior girder, BT-63 with 135 ft span

A.2.5 Quantitative Comparison of Load Distribution Factors

Figures A.53-A.56 show linear trendlines for distribution factors determined for all BT-63 girder cases examined relative to girder spacing. Discussion on the use of a linear trendline for the quadratic AASHTO equation is provided in Section 2.5.6. For all cases, the results of grillage models were fit quite well with linear equations having coefficient of determination greater than 0.97. For all of the cases grillage model gave less steep trendlines than the AASHTO LRFD equations. The maximum percentage difference in slope was found for the two lanes loaded exterior girder case which was 28.1% and the minimum percentage difference was found for the one lane loaded interior girder case (2.7%). These results indicate that girder spacing had a large impact on load distribution factors and that the effect was less for grillage models than for the AASHTO equations.

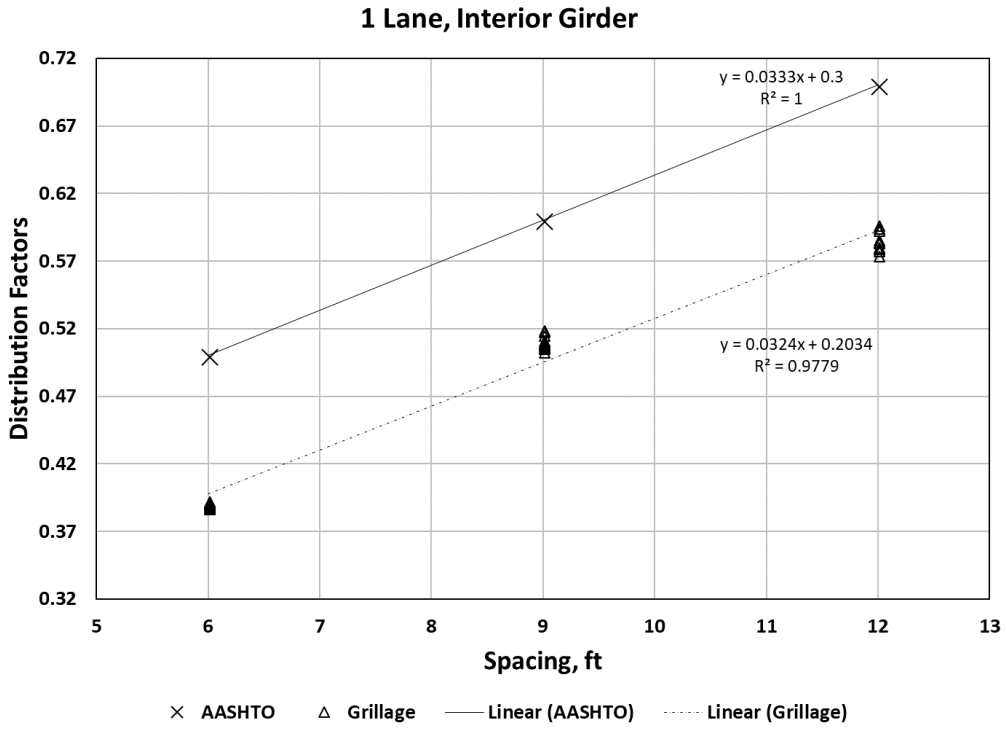

Figure A.53. Linear trendlines for effect of girder spacing on distribution factors for BT-63 girders, interior girders one lane loaded case

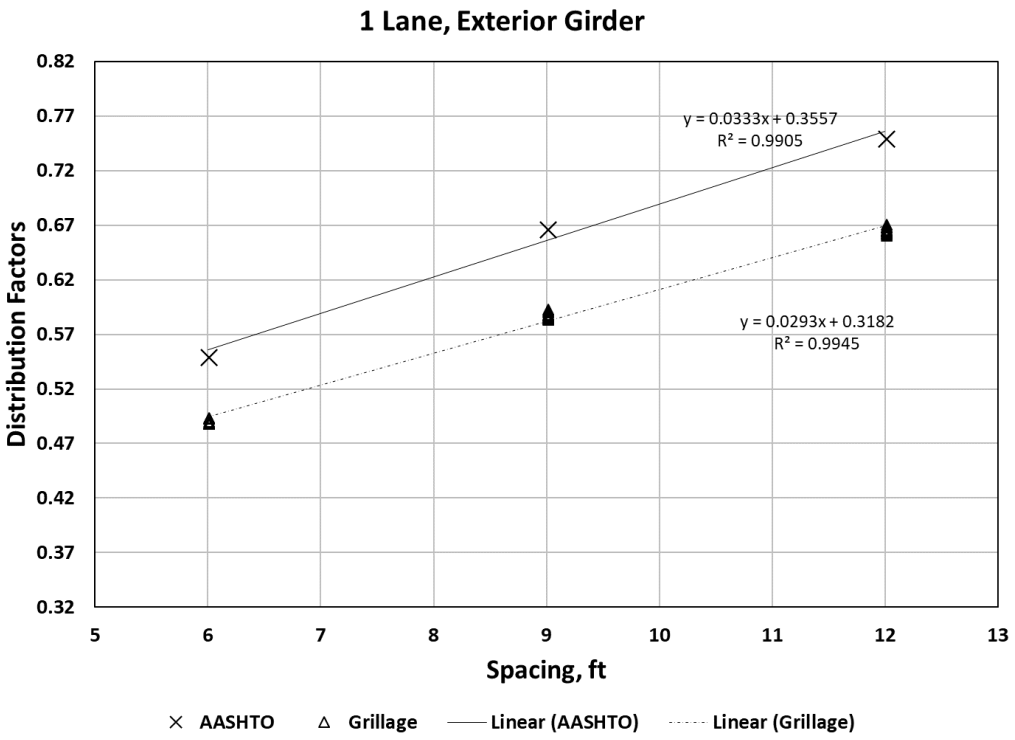

Figure A.54. Linear trendlines for effect of girder spacing on distribution factors for BT-63 girders, exterior girders one lane loaded case

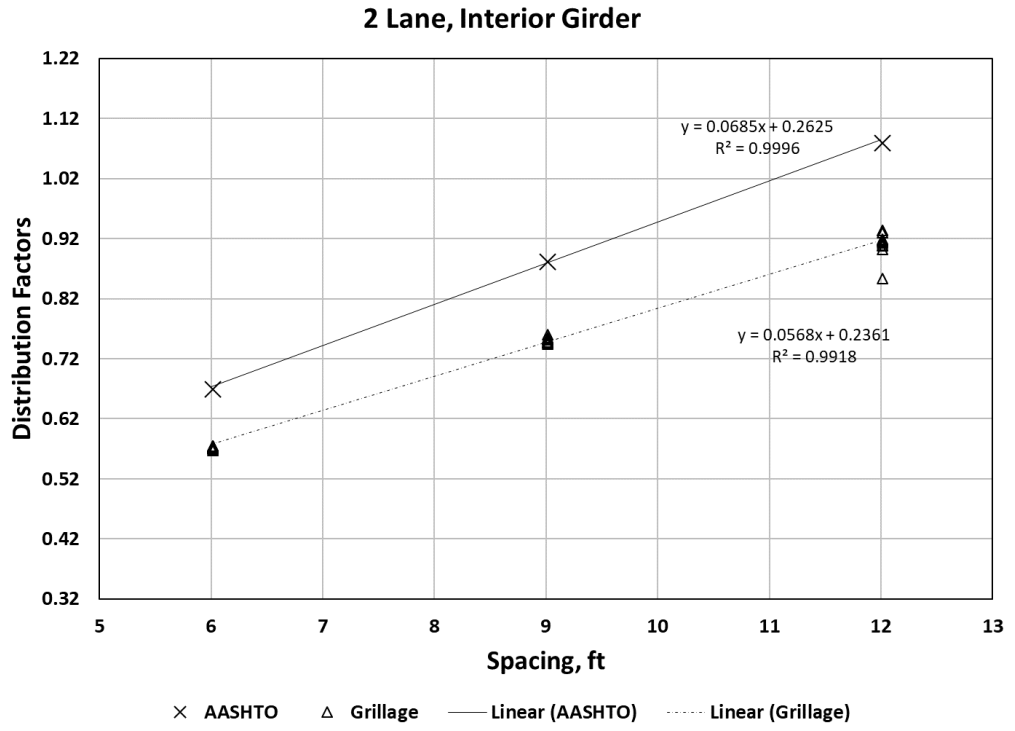

Figure A.55. Linear trendlines for effect of girder spacing on distribution factors for BT-63 girders, interior girders two lanes loaded case

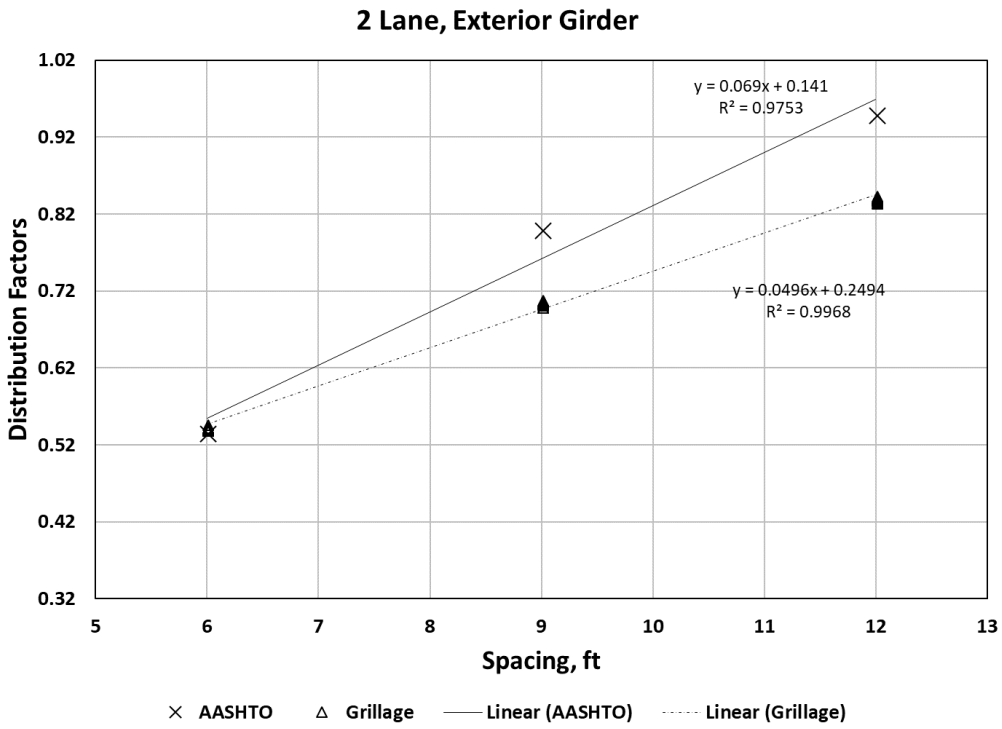

Figure A.56. Linear trendlines for effect of girder spacing on distribution factors for BT-63 girders, exterior girders two lanes loaded case

A.3 BT-72 Girders

A.3.1 Effects of Girder Spacing

The distribution factors calculated using the AASHTO LRFD equations and from the grillage models for BT-72 girders are shown in Figures A.57-A.59, A.60-A.62, A.63-A.65 and A.66-A.68. The trends of change in distribution factor relative to girder spacing are very consistent between girder BT-63 and BT-72 girders. Even the percentage difference between AASHTO and grillage model distribution factors for BT-72 girders are quite close to those for BT-63 girders which can be seen from comparing Figures A.41-A.43, A.44-A.46, A.47-A.49 and A.50-A.52 and Figures A.69-A.71, A.72-A.74, A.75-A.77, and A.78-A.80.

A.3.2 Effects of Diaphragms

The effects of diaphragms on distribution factors for BT-72 girders are similar to those for all the other girders discussed previously. A difference of about 1% to 2% is observed when the percentage differences between AASHTO and grillage model

factors for diaphragm and no diaphragm cases are compared as shown in Figures A.69-A.80.

A.3.3 Effects of Deck Thickness

Similar to the Type-III, Type-IV and BT-63 girders, the effects of deck thickness are not remarkable. The change in deck thickness makes a very small impact of about 1% to 2% on the difference between AASHTO and grillage model factors as shown in Figures A.69-A.80.

A.3.4 Effects of Span Length

The percentage differences between AASHTO and grillage model factors shown in Figures A.69-A.80 suggest only a 1% to 4% change in the percentage difference when the same configuration of bridge is compared with different span lengths.

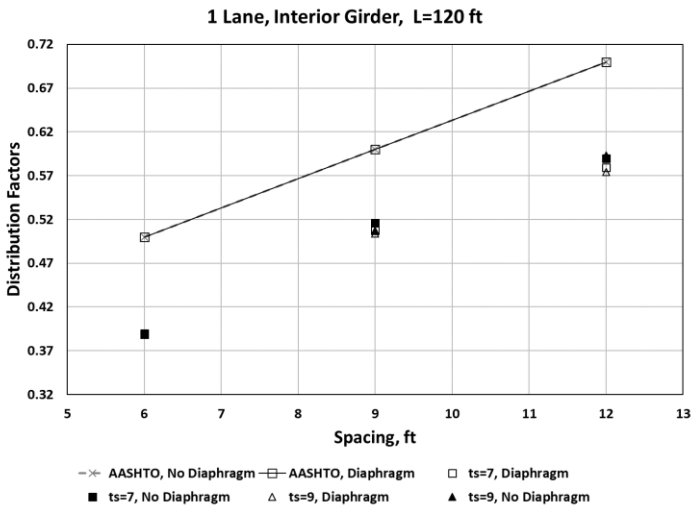

Figure A.57. Distribution factors for the interior girders, one lane loaded versus girder spacing, BT-72 with 120 ft span

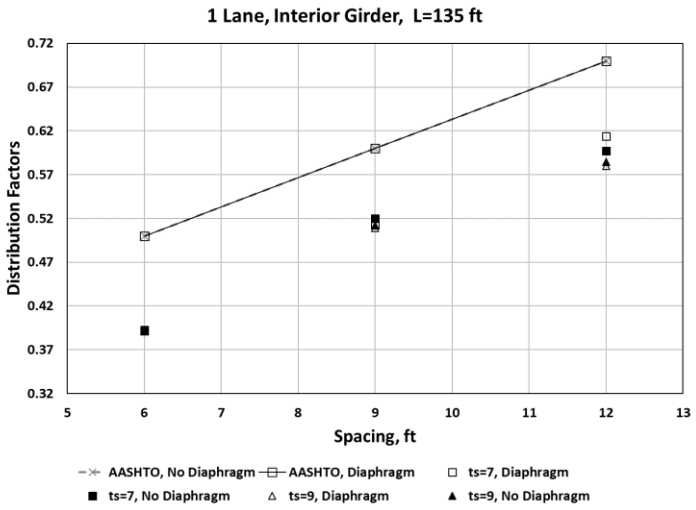

Figure A.58. Distribution factors for the interior girders, one lane loaded versus girder spacing, BT-72 with 135 ft span

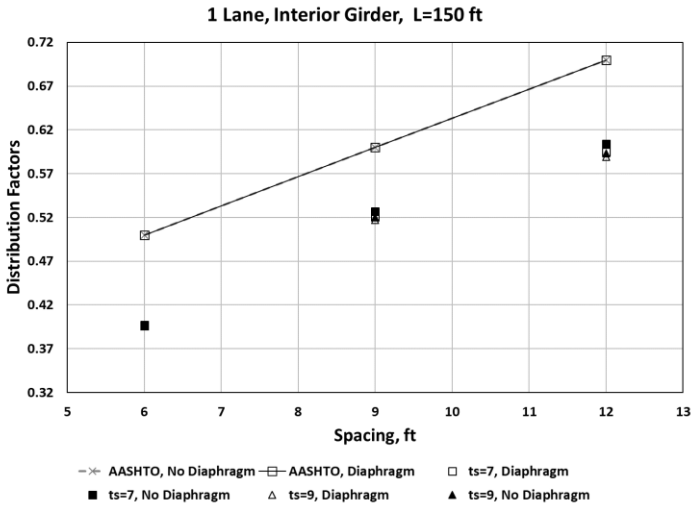

Figure A.59. Distribution factors for the interior girders, one lane loaded versus girder spacing, BT-72 with 150 ft span

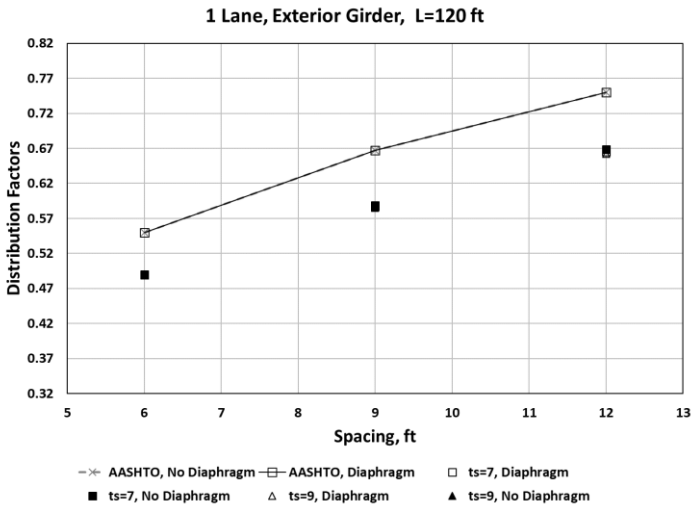

Figure A.60. Distribution factors for the exterior girders, one lane loaded versus girder spacing, BT-72 with 120 ft span

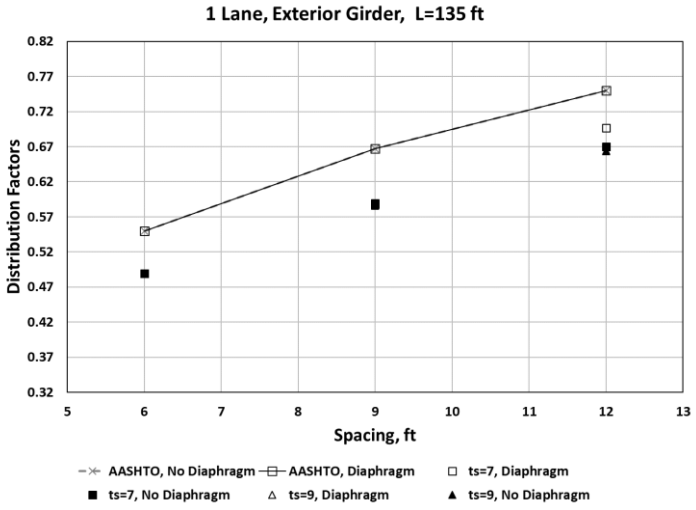

Figure A.61. Distribution factors for the exterior girders, one lane loaded versus girder spacing, BT-72 with 135 ft span

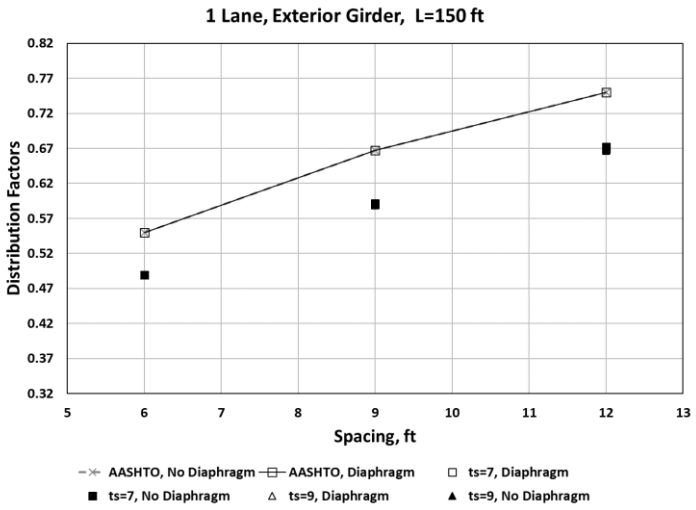

Figure A.62. Distribution factors for the exterior girders, one lane loaded versus girder spacing, BT-72 with 150 ft span

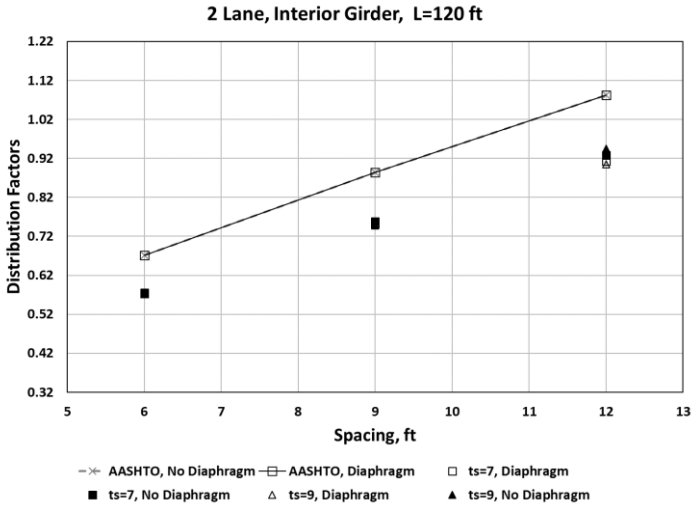

Figure A.63. Distribution factors for the interior girders, two lanes loaded versus girder spacing, BT-72 with 120 ft span

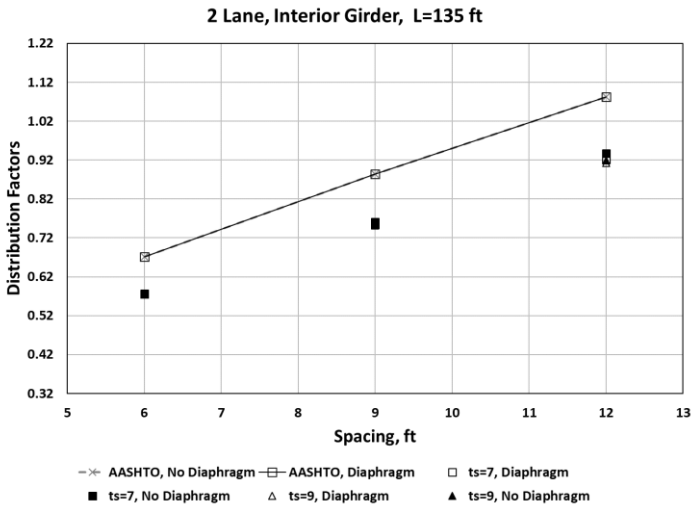

Figure A.64. Distribution factors for the interior girders, two lanes loaded versus girder spacing, BT-72 with 135 ft span

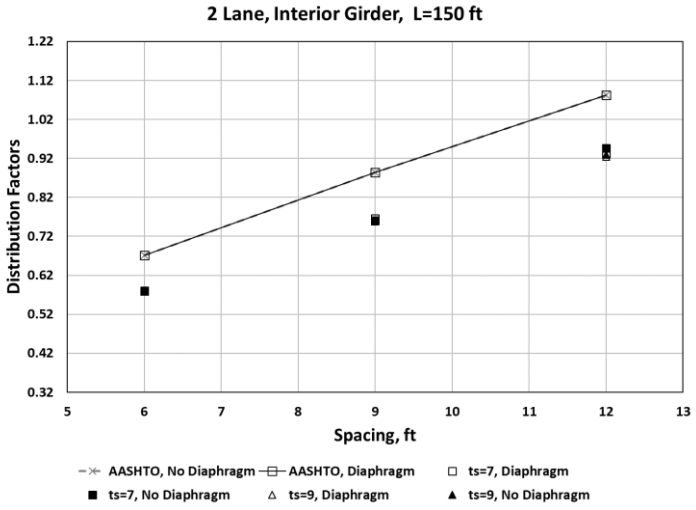

Figure A.65. Distribution factors for the interior girders, two lanes loaded versus girder spacing, BT-72 with 150 ft span

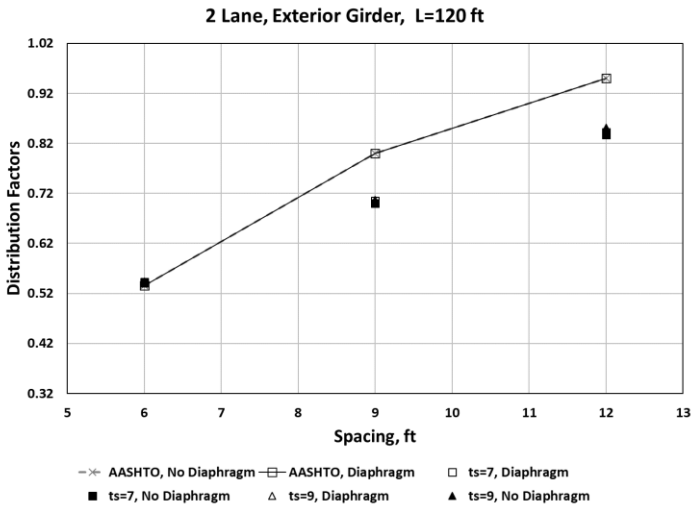

Figure A.66. Distribution factors for the exterior girders, two lanes loaded versus girder spacing, BT-72 with 120 ft span

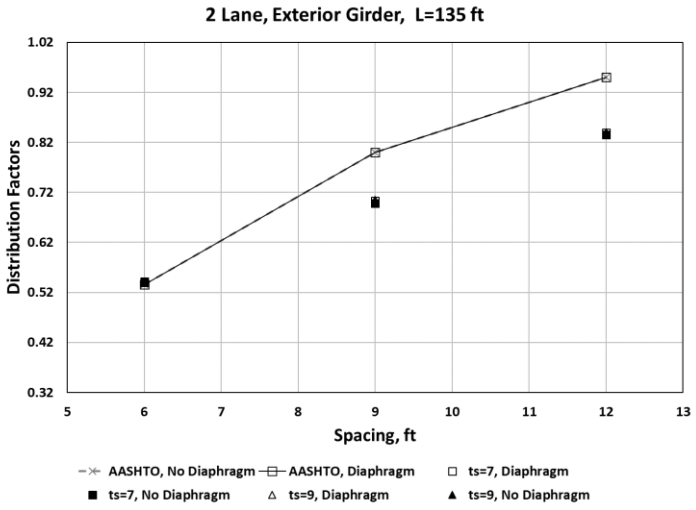

Figure A.67. Distribution factors for the exterior girders, two lanes loaded versus girder spacing, BT-72 with 135 ft span

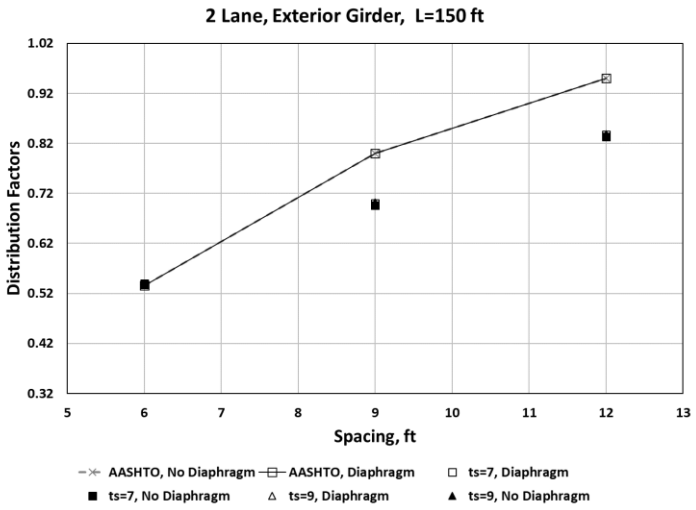

Figure A.68. Distribution factors for the exterior girders, two lanes loaded versus girder spacing, BT-72 with 150 ft span

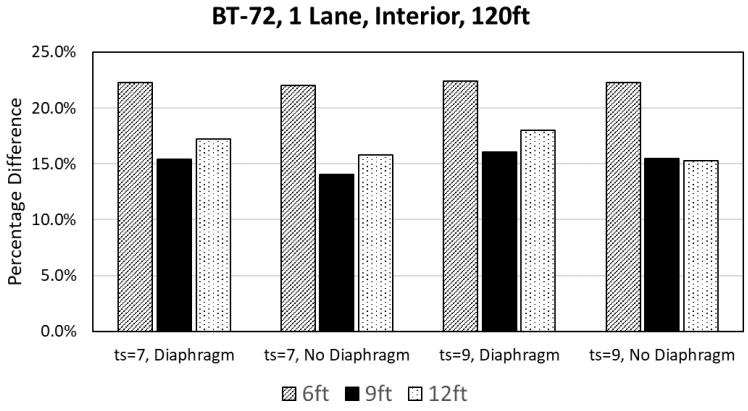

Figure A.69. Percentage difference between AASHTO equations and grillage models, for one lane loaded and interior girder, BT-72 with 120 ft span

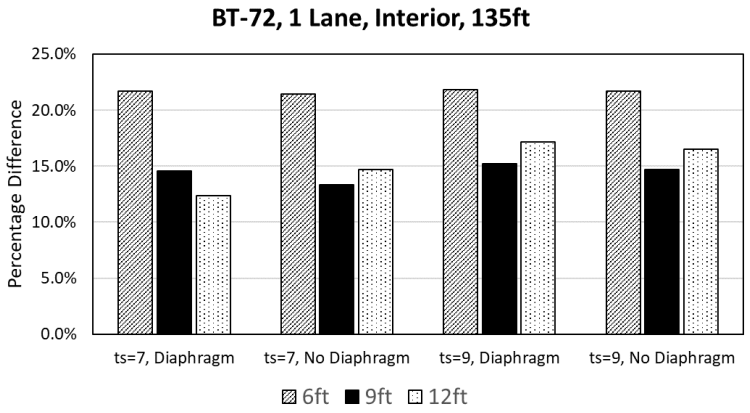

Figure A.70. Percentage difference between AASHTO equations and grillage models, for one lane loaded and interior girder, BT-72 with 135 ft span

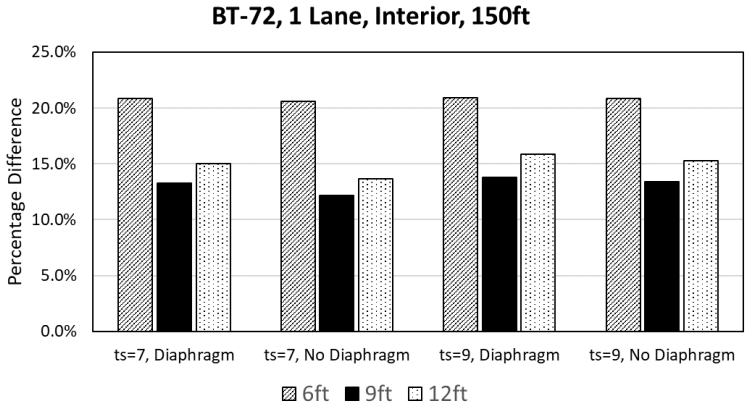

Figure A.71. Percentage difference between AASHTO equations and grillage models, for one lane loaded and interior girder, BT-72 with 150 ft span

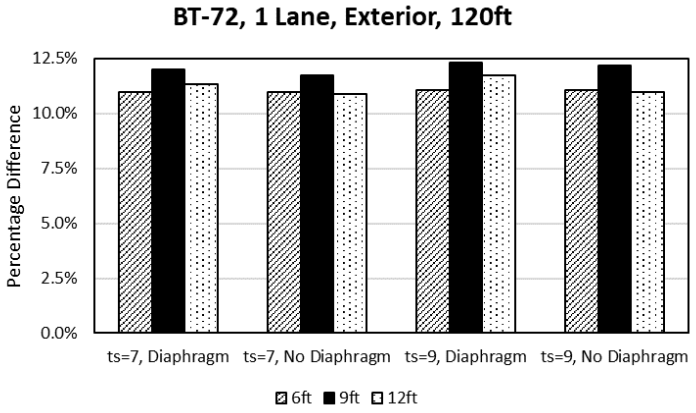

Figure A.72. Percentage difference between AASHTO equations and grillage models, for one lane loaded and exterior girder, BT-72 with 120 ft span

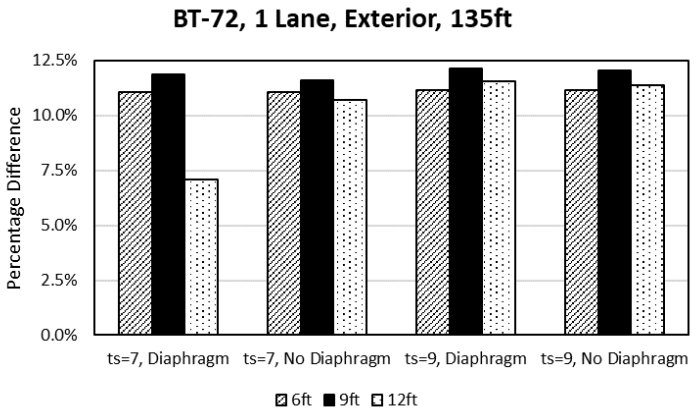

Figure A.73. Percentage difference between AASHTO equations and grillage models, for one lane loaded and exterior girder, BT-72 with 135 ft span

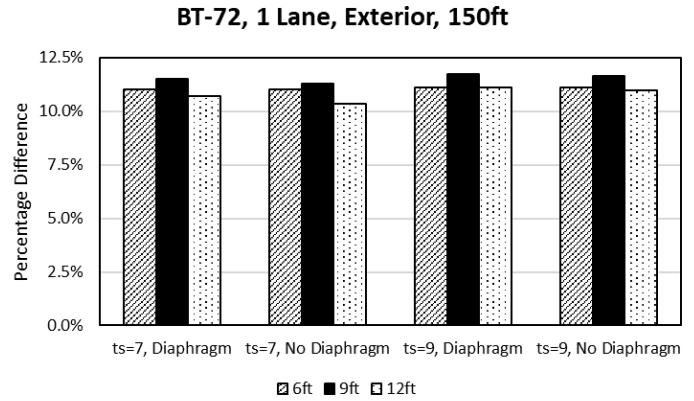

Figure A.74. Percentage difference between AASHTO equations and grillage models, for one lane loaded and exterior girder, BT-72 with 150 ft span

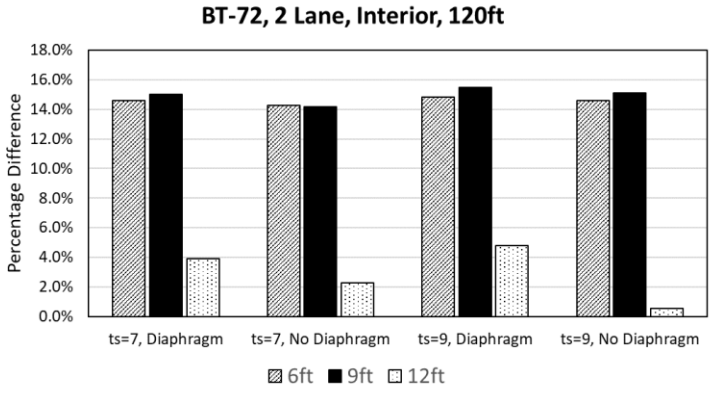

Figure A.75. Percentage difference between AASHTO equations and grillage models, for two lane loaded and interior girder, BT-72 with 120 ft span

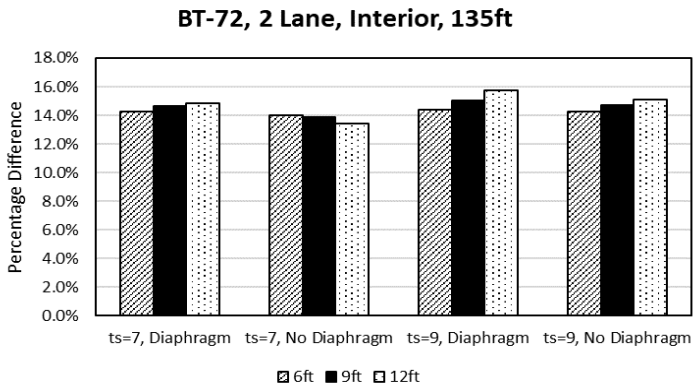

Figure A.76. Percentage difference between AASHTO equations and grillage models, for two lane loaded and interior girder, BT-72 with 135 ft span

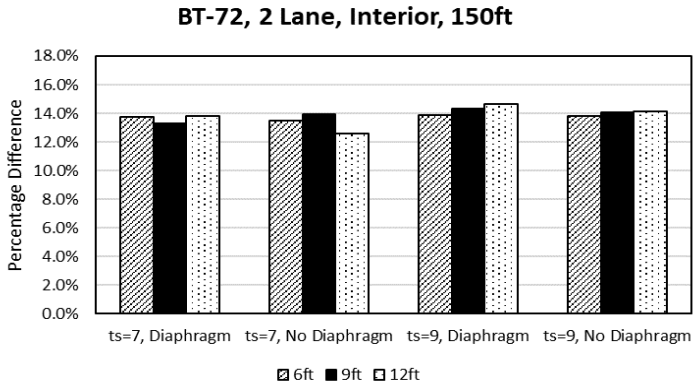

Figure A.77. Percentage difference between AASHTO equations and grillage models, for two lane loaded and interior girder, BT-72 with 150 ft span

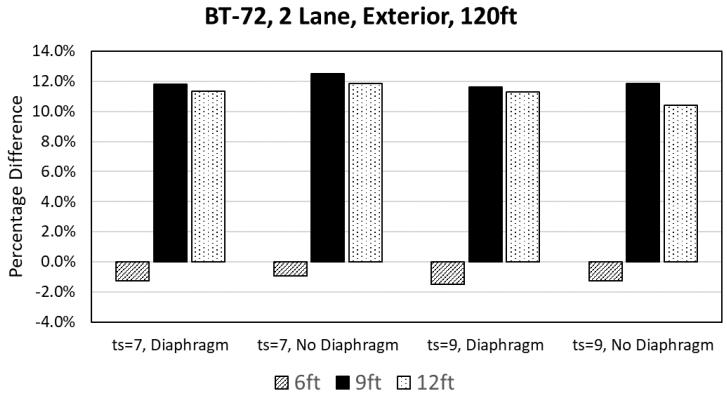

Figure A.78. Percentage difference between AASHTO equations and grillage models, for two lane loaded and exterior girder, BT-72 with 120 ft span

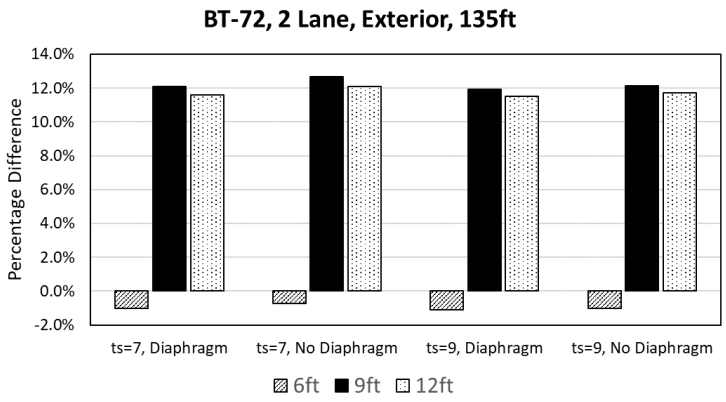

Figure A.79. Percentage difference between AASHTO equations and grillage models, for two lane loaded and exterior girder, BT-72 with 135 ft span

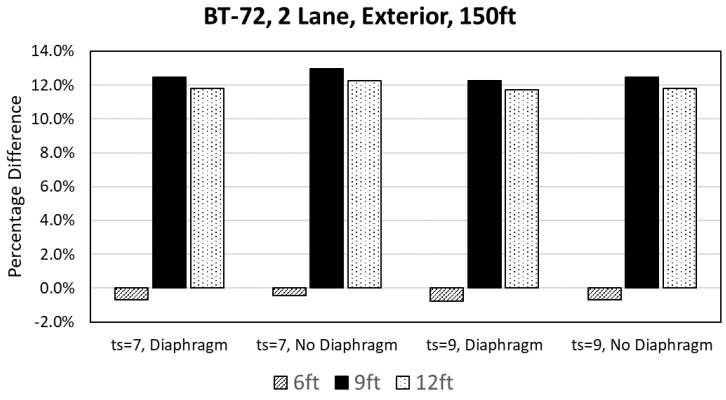

Figure A.80. Percentage difference between AASHTO equations and grillage models, for two lane loaded and exterior girder, BT-72 with 150 ft span

A.3.5 Quantitative Comparison of Load Distribution Factors

Figures A.81-A.84 show linear trendlines for BT-72 girder distribution factors determined from AASHTO LRFD and grillage models relative to girder spacing. Discussion on the use of a linear trendline for the quadratic AASHTO equation is provided in Section 2.5.6. Similar to results for BT-63 girders, the BT-72 load distribution factors determined from grillage models were fitted very well with linear equations with minimum coefficient of determination as 0.9751. For all of the cases, the trendlines from grillage model derived factors were less steep than the AASHTO LRFD equations. These results indicate that girder spacing had a large impact on load distribution factors and that the effect was less for grillage models than for the AASHTO equations.

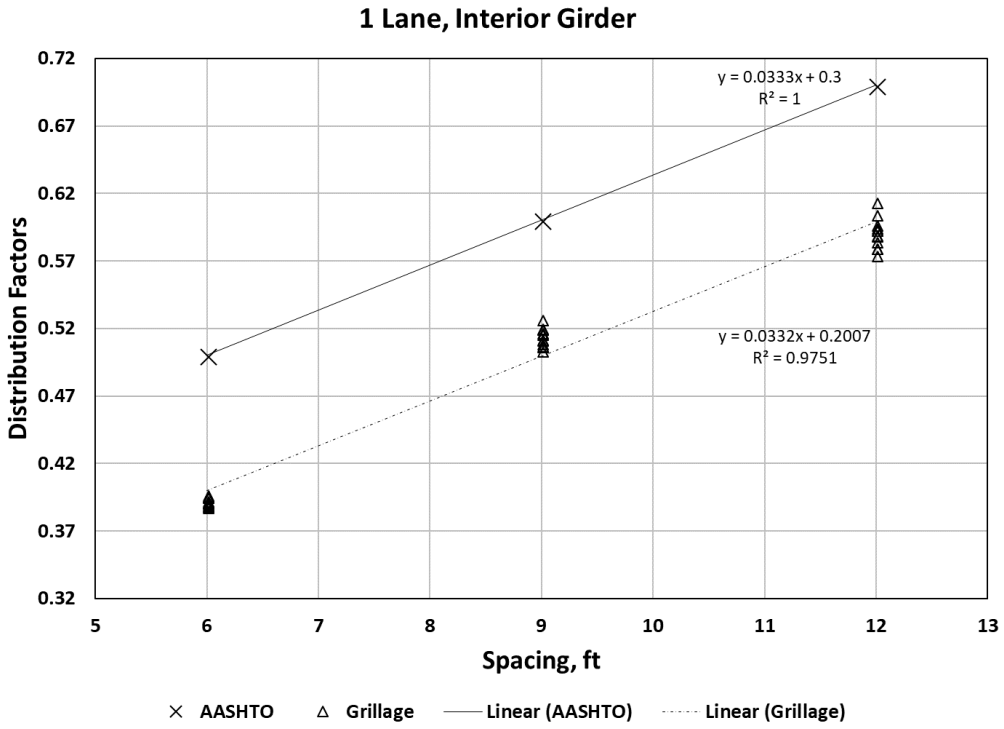

Figure A.81. Linear trendlines for effect of girder spacing on distribution factors for BT-72 girders, interior girders one lane loaded case

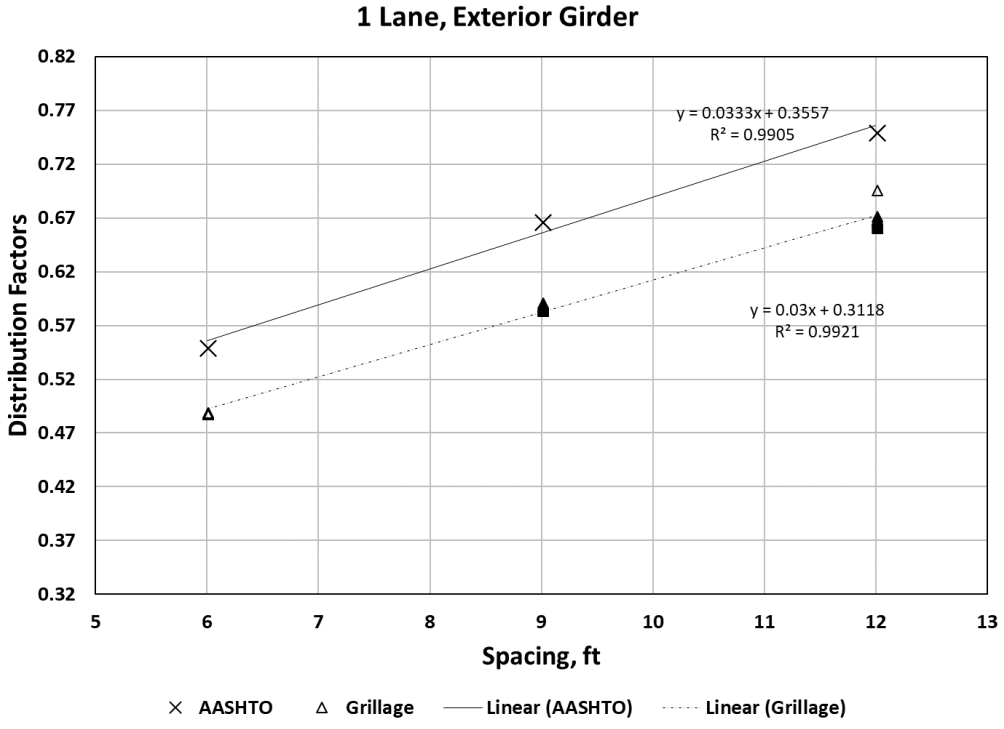

Figure A.82. Linear trendlines for effect of girder spacing on distribution factors for BT-72 girders, exterior girders one lane loaded case

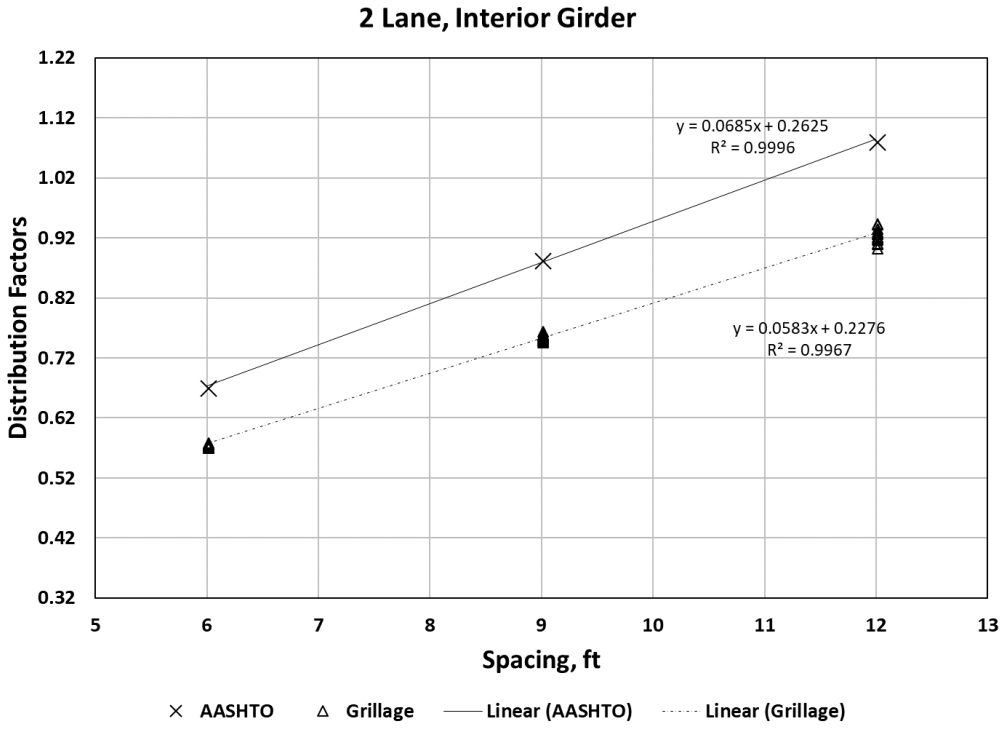

Figure A.83. Linear trendlines for effect of girder spacing on distribution factors for BT-72 girders, interior girders two lanes loaded case

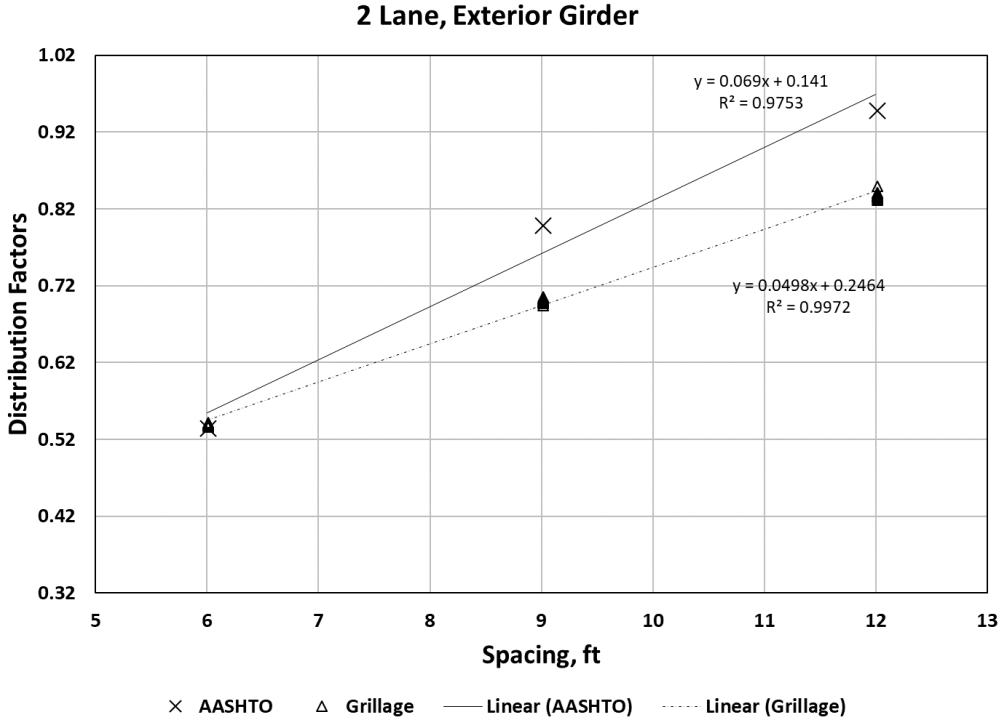

Figure A.84. Linear trendlines for effect of girder spacing on distribution factors for BT-72 girders, exterior girders two lanes loaded case

Appendix B: Distribution factor data

Table B.1. Distribution factors from STAAD and model parameters for Type II girders

Model Number	Spacing (ft)	L (ft)	Thickness (in.)	Diaphragm?	Max DF Ext. 1 Lane	Max DF Int. 1 Lane	Max DF Ext. 2+ Lane	Max DF Int. 2+ Lane
Grill1YD	6	30	7	y	0.525	0.417	0.501	0.499
Grill1ND	6	30	7	n	0.525	0.437	0.501	0.499
Grill2YD	6	30	9	y	0.525	0.416	0.501	0.499
Grill2ND	6	30	9	n	0.525	0.425	0.501	0.499
Gill13YD	6	42.5	7	y	0.526	0.403	0.500	0.500
Grill13ND	6	42.5	7	n	0.526	0.424	0.500	0.500
Grill14YD	6	42.5	9	y	0.526	0.402	0.500	0.500
Grill14ND	6	42.5	9	n	0.526	0.409	0.500	0.500
Grill3YD	6	55	7	y	0.527	0.399	0.500	0.500
Grill3ND	6	55	7	n	0.527	0.410	0.500	0.500
Grill4YD	6	55	9	y	0.527	0.398	0.500	0.500
Grill4ND	6	55	9	n	0.527	0.399	0.500	0.500
Grill19YD	6	67.5	7	y	0.527	0.398	0.500	0.500
Grill19ND	6	67.5	7	n	0.527	0.407	0.500	0.500
Grill20YD	6	67.5	9	y	0.526	0.397	0.500	0.500
Grill20ND	6	67.5	9	n	0.527	0.397	0.500	0.500
Grill5YD	9	30	7	y	0.628	0.562	0.680	0.700
Grill5ND	9	30	7	n	0.633	0.615	0.648	0.735
Grill6YD	9	30	9	y	0.626	0.555	0.685	0.694
Grill6ND	9	30	9	n	0.629	0.586	0.665	0.716
Grill15YD	9	42.5	7	y	0.625	0.542	0.686	0.692
Grill15ND	9	42.5	7	n	0.629	0.582	0.662	0.719
Grill16YD	9	42.5	9	y	0.624	0.533	0.692	0.686
Grill16ND	9	42.5	9	n	0.626	0.556	0.678	0.701
Grill7YD	9	55	7	y	0.625	0.532	0.691	0.687
Grill7ND	9	55	7	n	0.628	0.565	0.670	0.709
Grill8YD	9	55	9	y	0.624	0.523	0.697	0.680
Grill8ND	9	55	9	n	0.626	0.541	0.685	0.693
Grill21YD	9	67.5	7	y	0.624	0.533	0.690	0.688
Grill21ND	9	67.5	7	n	0.627	0.562	0.672	0.707
Grill22YD	9	67.5	9	y	0.629	0.525	0.696	0.681

Model Number	Spacing (ft)	L (ft)	Thickness (in.)	Diaphragm?	Max DF Ext. 1 Lane	Max DF Int. 1 Lane	Max DF Ext. 2+ Lane	Max DF Int. 2+ Lane
Grill22ND	9	67.5	9	n	0.624	0.540	0.685	0.692
Grill9YD	12	30	7	y	0.707	0.654	0.795	0.984
Grill9ND	12	30	7	n	0.713	0.713	0.755	1.030
Grill10YD	12	30	9	y	0.704	0.641	0.802	0.975
Grill10ND	12	30	9	n	0.708	0.679	0.774	1.006
Grill17YD	12	42.5	7	y	0.702	0.629	0.804	0.975
Grill17ND	12	42.5	7	n	0.706	0.674	0.772	1.011
Grill18YD	12	42.5	9	y	0.698	0.615	0.812	0.964
Grill18ND	12	42.5	9	n	0.701	0.642	0.792	0.987
Grill11YD	12	55	7	y	0.700	0.617	0.809	0.971
Grill11ND	12	55	7	n	0.703	0.654	0.782	1.000
Grill12YD	12	55	9	y	0.697	0.602	0.818	0.958
Grill12ND	12	55	9	n	0.698	0.624	0.801	0.977
Grill23YD	12	67.5	7	y	0.699	0.617	0.810	0.969
Grill23ND	12	67.5	7	n	0.701	0.649	0.786	0.994
Grill24YD	12	67.5	9	y	0.696	0.603	0.819	0.956
Grill24ND	12	67.5	9	n	0.696	0.621	0.804	0.971

Table B.2. AASHTO distribution factors for parametric models for Type II girders

Model Number	Spacing (ft)	L (ft)	Thickness (in.)	Diaphragm?	AASHTO Ext. 1 Lane	AASHTO Ext. 2 Lane	AASHTO Int. 1 Lane	AASHTO Int. 2 Lane
Grill1YD	6	30	7	y	0.660	0.536	0.600	0.671
Grill1ND	6	30	7	n	0.600	0.536	0.600	0.671
Grill2YD	6	30	9	y	0.660	0.536	0.600	0.671
Grill2ND	6	30	9	n	0.600	0.536	0.600	0.671
Gill13YD	6	42.5	7	y	0.660	0.536	0.600	0.671
Grill13ND	6	42.5	7	n	0.600	0.536	0.600	0.671
Grill14YD	6	42.5	9	y	0.660	0.536	0.600	0.671
Grill14ND	6	42.5	9	n	0.600	0.536	0.600	0.671
Grill3YD	6	55	7	y	0.660	0.536	0.600	0.671
Grill3ND	6	55	7	n	0.600	0.536	0.600	0.671
Grill4YD	6	55	9	y	0.660	0.536	0.600	0.671
Grill4ND	6	55	9	n	0.600	0.536	0.600	0.671
Grill19YD	6	67.5	7	y	0.660	0.536	0.600	0.671
Grill19ND	6	67.5	7	n	0.600	0.536	0.600	0.671
Grill20YD	6	67.5	9	y	0.660	0.536	0.600	0.671
Grill20ND	6	67.5	9	n	0.600	0.536	0.600	0.671
Grill5YD	9	30	7	y	0.800	0.800	0.720	0.884
Grill5ND	9	30	7	n	0.800	0.707	0.720	0.884
Grill6YD	9	30	9	y	0.800	0.800	0.720	0.884
Grill6ND	9	30	9	n	0.800	0.707	0.720	0.884
Grill15YD	9	42.5	7	y	0.800	0.800	0.720	0.884
Grill15ND	9	42.5	7	n	0.800	0.707	0.720	0.884
Grill16YD	9	42.5	9	y	0.800	0.800	0.720	0.884
Grill16ND	9	42.5	9	n	0.800	0.707	0.720	0.884
Grill7YD	9	55	7	y	0.800	0.800	0.720	0.884
Grill7ND	9	55	7	n	0.800	0.707	0.720	0.884
Grill8YD	9	55	9	y	0.800	0.800	0.720	0.884
Grill8ND	9	55	9	n	0.800	0.707	0.720	0.884
Grill21YD	9	67.5	7	y	0.800	0.800	0.720	0.884
Grill21ND	9	67.5	7	n	0.800	0.707	0.720	0.884
Grill22YD	9	67.5	9	y	0.800	0.800	0.720	0.884
Grill22ND	9	67.5	9	n	0.800	0.707	0.720	0.884
Grill9YD	12	30	7	y	0.900	0.950	0.840	1.082

Model Number	Spacing (ft)	L (ft)	Thickness (in.)	Diaphragm?	AASHTO Ext. 1 Lane	AASHTO Ext. 2 Lane	AASHTO Int. 1 Lane	AASHTO Int. 2 Lane
Grill9ND	12	30	7	n	0.900	0.866	0.840	1.082
Grill10YD	12	30	9	y	0.900	0.950	0.840	1.082
Grill10ND	12	30	9	n	0.900	0.866	0.840	1.082
Grill17YD	12	42.5	7	y	0.900	0.950	0.840	1.082
Grill17ND	12	42.5	7	n	0.900	0.866	0.840	1.082
Grill18YD	12	42.5	9	y	0.900	0.950	0.840	1.082
Grill18ND	12	42.5	9	n	0.900	0.866	0.840	1.082
Grill11YD	12	55	7	y	0.900	0.950	0.840	1.082
Grill11ND	12	55	7	n	0.900	0.866	0.840	1.082
Grill12YD	12	55	9	y	0.900	0.950	0.840	1.082
Grill12ND	12	55	9	n	0.900	0.866	0.840	1.082
Grill23YD	12	67.5	7	y	0.900	0.950	0.840	1.082
Grill23ND	12	67.5	7	n	0.900	0.866	0.840	1.082
Grill24YD	12	67.5	9	y	0.900	0.950	0.840	1.082
Grill24ND	12	67.5	9	n	0.900	0.866	0.840	1.082

Note: AASHTO distribution factors include *m*

Table B.3. Girder properties for Type II girder parametric bridge models

Model #	Diaph.	Length (ft)	Spacing (ft)	Slab (in.)	Int. A (in^2)	Int. J (in^4)	Int. I (in^4)	Ext. A (in^2)	Ext. J (in^4)	Ext. I (in^4)
1	*Y*	30	6	7	805.5	7387.4	68335.1	732.8	7387.4	66731.0
1	*N*	30	6	7	805.5	7387.4	68335.1	732.8	7387.4	66731.0
2	*Y*	30	6	9	930.3	7451.7	72106.1	836.7	7451.7	70200.3
2	*N*	30	6	9	930.3	7451.7	72106.1	836.7	7451.7	70200.3
3	*Y*	55	6	7	805.5	7387.4	68335.1	732.8	7387.4	66731.0
3	*N*	55	6	7	805.5	7387.4	68335.1	732.8	7387.4	66731.0
4	*Y*	55	6	9	930.3	7451.7	72106.1	836.7	7451.7	70200.3
4	*N*	55	6	9	930.3	7451.7	72106.1	836.7	7451.7	70200.3
5	*Y*	30	9	7	1023.8	7387.4	72032.9	841.9	7387.4	69052.5
5	*N*	30	9	7	1023.8	7387.4	72032.9	841.9	7387.4	69052.5
6	*Y*	30	9	9	1210.9	7451.7	76642.2	977.0	7451.7	72967.5
6	*N*	30	9	9	1210.9	7451.7	76642.2	977.0	7451.7	72967.5
7	*Y*	55	9	7	1023.8	7387.4	72032.9	841.9	7387.4	69052.5
7	*N*	55	9	7	1023.8	7387.4	72032.9	841.9	7387.4	69052.5
8	*Y*	55	9	9	1210.9	7451.7	76642.2	977.0	7451.7	72967.5
8	*N*	55	9	9	1210.9	7451.7	76642.2	977.0	7451.7	72967.5
9	*Y*	30	12	7	1242.1	7387.4	74744.4	951.0	7387.4	70943.5
9	*N*	30	12	7	1242.1	7387.4	74744.4	951.0	7387.4	70943.5
10	*Y*	30	12	9	1491.5	7451.7	80184.2	1117.3	7451.7	75277.6
10	*N*	30	12	9	1491.5	7451.7	80184.2	1117.3	7451.7	75277.6
11	*Y*	55	12	7	1242.1	7387.4	74744.4	951.0	7387.4	70943.5
11	*N*	55	12	7	1242.1	7387.4	74744.4	951.0	7387.4	70943.5
12	*Y*	55	12	9	1491.5	7451.7	80184.2	1117.3	7451.7	75277.6
12	*N*	55	12	9	1491.5	7451.7	80184.2	1117.3	7451.7	75277.6
13	*Y*	42.5	6	7	805.5	7387.4	68335.1	732.8	7387.4	66731.0
13	*N*	42.5	6	7	805.5	7387.4	68335.1	732.8	7387.4	66731.0
14	*Y*	42.5	6	9	930.3	7451.7	72106.1	836.7	7451.7	70200.3
14	*N*	42.5	6	9	930.3	7451.7	72106.1	836.7	7451.7	70200.3
15	*Y*	42.5	9	7	1023.8	7387.4	72032.9	841.9	7387.4	69052.5
15	*N*	42.5	9	7	1023.8	7387.4	72032.9	841.9	7387.4	69052.5
16	*Y*	42.5	9	9	1210.9	7451.7	76642.2	977.0	7451.7	72967.5
16	*N*	42.5	9	9	1210.9	7451.7	76642.2	977.0	7451.7	72967.5
17	*Y*	42.5	12	7	1242.1	7387.4	74744.4	951.0	7387.4	70943.5

Model #	Diaph.	Length (ft)	Spacing (ft)	Slab (in.)	Int. A (in^2)	Int. J (in^4)	Int. I (in^4)	Ext. A (in^2)	Ext. J (in^4)	Ext. I (in^4)
17	*N*	42.5	12	7	1242.1	7387.4	74744.4	951.0	7387.4	70943.5
18	*Y*	42.5	12	9	1491.5	7451.7	80184.2	1117.3	7451.7	75277.6
18	*N*	42.5	12	9	1491.5	7451.7	80184.2	1117.3	7451.7	75277.6
19	*Y*	67.5	6	7	805.5	7387.4	68335.1	732.8	7387.4	66731.0
19	*N*	67.5	6	7	805.5	7387.4	68335.1	732.8	7387.4	66731.0
20	*Y*	67.5	6	9	930.3	7451.7	72106.1	836.7	7451.7	70200.3
20	*N*	67.5	6	9	930.3	7451.7	72106.1	836.7	7451.7	70200.3
21	*Y*	67.5	9	7	1023.8	7387.4	72032.9	841.9	7387.4	69052.5
21	*N*	67.5	9	7	1023.8	7387.4	72032.9	841.9	7387.4	69052.5
22	*Y*	67.5	9	9	1210.9	7451.7	76642.2	977.0	7451.7	72967.5
22	*N*	67.5	9	9	1210.9	7451.7	76642.2	977.0	7451.7	72967.5
23	*Y*	67.5	12	7	1242.1	7387.4	74744.4	951.0	7387.4	70943.5
23	*N*	67.5	12	7	1242.1	7387.4	74744.4	951.0	7387.4	70943.5
24	*Y*	67.5	12	9	1491.5	7451.7	80184.2	1117.3	7451.7	75277.6
24	*N*	67.5	12	9	1491.5	7451.7	80184.2	1117.3	7451.7	75277.6

Table B.4. Continued properties for Type II girder parametric bridge models

Model #	Diaph.	Slab A (in^2)	Slab I (in^4)	Slab J (in^4)	Slab + Diaph. A (in^2)	Slab + Diaph. J (in^4)	Slab + Diaph. I (in^4)	End Slab A (in^2)	End Slab J (in^4)	End Slab I (in^4)
1	*Y*	272.8	2228.1	1286.3	439.1	6546.0	12299.4	302.7	5259.7	10862.5
1	*N*	272.8	2228.1	1286.3	X	X	X	136.4	1114.1	557.0
2	*Y*	350.8	4735.6	2367.8	517.1	9267.6	14073.0	341.7	6533.8	11983.2
2	*N*	350.8	4735.6	2367.8	X	X	X	175.4	2367.8	1183.9
3	*Y*	500.2	4084.9	2042.5	666.5	8689.7	13893.7	416.4	6331.6	12099.9
3	*N*	500.2	4084.9	2042.5	X	X	X	250.1	2042.5	1021.2
4	*Y*	643.1	8682.0	4341.0	809.4	13823.8	16683.6	487.9	8812.0	13770.0
4	*N*	643.1	8682.0	4341.0	X	X	X	321.6	4341.0	2170.5
5	*Y*	272.8	2228.1	1114.1	439.1	6546.0	12299.4	302.7	5259.7	10862.5
5	*N*	272.8	2228.1	1114.1	X	X	X	136.4	1114.1	557.0
6	*Y*	350.8	4735.6	2367.8	517.1	9267.6	14073.0	341.7	6533.8	11983.2
6	*N*	350.8	4735.6	2367.8	X	X	X	175.4	2367.8	1183.9
7	*Y*	500.2	4084.9	2042.5	666.5	8689.7	13893.7	416.4	6331.6	12099.9
7	*N*	500.2	4084.9	2042.5	X	X	X	250.1	2042.5	1021.2
8	*Y*	643.1	8682.0	4341.0	809.4	13823.8	16683.6	487.9	8812.0	13770.0
8	*N*	643.1	8682.0	4341.0	X	X	X	321.6	4341.0	2170.5
9	*Y*	272.8	2228.1	1114.1	439.1	6546.0	12299.4	302.7	5259.7	10862.5
9	*N*	272.8	2228.1	1114.1	X	X	X	136.4	1114.1	557.0
10	*Y*	350.8	4735.6	2367.8	517.1	9267.6	14073.0	341.7	6533.8	11983.2
10	*N*	350.8	4735.6	2367.8	X	X	X	175.4	2367.8	1183.9
11	*Y*	500.2	4084.9	2042.5	666.5	8689.7	13893.7	416.4	6331.6	12099.9
11	*N*	500.2	4084.9	2042.5	X	X	X	250.1	2042.5	1021.2
12	*Y*	643.1	8682.0	4341.0	809.4	13823.8	16683.6	487.9	8812.0	13770.0
12	*N*	643.1	8682.0	4341.0	X	X	X	321.6	4341.0	2170.5
13	*Y*	386.5	3156.5	1578.3	552.8	7617.9	13165.0	359.6	5795.7	11542.4
13	*N*	386.5	3156.5	1578.3	X	X	X	193.3	1578.3	789.1
14	*Y*	496.9	6708.8	3354.4	663.2	11545.7	15448.6	414.8	7672.9	12947.1
14	*N*	496.9	6708.8	3354.4	X	X	X	248.5	3354.4	1677.2
15	*Y*	386.5	3156.5	1578.3	552.8	7617.9	13165.0	359.6	5795.7	11542.4
15	*N*	386.5	3156.5	1578.3	X	X	X	193.3	1578.3	789.1
16	*Y*	496.9	6708.8	3354.4	663.2	11545.7	15448.6	414.8	7672.9	12947.1
16	*N*	496.9	6708.8	3354.4	X	X	X	248.5	3354.4	1677.2

Model #	Diaph.	Slab A (in^2)	Slab I (in^4)	Slab J (in^4)	Slab + Diaph. A (in^2)	Slab + Diaph. J (in^4)	Slab + Diaph. I (in^4)	End Slab A (in^2)	End Slab J (in^4)	End Slab I (in^4)
17	*Y*	386.5	3156.5	1578.3	552.8	7617.9	13165.0	359.6	5795.7	11542.4
17	*N*	386.5	3156.5	1578.3	X	X	X	193.3	1578.3	789.1
18	*Y*	496.9	6708.8	3354.4	663.2	11545.7	15448.6	414.8	7672.9	12947.1
18	*N*	496.9	6708.8	3354.4	X	X	X	248.5	3354.4	1677.2
19	*Y*	613.9	5013.3	2506.7	780.2	9761.6	14545.4	473.2	6867.6	12579.3
19	*N*	613.9	5013.3	2506.7	X	X	X	306.9	2506.7	1253.3
20	*Y*	789.3	10655.1	5327.6	955.6	16102.0	17842.7	560.9	9951.0	14507.0
20	*N*	789.3	10655.1	5327.6	X	X	X	394.6	5327.6	2663.8
21	*Y*	613.9	5013.3	2506.7	780.2	9761.6	14545.4	473.2	6867.6	12579.3
21	*N*	613.9	5013.3	2506.7	X	X	X	306.9	2506.7	1253.3
22	*Y*	789.3	10655.1	5327.6	955.6	16102.0	17842.7	560.9	9951.0	14507.0
22	*N*	789.3	10655.1	5327.6	X	X	X	394.6	5327.6	2663.8
23	*Y*	613.9	5013.3	2506.7	780.2	9761.6	14545.4	473.2	6867.6	12579.3
23	*N*	613.9	5013.3	2506.7	X	X	X	306.9	2506.7	1253.3
24	*Y*	789.3	10655.1	5327.6	955.6	16102.0	17842.7	560.9	9951.0	14507.0
24	*N*	789.3	10655.1	5327.6	X	X	X	394.6	5327.6	2663.8

Table B.5. Properties for grillage models of selected Oklahoma bridges (part 1)

Bridge	Length (ft)	Spacing (ft)	Slab (in.)	Int. A (in^2)	Int. J (in^4)	Int. I (in^4)	Ext. A (in^2)	Ext. J (in^4)	Ext. I (in^4)
Little River Overflow	34.83	11.75	9	1468.1	7451.7	79913.1	1105.7	7451.7	75098.3
I244 A	30.5	7.67	7	1053.7	7387.4	72448.6	889.9	7387.4	69928.5
I244 C	46	7.67	7	960.1	7387.4	71085.7	818.8	7387.4	68601.7

Table B.6. Properties for grillage models of selected Oklahoma bridges (part 2)

Bridge	Slab A (in^2)	Slab J (in^4)	Slab I (in^4)	Slab + Diaph. A (in^2)	Slab + Diaph. J (in^4)	Slab + Diaph. I (in^4)	Slab + end A (in^2)	Slab + end J (in^4)	Slab + end I (in^4)
Little River Overflow	407.3	5498.6	2749.3	573.6	10148.5	14628.4	369.9	6974.3	12377.9
I244 A	340.5	2780.6	1390.3	544.6	6588.9	15144.4	374.4	5281.2	13370.8
I244 C	443.3	3620.5	1810.3	619.6	7918.0	14178.4	397.9	5945.7	12407.6

Appendix C: Strand Draw-in Data

Table C.1. Draw-in data for specimen PC3

Beam Age (days)	NW (in.)	NE (in.)	SW (in.)	SE (in.)
1 (release)	0.120	0.077	0.069	0.069
7	0.138	0.090	0.083	0.097
14	0.139	0.098	0.083	0.098
15	0.139	0.099	0.083	0.099
21	0.139	0.099	0.083	0.101
28	0.139	0.100	0.083	0.104
29	0.139	0.100	0.083	0.105
35	0.139	0.104	0.083	0.105
42	0.139	0.106	0.083	0.107
56	0.139	0.106	0.083	0.107
63	0.140	0.106	0.084	0.107

Note: Strand designations are based on beam casting position for two strands

Table C.2. Draw-in data for specimen PC4

Beam Age (days)	NW (in.)	NE (in.)	SW (in.)	SE (in.)
1 (release)	0.089	0.047	0.068	0.054
7	0.095	0.083	0.103	0.071
14	0.095	0.083	0.103	0.071
15	0.095	0.083	0.104	0.071
21	0.095	0.083	0.104	0.072
28	0.095	0.090	0.104	0.072
29	0.096	0.090	0.104	0.072
35	0.096	0.090	0.104	0.072
42	0.096	0.090	0.104	0.072
56	0.096	0.091	0.104	0.073
63	0.096	0.091	0.104	0.073

Note: Strand designations are based on beam casting position for two strands

Table C.3. Draw-in data for specimen PC5

Beam Age (days)	NW (in.)	NE (in.)	SW (in.)	SE (in.)
1 (release)	0.073	0.087	0.045	0.064
7	0.094	0.105	0.068	0.091
14	0.099	0.105	0.072	0.095
21	0.099	0.108	0.072	0.095
22	0.1	0.112	0.072	0.095
28	0.101	0.112	0.073	0.098
35	0.102	0.112	0.073	0.098
49	0.108	0.112	0.078	0.098
56	0.123	0.126	0.081	0.102
63	0.125	0.126	0.081	0.102
70	0.125	0.129	0.107	0.102

Note: Strand designations are based on beam casting position for two strands

Table C.4. Draw-in data for specimen PC6

Beam Age (days)	NW (in.)	NE (in.)	SW (in.)	SE (in.)
1 (release)	0.077	0.077	0.070	0.079
7	0.101	0.097	0.095	0.094
14	0.101	0.104	0.095	0.094
21	0.101	0.104	0.096	0.094
22	0.102	0.105	0.095	0.095
28	0.102	0.105	0.095	0.095
35	0.102	0.112	0.096	0.095
49	0.102	0.112	0.100	0.095
56	0.102	0.112	0.100	0.095
63	0.105	0.112	0.100	0.096
70	0.108	0.123	0.105	0.096

Note: Strand designations are based on beam casting position for two strands

Table C.5. Draw-in data for specimen PC7

Beam Age (days)	NW (in.)	NE (in.)	SW (in.)	SE (in.)
1 (release)	0.068	0.078	0.068	0.040
7	0.091	0.094	0.098	0.100
14	0.091	0.117	0.098	0.100
28	0.101	0.117	0.099	0.101
35	0.101	0.117	0.099	0.101
42	0.101	0.118	0.099	0.100
49	0.101	0.118	0.099	0.105
56	0.101	0.121	0.099	0.105

Note: Strand designations are based on beam casting position for two strands

Table C.6. Draw-in data for specimen PC8

Beam Age (days)	NW (in.)	NE (in.)	SW (in.)	SE (in.)
1 (release)	0.070	0.067	0.066	0.071
14	0.086	0.096	0.099	0.092
21	0.088	0.098	0.103	0.097
28	0.094	0.099	0.103	0.101
35	0.096	0.099	0.106	0.101
42	0.096	0.101	0.109	0.101
49	0.096	0.101	0.109	0.104
56	0.097	0.102	0.110	0.104

Note: Strand designations are based on beam casting position for two strands

Table C.7. Draw-in data for specimen PC9

Beam Age (days)	NW (in.)	NE (in.)	SW (in.)	SE (in.)
1 (release)	0.071	0.072	0.044	0.072
14	0.100	0.095	0.069	0.096
21	0.100	0.097	0.069	0.096
28	0.102	0.101	0.069	0.099
35	0.103	0.101	0.069	0.099
42	0.102	0.101	0.073	0.099
49	0.106	0.101	0.074	0.099
56	0.106	0.105	0.074	0.099

Note: Strand designations are based on beam casting position for two strands

Table C.8. Draw-in data for specimen PC10

Beam Age (days)	NW (in.)	NE (in.)	SW (in.)	SE (in.)
1 (release)	0.081	0.062	0.054	0.032
7	0.100	0.091	0.079	0.067
14	0.096	0.094	0.090	0.080
21	0.096	0.094	0.090	0.080
28	0.096	0.097	0.094	0.085
35	0.096	0.097	0.094	0.085
42	0.096	0.097	0.094	0.089
49	0.096	0.098	0.094	0.089

Note: Strand designations are based on beam casting position for two strands

Table C.9. Draw-in data for specimen PC11

Beam Age (days)	NW (in.)	NE (in.)	SW (in.)	SE (in.)
1 (release)	0.065	0.068	0.062	0.072
7	0.095	0.093	0.092	0.097
14	0.096	0.104	0.094	0.103
21	0.096	0.104	0.094	0.107
28	0.100	0.114	0.097	0.107
35	0.101	0.115	0.099	0.107
42	0.108	0.115	0.104	0.107
49	0.108	0.116	0.104	0.107

Note: Strand designations are based on beam casting position for two strands

Table C.10. Draw-in data for specimen PC12

Beam Age (days)	NW (in.)	NE (in.)	SW (in.)	SE (in.)
1 (release)	0.076	0.077	0.073	0.073
3	0.099	0.108	0.103	0.100
7	0.101	0.108	0.105	0.103
14	0.101	0.123	0.110	0.104
21	0.104	0.123	0.112	0.115
28	0.104	0.123	0.112	0.115

Note: Strand designations are based on beam casting position for two strands

Table C.11. Draw-in data for specimen PC13

Beam Age (days)	NW (in.)	NE (in.)	SW (in.)	SE (in.)
1 (release)	0.092	0.080	0.067	0.069
3	0.121	0.115	0.099	0.093
7	0.121	0.113	0.097	0.097
14	0.125	0.115	0.103	0.097
21	0.129	0.123	0.103	0.097
28	0.130	0.122	0.103	0.097

Note: Strand designations are based on beam casting position for two strands